:

Bacterial filamentation as a survival strategy: identification and characterisation of a novel cell division inhibitor in *Escherichia coli*

Shirin Ansari

A thesis submitted in fulfilment of the requirements for

the degree of Doctor of Philosophy

February 2019

UNIVERSITY OF TECHNOLOGY SYDNEY

Certificate of Authorship/ Originality

I, Shirin Ansari declare that this thesis is submitted in fulfilment of the requirements for the award of Doctor of Philosophy, in the i3 Institute, Faculty of Science at the University of Technology Sydney. This thesis is wholly my own work unless otherwise reference or acknowledged. In addition, I certify that all information sources and literature used are indicated in the thesis. This document has not been submitted for qualifications at any other academic institution.

This research is supported by an Australian Government Research Training Program Scholarship.

Signature of Student:

Production Note:
Signature removed prior to publication.

Date: 20/2/2019

Acknowledgements

What a journey! I could not have done this without the help of some wonderful people along the way. First and foremost, to my supervisors, Cath Burke and Liz Harry, thank you for the opportunity, support and guidance over the years. I have learnt so much from you both and you have played a huge part in me becoming the scientist I am today.

To Iain Duggin, I cannot even begin to thank you for all your science wisdom and knowledge, all the while expecting nothing in return. This has meant the world to me. Thank you for taking the time to listen to my ideas and helping develop them.

I would also like to thank all the Harry Lab members, past and present, especially Isa, Ken, Daniel, Nural, Amy and Riti. It has been a pleasure working with such amazing people and of course enjoying all the baked goodies for morning tea! I will cherish all our great memories of love and laughter. It will be hard to find better lab buddies! A special shout-out to Penny and Naomi, your friendship has gotten me through some very difficult times, I appreciate it more than you can imagine.

Huge thanks to my parents, Rehmat and Sharaf. You both have loved me unconditionally and always encouraged me to pursue my dreams. The person I am today is because of you both. Also to Mecki, Nagma, Amaan and Nonu, thanks for being there for me no matter what and delivering food to my place so I didn't have to deal with cooking.

Finally to my loving fiancé, James (Dr. Baby), thank you is not enough for everything you have done for me! You have believed in me when I didn't and have picked me up

every time I couldn't go on. Thank you for your patience and love, especially in the last few weeks. I am really looking forward to our post-thesis life and all the adventures I am sure that await us.

On a more professional note, I would like to thank and acknowledge Dr. James Walsh's help in writing script in Mathematica that allowed me to automate and generate a lot of my bioinformatics analysis. Also thank you for all your maths wisdom. Without this I may not have come as far as I did.

Abstract

Bacterial cell division is tightly regulated to ensure that division occurs at the correct time and position in order to create two viable, genetically identical, daughter cells. In addition to correct timing and positioning, the inhibition of division is also important for survival in certain conditions. This inhibition of division results in filamentous cells, a process where cell growth and DNA replication continues in the absence of division, resulting in elongated cells. This is an important survival mechanism utilised by several bacteria in response to an environmental stimuli, including during pathogenesis and exposure to antibiotics. However, the underlying mechanisms of filamentation and regulators of cell division that enable this unique morphology remain largely unknown. A recent high-throughput over-expression screen in *Escherichia coli* identified several potential division inhibitors, including *ymfM*, a gene encoded within the e14 prophage. The overall aim of this thesis was to understand the biological condition in which YmfM may be functioning, as well as how it may be acting to inhibit division.

The initial aim of this thesis was to verify the genes from the original screen that are responsible for causing filamentation. From this the expression of *ymfM* was shown to cause a complete inhibition of cell division and became the primary focus of this work.

The e14 prophage is thought to encode for an SOS inducible cell division inhibitor, SfiC. However the exact gene responsible for this is unknown. In this thesis, YmfM was identified to be SfiC and is up-regulated by the SOS response. The inhibition of cell division during SOS has traditionally been attributed to SulA, which inhibits FtsZ polymerization and is activated by the RecA pathway. However, we have identified the

likely role of *ymfM* in inhibiting division during SOS, suggesting that alternative pathways exist during stress.

Bioinformatics analysis identified the context in which *ymfM* functions; it is conserved to *E. coli* and closely related gram-negative bacteria. Further, it was shown to be likely that *ymfM* functions with two other genes within the e14 prophage, *ymfL* and *oweE*. Finally, the initial characterisation of the mechanism of action of YmfM indicates that it inhibits division at the level of FtsZ ring assembly (early stages of division) and is independent of known cell division inhibitors SulA, MinC and SlmA.

While more work is needed to fully characterise YmfM, this work highlights that there are multiple pathways which may inhibit cell division during stress and raises the question of the beneficial role of prophage encoded inhibitors for bacterial survival. Having a greater understanding of filamentation will not only enable us to understand the intricacies of cell division inhibition, but also how bacteria are able to cope with stress.

Table of Contents

Certificate of Authorship/ Originality I
Acknowledgements II
Abstract IV
Table of Contents VI
List of Figures and Tables XII
Publications and Conference Proceedings XVI
Abbreviations XVIII
Chapter 1. Introduction 1
1.1 Introduction 2
1.2 Overview of bacterial cell division 4
1.2.1 Formation of the Z ring 5
1.2.2 Late division proteins: making of the divisome 10
1.2.3 Spatial and temporal regulators of Z ring assembly 12
1.3 Morphological plasticity and bacterial filamentation 16
1.3.1 Bacterial Filamentation 17
1.4 Filamentation Regulators 23
1.4.1 SulA as part of the SOS response 23
1.4.2 DamX 27
1.4.3 Prophage-encoded inhibitors 27
1.5 The role of prophages in bacterial fitness 32
1.6 Thesis Aims 34
Chapter 2. Methods and Materials 37
2.1 Chemicals, Reagents and Solutions 38
2.2 *Escherichia coli* Strains and Growth Conditions 39
2.3 Plasmids used in this Study 43
2.4 General DNA Methods 45
2.4.1 Extraction and purification of *E. coli* DNA from bacterial cultures 45
2.4.2 Polymerase Chain Reaction (PCR) 46

2.4.3 Determining DNA concentration 49
2.4.4 Agarose Gel Electrophoresis 49
2.4.5 DNA sequencing 50
2.5 Transformation of Plasmid DNA into *E. coli* Strains 51
2.5.1 Preparation of electro-competent *E. coli* cells 51
2.5.2 Electroporation of competent *E. coli* cells 51
2.6 Growth Curves 53
2.6.1 96-well plates 53
2.6.2 50mL flasks 53
2.7 Construction of Deletion Mutants Using Lambda Recombination 55
2.7.1 Amplification of kanamycin cassette for the deletion of *sulA* and *ymfM*: 55
2.7.2 Transformation of kanamycin resistance cassette and selection of successful insertion into *sulA* and *ymfM* 56
2.7.3 Removal of Kanamycin Cassette 56
2.8 Over-Expression of Genes From Inducible Plasmid, pBAD24 58
2.8.1 Cloning of genes into expression plasmid, pBAD24 58
2.8.2 Over-expression of genes from pBAD24 62
2.9 Induction of the SOS Response 63
2.9.1 Induction through the activation of a temperature sensitive RecA-mutant, RecA441 63
2.9.2 Chemical induction of the SOS response using norfloxacin 64
2.10 Microscopy Methods 65
2.10.1 Immunofluorescence microscopy (IFM) 65
2.10.2 Preparation of cells expressing YmfM-GFP for live cell fluorescence microscopy 68
2.10.3 Phase-contrast and Fluorescence Microscopy 68
2.10.4 Image analysis of microscopy images 69
2.11 Coulter Counter Analysis of Cell Length 70
2.11.1 Graphing coulter counter data 70
2.11.2 Statistical analysis of the coulter counter data 70
2.12 Western Blot Analysis 72
2.12.1 Whole cell protein extraction for western blotting 72

2.12.2 SDS-polyacrylamide gel 73
2.12.3 Western Transfer 73
2.12.4 Immunodetection and quantification 73
2.13 Quantitative Real-Time PCT to Determine Gene Expression Levels 75
2.13.1 Primer design and validation 75
2.13.2 RNA extraction 76
2.13.3 Synthesis of complementary DNA (cDNA) 77
2.13.4 qRT-PCR to determine gene expression 77
2.14 Protein Production of YmfM 79
2.14.1 Cloning of *ymfM* into pETMCSIII 79
2.14.2 Transformation of pET-his$_6$-ymfM 81
2.14.3 Small-scale overproduction of YmfM 81
2.14.4 Checking for YmfM overproduction and solubility 81
2.15 Bioinformatics Analysis of *ymfM* 83
2.15.1 Identifying Organisms containing *ymfM* 83
2.15.2 Gene and Genome Sequences 83
2.15.3 Presence Correlation Analysis 84
2.15.3 Conditional Probability 84
2.15.4 Mutual Information 85
2.15.5 Directional Probability 86
2.15.6 Phylogenetic tree of *ymfL* homologs found in *E. coli*. 86
2.15.7 Cross correlation of transcriptional upregulation. 87
Chapter 3. Validation of an *E. coli* over-expression screen 88
3.1 Introduction 89
3.1.2 Chapter Aims and Objectives 95
3.2 Results 96
3.2.1 Confirmation of genes from filamentous clones from shot-gun library responsible for cell division inhibition 96
3.3 Discussion 104
Chapter 4. The biological role of YmfM: a potential role in the SOS response 110
4.1 Introduction 111
4.1.1 The SOS Response 111

4.1.2 Induction of prophages during SOS 113
4.1.3 The e14 prophage of *E. coli* 115
4.1.4 Identification of another SOS-induced cell division inhibitor, SfiC: 116
4.1.5 Chapter Aims and Objectives: 119
4.2 Results 120
4.2.1 Determining the gene responsible for the *sfiC* phenotype 120
4.2.2 YmfM is involved in the inhibition of division during the SOS response genetically induced by RecA: 121
4.2.3 Contribution of *ymfM* to the filamentation seen during norfloxacin-induced SOS 126
4.2.4 Contribution of the entire e14 prophage to norfloxacin-induced filamentation: 133
4.2.5 RecA-independent filamentation mechanism during SOS: 137
4.2.6 Changes in expression of *ymfM* during SOS-inducing conditions 139
4.3 Discussion 146
4.3.1 *ymfM* is the previously identified cell division inhibitor, SfiC: 146
4.3.2 *ymfM* is a cell division inhibitor during RecA-induced SOS: 146
4.3.3 Finding the biological SOS condition in which YmfM is needed to inhibit division: 149
4.3.4 Why does *ymfM* respond differently to genetic and chemical induction of the SOS response? 151
4.3.5 Future directions: 153
4.3.6 Conclusions 154
Chapter 5. A bioinformatics analysis of *ymfM* 156
5.1 Introduction 157
5.1.1 Chapter Aims and Objectives: 160
5.2 Results 162
5.2.1 The conservation of *ymfM* 162
5.2.2 Community profiling of the genes within e14 prophage 169
5.2.3 The co-dependency and directional dependency of genes within the e14 prophage 171
5.2.4 Phylogenetic analysis of *ymfL* 175
5.2.5 Transcriptional cross-correlation of genes from the e14 prophage from published transcriptional databases 177

5.3 Discussion 181
5.3.1 YmfM is conserved within *E. coli* and is not environment specific 181
5.3.2 Transcriptional regulation of functional systems 185
5.3.3 Conclusion 187
Chapter 6. The mechanism of action of YmfM 188
6.1 Introduction 189
6.1.1 Overview of cell division 189
6.1.2 FtsZ structure 190
6.1.3 Identified modes of FtsZ inhibition 190
6.1.4 YmfM, a potential cell division inhibitor 192
6.1.5 Chapter Aims and Objectives: 193
6.2 Results 195
6.2.1 Detecting Z ring formation in cells induced to express *ymfM* 195
6.2.2 Measurement of cellular levels of FtsZ in *ymfM*-expressed cells 200
6.2.3 Inhibition of cell division by YmfM does not rely on known *E. coli* cell division regulators SulA, MinC and SlmA. 203
6.2.4 Cellular localisation of YmfM during filamentation, using GFP 209
6.2.5 Optimisation of the over-expression and purification of YmfM for future *in vitro* studies 215
6.3 Discussion 222
6.3.1 YmfM targets early stages of division and is independent of the known cell division inhibitors, SulA, MinC and SlmA 222
6.3.2 Does YmfM interact directly with FtsZ? 224
6.3.3 Localisation of YmfM using fluorescence microscopy 227
6.3.4 Conclusions 229
Chapter 7. General Discussion 230
7.1 Introduction 231
7.2 Identification of novel cell division inhibitors: 232
7.3 YmfM is an SOS-inducible cell division inhibitor: 235
7.4 The regulatory pathway of *ymfM* 239
7.5 YmfM inhibits division by targeting Z ring formation 241
7.6 The broader context of YmfM and cell division inhibitors 244

7.7 Concluding remarks 245
Appendix 246
Supplementary Data 246
References 251

List of Figures and Tables

Figure 1.1. Overview of the cell cycle in *E. coli*..... 5
Figure 1.2. A simple schematic of the polymerisation of FtsZ into a Z ring..... 7
Figure 1.3. The recruitment hierarchy of cell division proteins to the division site in *E. coli*..... 11
Figure 1.4 Regulation of the positioning of the Z ring by the Min System and Nucleoid Occlusion in *E. coli*..... 14
Figure 1.5.Filamentation of freshwater bacteria, *Flectobacillus* spp. in response to predation threat..... 18
Figure 1.6. Uropathogenic infection cycle during urinary tract infections..... 20
Figure 1.7. Schematic overview of the SOS response in *E. coli*..... 26
Figure 3.1.Cell length distribution of the over-expression of genes *ycjY* and *ykfI* in *DH5a*..... 98
Figure 3.2. Cell length distribution of the over-expression of genes *ymfM* and *ytfB* in *DH5a*..... 100
Figure 3.3. Growth curve comparing the growth of individual ORF and their original clones..... 102
Figure 4.1. A schematic diagram showing the gene arrangement of the e14 prophage..... 114
Figure 4.2. Cell length analysis of the over-expression of *ymfL* in *E. coli*..... 119
Figure 4.3. Cell volume distribution of WT, Δ*ymfM*, Δ*sulA,* and Δ*sulA*Δ*ymfM* after genetic induction of the SOS response by a temperature-sensitive *recA* mutant, *recA441*..... 122
Figure 4.4. Morphological changes of *E. coli* cells exposed to varying concentrations of norfloxacin..... 126
Figure 4.5.Cell volume distribution of WT and mutant *E. coli* treated with Norfloxacin..... 129
Figure 4.6. Cell volume distribution of *e14* mutant treated with Norfloxacin..... 134
Figure 4.7. Cell volume distribution of wild-type and Δ*recA E. coli* K-12 strains treated with norfloxacin..... 137

Figure 4.8.Gene expression profile of *E. coli* treated with 100 ng/mL Norfloxacin..... 139
Figure 4.9. The requirement of minimal media for RecA441 activity..... 142
Figure 4.10. Gene expression profile of *E. coli* during pBAD-*ymfM* expression..... 144
Figure 5.1 The arrangement of the e14 prophage genome within *E. coli*..... 156
Figure 5.2. Nucleotide sequence conservation of all *ymfM* homologs..... 162
Figure 5.3 A phylogenetic tree of *Escherichia coli* strains showing the presence and absence of various components of the e14 prophage..... 165
Figure 5.4 The percentage of genomes of *E. coli* containing genes from the e14 prophage..... 166
Figure 5.5 Conditional probability for the presence of each gene from the e14 prophage given the presence of any other gene..... 168
Figure 5.6 Mutual information for all gene combinations of the e14 prophage.... 171
Figure 5.7 Directional probability for all gene combinations of the e14 prophage..... 172
Figure 5.8 Phylogenetic tree of *ymfL* homologs found in *E. coli*..... 174
Figure 5.9 Cross correlation of changes within gene transcriptional levels within the e14 prophage..... 177
Figure 5.10 Scatterplots of all transcription data for all combinations of *ymfL*, *ymfM* and *ymfN* in the *E. coli* Gene Expression Database..... 178
Figure 6.1.BW25113 pBAD-*ymfM* induced filaments have no Z rings..... 194
Figure 6.2. Optimisation of immunofluorescence microscopy for detecting the formation of Z rings in filamentous *E. coli*..... 196
Figure 6.3. Western blot to determine cellular FtsZ levels in pBAD-*ymfM* expressed cells..... 199
Figure 6.4. Western blot to determine specificity of the antibody to FtsZ..... 200
Figure 6.5. Filamentation caused by the over-expression of pBAD-*ymfM* is independent of the cell division inhibitor, SulA..... 202
Figure 6.6. Filamentation caused by the over-expression of pBAD-*ymfM* is independent of the division regulator, the Min system..... 204
Figure 6.7. Filamentation induced by pBAD-*ymfM* is independent of the nucleoid occlusion protein, SlmA..... 205

Figure 6.8. Cell size distribution comparison of untagged and GFP tagged *ymfM*..... 209
Figure 6.9. Live-cell fluorescent imaging of YmfM-GFP..... 211
Figure 6.10. Examples of abnormal cell shape observed from YmfM-GFP..... 212
Figure 6.11. 15% SDS-PAGE of the initial overproduction of His_6-YmfM from pETMCSIII in expression strain C41-DE3..... 215
Figure 6.12. SDS PAGE analysis of His_6-YmfM expressed from plasmid pETMCSIII in strain C43-DE3..... 217
Figure 6.13. Phase-contrast microscopy of C43-DE3 cells expressing pET-his_6-*ymfM*..... 218
Figure 6.14. SDS-PAGE analysis of possible extracellular YmfM into the media during overproduction..... 219

Table 2.1 Solutions and their working compositions..... 37
Table 2.2 *E. coli* strains used in this study..... 39
Table 2.3 Media used for bacterial growth..... 42
Table 2.4 Antibiotics used for selection in *E. coli*..... 42
Table 2.5 Plasmids constructed and used in this study..... 43
Table 2.6 List of primers used to delete genes *ymfM* and *sulA*..... 54
Table 2.7 List of Primers used to amplify genes of interest to be cloned into pBAD24..... 58
Table 2.8 Primers used for quantitative real-time PCR (qRT-PCR)..... 75
Table 2.9 Primers used to clone *ymfM* into pETMCSIII..... 78
Table 3.1 The genetic loci, clone name and genes present in each clone that caused filamentation from the original screen..... 91
Table 3.2 Mean cell length and fold increase of length, of genes of interest and their original clones under repression (0.2 % glucose) and induction (0.2% arabinose)..... 101
Table 4.1 Average[a] cross correlation[b] analysis of cell volume distribution during pBAD-*rec441* expression..... 123
Table 4.2 Average cross correlation analysis of cell volume distribution during Norfloxacin exposure..... 130
Table 4.3 Average cross correlation analysis of cell volume distribution during Norfloxacin exposure..... 135
Table 4.4 A comparison of log2 fold change of gene expression during norfloxacin exposure..... 140
Table 5.1 The distribution of *ymfM* homologs in organisms based on nucleotide sequence..... 161
Table 6.2 Number of Z rings detected in *ymfM*-induced filament via immunofluorescence microscopy..... 197
Table 6.3 Mean cell volume (μm^3) of *ymfM* expressed from pBAD-*ymfM* in mutant backgrounds, as determined by the coulter counter..... 206

Publications and Conference Proceedings

Publications:

Mediati D, Burke C, **Ansari S**, Harry EJ, Duggin IG (2018) High-throughput sequencing of phenotypically enriched DNA libraries: discovering mediators of reversible bacterial filamentation, Under Review at BMC Genomics

Ansari, S (2016) Bacterial filamentation as a survival strategy. ASM Syntrophy, Volume 17 Issue 4 Page 3

Conferences proceedings:

1. **Ansari S**, Burke C, Duggin IG, Harry EJ (2014) Bacterial filamentation as a survival strategy: identification and characterisation of genes causing filamentation in *Escherichia coli,* **Australian Society for Microbiology Annual Scientific Conference, Melbourne, Poster Session**

2. **Ansari S**, Burke C, Bottomley A, Duggin IG, Harry EJ (2015) Bacterial filamentation as a survival strategy: identification and characterisation of genes causing filamentation in *Escherichia coli,* **BacPath 13: Molecular Analysis of Bacterial Pathogens, Melbourne, Poster Session**

3. **Ansari S**, Burke C, Bottomley A, Duggin IG, Harry EJ (2016) Bacterial filamentation as a survival strategy: identification and characterisation of genes causing filamentation in *Escherichia coli,* **Australian Society for Microbiology Annual Scientific Conference, Perth, Poster Session**

4. **Ansari S**, (2016) Bacterial filamentation as a survival strategy: identification and characterisation of genes causing filamentation in *Escherichia coli,* **East Coast Bacillus Meeting, Sydney, Oral Presentation**

Awards:

BD Award, ASM NSW-ACT Branch Prize for an Oral Presentation (2016)

ASM 3 Minute Thesis Award for an Oral Presentation (2016)

Abbreviations

aa	Amino acid
Ab	Antibody
ADP	Adenosine 5'-diphosphate
AGRF	Australian Research Genome Facility
ATP	Adenosine 5'-triphosphate
B.	Bacillus
BACTH	Bacterial two hybrid system
BP	Band pass
bp	Base pair(s)
BSA	Bovine serum albumin
°C	Degrees Celsius
CFU	Colony forming unit
Da	Dalton(s)
DAPI	4'6-diamidino-2-phenylindole
Δ	Deletion of gene
DNA	Deoxyribonucleic Acid
E.	*Escherichia*
ECL	Enhanced chemi-luminescence
EDTA	Ethylenediaminetetraacteic acid
et al.	and others
fts	Filamentation temperature sensitive
g	Centrifugal force
g	Gram(s)
gDNA	Genomic DNA
GDP	Guanosine diphosphate
GFP	Green fluorescent protein
GTP	Guanosine triphosphate
h	Hour(s)
IFM	Immunofluorescence microscopy

IgG	Immunoglobulin G
IPTG	isopropyl-1-thio-β-D-galactopyranoside
kb	Kilobase(s)
L	Litre(s)
m	Milli- (10^3)
M	Moles per litre
mg	milligram
min	Minute(s)
mL	Millilitre(s)
MQW/MilliQ	Milli-Q purified water
MSA	Mineral salts A
n	Nano- (10^3)
N/A	Not applicable
NEB	New England Biolabs
OD_{600}	Optical Density at 600nm
ORF	Open reading frame
PAGE	Polyacrylamide gel electrophoresis
PBP	Penicillin binding protein
PBS	Phosphate buffered saline
PCR	Polymerase chain reaction
pH	Power of Hydrogen
RNA	Ribonucleic Acid
rpm	Revolutions per minute
S.D	Standard deviation
SDS	Sodium dodecyl sulphate
SDS-PAGE	Sodium dodecyl sulfate-polyacrylamide gel electrophoresis
spp.	Species
TEV	Tobacco Etch Virus
Tris	Tris(hydroxymethyl)methylamine
ts	Temperature sensitive
UV	Ultraviolet
V	Volts(s)
v/v	Volume per volume

w/v	Weight per volume
μ	Micro- (10^6)

Chapter 1. Introduction

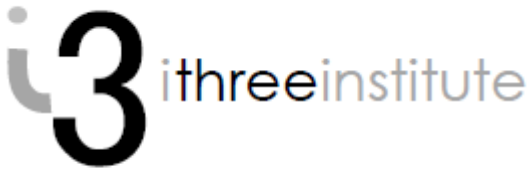

1.1 Introduction

Cell division is an essential process that is required for the survival and propagation of all living organisms. Bacterial cell division occurs via the invagination of the cell envelope to produce a septum between two newly replicated chromosomes [1, 2]. This leads to the eventual splitting of the cell, producing two new daughter cells. Since division is central to the survival of bacteria, this process is almost always tightly spatially and temporally regulated to ensure the production of two genetically identical and viable cells. However, many aspects of the nature of this regulation remain unknown. In particular, the regulation of growth and division under the variety of stresses imposed on bacteria by the environment they inhabit.

Escherichia coli, a Gram-negative, rod-shaped bacterium, is a model organism that has been extensively studied in molecular and cell biology. While much is known about how *E. coli* grows and divides under standard laboratory conditions, which is relatively stress-free and nutrient rich, less is known about how this bacterium regulates cell growth and division under a variety of environmental conditions that it naturally inhabits. One documented response to stress in *E. coli* is filamentation where division is inhibited but cell growth and elongation continue [3]. However, relatively little is known about the regulatory pathways that can lead to filamentation.

Understanding the regulation pathways of cell division (and filamentation) not only broadens the current knowledge of this process but is of scientific importance given the rise of antibiotic resistance. This importance is two-fold. Firstly, bacteria such as *E. coli* are able to respond and adapt to certain antibiotics by filamenting, and this response is

suggested to aid in the development of antibiotic resistance [4] . An understanding of filamentation regulation pathways will subsequently give insight into the development of resistance. Secondly, there is the possibility that novel antibiotics that target the molecular mechanism of action used by cell division inhibitors could be developed to kill bacteria. As cell division is well conserved on a molecular level and proteins involved are largely unique to bacteria, cell division is an attractive novel antibacterial target [2]. This has led in recent years to the development of several novel compounds targeting the essential division protein, FtsZ [5].

This introduction chapter begins by first reviewing the current molecular understanding of the cell division machinery in *E. coli.* Following this, several cases of environmental filamentation are reviewed, such as that seen during pathogenesis and exposure to antibiotics. This is followed by a summary of the known cell division inhibitors that give rise to filamentation and their regulation pathways, including those encoded within prophages. An overview of the beneficial role of prophages in bacteria is then explored. Finally, the overall project aims of this thesis are detailed.

1.2 Overview of bacterial cell division

Cell division in *E. coli* occurs via binary fission, a process involving the formation of a septum at the cell centre (mid-cell) (Figure 1.1) [6]. This process is coordinated with chromosome replication such that septation does not occur before DNA replication and segregation is complete (Figure 1.1). Division occurs in three stages and involves over 20 essential and accessory proteins [7]. The early stage of division begins with the formation of the Z ring at the future division site. The Z ring comprises bundles of FtsZ filaments tethered to the cell membrane by FtsA and ZipA [8]. The formation of the Z ring is spatially and temporally regulated by multiple systems including the Min system and Nucleoid Occlusion (NO), with new systems still being identified [9-12]. These systems function to ensure division occurs at the right time and place to give rise to viable progeny. The second stage of division occurs once a stable Z ring forms and the late division proteins bind to the Z ring to form the divisome. The fully formed divisome performs cytokinesis, the final stage of division, by invaginating the cell envelope, and eventually splitting of the cell to produce two daughter cells [1, 2, 6].

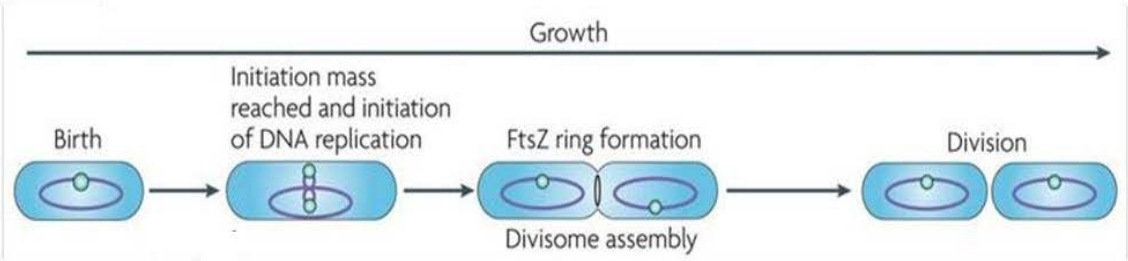

Figure 1.1. Overview of the cell cycle in *E. coli*

The bacterial cell cycle begins with the birth of a new daughter cell. Chromosome (purple oval) replication occurs at a single origin, the *oriC* (green circle). Replication proceeds bi-directionally around the chromosome and terminates at the opposite region of the *oriC*. Chromosomes are maintained in a condensed, yet highly dynamic structure known as the nucleoid. Division is initiated during DNA segregation with the formation of a Z ring and the divisome. Finally, the Z ring constricts, driving septal wall synthesis, and invagination of the cell membranes to give rise to two new daughter cells. Adapted from [13]

1.2.1 Formation of the Z ring

FtsZ

FtsZ is a highly conserved tubulin-like protein in bacteria that forms a ring-like structure (Z ring) at the future division site (typically mid-cell). This ring acts as a scaffold for the assembly of the downstream divisome proteins and directs the synthesis of septal peptidoglycan [14, 15]. While the amino acid sequence of FtsZ shows little similarity to eukaryotic tubulin, their tertiary structures are very similar, suggesting they share common ancestry [16]. Although the structure of *E. coli* FtsZ has not been determined, solved structures from several other species show FtsZ has a conserved fold (Figure 1.2

A) [16-19]. This includes two independent domains, the N-terminal (NTD) and C-terminal (CTD) domains which are connected via a central helix [16]. The NTD contains the GTPase/ nucleotide binding site and the CTD contains the catalytic T7 loop as well as the disordered C-terminal tail, needed for the interaction of FtsZ with several division proteins [20, 21].

Polymerisation of FtsZ

FtsZ monomers assemble in a linear head-to-tail manner to form short polymers known as protofilaments (shown schematically in Figure 1.2 B) [17]. Polymerisation is dependent on FtsZ monomers binding guanosine triphosphate (GTP). Upon binding GTP, the T7 loop of one FtsZ monomer inserts into the GTP binding domain of the next, activating the GTPase activity of FtsZ. The hydrolysis of GTP to GDP triggers the disassembly of the protofilaments, and drives the rapid turnover of polymeric and monomeric FtsZ [22].

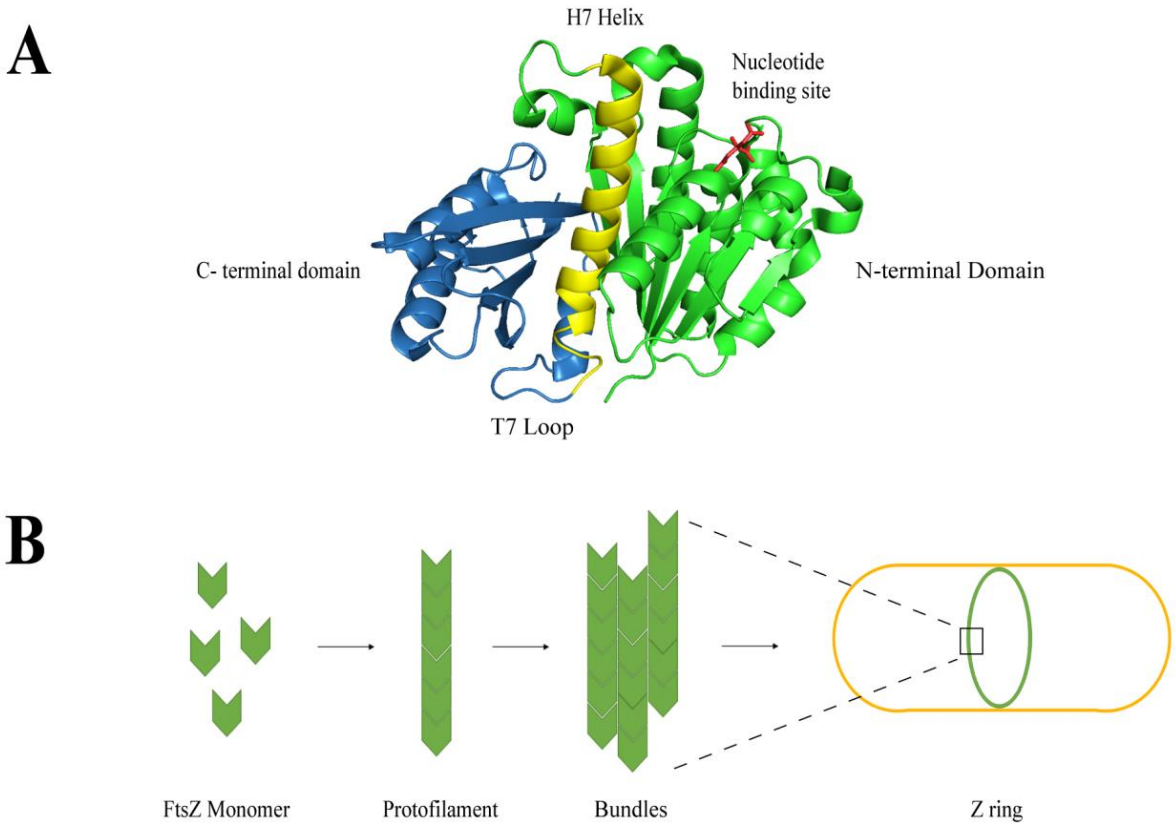

Figure 1.2. A simple schematic of the polymerisation of FtsZ into a Z ring

A) The crystal structure of FtsZ from the rod-shaped bacterium, *Bacillus subtilis* (Protein data bank entry 2VXY). FtsZ contains two independently folding domains, the N-terminal domain (green) and the C-terminal domain (blue), connected via the central core H7 helix (yellow). GTP binds at the nucleotide binding site, which causes the polymerisation of FtsZ monomers in a linear head to tail manner, with the T7 loop of one monomer inserting into the nucleotide binding site of the next. Citric acid (red) is shown bound at the nucleotide binding site in the crystal structure. B) A simplified schematic overview of FtsZ monomers polymerising into protofilaments and laterally associating with each other, eventually leading to the formation of the Z ring at the site of division (mid-cell).

Tethering and stabilisation of the Z ring

FtsZ is a cytoplasmic protein and so binding of FtsZ protofilaments to the inner membrane is mediated by membrane associated proteins [23]. In *E. coli* this is accomplished by essential proteins FtsA and ZipA, which bind to the C-terminal core peptide of FtsZ [24].

FtsA is the second most conserved division protein in bacteria after FtsZ [1]. It is part of the actin family with structural homology to three of the four sub-domains of actin [25]. FtsA is an ATPase, although the exact role of ATP hydrolysis is currently unclear [23]. FtsA binds the membrane via its C-terminal amphiphatic helix and its ability to bind the membrane is important for tethering the Z ring [26]. *In vitro* reconstitution of FtsZ-FtsA showed that FtsA is able to form actin-like protofilaments [27]. It is thought that FtsA polymerisation is important for Z ring integrity and aids in its curvature. This is consistent with *in vitro* reconstitution of FtsZ-FtsA systems on supported lipid bi-layers where spirals and rings were observed [28].

A similar membrane mediation role is also fulfilled by ZipA in *E. coli* [29]. FtsA and ZipA both rely on FtsZ for their recruitment, being unable to localise at the site of division in cells that are unable to form Z rings [2, 30]. These are essential division proteins, since deletion of one leads to non-functional Z rings and deletion of both prevents Z ring formation [8, 31]. This is thought to be due to a role for ZipA in stabilising FtsZ monomers, while FtsA stabilises polymerised FtsZ [32]. An imbalance in the FtsA to FtsZ ratio can lead to inhibition of cell division, with overproduction of FtsA resulting in filamentous cells [33, 34].

FtsA and ZipA not only tether the Z ring to the membrane but are also needed for the localisation of downstream division proteins, including FtsN [35], However some mutants of FtsA can bypass the need for ZipA [36]. ZipA is thought to promote higher order FtsZ structures such as protofilament bundling which allow for the localisation of the late division proteins [32].

Z ring dynamics

FtsZ bound to the membrane by FtsA is able to deform the membrane *in vitro* in a GTP dependent manner [37, 38], suggesting that the Z ring provides at least part of the contractile force needed to pull the inner membrane during constriction [37, 39]. Recent advances in super resolution microscopy have revealed the Z ring to in fact be a discontinuous and heterogeneous distribution of FtsZ protofilaments throughout the ring [40, 41]. However the presence of the Z ring alone is not enough to provide constriction *in vivo* [42], indicating that later components of the divisome are also needed.

It is now thought that Z ring dynamic treadmilling, and cell wall remodelling work together to facilitate constriction [15]. Treadmilling occurs when monomers preferentially bind to one end of a filament and dissociate from the other, causing the filament to move in the direction of preferential binding [15]. FtsZ protofilaments were first observed to treadmill on a lipid bilayer *in vitro* [28] and more recently this has been observed *in vivo* in both *B. subtilis* and *E. coli* [43, 44]. These recent studies were a real breakthrough in this field, showing that treadmilling was dependent on GTPase activity and how this dynamic movement guided septal wall synthesis.

1.2.2 Late division proteins: making of the divisome

Following Z ring assembly, the late division proteins are recruited in a sequential manner and are required for peptidoglycan synthesis and constriction of the cell (Figure 1.3)[2]. These are FtsE, FtsX, FtsK, FtsQ, FtsL, FtsB, FtsW, FtsI (PBP3), and FtsN. FtsA and ZipA are needed for the recruitment of the downstream division protein, FtsK [8]. FtsK belongs to a family of proteins involved in chromosome segregation and is thought to coordinate this process with septation [45]. FtsQ, FtsB and FtsL are membrane proteins that form a complex prior to septal ring localisation, and have a possible role in the synthesis of the septal peptidoglycan [2, 46]. FtsW recruits the penicillin binding protein, FtsI (PBP3) which is involved in synthesising the septal peptidoglycan [1]. Finally, FtsN, a protein which contains a murein (peptidoglycan) binding domain, stimulates peptidoglycan synthesis and constriction [6, 47].

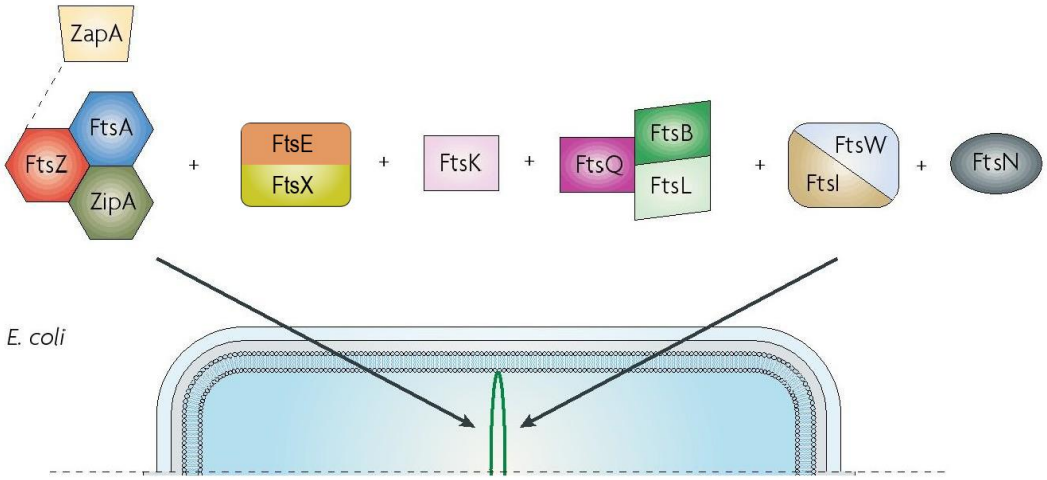

Figure 1.3. The recruitment hierarchy of cell division proteins to the division site in *E. coli*.

Divisome proteins in *E. coli* are recruited in an almost linear and sequential manner. FtsZ is first to localise to midcell, where it polymerises into a ring. This is followed by the arrival of FtsA and ZipA, which tether Z ring to the cell membrane and are needed for the recruitment of the late division proteins. The late division proteins include, the FtsE, FtsX, FtsK, FtsQ, FtsL FtsB, FtsW, FtsI and FtsN. Proteins FtsQLB form a complex prior to midcell localisation. FtsW recruits the PBP, FtsI. FtsN is the last divisome protein to arrive and activates septal peptidoglycan synthesis. Modified from [2]

1.2.3 Spatial and temporal regulators of Z ring assembly

Positioning of the division apparatus to mid-cell has to be spatially and temporally regulated in order to give rise to viable progeny. Known regulators include inhibitors of Z ring assembly and inhibitors of Z ring formation at inappropriate sites such as over chromosomes or at the DNA-free poles. The Min system and nucleoid (chromosomal mass) occlusion (NO) are two examples of such negative regulators of FtsZ assembly in *E. coli*, providing spatial and temporal control to ensure correct positioning of the Z ring at mid-cell (Figure 1.4) [6, 48].However alternative spatial regulators also exist [9, 10] .

Nucleoid occlusion prevents the formation of the Z ring over the region of the cell occupied by the unsegregated nucleoid (Figure 1.4). This ensures that cytokinesis does not occur over DNA, which would result in daughter cells with incomplete genetic information that would therefore be non-viable. Thus, during the cell cycle, NO helps ensure that chromosomes have completed replication and have separated before cell division can occur between them [6, 49]. NO is mediated via SlmA in *E. coli* which inhibits FtsZ polymerisation in the vicinity of chromosomes [50]. The antagonistic activity of SlmA occurs when it is bound to specific SlmA-binding sites (SBS) on the chromosome [11, 51]. Two mechanisms of action have been proposed: Cho *et al.* [11] suggest that SlmA disassembles FtsZ polymers and requires the GTPase activity of FtsZ, whereas Tonthat *et al.* [52, 53] propose that the action of SlmA does not prevent assembly of FtsZ protofilaments, but instead acts by preventing these polymers from forming the Z ring. Although the exact mechanism of SlmA action remains unclear, it is apparent that SlmA is part of the NO system that regulates FtsZ polymerisation in space, effectively

preventing premature septation over chromosomes that have not completely replicated or segregated [49].

Systems which couple the divisome location to the nucleoid play an important role in coordinating division; however, they require an additional mechanism (the correct positioning of the nucleoid) to localise the divisome to the centre of the cell [9]. To date, one independent localization mechanism that positions the division ring formation without the need for additional underlying systems has been identified: the Min system [54] (Figure 1.4). The Min system comprises of proteins MinC, MinD and MinE. These proteins work together to prevent Z ring formation at the cell poles by locally inhibiting Z ring formation [55-59]. To achieve this, the distribution of the Min proteins forms an oscillatory spatiotemporal pattern which oscillates from pole to pole of the cell [60]. On a molecular level, MinD binds to the cell membrane in an ATP dependent manner before dimerising [61, 62]. MinE is able to bind to the membrane and interacts with MinD to accelerate the hydrolysis of ATP to ADP resulting in the release of MinD dimer from the membrane [63, 64]. The non-linear MinD dimerization and MinDE interactions are sufficient to cause the oscillatory pattern which gives rise to an average minimum concentration of Min proteins at mid-cell, allowing for Z ring to form [65, 66]. MinC is able to bind to the oscillating MinD which co-localises it to the cell poles [67-70]. MinC is the inhibitor of FtsZ polymerisation as its N-terminal domain directly interacts with FtsZ [71, 72]. The Min system is non-essential in *E. coli* as deletion of these proteins, still results in Z ring formation and division [73]. However, in its absence division can occur at the cell poles, leading to the production of chromosome-less mini-cells [6, 55]. The deletion of the Min system also causes a decrease mid-cell localisation precision of Z rings [74].

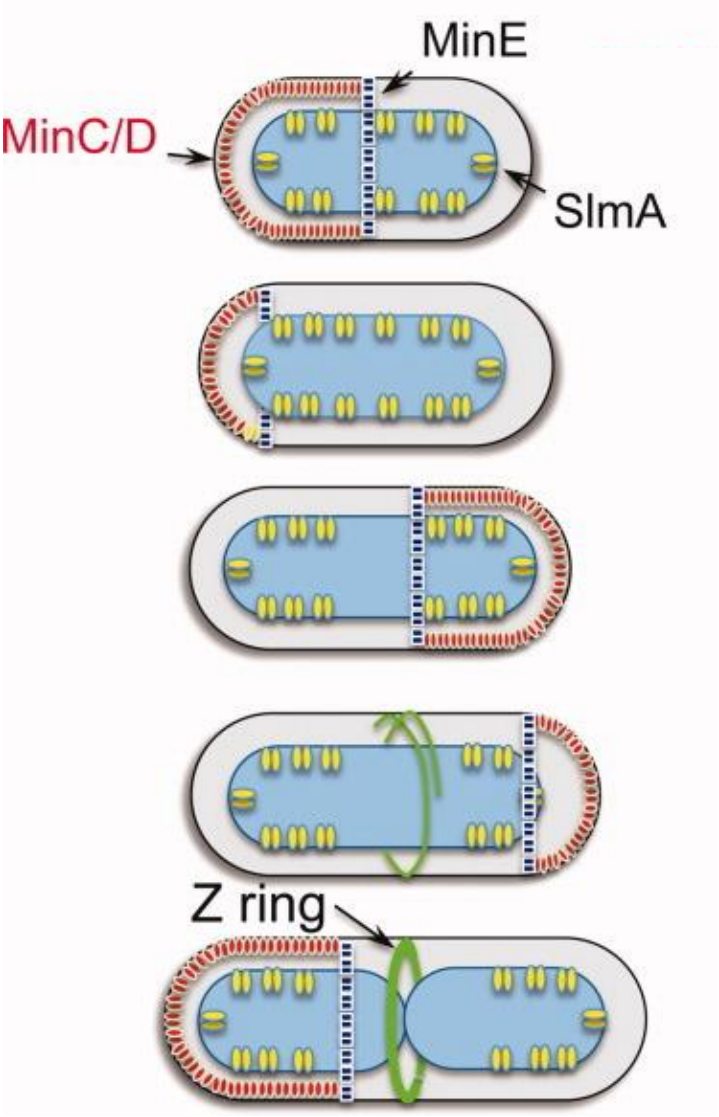

Figure 1.4. Regulation of the positioning of the Z ring by the Min system and Nucleoid Occlusion in *E. coli*

The Min and Nucleoid Occlusion system provide spatial and temporal regulation of the Z ring in *E. coli*. SlmA, the NO protein (yellow) prevents the formation of the Z ring and consequently division over the nucleoid (chromosomal mass). This ensures that cytokinesis does not occur over DNA (blue oval), which would give rise to two non-viable daughter cells. The Min system (red and blue), acts by antagonizing the ability of FtsZ (green) to form a ring at cell poles and thus prevents the production of mini-cells lacking chromosomes. This is achieved by MinC binding to membrane bound MinD. The oscillatory behaviour is mediated by the non-linear interactions between MinD and MinE. Thus an overall effect of maximum inhibition of Z ring formation at cell poles, and minimum inhibition at the cell centre, is achieved, as shown in this diagram. Adapted from [75].

Although the Min and NO systems play an important role in influencing Z ring positioning, these systems in *E. coli* are non-essential for Z ring positioning. In double mutant strains (both SlmA and Min proteins deleted), over-expression of FtsZ partially rescues some mini-cell formation with an increased frequency of Z rings forming at mid-cell [50]. This has also been seen in *Bacillus subtilis*, where even in the absence of the Min and NO systems, Z rings were able to form accurately at mid-cell (although at a reduced frequency) [76]. Furthermore, several other bacterial species do not have either system, suggesting that other regulators must be in place to ensure the correct positioning of the Z ring [1].

The Min and NO mechanisms for regulation and control of positioning of the Z-ring have been described in bacterial cells that are under standard laboratory conditions (nutrient rich and fairly stress-free), and may not represent how *E. coli* regulates growth and division under a variety of conditions in the environments that it naturally inhabits. SulA is an example of a negative regulator of division that is induced as part of the SOS response, during stressful conditions (discussed below). Although such regulators of cell division are known, there is still a significant gap in our knowledge about other regulatory systems that may play a role in response to other environmental stressors. For example, there are situations in which bacteria can benefit from delaying cell division under certain environmental stressors, as will be discussed below.

1.3 Morphological plasticity and bacterial filamentation

Bacteria exist in a variety of different environments where they must deal with often changing conditions, to survive and prevail. Bacteria must therefore coordinate cell metabolism, growth, and division to deal with environmental changes such as osmotic stress, predation, competition from other organisms and exposure to antimicrobials [77]. These stressors provide selective pressure on bacteria to adapt to minimize the impact of the stress, with bacteria that successfully adapt developing an enhanced chance of survival [78]. Typical adaptations include biofilm formation, production of toxins and enzymes, change in cell surface structure and increased motility [79-81]. One particular way bacteria cope with environmental insults is to alter their cell shape.

Bacterial cells come in all shapes and sizes ranging from rods, cocci, spirals and long cells. These variations in cell shape provide bacteria with certain advantages that enable them to survive their surrounding environment [82]. For example, being a small spherical cell in the presence of a predatory protozoan means that the cell may elude capture [78]. However, during growth on surfaces subjected to liquid forces, being rod-shaped would be more advantageous than being round, as there is an increase in surface area attachment, thus reducing the chances of being eliminated by the forces of liquid flow [78, 83]. Bacteria that are spiral shaped are able to move through viscous liquids more efficiently than rod cells [84]. This may explain how *Campylobacter jejuni* and *Helicobacter pylori* (spiral-shaped bacterium) are able to move through the gastrointestinal mucus of the host [85, 86].

1.3.1 Bacterial Filamentation

From these morphological variations it is evident that cell shape provides survival advantages in certain conditions. Therefore morphological plasticity, or changing cell shape, is one way that bacteria are able to deal with changing environmental pressures. One specific morphological response is filamentation. Bacterial filamentation is the process in which cell growth and DNA replication continues in the absence of cell division, resulting in the formation of elongated cells [3, 82]. This alternative morphology is advantageous during times of low nutrient availability, and aids in attachment, motility and differentiation during pathogenesis [3, 78, 87].

Protection against predation and phagocytosis

Filamentation is well documented in the aquatic environment, where some species of freshwater bacteria display morphological plasticity when under predation stress (Figure 1.5.). Protozoa are the major consumers of bacteria and graze on them by either beating their flagella to draw the prey inwards or by filtering water to trap bacteria in a sieving apparatus [88]. Both these methods are effective in a size dependent manner, such that protists are more efficient in capturing bacterial cells within a certain size range [78, 79]. By reducing or increasing their size, bacterial cells can evade capture, thus giving them a better chance of survival [78]. Studies looking at the mechanisms of bacterial adaptation to predation in the freshwater bacteria, *Flectobacillus* spp., found that up to 90% of the bacterial population became filamentous in the presence of protozoa [89]. Interestingly, when bacteria were physically separated from the protists by a membrane barrier, and were therefore not under direct threat of being ingested, they still became filamentous [90]. This suggests that chemical stimuli which diffuse through the membrane barrier are

released by the predator and are recognised by bacteria, alerting them of the threat near-by and triggering filamentation [90]. When the predation threat was removed, these cells reverted back to rod-shaped cells. This example provides insight into how changing cell shape, in particular becoming filamentous, is a survival strategy employed by bacteria during stressful situations and ensures the continuation of the bacterial population.

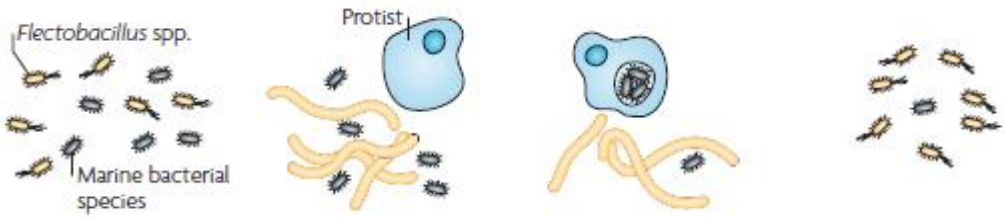

Figure 1.5.Filamentation of freshwater bacteria, *Flectobacillus* spp. in response to predation threat.

In the presence of predation, *Flectobacillus* spp. cells differentiate into filamentous cells, thus preventing their capture by protists. Once the predation threat is removed, bacterial cells revert back to their bacillary form. Adapted from [3].

Similar behaviour has also been observed in bacteria of clinical significance, with filamentation playing a vital role in causing antibiotic resistance, and ensuring survival and ongoing pathogenesis (infection) during many established human diseases. Filamentation of *Haemophilus influenzae* has been observed during otitis media (middle-ear infection) [91], and it has been suggested that this form provides protection from phagocytes of the innate immune system [3]. Macrophages and other phagocytic cells form part of the immune response and are similar to protozoa in the way in that they capture, internalise and kill bacterial cells. Similar to protists, macrophages recognise and

internalise bacteria in a size dependent manner, and are less efficient at capturing and ingesting filamentous cells [92, 93].

Resistance to phagocytosis is also well documented in uropathogenic *E. coli* (UPEC) during urinary tract infections (UTI) [94, 95] and is associated with increased virulence and continuing infection [94-96]. UPEC are responsible for nearly 90 % of all UTIs, and their ability to become filamentous is part of its ongoing pathogenesis (Figure 1.6), with filaments reaching up to 50 times longer than their bacillary counterparts [3, 97]. UPEC are able to cause infection by colonising bladder epithelial cells where they form biofilm-like intracellular bacterial communities [83, 98]. It is during this intracellular growth that a subpopulation of the bacteria differentiates into filaments [99, 100]. This change in morphology provides several advantages during infection and aids in proliferation of the bacteria to continue infection. Similar to what is seen in freshwater bacteria [90], filamentation protects these cells from being engulfed and, therefore, eliminated by the innate immune response. During infection, there is an increased influx of neutrophils and macrophages at the site of infection; however these phagocytic cells are unable to effectively clear filamentous cells, and preferentially engulf bacillary cells [94, 98, 101, 102]. When filamentation is inhibited, UPEC are less effective in causing infection, thus further highlighting the importance of filamentation during pathogenesis [96].

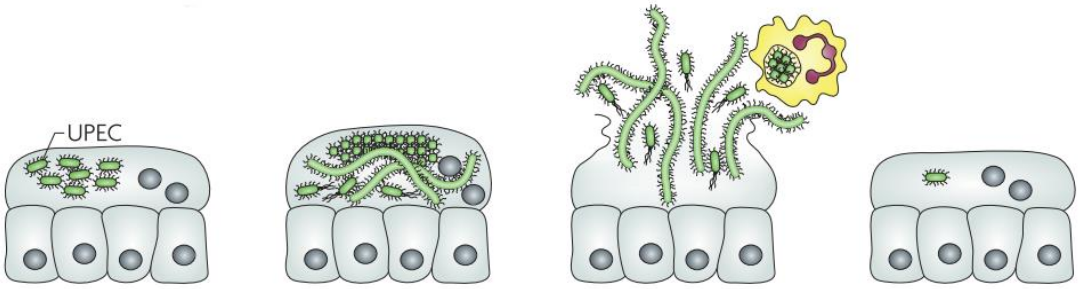

Figure 1.6.Uropathogenic infection cycle during urinary tract infections.

UPEC are able to colonize bladder epithelial cells forming intracellular bacterial communities. During intracellular growth, a subpopulation of bacterial cells becomes filamentous. These filamentous cells are able to evade phagocytosis by innate immune cells (e.g. neutrophils) and re-infect surrounding epithelial cells to continue infection. Adapted from [3]

Filamentation has also been linked to survival post-ingestion by macrophages. Although the exact mechanisms remain unknown, filamentation has been observed in *Mycobacterium tuberculosis* (the causative agent of tuberculosis) and *Salmonella spp.* within macrophages, which is speculated to contribute to survival within the macrophage [103, 104].

Nutrient availability

Bacteria need to overcome changes in nutrient availability and filamentation in response to such stress has been observed. Wrainwright *et al.*[105], found that *E. coli* became filamentous during growth on surfaces with low nutrient availability. These observations suggest that by becoming filamentous, bacteria can increase their surface area without

significantly increasing cell volume, thus allowing the cell to expand out and access areas that may be more nutrient rich[105]. This has implications for how *E. coli* may survive on surfaces such as hospitals and non-sterile equipment [105]. Filamentous *E. coli* cells retain their motility, so not only are they able to attach to surfaces due to an increased surface-area but also move using flagella movements like their bacillary counterparts to move toward or away from nutrients and threats, respectively [106].

Increased surface area caused by filamentation is not only advantageous for nutrient acquisition but also for increased surface attachment [82] During UTIs, UPEC encounter liquid forces when they are growing on the surface of bladder epithelial cells. Type 1 pili are expressed along the lengths of the cell membrane and this allows maximum contact and attachment with the surface of bladder [83].

Antibiotic exposure

Exposure to certain antibiotics such as β-lactams which target penicillin binding proteins, and DNA damaging antibiotics such as mitomycin C and fluoroquinolones are known to cause filamentation in bacteria [107-109] . When exposed to sub-inhibitory concentrations of ceftaxamide (β-lactam), *Burkholderia pseudomallei* (which causes melioidosis) becomes filamentous. Once the antibiotic is removed, these filamentous cells are able to re-divide [110]. When re-exposed to a higher dosage of antibiotic treatment, these cells are more resistant. This means that filamentation is a transition state which drives tolerance and resistance to antibiotics. The development of antibiotic resistance through filamentation has been reported in *E. coli*, where it is thought to be mediated through the activation of the bacterial stress response (discussed below) and increase in mutation rates. *E. coli* cells under sub-inhibitory concentrations of ciprofloxacin

(fluoroquinolone) are not only able to become filamentous but undergo asymmetrical division, where short cells bud off at the end of the filament [4]. These short cells became resistant to the same concentration of ciprofloxacin. Bos et al. [4], proposed that filamentation is the first stage of the emergence of resistance as it allows an opportunity for the cell to generate and select for advantageous chromosomal mutations within the multinucleated filaments. While more work is needed to fully understand the molecular mechanism giving rise to resistance during filamentation, this has serious implications on the effectiveness of antibiotic treatment and the development of resistance.

1.4 Filamentation Regulators

It is clear that filamentation is a reversible state for bacteria, which not only provides a survival advantage to overcome environmental challenges, but also aids in prolonging infection [96]. The ability of bacteria to efficiently become filamentous and then revert back to rod-shaped cells, depending on their environmental interactions, means that this process is likely highly regulated. However, knowledge of these regulators and their molecular mechanisms are limited. There is clearly an inherent gap in our knowledge which requires further examination to identify the factors involved. This section will review all known regulators which inhibit division leading to filamentation.

1.4.1 SulA as part of the SOS response

Bacteria respond to DNA damage through the activation of the SOS response, which controls the repair of DNA lesions. Typical SOS inducing conditions include oxidative stress, antibiotics or UV exposure [111]. All of these conditions activate the SOS response by generating single-stranded DNA (ssDNA) breaks. The activation of the SOS response is coordinated by two regulatory proteins, RecA and LexA (Figure 1.7) [112, 113]. LexA represses over 40 genes in *E. coli* under normal growth conditions [114]. Following DNA damage, RecA binds to ssDNA breaks forming a RecA-DNA filament, which facilitates the self-cleavage of LexA and the up-regulation of LexA controlled genes [115].

A key part of the SOS response is the inhibition of division, which allows sufficient time for DNA repair to occur before committing to producing the next round of offspring, minimising the transmission of defective DNA [116]. This is facilitated by the cell

division inhibitor, SulA, which is under the regulatory control of LexA. SulA is perhaps one of the most studied filamentation regulators and molecular studies show that it directly interacts with FtsZ [30, 55, 117]. SulA acts by sequestering FtsZ monomer away from the pool available for Z ring assembly and increasing the critical concentration needed for polymerization [118, 119]. SulA affects polymerization of FtsZ by inhibiting its GTPase activity [120, 121] and this is consistent with the fact that FtsZ mutants which are impaired in GTPase activity are resistant to the inhibitory effects of SulA [122]. The crystal structure of SulA in complex with FtsZ from *Pseudomonas aeruginosa*, shows that SulA is a dimer which does in fact bind the T7 loop of FtsZ [117]. The T7 loop is needed to insert into the GTP binding pocket of the next FtsZ monomer, driving polymerization of FtsZ. When DNA damage is repaired, SulA is degraded via the cytoplasmic protease, Lon, and FtsZ polymerisation and cell division resumes [96, 123].

SulA has been implicated in the filamentation response of UPEC during bladder infection. Justice *et al.*[96], investigated the role of SulA inhibition of cell division of UPEC in a mouse model. Results showed that unlike the wild-type strain, a Δ*sulA* UPEC strain was unable to become filamentous in mouse bladders [96]. It was concluded that SulA is required for filamentation during bladder infection. Furthermore it has been suggested that the overall SOS response is needed for bacteria to evade the host's immune response. When *lexA* and *recA*, were inactivated by a point mutation in UPEC strain, UTI-89, there was an attenuation of infection and bacterial burden within the mouse bladders [124]. These strains persisted in infection in immune-compromised (TLR4-deficient) mice, to a similar degree as wild-type UTI-89 [124]. These two studies put forward the notion that SulA, as part of the SOS response, is activated in response to host mediated defence mechanisms, resulting in filamentous bacterial cells.

Interestingly, an *in vitro* human bladder infection model has suggested that a SulA-independent mechanism is also responsible for the filamentation observed during UTIs [125]. This *in vitro* model used a flow chamber culture and infection system, including a urine flow to reflect the hydrodynamic environment within the bladder. This recapitulated the infection process of invasion, escape and secondary infection. The study found that the degree of filamentation increased with increased concentration of urine. More recently, the cell division inhibitor, DamX (detailed below), has been implicated as this SulA-independent filamentation response during *in vitro* and *in vivo* bladder infection by UPEC [126].

The current understanding of the filamentation response of UPEC during UTI's is that the SOS response causes filamentation in response to host immune cells and DamX causes filamentation in response to the shift from intracellular growth to being exposed to highly concentrated urine on the surface of the bladder cell. This highlights the fact that several regulators exist, and can even function to cause filamentation within the same environment.

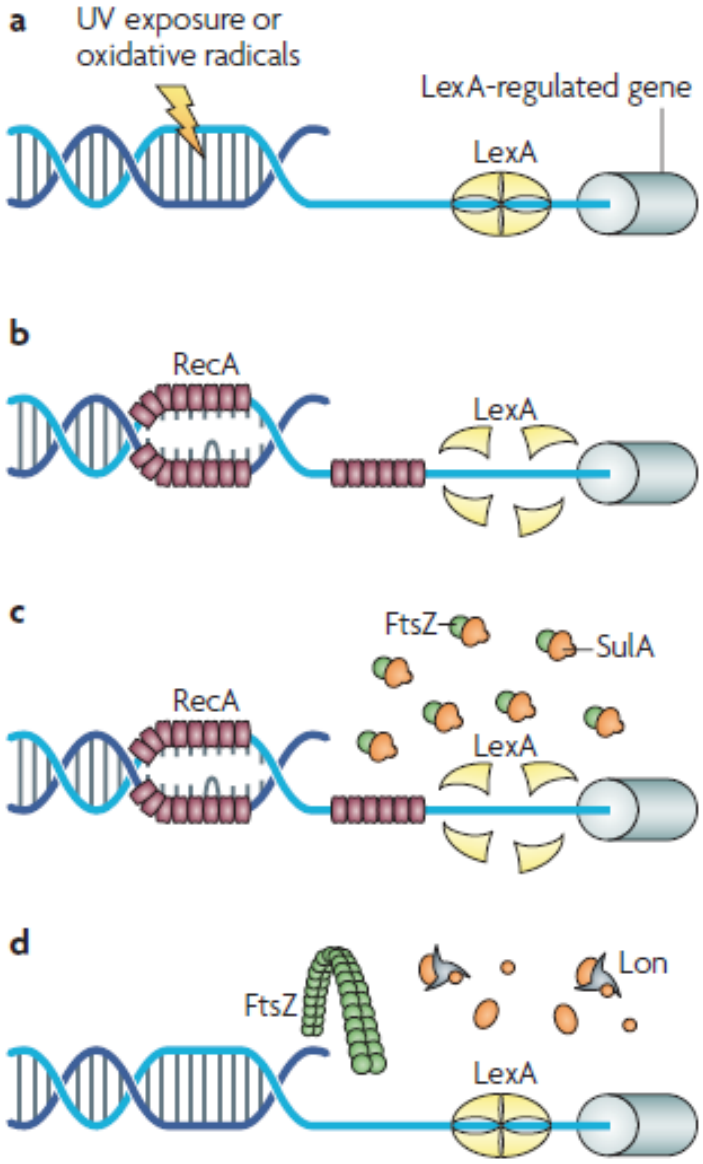

Figure 1.7. Schematic overview of the SOS response in *E. coli*

The SOS response allows microorganisms' time to repair DNA damage before committing to cell division. This response is initiated after a DNA-damaging event such as exposure to UV, exposure to antibiotics or oxidative stress, which causes single-stranded DNA (ssDNA) breaks (a). RecA binds to these ssDNA breaks and polymerises to form activated RecA. This stimulates the autoproteolysis of the transcriptional repressor LexA and the up-regulation of the SOS response genes (b). SulA is activated during this response and directly interacts with and prevents the polymerisation of FtsZ into a Z ring (c). Once the DNA damage is repaired, LexA repression of the SOS regulon is reinstated. SulA is degraded by the protease Lon, allowing Z ring polymerisation and cell division. Adapted from [3]

1.4.2 DamX

DamX, causes filamentation when over-expressed, with evenly spaced nucleoids along the length of the cell, suggesting some involvement in cell division [127]. DamX contains a SPOR (sporulation related repeat) domain, which is a small peptidoglycan binding domain [128]. Many of the SPOR domain-containing proteins are involved in cell division, as this domain is sufficient for the localisation to and binding of the septal peptidoglycan [128, 129]. In *E. coli*, four proteins have been identified so far to contain a SPOR domain, and include FtsN, DamX, DedD and RplA [47]. All four proteins are involved in cell division [47]. FtsN is better characterised of the four and is important in stimulating septal peptidoglycan synthesis and constriction. DamX localises to the site of division [47, 129]. Bacterial two-hybrid experiments revealed that DamX interacts strongly with itself, FtsQ and FtsN, and weakly with FtsZ, FtsA and FtsI [129]. More work is needed to show definitively how DamX interacts with the divisome components, its role in cell division and why its over-expression results in filamentation. Since DamX has recently been implicated in the filamentation of UPEC during bladder infections (discussed above), understanding the molecular mechanisms of DamX may give insight into how UPEC are able to transit between rod and filamentous phenotypes [126]. Mutants of *damX*, result in increased sensitivity to bile salts [130, 131], the main component of bile in the human digestive tract, suggesting a role in allowing *E. coli* and *Salmonella spp.*, another enteric organism, to survive such environments.

1.4.3 Prophage-encoded inhibitors

Temporal cell division inhibitors are also encoded within prophages, which are viral (phage) DNA incorporated within the host (bacterial) chromosome. Phages can undergo two lifecycles while infecting their bacterial hosts, the lytic or lysogenic cycle. During the lytic stage, these elements use their host cellular machinery to replicate and produce phage particles, eventually leading to the lysis of the host cell [132]. During the lysogenic cycle phage DNA is incorporated and maintained as part of the host chromosome (now referred to as prophage) [132].Phage encoded inhibitors are thought to be used by the phage to control the cell cycle during lytic growth. In *E. coli*, several inhibitors have been identified and include, CbtA (YeeV) from prophage CP4-44, Kil from bacteriophage λ and Rac, DicB and DicF from prophage Qin, CbtA from prophage CP4-44 and SfiC from prophage e14 [133-137].

Toxin-Antitoxin Systems

At least 33 toxin and antitoxin pairs have been identified in *E. coli,* some of which are encoded within prophages and play diverse roles by affecting a number of cellular processes, including inhibiting cell division [138]. During normal cell growth, toxin and its complementary antitoxin form a stable complex, preventing the activity of the toxin. However, under adverse conditions, stress-induced proteases degrade the antitoxin, activating the toxin. Toxin proteins have been shown to increase the virulence of *E. coli*, creating persister cells and influencing biofilm formation [139]. Persister cells are those that are able to withstand antibiotic treatment by going into a dormant state, even though they are genetically susceptible to the drug [138]. Toxins also provide endurance under oxidative stress, and limited nutrient environments, supporting the idea that these systems play an important role in adapting to adverse environments [140].

CbtA (YeeV), as part of the CbtA/CbeA toxin/antitoxin system is an example of a cell division inhibitor that interacts with FtsZ, preventing its polymerisation [137, 141, 142]. Furthermore, it also inhibits the polymerisation of MreB, another cytoskeleton protein that interacts with FtsZ in *E. coli* and is required for maintaining cell shape [137, 142, 143]. Inhibition of both proteins leads initially to filamentation of the cell, followed by the formation of lemon-shaped cells [137, 142]. Through a bacterial two-hybrid system, CbtA has been shown to interact with the H6/H7 loop of FtsZ [142]. The H6/H7 region is within the N-terminal domain of FtsZ, and this is the first example of an inhibitor targeting this region. Previously identified inhibitors such as MinC and SlmA are known to bind the C-terminal region of FtsZ and SulA binds the T7 loop [117, 119, 144-146]. Given that toxins are able to interact with division and cell shape components, it is of interest to see if these inhibitory effects convey a beneficial role to *E. coli* under particular environmental conditions, if at all.

Kil

Kil of bacteriophage λ, inhibits cell division when expressed leading to filamentation and eventual cell death [133]. *In vitro* experimentation shows that mutations within FtsZ that are resistant to the effects of Kil are found within the T7-loop and GTP-binding domain. [147]. These FtsZ mutants are also resistant to the inhibitory effects of SulA suggesting the Kil may be functioning to inhibit division in a similar manner to SulA. Furthermore, the characterisation of this inhibitor shows that it disrupts FtsZ protofilament bundling and reduces the GTPase activity of FtsZ *in vitro*, suggesting that it works by a sequestration method similar to SulA [148].

DicB/DicF

DicB and DicF are both encoded within the same operon from prophage Qin. Expression of DicB inhibits division leading to filamentation [149, 150]. This is achieved by DicB indirectly targeting FtsZ through the inhibitory actions of MinC [151]. DicB competes with MinD and binds to the C-terminal domain of MinC forming a DicB/MinC complex [67, 134]. Formation of the DicB/MinC complex activates inhibitory action of MinC, however unlike MinD/MinC, the DicB complex is not spatially regulated by MinE [134]. Instead it requires ZipA to recruit its inhibitory actions to the division ring [152]. While both systems utilise MinC to inhibit division, their mechanisms reflect the difference between spatial and temporal regulators.

DicF, on the other hand encodes for a small RNA (sRNA), which causes the antisense inhibition of *ftsZ* mRNA, preventing FtsZ translation [135]. As well as targeting *ftsZ*, through computational and experimental approaches, *dicF* has been shown to target *xylR* and *pykA*, genes responsible for xylose uptake and synthesis of pyruvate kinase, respectively [135]. *dicF* and *dicB* are up-regulated during exposure to certain fluoroquinolone and β-lactam antibiotics, with DicB implicated in aiding survival of *E. coli* during treatment with β-lactam antibiotics [153].

SfiC

Finally, SfiC which is encoded on the e14 prophage is thought to be activated during genetic activation of the SOS response. This is because, when the SOS response was induced using a temperature sensitive RecA mutant (*recA441*), it contributed to the filamentation response, and is thought be an alternative inhibitor to SulA [136]. Initial characterisation of this inhibitor revealed that FtsZ is most likely the target, as point mutations in *ftsZ* that confer resistance to the inhibitory effects of SulA, also conferred resistance to SfiC [136, 154]. The gene responsible for the SfiC phenotype has not been identified yet, although based on prophage arrangement, it is likely encoded by genes *ymfL* or *ymfM* of the e14 prophage [155], and is explored further as part of this thesis.

1.5 The role of prophages in bacterial fitness

While phages are often thought to be parasitic upon bacteria, when integrated into the chromosome their relationship can become symbiotic, with prophages playing a very important role in survivability, adaptation and virulence of their bacterial host [156]. Prophages can encode for virulence factors which aid in the pathogenicity of their host. This includes the extracellular toxins of botulism (*Clostridium botulinium*), diphtheria (*Corynebacterium diptheriae*), cholera (*Vibrio cholerae*) and shiga toxin (*E. coli* O157:H7) [157].

As well as virulence factors, prophages are able to mediate horizontal gene transfer between bacteria via transduction [158]. It is thought that when packaging their own DNA, phages can mis-package host DNA into their capsids, allowing the transfer of beneficial traits such as antibiotic resistance [158]. Using real-time PCR (qPCR), Colomer-Lluch*et al.*[159], showed that phage DNA isolated from urban sewage and river water samples contained genes encoding β-lactamases (enzyme causing resistance to β-lactam antibiotics), showing that phage have the capacity to harbour antibiotic resistance traits. Furthermore, phages isolated from retail chicken samples were able to successfully transduce resistance genes encoding kanamycin, tetracycline, chloramphenicol and ampicillin into the previously susceptible lab strain of *E. coli* [160].

Phages not only contribute to the biology of pathogenic bacteria but are also beneficial to non-pathogenic bacteria in their overall fitness and adapting to their environment. The *E. coli* strain K-12, contains nine cryptic prophages [153]. Cryptic prophages are phages which have lost the ability to induce cell lysis and phage particle production, remaining

for the most part dormant within the host chromosome [161]. However, they are still beneficial for the biology of the bacterium. When these prophages were deleted from K-12, either individually, or all nine, the new mutant strains were less able to respond to the various growth conditions tested. Deletion of all nine resulted in increased sensitivity to nalidixic acid, oxidative stress, and acid stress, as well as a decrease in the ability to form biofilms [153]. These results highlight the importance of cryptic prophages on the physiology of *E. coli*.

It is apparent from the examples provided here that prophages play a very important role in the ecology of several bacterial species. However, what has not been explored yet is whether the cell division inhibitors encoded within prophages also have a beneficial role. Traditionally, phages when inducing lytic growth would employ inhibition to delay the cell cycle in order to optimise the production of viral particles [162]. However, given that many of the cell division inhibitors described above are from cryptic prophages and presumably cannot benefit the phage, it raises the question of whether these inhibitors are now beneficial for the host. That is, does *E. coli* use these genes to inhibit division to adapt and survive under specific environmental conditions?

1.6 Thesis Aims

Knowing when and where to divide is crucial for any bacterial population, thus several regulators must be in place to allow rapid responses to changing environments, such as those seen during filamentation. Although some proteins have been described recently which directly interact with FtsZ and the divisome, their biological relevance in causing filamentation still remains unknown. There is still a significant gap in our knowledge of the underlying mechanisms of filamentation and regulation of cell division requires further examination to identify the factors involved.

To address this, the overall objective of this thesis was to identify novel genes involved in the inhibition of cell division, to understand the environmental conditions in which they may be acting, and how they may be mediating the inhibition of division.

Prior to this study, a novel, high-throughput screening system was developed in our lab to identify potential cell division regulators [163]. This involved the over-expression of an *E. coli* shotgun genomic expression library. The use of over-expression to identify novel genes does not rely on creating the environmental conditions that lead to filamentation, but instead allows for the selection of genes that when expressed at high levels will make cells filamentous. Clones which caused filamentation when expressed were isolated using a high-throughput flow cytometry sorting system and sequenced to identify potential genes responsible for cell division inhibition.

The sequenced DNA fragments from this screen often contained multiple genes. Therefore as an initial step, the aim of Chapter three was to confirm which genes from

the original screen were responsible for the filamentation phenotype. Four genes of previous unknown function were selected and over-expressed to determine whether they were responsible for the inhibition of division observed in the screen. Through this, over-expression of the gene *ymfM* from a multi-copy plasmid was identified to be responsible for the cell division inhibition. This made *ymfM* an ideal candidate for further investigation and became the primary focus of this PhD.

The remainder of this thesis was focused on characterising the novel cell division inhibitor, YmfM, encoded within the e14 prophage of *E. coli*.

Chapter four aimed to understand the biological role of YmfM during the SOS response. The e14 prophage is known to contain a cell division inhibitor, SfiC, which is thought to be activated during the SOS response, although the exact identity of this inhibitor was unknown [136, 155]. We hypothesised that YmfM was this previously unidentified inhibitor. To test this, gene expression levels of *ymfM* during antibiotic induced SOS were tested using quantitative real-time PCR (qPCR) to see if *ymf*M was induced in response to an SOS stimuli. As well as this, genetic experiments activating the SOS response through a temperature sensitive RecA mutant (*recA441*) were conducted to measure changes in the degree of filamentation in the absence of *ymfM*.

Chapter five aimed to understand the context in which ymfM functions. This was achieved via a bioinformatics analysis of *ymfM* and the e14 prophage. This determined the conservation of *ymfM* within bacteria and the potential regulatory pathway of YmfM to give insight into when and where YmfM may be functioning to inhibit division.

Finally, the aim of Chapter five was to examine the molecular mechanism of how YmfM inhibits division. In particular, it aimed to determine whether YmfM interacts directly with FtsZ or indirectly through known cell division inhibitors.

By identifying and analysing YmfM's biological role, environmental cues and molecular mechanism, this work aimed to provide a broad understanding of a novel cell division inhibitor. Identifying and characterising cell division inhibitors are not only important to give us insight into how this highly conserved process is regulated, but also give us insight into how bacteria survive different environments.

Chapter 2. Methods and Materials

2.1 Chemicals, Reagents and Solutions

The chemicals and reagents used throughout this work were typically analytical reagent grade and were obtained from Amresco, BDH Chemicals or Sigma unless otherwise specified. Commonly used buffers and solutions are listed in Table 2.1.

Table 2.1 Solutions and their working compositions

Buffer/Solution	Composition [a,]
APS	10% ammonium persulfate
EDTA (0.5 M)	18.6% EDTA, 2% NaOH, pH 8.0
PBS	137 mM NaCl, 2.7 mM KCl, 10 mM Na_2HPO_4, 1.8 mM KH_2PO_4; pH 7
GTE	50 mM glucose, 20 mM Tris-Cl, 10 mM EDTA, pH 7.5
TE	10 mM Tris-HCl, 1mM EDTA, pH 7.5
TBE	89 mM Tris-HCl, 89 mM boric acid, 2.5 mM EDTA, pH 8.3
TBS	50 mM Tris-HCl, 150 mM NaCl
TS	200 mM Tris-Cl, 100 mM NaCl
Coomassie Blue Stain	50% Ethanol (v/v), 10% Glacial Acetic acid ≥ 99.85% (v/v), 0.5% Coomasie R-250(w/v)
Destaining buffer	20% Ethanol (v/v), 10% Glacial Acetic acid ≥ 99.85% (v/v)
SDS-PAGE loading buffer (2X)	0.62 M Tris-HCl pH 6.8, 10% SDS, 20% Glycerol (v/v), 0.1% Bromophenol blue
SDS-PAGE loading buffer (1X)	SDS-PAGE loading buffer (2X) with 10% of 2-Mercaptoethanol (v/v)
SDS-PAGE running buffer (10X)	14.42% Glycine, 3%, Tris, 1% SDS

a All buffers and solutions were made up in MilliQ® purified water (MQW; Millipore) and are listed at the normal working concentration (1 x) or stated otherwise. All percentages are given as weight per volume (w/v) unless stated otherwise.

2.2 *Escherichia coli* Strains and Growth Conditions

All *E. coli* strains used in this thesis are listed in Table 2.2. *E. coli* cells were grown on LB agar (1.5% w/v) plates at 37ºC, unless stated otherwise. Antibiotics (Table 2.4) were supplemented, where appropriate. Broth cultures were grown in 50 mL falcon tubes or 250 mL flasks, incubated with vigorous shaking (250 rpm) at 37ºC, unless otherwise stated. Growth was monitored by recording the absorbance at 600 nm (OD_{600}) using a spectrophotometer (UV-1601 UV-visible spectrophotometer; Shimadzu). *E. coli* strains were stored as stationary phase cultures suspended in 20% (v/v) glycerol at -80ºC

Table 2.2.*E. coli* strains used in this study

Strain	Genotype and Relevant Characteristics	Source
DH5α	F– *hsdR17 deoR recA1 endA1 phoA supE44 thi-1 gyrA96 relA1*	Lab Stock
MG1655	rph1 ilvG rfb-50	Lab Stock
BW25113 (wild-type)	F-, *Δ(araD-araB)567*, *ΔlacZ4787*(::rrnB-3), λ^-, *rph-1*, *Δ(rhaD-rhaB)568*, *hsdR514*	[164]
JW0941-1 (Δ*sulA*)	BW25113Δ*sulA*	[165]
JW1134-1 (Δ*ymfM*)	BW25113Δ*ymfM*	[165]
JW5641-1 (Δ*slmA*)	BW25113Δ*slmA*	[165]
Δ*sulA*Δ*ymfM*	BW25113Δ*sulA*Δ*ymfM*	This study
Δ*e14*	BW25113Δ*e14*	[153]
Δ*e14*Δ*sulA*	BW25113Δ*e14*Δ*sulA*	This study
TB28	MG1655 *ΔlacIZYA::frt*	[166]

TB43	TB28Δ*minCDE*::*frt*	[50]
JKD-2	*ftsZ*::kan *recA56* (native FtsZ in inactivated with a KanR casette, RecA56 mutation) Harbouring plasmid, pKD3a AmpR; temperature-sensitive pSC101 derivative containing *ftsAZ* and *envA*	Lab Stock
JM12	F-,*thr-1*, *araC14*, *leuB6*(Am), *Δ(gpt-proA)62*, *lacY1*, *tsx-33*, *qsr'-0*, *glnX44*(AS), *galK2*(Oc), *λ*-, *Rac-0*, *hisG4*(Oc), *fbC1*, *recA441*(ts), *rpsL31*(strR), *kdgK51*, *xylA5*, *mtl-1*, *argE3*(Oc), *thiE1*	[167]
BL21-DE3	*fhuA2 [lon] ompT gal (λ DE3) [dcm] ΔhsdS. λ DE3 = λ sBamHIo ΔEcoRI-B int::(lacI::PlacUV5::T7 gene1) i21 Δnin5*	Lab Stock
BL21-AI	*B F– ompT gal dcm lon hsdSB(rB- mB-) araB::T7RNAP-tetA*	Gift from Iain Duggin (University of Technology Sydney)
C41-DE3	*B F– ompT gal dcm hsdSB (rB- mB-)(DE3)*	Gift from Iain Duggin (University of Technology Sydney)
C43-DE3	F – *ompT hsdSB (rB- mB-) gal dcm* (DE3)	Gift from Roberta Davis (University of New South Wales)
B834-DE3	*F- gal dcm met* (DE3)	Gift from Iain Duggin (University of Technology Sydney)

Table 2.3. Media used for bacterial growth

Media	Composition
Luria-Bertani (LB) broth	10 % sodium chloride, 1% tryptone, 0.5% yeast extract
M63	0.2 % ammonium sulphate, 1.3 % potassium phosphate, 0.4% glucose, 0.5 mg/L ferrous sulphate, 1 mM magnesium sulphate, 0.4% casamino acids, trace elements

Media were made up in MilliQ and are listed at the normal working concentration (1 x). All percentages are given as weight per volume (w/v) unless stated otherwise.

Table 2.4. Antibiotics used for selection in *E. coli*

Antibiotics[a]	Working Concentration
Ampicillin	100 µg/mL
Kanamycin	50 µg/mL
Norfloxacin	100 ng/mL
Cephalexin	2 µg/mL

[a]Stock solutions were made by dissolving antibiotics in either MilliQ or Acetic acid (for norfloxacin) and filter sterilising (0.2 µm filter). Antibiotic solutions were stored at -20°C (long-term) or at 4°C (short-term)

2.3 Plasmids used in this Study

A list of plasmids used in this thesis is described in

Table 2.5.

Table 2.5. Plasmids constructed and used in this study

Plasmid	Description	Source
pBAD24	Plasmid pBAD24 containing an arabinose inducible promoter (P_{araB}), Amp^r	[168]
pBAD-*ycjY-clone*	Genes *ycjZ** and *ycjY* cloned into the MSC of pBAD24, Amp^r. Clone D2-3B	[163]
pBAD-*ykfI-clone*	Genes *yafW*,yfkI* and *thrW* cloned into the MSC of pBAD24, Amp^r. Clone D2-8D	[163]
pBAD-*ytfB-clone*	Genes *ytfB** cloned into the MSC of pBAD24, Amp^r. Clone D2-5G	[163]
pBAD-*ymfM-clone*	Genes *ymfL*,ymfM* and *oweE** cloned into the MSC of pBAD24, Amp^r. Clone D1-8E	[163]
pBAD-*ycjY*	The ORF of gene *ycjY* cloned into the MCS of pBAD24, Amp^r	This study
pBAD-*ykfI*	The ORF of gene *ykfI* cloned into the MCS of pBAD24, Amp^r	This study
pBAD-*ytfB*	The ORF of gene *ytfB* cloned into the MCS of pBAD24, Amp^r	This study
pBAD-*ymfM*	The ORF of gene *ymfM* cloned into the MCS of pBAD24, Amp^r	This study
pBAD-*ymfL*	The ORF of gene *ymfL* cloned into the MCS of pBAD24, Amp^r	This study

pBAD-*recA441*	The ORF of the mutant *recA* gene, *recA441* cloned into the MCS of pBAD24, Amp^r	This study
pBAD-*gfp-ymfM*	The ORF of gene *ymfM* and superfolder gfp at the N-terminal site cloned into the MCS of pBAD24, Amp^r	This study
pBAD-*ymfM-gfp*	The ORF of gene *ymfM* and superfolder *gfp* at the C-terminal site cloned into the MCS of pBAD24, Amp^r	This study
pETMCSIII	High-copy plasmid contains the bacteriophage T7 promoter for IPTG inducible protein expression. Contains an N-terminal 6 x His tag (His_6), Amp^r	[169]
pET-His_6-*ymfM*	The ORF of gene *ymfM* cloned into the MCS of pETMSCIII, Amp^r	This study
pKD46	Lambda red recombinase expression under arabinose inducible promoter (P_{araB}) , Amp^r	[164]
pCP20	Contains the yeast Flp recombinase gene, *flp*, on a temperature sensitive replicon, Amp^r	[170]

Amp^r = Ampicillin resistance

2.4 General DNA Methods

2.4.1 Extraction and purification of *E. coli* DNA from bacterial cultures

Chromosomal DNA

Chromosomal DNA was extracted and purified using the PureLink™ Genomic DNA mini kit (ThermoFisher Scientific) following the manufacturer's instructions. In summary, a volume of 1mL of overnight culture of the required strain was centrifuged for 2 minutes at 10,000 x *g*. The cell pellet was resuspended in 180 µL PureLink™ genomic digestion buffer and 20 µL of Proteinase K and incubated at 55ºC for 60 minutes until lysis was complete. A volume of 20 µL of RNase A (provided with the kit) was added to the lysate and mixed for 10 seconds on the vortex. The sample was then incubated for 2 minutes at room temperature. A volume of 200 µL of PureLink™ genomic Lysis/Binding buffer was added to the sample and mixed for 20 seconds by vortexing until a homogenous solution was obtained. 200 µL of 100% ethanol was added to the lysate and mixed well by vortexing for 5 seconds. The lysate (approximately 650 µL) was loaded onto a PureLink™ spin column in a collection tube and centrifuged at 10,000 x *g* for 1 minute at room temperature. The flow through liquid was discarded and the column was washed twice with wash buffer 1 and wash buffer 2. The column was dried with a final spin for 3 minutes at 10,000 x *g*. DNA was eluted using 200 µL of PureLink™ genomic elution buffer into a new 1.5 mL Eppendorf tube.

Plasmid DNA

Plasmid DNA was extracted and purified using PureLink™ Quick Plasmid Miniprep kit (ThermoFisher Scientific) following the manufacturer's instructions. In summary, 3 mL of overnight culture of *E. coli* strain harbouring desired plasmid was centrifuged at 10,000 x *g*. Cell pellet was resuspended with 250 µL of resuspension buffer. Cells were lysed by adding 250 µL of lysis buffer and mixing by gently inverting the tube. A volume of 350 µL of the precipitation buffer was added and sample mixed by inverting. The precipitate was separated from the supernatant via centrifugation at 10,000 x *g* for 10 minutes. The supernatant was loaded onto a spin column and spun for 1 minute at 10,000 x *g*. The column was washed using 700 µL of the wash buffer and spun at 10,000 x *g* for 1 minute. The column was dried and excess wash buffer removed with a 2 minute spin at 10,000 x *g*. Plasmid DNA was eluted using 50 µL of TE buffer into a new 1.5 mL Eppendorf tube.

2.4.2 Polymerase Chain Reaction (PCR)

PCR was used in this study for cloning genes into plasmids, confirming correct insertion of genes into plasmids and for the deletion of genes from the chromosome. Single-stranded oligonucleotide primers for PCR were generated by IDT and supplied in a lyophilised form. Primers were dissolved in MilliQ to a final concentration of 100 µM and stored at –20°C. Primers used are listed below in relevant Tables.

PCR using Phusion® High-Fidelity DNA Polymerase

PCR with Phusion® polymerase (New England Biolabs) was used for the amplification of genes for cloning and deletions. Each reaction was set up with Phusion HF buffer (1 x v/v), dNTPs (200 µM), forward and reverse primers (0.5 µM), template DNA (100 ng), 1 unit of Phusion DNA polymerase and sterile MilliQ water to a final volume of 50 µL.

PCR reactions were subjected to the following temperature cycling using a thermocycler (Mastercycler; Eppendorf): 98ºC for 1 minute (initial denaturation of the template), followed by 30 cycles of 98ºC for 10 seconds (template denaturation), XºC for 30 seconds (primer annealing), and extension at 72ºC for Y seconds (extension), followed by a final extension step was at 72ºC for 10 minutes. XºC for each primer is listed in their respective tables, and Y was 30 seconds per kb of amplicon to be amplified.

The PCR products were analysed via agarose gel electrophoresis (Section 2.4.4) and cleaned using the PureLink™ PCR purification kit (ThermoFisher Scientific) following the manufacturer's instructions. Concentration of PCR product was determined using the Nanodrop spectrophotometer (OD_{260nm}) (Section 2.4.3). PCR products were stored at -20ºC until further use.

PCR using Taq DNA polymerase

PCR with Taq DNA polymerase (New England Biolabs) was used for colony PCR to confirm correct insertion of gene into plasmids. A volume of 20 µL of sterile MillQ was

added to each PCR tube. A colony was selected from plates and resuspended in the water. Cells were lysed using a thermocycler, for 5 minutes at 95ºC. Samples were then placed on ice as the following reaction was set up. The following were added to each PCR tube and made to a final reaction volume of 25 µL: Thermopol buffer (1 x v/v), dNTPs (200 µM), forward and reverse primers (0.2 µM), 1 unit of Taq DNA polymerase.

PCR reactions were subjected to the following temperature cycling using a thermocycler: 95ºC for 30 seconds (initial denaturation of the template), followed by 30 cycles of 95ºC for 15 seconds (template denaturation), XºC for 30 seconds (primer annealing), and extension at 68ºC for Y seconds (extension), followed by a final extension step was at 68ºC for 5 minutes. XºC for each primer is listed in their respective tables, Y was 1 minute per kb to be amplified.

The PCR products were analysed via an agarose gel electrophoresis to confirm correct insertion of DNA product into plasmid (Section 2.4.4).

2.4.3 Determining DNA concentration

Concentration of genomic and plasmid DNA was determined on the Nanodrop™ spectrophotometer. Absorbance at 260nm was blanked using either water or elution buffer. A volume of 2 µL of DNA sample was used to determine DNA concentration (ng/µL).

2.4.4 Agarose Gel Electrophoresis

Agarose gels were used for visualisation of PCR product of the correct size and quality of either genomic or plasmid DNA. Agarose (Sigma) at 1% (w/v) was dissolved in electrophoresis buffer (TBE). Gels were cast on a horizontal slab gel apparatus (Bio-rad) with a well-forming comb in place. Gels contained 60 ng/mL of GelRed® (Biotium) to visualise the DNA under UV light. The DNA sample was prepared in 6X gel loading dye purple (New England Biolabs) and loaded into the pre-cast wells. A 1 kb DNA ladder (New England Biolabs) was used to estimate size of DNA product ranging from 500 bp to 10 kb. Agarose gels were run submerged under a volume of 1 x TBE electrophoresis buffer that lay above the surface of the gel at 90 V for approximately 1 hour. The gels were visualised via exposure to short-wavelength UV light (254 nm) using a transilluminator (Ingenius3; Syngene) and recorded as a digital image using a charge-coupled device (CCD) camera (Synoptics CAM-FLXCM; Syngene) linked to GeneSys molecular imaging software, version 1.5.0.0 (Syngene).

2.4.5 DNA sequencing

Sanger sequencing was used to determine correct insertion of gene sequence into plasmid or correct disruption of a gene on the chromosome. For plasmid constructs, purified plasmid, as described in Section 2.4.1, was used. For gene disruptions on the chromosome, purified PCR product, as described in Section 2.4.2 was used. Samples, along with appropriate primers, were then sent to the Australian Genome Research Facility (AGRF; University of Queensland, Australia), where sequencing reactions were performed. Sequencing data was analysed using the Lasergene® (DNASTAR) software.

2.5 Transformation of Plasmid DNA into *E. coli* Strains

2.5.1 Preparation of electro-competent *E. coli* cells

The *E. coli* strain that was to be made electro-competent, was grown overnight in LB at 37ºC with shaking at 250 rpm. The following day, cultures were diluted to Optical Density (OD_{600}) of 0.05 in 500 mL of LB. Cells were grown to an OD_{600} ranging from 0.6 to 0.8, after which they were chilled on ice for 30 minutes. Cells were centrifuged at 2 000 x *g* at 4ºC for 10 minutes and the supernatant discarded. The pellet was resuspended in 500 mL ice-cold sterile MilliQ water and centrifuged again at 2 000 x *g* for 10 minutes at 4ºC. The pellet was resuspended in 250 mL of ice-cold sterile 10% glycerol (v/v), and centrifuged at 2 000 x *g* for 15 minutes at 4ºC. The cells were resuspended again in 20 mL of 10% glycerol and centrifuged at 2 000 x *g* for 20 minutes. Finally, the cells were resuspended in 5 mL of 10% glycerol to achieve a 100x concentration. Cells were either used immediately for electroporation or were aliquoted in 100 µL volumes into Eppendorf tubes, snap frozen using liquid nitrogen and stored at -80ºC for later use.

2.5.2 Electroporation of competent *E. coli* cells

A concentration of 50 ng (unless otherwise stated) of desired plasmid was added to 50 µL of competent cells on ice. This was then transferred into a pre-chilled 0.2cm electroporation cuvette (BioRad, USA), ensuring no bubbles were produced during the process. The cells were electroporated using PowerPac Basic (BioRad, USA) electroporation machine at 25µF (capacitance), 2.5kV (voltage) and 200 ohm (resistance).

For a successful transformation, the time constant for the pulse was between 4 to 5 milliseconds. Once electroporated, the cells were immediately transferred into 1mL of LB broth to recover for 1 hour at 37ºC. 100µL undiluted cells were plated out onto antibiotic selective LB agar plates. The remainder of the sample was concentrated by 10 times and plated onto another plate. Plates were incubated overnight at 37ºC (unless otherwise stated).

2.6 Growth Curves

2.6.1 96-well plates

Growth curves of DH5α containing plasmid, pBAD-(gene of interest) under both arabinose induction and glucose repression were performed for results outlined in Chapter 3. This was done using the Biotex Synergy HTX 96-well plate reader. Overnight cultures grown in LB with Ampicillin 100 µg/mL and 0.2% glucose were diluted to OD_{600} = 0.04 in the same media the following morning and grown to mid-exponential phase. Samples were washed in fresh LB and diluted to an OD_{600} = 0.04 in LB with either 0.2% glucose or 0.2% arabinose and Ampicillin 100 µg/mL. Duplicates of each culture were aliquoted at 200µL each into a 96-well plate. The plate reader was set up to take OD_{600} measurements every 15 minutes for 6 hours, incubated at 37ºC with continuous shaking. Data was exported into excel and plotted onto a semi-logarithmic graph.

2.6.2 250mL flasks

Strain for which growth curve was to performed was grown overnight in 5 mL of LB, supplemented with antibiotics if necessary, at 37ºC. Overnight cultures were diluted in 50 mL of LB (antibiotics added if necessary) to an OD_{600} = 0.01. Cultures were grown over a period of 6 hours. Growth was monitored and recorded using a spectrophotometer by removing a 1mL aliquot and using a cuvette, every 30 minutes. Growth curves were performed in biological triplicates. Time point and OD values were exported into excel and plotted onto a semi-logarithmic graph. This method was used to measure growth rate of mutant strains (Table 2.2) constructed in this study as well as the number of generations

needed to induce expression of genes from pBAD24 . Mutant strains did not affect growth rate as compared to wild-type. Generation (doubling) time was calculated by determining the time (minutes) it took for the OD_{600} value to double when in exponential growth phase.

2.7 Construction of Deletion Mutants Using Lambda Recombination

Lambda Red recombination [164, 165] was used to generate various gene deletions in *E. coli* strains (Table 2.2).

2.7.1 Amplification of kanamycin cassette for the deletion of *sulA* and *ymfM*:

Genomic DNA of JW0941 and JW1134, containing insertions of a kanamycin resistance cassette to replace the open reading frame of *sulA* and *ymfM* respectively, was used to make subsequent gene deletions. Primers (Table 2.6) were designed approximately 100 bp upstream and downstream to genes of interest on the chromosome, in order to amplify the kanamycin cassette as well as the flanking DNA sequence needed for homologous recombination. Phusion polymerase (NEB) was used to amplify DNA sequence (Section 2.4.2) and the reaction was cleaned up using a PureLink™ PCR purification kit (ThermoFisher Scientific) as per the manufacturer's instructions.

Table 2.6 List of primers used to delete genes *ymfM* and *sulA*

Gene	Forward or Reverse	Sequence (5' – 3')[a]	Annealing Temp (°C)
ymfM	F	TACAAAATTTTTTGCATTTCAGAAAGTAATGACGC	57
	R	TCCCATACATAGCCGGTTAATTTAGTGC	
sulA	F	GGGATCTGCTCAATATTAACTCTACCGATATCTTC	58
	R	TAAAAGAATGATTCACATTAACGGATCCGTTAACTA	

2.7.2 Transformation of kanamycin resistance cassette and selection of successful insertion into *sulA* and *ymfM*

Background strains (JW0941 and Δe14) were made electro-competent and transformed with recombinase plasmid pKD46 and selected on LB agar plates containing 100 µg/mL ampicillin at 30ºC. The strain now containing the plasmid was made electro-competent again using LB media containing 100 µg/mL ampicillin and 0.2% arabinose at 30ºC.

Amplified DNA was transformed into recipient strain by using 50 ng of DNA and 50µL of competent cells. Cells were allowed to recover in LB media for 1 hour at 30ºC. Transformation was plated onto LB agar plates containing 50µg/mL Kanamycin and incubated overnight at 37ºC

PCR was used to confirm insertion of the kanamycin resistance cassette at the correct site on the chromosome using primers upstream and downstream to the gene of interest. PCR products were visualised on a 1% agarose gel to confirm products of the expected size.

The newly constructed mutant strains were cured of plasmid pKD46 through incubation of LB streak plates at 42ºC overnight. Loss of the plasmid was confirmed by lack of ampicillin sensitivity on LB agar plates.

2.7.3 Removal of Kanamycin Cassette

Mutant strains were made electro-competent and 50 µL of cells were transformed with plasmid pCP20 and incubated on 100 µg/mL ampicillin plates at 30ºC overnight. A few colonies were then re-streaked onto LB plates and incubated overnight at 42ºC. Loss of cassette and plasmid was confirmed by assaying sensitivity to ampicillin and kanamycin on LB agar plates.

2.8 Over-Expression of Genes From Inducible Plasmid, pBAD24

2.8.1 Cloning of genes into expression plasmid, pBAD24

Plasmid pBAD24 was extracted following the instructions outlined in Section 2.4.1. The plasmid was linearised using restriction enzyme *NcoI* (New England Biolabs). The reaction was set up using 1 µg of plasmid, 1 x NEBuffer™ 3.1 (v/v), 1 µL (10 units) of *NcoI* in a final volume of 50 µL. Samples were incubated at 37ºC for 1 hour, after which the enzyme was heat inactivated at 80ºC for 20 minutes. Linear ends of pBAD24 were dephosphorylated by adding 5 units of Antarctic phosphatase (New England Biolabs) and 6 µL of 1 x Antarctic phosphatase reaction buffer (v/v) to the 50 µL reaction. Sample was incubated at 37ºC for 30 minutes followed by a heat inactivation step of 80ºC for 2 minutes. Linearised plasmid was cleaned up using the PureLink™ PCR purification kit (ThermoFisher Scientific) following the manufacturer's instructions. Concentration of purified linear plasmid was determined using the Nanodrop spectrophotometer (Section 2.4.3) and visualised on an agarose gel (Section 2.4.4).

Primers used to amplify genes of interest to be cloned into pBAD24 are listed in Table 2.7. Primers were designed so that genes of interest could be cloned into pBAD24 using the Gibson Assembly master mix (New England Biolabs). PCR reactions were set up following Section 2.4.2.

Table 2.7. List of Primers used to amplify genes of interest to be cloned into pBAD24

Gene	Forward or Reverse	Sequence (5' – 3')[a]	Annealing Temp (°C)
ykfI	F	AGCAGGAGGAATTCACC**ATGAAAACTTTACCTGCAATAAC**	52
	R	AGGATCCCCGGGTAC**TCATCGTACTACGTTGTTACG**	
ycjY	F	AGCAGGAGGAATTCACC**ATGATGAATAATAAAGTCAGCTTC**	52
	R	AGGATCCCCGGGTAC**TTACAGAGTTTCCTCAAAGAAC**	
ytfB	F	AGCAGGAGGAATTCACC**ATGCCCGGGCGCTTTGAA**	64
	R	AGGATCCCCGGGTAC**CTACCGCGCACGAATAAAACTGC**	
ymfM	F	AGCAGGAGGAATTCACC**ATGAACAGTTTAACAACACACTAC**	50
	R	AGGATCCCCGGGTAC**CTATTTCCCTGAATTTACGAC**	
ymfL	F	AGCAGGAGGAATTCACC**GTGGGTAAGCATCACTGGAAAATAG**	55
	R	AGGATCCCCGGGTAC**TCATGCGTTAGTTTCTCCACAA**	
recA441	F	AGCAGGAGGAATTCACC**ATGGCTATCGACGAAAACAA**	54
	R	AGGATCCCCGGGTAC**TTAAAAATCTTCGTTAGTTTCTGCT**	
ymfM-msfgfp *ymfM*	F	AGCAGGAGGAATTCACC**ATGAACAGTTTAACAACACACTAC**	56
	R	CTACCACTTTCACGGGT**TTTCCCTGAATTTACGACG**[b]	

	gfp	F	CAGGGAAAACCCGTGAAAGTGGTAGTATCGGGTCC**ATGCGTAAAGGTGAAGAAC**[c]	56
		R	AGGATCCCCGGGTAC**TTATTTGTAGAGTTCATCCATG**	
msfgfp-ymfM	*gfp*	F	AGCAGGAGGAATTCACC**ATGCGTAAAGGTGAAGAAC**	57
		R	CTACCACTTTCACGGGT**TTTGTAGAGTTCATCCATGC**[d]	
	ymfM	F	CTCTACAAAACCCGTGAAAGTGGTAGTATCGGGTCC**ATGAACAGTTTAACAACACACTAC**[e]	59
		R	AGGATCCCCGGGTAC**CTATTTCCCTGAATTTACGAC**	
pBAD24		F	ATGCCATAGCTTTTTATCC	40
		R	GATTTAATCTGTATCA	

[a] nucleotides in bold are for the region of the primer that are homologous to the gene of interest, whilst the regions not in bold are homologous to pBAD24. The bold region was used to calculate annealing temperature during PCR amplification of gene of interest.

[b and e] Bold regions homologous for ymfM and non-bold are homologous for gfp

[c and d] Bold regions homologous for gfp and non-bold are homologous for ymfM

Insertion of each gene into the linearised pBAD24 was achieved using the Gibson Assembly Mater Mix (New England Biolabs), with a 3:1 insert to vector (50 ng) ratio. Reaction was set up with 1 x Gibson Assembly master mix (v/v) in a final volume of 20 µL, as per the manufacturer's instructions. The reaction was incubated in a thermocycler for 15 minutes at 50^{o}C, and stored at -20^{o}C until needed for subsequent transformation.

A volume of 2 µl of the Gibson assembly reaction, containing the assembled plasmid, was used to transform into electro-competent DH5α cells and recovered onto Luria-Bertani (LB) agar plates containing ampicillin (100 µg/mL). Colonies were screened for successful insert via colony PCR using pBAD24 forward and reverse primers (Table 2.7) following the protocol outlined in Section 2.4.2. These primers are designed to be up-stream and down-stream of the multiple cloning site (MCS). Successful insertion was determined by the presence of a PCR product of the expected size, on a 1% agarose gel. Unsuccessful insertion resulted in the presence of a PCR product around 100 base-pairs, due to the amplification of the multiple cloning site.

Plasmid containing genes of interest were sent to the Australian Genome Research Facility (AGRF) for Sanger sequencing. pBAD24 forward and reverse primers (Table 2.7) were used for sequencing from each end of the insert.

2.8.2 Over-expression of genes from pBAD24

Table **2.5** has a list of genes cloned into pBAD24, used for over-expression studies. All over-expression studies in this thesis were conducted using the following protocol.

Cultures of desired *E. coli* strain containing pBAD24 cloned with gene of interest were grown overnight in 5mL LB with ampicillin (100 µg/mL) and 0.2% glucose at 37ºC. The following morning overnight cultures were diluted to OD_{600} = 0.04 in 20mL LB with ampicillin (100 µg/mL) and 0.2% glucose (for repression from the pBAD24 promoter). Cultures were grown at 37ºC to mid-exponential phase. A 1mL aliquot of the culture was collected and fixed with 3% formaldehyde.

The rest of the culture was pelleted by centrifugation at 2, 000 x *g*, and resuspended in an equal volume of fresh LB to remove the glucose. Cultures were further diluted to an OD_{600}=0.04 in 20mL LB with ampicillin (100 µg/mL) and 0.2% arabinose (to induce expression), and grown for 4 generations (approximately 2 hours) at 37ºC. A 1mL culture was taken and fixed with 3% formaldehyde.

Fixed samples were viewed under microscope for phenotypic changes using phase-contrast microscopy (Section 2.10.3). Cells lengths were measured either manually from microscopy images (Section 2.10.3) or using the Coulter counter (Section 2.11).

2.9 Induction of the SOS Response

2.9.1 Induction through the activation of a temperature sensitive RecA-mutant, RecA441

The strain JM12 [167] contains the *recA* mutation *recA441*. This mutant contains two amino acid substitutions, E38K and I298V [171]. Mutation, E38K, is responsible for the constitutive expression of the SOS response, and I298V, is responsible for its temperature-dependent induction. In this mutant, RecA expression is activated at the non-permissive temperature of 42ºC, thereby inducing the SOS response without the need for external means to DNA damage.

Forward and reverse primers (Table 2.7) were used to amplify the mutant *recA* gene from JM12 genomic DNA following protocol detailed in Section 2.4.2. *RecA441* was cloned into pBAD24 as outline in Section 2.8.1, and transformed into strains, BW25113 (wild-type), Δ*sulA,* Δ*ymfM,* Δ*sulA*Δ*ymfM* (Table 2.2).

For strains containing pBAD-*recA441*, cultures were grown as outlined in Section 2.8.2 with slight variations. Overnight cultures in LB and 0.2% glucose repressed cultures were grown at 30ºC instead of 37ºC. Induced expression was achieved with 0.2% arabinose, 100 µg/mL adenine and growth at 42ºC for 2 hours. Adenine was added as it is reported that combination of growth at 42ºC and adenine allows RecA to acquire its protease activity [136]. Fixed samples were analysed on the coulter counter as detailed in Section 2.11.

2.9.2 Chemical induction of the SOS response using norfloxacin

Determining the concentration needed to induce filamentation

Overnight cultures of *E. coli* BW25113 grown in LB at 37ºC, were diluted to an OD_{600} = 0.04, in LB and incubated at 37ºC with shaking at 250 rpms. These were grown to mid-exponential phase. A 1 mL the sample was fixed with final concentration of 3% formaldehyde (no treatment sample). With the remainder of the culture, a fresh dilution to and OD_{600} = 0.04 was performed in LB containing varying concentrations of Norfloxacin (Sigma). This included 50, 100, 150, 200 and 250 ng/mL. Cultures were grown over a period of 2 hours, during which 1mL samples were taken at 60 and 120 minutes and fixed with 3% formaldehyde. Cells were imaged using phase-contrast microscopy as described in Section 2.10.

Induction of the SOS response using 100 ng/mL of norfloxacin

Overnight cultures of *E. coli* (Wild-type, Δ*sulA*, Δ*ymfM*, Δ*sulA*Δ*ymfM*, Δ*e14*, Δ*e14*Δ*sulA* and Δ*recA*) grown in LB at 37ºC, were diluted to an OD_{600} = 0.04, in LB and incubated at 37ºC with shaking at 250 rpms. These were grown to mid-exponential phase. A 1 mL sample of these cells was fixed with final concentration of 3% formaldehyde (No treatment sample). With the remainder of the culture, a fresh dilution to and OD_{600} = 0.04 was performed in LB containing 100 ng/mL Norfloxacin (Sigma). Cells were grown with norfloxacin over a period of two hours, during which 1mL samples were taken at both 60 and 120 minutes and fixed with 3% formaldehyde. Experiments were repeated to obtain three biological replicates. Cells were analysed on the coulter counter as described in Section 2.11.

2.10 Microscopy Methods

2.10.1 Immunofluorescence microscopy (IFM)

IFM was used for the detection of the FtsZ protein in various *E. coli* strains, under various growth conditions, specified in the text below. The IFM method used in this study is based on the method previously described in [172], with slight variations, detailed below.

Growth conditions

pBAD-ymfM induced cells

Overnight cultures of strain BW25113 containing pBAD-*ymfM* were diluted to an OD of 0.05 the following morning in fresh LB with 100 µg/mL ampicillin and 0.2% glucose. Cells were grown to mid-exponential phase at 37ºC and 250 rpm, after which a 780µL sample was taken and prepared for immunofluorescence microscopy. The remainder of the culture was centrifuged and resuspended in an equal volume of fresh LB to wash out glucose. Cells were then re-diluted to an OD of 0.04 in LB with 100 µg/mL ampicillin and 0.2% arabinose. Cultures were grown for 90 minutes in LB with shaking after which a 780µL sample was taken to be prepared for immunofluorescence microscopy.

Cephalexin treated cells

Overnight cultures of BW25113 were diluted to an OD of 0.05 in LB or LB with 2 µg/mL cephalexin and grown to mid-exponential phase at 37ºC with 250 rpm shaking. A volume

of 780µL of cells from each sample was taken to be prepared for immunofluorescence microscopy.

FtsZ-depleted cells

The strain JKD-2, containing the plasmid pKD3a, was used to deplete cells of FtsZ. JKD-2 has the native FtsZ inactivated by a kanamycin resistance cassette. Plasmid pKD3a contains an ampicillin resistance gene, and is a temperature-sensitive pSC101 derivative plasmid containing the *ftsZ* gene. When grown at the permissive temperature of 30ºC, FtsZ is produced from the plasmid and cell division occurs. During non-permissive growth of 42ºC, the plasmid is lost overtime, thereby depleting the levels of FtsZ in the cell. This strain was grown overnight in LB and 100 µg/mL ampicillin at 30ºC at 250 rpm. The following morning cells were diluted to an OD of 0.05 in fresh LB with 100 µg/mL ampicillin and grown to mid-exponential phase at 30ºC with shaking at 250 rpm. The culture was then diluted to an OD of 0.05 in either LB or LB with 100 µg/mL ampicillin. LB only cultures were grown at the non-permissive temperature of 42ºC and LB with ampicillin grown at 30ºC, until mid-exponential phase of growth was reached. A volume of 780 µL of cells from each sample was taken to be prepared for immunofluorescence microscopy.

Fixation of cells

Cells were fixed with $NaPO_4$ (30 nM), formaldehyde (2.4%), glutaraldehyde (0.04%). Samples were incubated at room temperature for 15 minutes followed by 45 minutes on ice. Samples were then centrifuged to pellet cells and the supernatant discarded. Cell

pellets were washed twice with phosphate-buffered saline (PBS), pH 7.4. Cells were then resuspended in 200 µL of GTE buffer. Samples were kept on ice until the next step.

Microscopy slide preparation

A volume of 20 µL of poly-L-lysine was added to each well of a 15-well slide. After 1 minute, the liquid was aspirated off and the wells washed once with 25 µL of MQW. The wells were allowed to air dry before 10 µL of fixed cells was added to each well. Cells were allowed to sit on the slide for 1 minute after which excess sample was aspirated. Wells were washed twice with 25 µL of PBS, and then aspirated to allow complete dryness.

Immunostaining

Wells were rehydrated by adding PBS and incubating at room temperature for 4 minutes. The PBS was then aspirated. Each well was then incubated with PBS containing 2% w/v BSA (BSA-PBS) for 15 minutes at room temperature in a humidity chamber. The humidity chamber was constructed by adding wet tissue paper to a petri dish. The solution was then aspirated and 20 µL of the primary antibody, αFtsZ (anti-sera), in a 1 in 10,000 dilution in BSA-PBS, was added to each well. This was then allowed to incubate overnight in a humidity chamber at 4°C. The following morning, the primary antibody was aspirated off and each well was washed 10 times with PBS to remove any unbound antibody. A volume of 20 µL of Alexa488-conjugated secondary antibody, αRabbit IgG (Invitrogen), diluted 1 in 10,000 in BSA-PBS was added to each well. The slide was incubated for 2 hours in the dark, at room temperature in the humidity chamber. Wells were washed 10 times with PBS to remove excess secondary antibody. Finally 2 µL of

DAPI (4'6-diamidino-2-phenylindole), at a final concentration of 2 μg/mL in 50% (v/v) glycerol in PBS solution was added to each well. A coverslip (24 x 54 mm) was placed over the wells and the edges sealed with nail polish. Cell morphology and FtsZ localisation was then examined using phase-contrast and fluorescence microscopy (Section 2.10.3).

2.10.2 Preparation of cells expressing YmfM-GFP for live cell fluorescence microscopy

Live cell imaging was used for YmfM-GFP constructs. GFP was fused with YmfM on either the N-terminal or C-terminal. See section 2.8 for overview of cloning genes into pBAD24. Cells were grown as outlined in section 2.8.2, with slight variations. Cells were induced with 0.2% arabinose for only an hour. Agarose pads (detailed below) were used to mount cells on a slide.

2.10.3 Phase-contrast and Fluorescence Microscopy

Cells were visualised using phase-contrast and fluorescence on a Zeiss Axioplan 2 fluorescent microscope. The Zeiss Axioplan microscope was equipped with a Plan ApoChromat (100x NA 1.4; Zeiss) objective lens to allow visualisation at 100 x magnification. The light source was a 100 W high pressure mercury lamp passed through the following filter blocks for visualising Alexa 488 and GFP (Filter set 09, Zeiss; 450 – 490 nm BP excitation filter, 515 nm long pass (LP) barrier filter), for visualising DAPI (Filter set 02, Zeiss; 365 nm excitation filter, 420 nm long pass (LP) barrier filter). Images

were collected using the AxioCamMRm camera and processed using the AxioVision 4.8 software (Zeiss). Images were exported as TIFF files.

With the exception of IFM, agarose pads were used for mounting cells. Agarose pads (2% w/v agarose in MilliQ) were made using gene frames (ThermoFisher Scientific) on a glass slide. A volume of 2µl of fixed cells was added onto the pad and a glass coverslip (22 x 22 mm) was placed over each agarose pad.

2.10.4 Image analysis of microscopy images

The cell lengths from phase-contrast and fluorescent images obtained with the Zeiss Axioplan 2 fluorescence microscope, were measured directly from the digital micrographs using the AxioVision software, version 4.8 (Zeiss), with appropriate scaling. Approximately 100 cells were measured from each data set (unless specified otherwise) using the length tool to draw a line from one end of the cell to another. The distance was recorded in micrometers (µm) and length measurements were exported from the AxioVision software into Excel (Microsoft) to allow calculation of the mean cell length and standard deviation for each data set. For IFM, the presence of Z rings was determined by counting the number of cells with a fluorescent signal (Z rings were scored as bands across the width of the cell). The number of cells containing Z rings was then added as an additional column in the Excel spreadsheet containing cell lengths data.

2.11 Coulter Counter Analysis of Cell Length

A Coulter counter (Beckman) measures the size of particles, such as bacterial cells, suspended within an electrolyte buffer. This size is reported as a volume (μm^3), and in the case of rod-shaped bacteria such as *E. coli* is proportional to the cell length. A volume of 100µL of fixed cells was added to 9.9mLs of Isoflow buffer (Beckman). Of this, 200µL was run through a 50µm aperture tube, and data collected over 400 bins ranging from 0.6 $\mu m^3$to 100μm^3. Data was exported in excel as a table of bin width and number of cells per bin.

2.11.1 Graphing coulter counter data

The coulter counter data was plotted as a histogram with the cell volume along the x-axis and percentage of cells on the y-axis, in Mathematica (Wolfram).

2.11.2 Statistical analysis of the coulter counter data

The Coulter counter counts hundreds of thousands of cells per sample run, meaning that even very small differences between populations will be statistically significant. This includes the normal low levels of variability between two samples from the same strain, and does not necessarily indicate biological significance. As such, statistical analysis was not used to determine significant differences between strains. Instead, differences were determined visually from the distribution graph and using a cross correlation function, calculated in Mathematica (Wolfram). Cross correlation gives a measure of how similar

two distributions are, with a value of 1 being identical, a value of 0 being un-correlated and -1 being anti-correlated.

2.12 Western Blot Analysis

Western blot analysis was performed to detect FtsZ in BW25113 (wild-type) cells expressing *ymfM* from pBAD-*ymfM*. Wild-type cells containing pBAD24 only, and FtsZ depletion strain, JKD-2 were used as controls.

2.12.1 Whole cell protein extraction for western blotting

Cell lysates for western blot analysis were prepared in the following way. Wild-type cells containing either pBAD24 or pBAD-*ymfM* were grown under 0.2% glucose repression and 0.2% arabinose induction as specified in Section 2.8.2, with a slight variation; induction with arabinose occurred for only 90 minutes. Depletion of FtsZ was carried a detailed in Section 2.10.1. A volume of 10 mL was taken from each culture and centrifuged at 2,000 x g for 5 minutes. The supernatant was discarded and the pellets resuspended in 250 µL of lysis buffer and incubated at 37ºC for 30 minutes. Protein concentration of each sample was measured using the Bradford Assay, in which 10 µL of sample was added to 200 µL of Bradford reagent (Bio-Rad) made to a final volume of 1 mL in MilliQ. The OD was measured at 595 nm. Protein concentration was determined from a standard curve. To the lysed samples 250 µL of 1 x SDS loading buffer was added and samples were heated at 95ºC for 5 minutes. The sample was centrifuged for 2 minutes at 10,000 x *g* in a microfuge to remove cell debris.

2.12.2 SDS-polyacrylamide gel

A pre-cast 4 – 15% gradient gel (Bio-rad) was transferred to a Protean 3 (Biorad) gel-running tank and submerged in 1 x SDS PAGE running buffer. The comb was removed from the gel and approximately 5 μg of protein (based on Bradford assay) was loaded into each well. 10 μL of Prestained Protein Standards (Invitrogen) was also loaded. Proteins were separated by electrophoresis at 175V for ~45 minutes. Following electrophoresis, the gel was either prepared for Western blotting or stained in coomassie staining solution for 2 hours before destaining overnight in destain solution.

2.12.3 Western Transfer

Immunoblot polyvinylidene difluoride (PVDF) membrane (BioRad) was cut to the same size as the SDS-PAGE gel. The membrane was submerged briefly in 100% (v/v) methanol before being rinsed in sterile MQW and then equilibrated in western transfer buffer for 5 minutes. Protein was transferred from the gel to the PVDF membrane by electroblotting in western transfer buffer using Mini Trans-Blot apparatus (BioRad) at 60 V for 1 hour.

2.12.4 Immunodetection and quantification

After Western transfer, the PVDF membrane was blocked in blocking buffer (TBST + 5% (w/v) skim milk) for 2 hours with gentle shaking. The membrane was then incubated with the primary antibody, Anti-FtsZ, diluted (1: 10,000) in blocking solution overnight at 4^{o}C. The blot was rinsed 3 times with TBST for 20 minutes each at room temperature

and gentle shaking. The membrane was then incubated with the secondary antibody (Horseradish peroxidase conjugated Anti-Rabbit, Promega) diluted (1: 10,000) in blocking solution, for 2 hours are room temperature with gentle shaking. The membrane was washed 3 times with TBST for 20 minutes each at room temperature and gentle shaking to remove excess antibody.

Following this, the blot was incubated with the ECL (enhanced chemiluminescence; GE Healthcare) kit reagents and prepared for chemiluminescent detection according to the manufacturer's instructions. The membrane was then scanned for chemiluminescent reaction between the ECL reagents and the horseradish peroxidase-conjugated secondary antibody, using the ChemiDoc XRS+ imaging system (Bio-Rad). Chemiluminescent reaction was acquired 6 times over 300 seconds to ensure that at least one of the images acquired would represent the peak-point of the reaction. Band intensities were analysed using ImageJ.

2.13 Quantitative Real-Time PCT to Determine Gene Expression Levels

2.13.1 Primer design and validation

Primers (Table 2.) were designed using the online tool available on the Integrated DNA Technology website (http://sg.idtdna.com/scitools/Applications/RealTimePCR). Genes of interest included, *ymfM, sulA, ymfL, croE* and *cohE*. Housekeeping genes included, *16srRNA* and *secA*. Primers were validated for specificity by PCR amplification of target sequences using BW25113 genomic DNA and confirming the presence of only one product of the correct size (approximately 100bp) by 2% agarose gel electrophoresis.

Primers were tested for efficiency by performing qPCR as detailed below on gDNA serially diluted from 10^0 to 10^{-5} in triplicates. CT values were plotted on a semi-log graph to generate a standard curve. The slope of the line was used to determine efficiency using the online qPCR Efficiency Calculator (ThermoFisher Scientific).

Table 2.8 Primers used for quantitative real-time PCR (qRT-PCR)

Gene	Forward/Reverse	Sequence (5' – 3')

ymfM	F	TACCAGGTGACAGGGAAATTG
	R	GTTAACTTGTCGCAAAGGACTG
ymfL	F	GCACTCACTTCATTGCTGATG
	R	CCAGCAGACGCTGGTTAATA
croE	F	GCTCAACACCTGGCTACTTAC
	R	CGTAATTGCACCTGATGTGTATTG
cohE	F	GTAGGATGGCTCGATCAAGAAC
	R	CCCATGATATGACAGGGACTAATG
sulA	F	GGGCTACCCTTAACGAAAGTAA
	R	GTAATTGCCCGTGCGTAAAG
16S rRNA	F	GCAAGCGTTAATCGGAATTACTG
	R	TGGAATTCTACCCCCCTCTACG
secA	F	CCAGAACTACTTCCGTCTGTATG
	R	ACGGTATCCAGCTTGTAGATTG

2.13.2 RNA extraction

A volume of 1mL was taken from a culture of BW25113 incubated with norfloxacin at 60 minutes and 120 minutes as well as a no treatment control (see 2.9.2 for a detailed overview of the experiment). Cells were pelleted at maximum speed in a microfuge for 2 minutes. The supernatant was discarded and the pellet was snap frozen in liquid nitrogen. Pellets were kept in the -80°C freezer until further use.

RNA was extracted from the cell pellets using a PureLink RNA minikit (Invitrogen) as per the manufacturer's instructions. DNA was degraded using DNase I (RNase free) (NEB) for 30 minutes at 37ºC and heat inactivated at 75ºC for 10 minutes. RNA was cleaned up after DNase I treatment using the RNA minikit as per the manufacturer's

instructions. The RNA concentration was measured using the Nanodrop spectrophotometer, and the 260/280nm and 260/230nm ratios were recorded to determine purity.

2.13.3 Synthesis of complementary DNA (cDNA)

Reverse transcription (RT) of RNA to cDNA was performed using Superscript III Reverse Transcriptase (Invitrogen) as per the manufacturer's instructions. A control of no RT was also included where no transcriptase enzyme was added to the reaction. Successful synthesis of cDNA was determined by PCR using Phusion polymerase. Primers for 16sRNA (Table 2) were used to amplify the gene target and reactions were run on a 2% agarose gel to confirm a product of correct size

2.13.4 qRT-PCR to determine gene expression

Reaction set up

A 1:3 dilution of the synthesised cDNA and no RT reaction, was made using Ultrapure distilled water (Invitrogen). A 3-times PCR reaction was set up for each gene target using the primers listed in Table 2, and following the manufacturer's instructions for iTaq Universal SYBR Green Supermix (Bio-Rad). The final primer concentration was 300nM and 2µL of either the diluted cDNA or no RT was used per reaction. The no RT control was used to determine the background noise or genomic DNA contamination of the PCR. For each biological replicate, the reaction was split into three technical replicates by aliquoting 10µL of the reaction into three wells of a MicroAmp Fast Optical 96-well reaction plate (ThermoFisher Scientific).

Running PCR

Real-time PCR was run on the Applied Biosystems QuantStudio 6 Flex Real-time PCR Machine (ThermoFisher Scientific), using the Quantstudio Real-Time PCR Software, Version 1.1. The Comparative CT (ΔΔCT) option and Sybr green reagent setting was selected for the PCR run over a period of 40 cycles. The PCR cycling conditions included three stages. The first hold stage included 50ºC for 2 minutes followed 95ºC for 10 minutes. The PCR stage consisted of 95ºC for 15 seconds and 60ºC for 1 minute which cycled 40 times. The third Melt Curve stage included 95ºC for 15 seconds, 60ºC for 1 minute and 95ºC for 15 seconds.

Analysis of CT values

Raw CT values were exported into Excel. ΔΔCT value (log_2 fold change) of gene expression was determined for each biological replicate using the following formula shown below. The ΔΔCT value from each biological replicate were then used to determine the average fold change

$$\frac{\text{Control genes (CT value of no treatment – CT value of treatment)}}{\text{Target gene (CT value of no treatment – CT value of treatment)}}$$

2.14 Protein Production of YmfM

2.14.1 Cloning of *ymfM* into pETMCSIII

The gene, *ymfM* was cloned into plasmid pETMSCIII for protein over-production. Primers used are listed in Table 2.9 and PCR product amplified and purified following protocol in Section 2.4.2.

Plasmid was extracted as detailed in Section 2.4.1. Plasmid (1 µg) and PCR product (500 ng) were digested with restriction enzymes, *NdeI* and *NcoI* and NEBuffer 2.1 in a final volume of 50 µL. Digestion was allowed to occur for 1 hour at 37ºC followed by heat inactivation at 80ºC for 20 minutes. Digestion reactions were cleaned up using the PureLink™ PCR purification kit (ThermoFisher Scientific) following the manufacturer's instructions. Concentration of DNA was determined using the Nanodrop spectrophotometer and visualised on an agarose gel.

Table 2.9. Primers used to clone *ymfM* into pETMCSIII

Gene	Forward or Reverse	Sequence (5' – 3')	Annealing Temperature (ºC)
ymfM	F	GCCGCATATGAACAGTTTAACAACACACTACCG	60
	R	GCCGCCATGGCTATTTCCCTGAATTTACGACG	
pET	F	CTATAGGGAGACCACAAC	54
	R	CTTTCGGGCTTTGTTAGC	

Linearised plasmid (50 ng) and insert DNA were ligated using T4 DNA Ligase (New England Biolabs) in a 3 : 1 insert to vector ratio. Reaction was set up using 1 x T4 DNA Ligase reaction buffer (v/v) and 1 µL Ligase in a final volume of 20 µL. The samples were incubated overnight at 16ºC in a thermocycler and heat inactivated at 65ºC for 10 minutes. A negative ligation control was used where no insert was added to the reaction.

A volume of 3 µL of the ligation reaction was added to 50 µL of electro-competent cells and transformed into DH5α and selected on 100 µg/mL ampicillin LB plates. See Section 2.5 for detailed overview of transformation.

Forward and reverse primers (pET-F and pET-R) were used to perform colony PCR to determine successful insertion. Successful insertion was determined by the presence of a PCR product of the expected size, on a 1% agarose gel. Unsuccessful insertion resulted in the presence of a PCR product around 100 base-pairs, due to the amplification of the multiple cloning site.

Plasmid containing genes of interest were sent to the Australian Genome Research Facility (AGRF) for Sanger sequencing. pET-F and pET-R were used for sequencing from each end of the insert.

2.14.2 Transformation of pET-his$_6$-ymfM

Plasmid, pET-his$_6$-*ymfM* was transformed into electro-competent cells of the strains, BL21-DE3, BL21-AI, C41-DE3. C43-DE3, B834-DE3 and RIPL as outlined in Section 2.5. Cells were recovered on LB 100 µg/mL ampicillin plates.

2.14.3 Small-scale overproduction of YmfM

Strain C43-DE3 harbouring pET-his$_6$-*ymfM* was grown overnight in LB with 100 µg/mL ampicillin at 37ºC. The following morning sample was diluted to an OD_{600} of 0.05 into 5 mL of fresh LB with 100 µg/mL ampicillin. Cells were grown at 37ºC until mid-exponential phase (OD_{600} = 0.5). A volume of 1 mL of the culture was taken and cells harvested for later use. To the remainder of the sample, 1mM of IPTG was added to induce protein overproduction. The induced cells were grown at 37ºC for 3 hours with shaking at 200 rpm. Varying induction temperatures were also tested; 30ºC (4 hours), 25ºC (4 hours), 18ºC (6 hours), and 10ºC (24 hours). Subsequently, 2 x 1 mL of the cells were harvested by centrifugation at 10, 000 x *g* for 5 minutes at 4ºC. Pellets were either prepared for SDS-PAGE immediately or stored at -20ºC for later use.

2.14.4 Checking for YmfM overproduction and solubility

To check for protein overproduction, un-induced and induced cell pellets were normalised to OD_{600} = 10 by resuspension in TS buffer. To this an equal volume of 1 x SDS loading buffer was added. The samples were vortexed and incubated for 10 minutes at 95ºC.

Cellular debris was removed by centrifuged at 10,000 x *g* for 5 minutes. A volume of 15 µL of each sample was loaded onto an SDS-PAGE and proteins were separated by electrophoresis at 175V for ~45 minutes in 1 x SDS PAGE running buffer. Following electrophoresis, the gel was stained in coomassie staining solution for 2 hours before destaining overnight in destain solution.

To check for protein solubility cell pellets were normalised to OD_{600} = 10 by resuspension in TS buffer. Samples were sonicated on ice at 15 second intervals. Lysed cells were centrifuged at 10, 000 x *g* for 15 minutes at 4ºC. The soluble supernatant was removed into a new tube. The insoluble pellet was resuspended in equal volume TS buffer. An equal volume of 1 x SDS loading buffer was added to both the soluble and insoluble fraction. Equal A volume of 15 µL of each sample was loaded onto an SDS-PAGE gel and incubated for 10 minutes at 95ºC. Cellular debris was centrifuged at 10, 000 x *g* for 5 minutes. A volume of 15 µL of each sample was loaded onto an SDS-PAGE and proteins were separated by electrophoresis at 175V for ~45 minutes in 1 x SDS PAGE running buffer. Following electrophoresis, the gel was stained in coomassie staining solution for 2 hours before destaining overnight in destain solution.

2.15 Bioinformatics Analysis of *ymfM*

2.15.1 Identifying organisms containing *ymfM*

The nucleotide sequence for *ymfM* was obtained from NCBI Nucleotide (https://www.ncbi.nlm.nih.gov/nuccore/NC_000913.3?report=fasta&from=1203822&to=1204160 accessed on 24/8/2017). This sequence was then queried against a non-redundant nucleotide collection (consisting of GenBank, EMBL, DDBJ, PDB and RefSeq sequences) using Blastn (MegaBlast) (https://blast.ncbi.nlm.nih.gov/ accessed on 12/11/2017) [173]. The max expected value was set to 10^{-10} and Max target sequences parameter was set to 5000 (excess above the 218 hits found). Organisms and taxonomies were then classified using the taxonomy assigned to the hit sequences within Blast's taxonomy report.

The percentage conservation of *ymfM* was determined by aligning all the homolog sequences and taking the mode of each nucleotide. This was achieved using a custom script written in Mathematica (Wolfram) (available upon request). For each base in the consensus sequence the fraction of hits with the same base at that position was calculated.

2.15.2 Gene and Genome Sequences

The sequences of genes contained within the e14 prophage were acquired from NCBI Gene (https://www.ncbi.nlm.nih.gov/gene) for strain K-12 substr. MG1655 of *E. coli* (NCBI Reference Sequence NC_000913.3). The locations of the genes within the genome are shown in Table S1 (See Supplementary Data).

Details of all complete genome sequences for *E. coli* were obtained from NCBI Genome (https://www.ncbi.nlm.nih.gov/genome/genomes/167) by selecting for all complete and all chromosome sequences. A short custom Mathematica script (Wolfram) was then used to download a FASTA file for each genome (available upon request)

The phylogenetic tree of *E. coli* strains was obtained from the accompanying Genome Tree report (https://www.ncbi.nlm.nih.gov/genome/tree/167? accessed on 24/8/2017) and was coloured based on presence/absence using Figtree v1.4.3 (http://tree.bio.ed.ac.uk/software/figtree/).

2.15.3 Presence Correlation Analysis

Each gene in the e14 prophage of K-12 substr. MG1655 was aligned against each *E.coli* complete genome using a Mathematica program which implements a downloaded version of Blastn (ncbi-blast-2.5.0+ https://blast.ncbi.nlm.nih.gov/accessed on 24/8/2017). For each alignment the expected value parameter was set to 10^{-10}. Genomes containing hits below this expected value were classed as containing a homolog.

2.15.3 Conditional Probability

Conditional probabilities, the probability that a gene ($gene_j$) is present when another gene ($gene_i$) is known to be present, is given by the joint distribution divided by the marginal distribution for a gene. Taking the kolmogorov definition the conditional probability can be written as

$$P(gene_j|gene_i) = \frac{P(gene_j, gene_i)}{P(gene_i)}$$

These conditional probabilities were calculated by counting the number of genomes that $gene_i$and $gene_j$were present together divided by the number of genomes where $gene_i$ was present.

2.15.4 Mutual Information

The mutual information [174], I, shared between two genes of e14 prophage is given by

$$I(gene_i; gene_j) = \sum_{i_p, j_p} p(i_p, j_p) \ln\left(\frac{p(i_p, j_p)}{p(i_p)p(j_p)}\right)$$

Where $i_p$and $j_p$denotes the presence or absence of $gene_i$and $gene_j$respectively. Mutual information values were normalized to form a metric between 0 and 1 by dividing by the maximum self information if of $gene_i$or $gene_j$. These values were calculated using a custom script in Mathematica (Wolfram).

2.15.5 Directional Probability

Directional probability for all gene combinations of the e14 prophage was calculated by filtering for asymmetry in the conditional probabilities. In particular, conditional probabilities were filtered to find cases where in genomes where $gene_j$ was present, $gene_i$ would almost always be present (>95%), however, in the genomes where $gene_i$ was present, $gene_j$ would only sometimes be present (<80 %). These conditions can be written formally as $P(gene_i|gene_j) > 0.95$ and $P(gene_j|gene_i) < 0.8$ respectively.

2.15.6 Phylogenetic tree of *ymfL* homologs found in *E. coli*.

The regions of *E. coli* genomes with homology to *ymfL* were extracted into a FASTA file using a Mathematica script. These homologous regions were input into the MAFFT version 7.112 server [175] (https://mafft.cbrc.jp/alignment/software/) with default options to generate the phylogenetic tree output.

For each *ymfL* homolog detected, the region stretching from 1000 base pairs to either side of the *ymfL* homology sequence was extracted and queried using MegaBlast (with the same settings as presence correlation analysis) against the K-12 substr. MG1655 *ymfM* sequence to detect whether *ymfL* and *ymfM* were adjacent. An expected value of 10^{-10} was used as a cut off for presence.

The phylogenetic tree output from MAFFT was coloured according to whether *ymfM* was adjacent using Figtree v1.4.3 (http://tree.bio.ed.ac.uk/software/figtree/).

2.15.7 Cross correlation of transcriptional upregulation.

Transcription qRT-PCR data was downloaded from the *E. coli* Gene Expression Database (GenExpDB) (https://genexpdb.okstate.edu/) by searching for "ymfM", selecting the download from the options and selecting all data. In total 855 experimental conditions were acquired for the e14 prophage. The normalized cross correlation for transcription levels of each pair of genes was calculated using the Correlation function in Mathematica (Wolfram). If we let x be the transcriptional ($\log_2$ fold change) data of one gene and y be the transcriptional ($\log_2$ fold change) data of the second gene, the normalized cross-correlation was given by:

$$\sum_{x,y} \frac{(x-\bar{x})(y-\bar{y})}{\sigma_x \sigma_y n}$$

Where $\bar{x}$and $\bar{y}$ are the means of x and y respectively, σ_x and σ_y are the standarddeviations of x and y respectively, and n is the number of transcriptional values.

Chapter 3. Validation of an *E. coli* over-expression screen

3.1 Introduction

Bacterial cell division is an essential process which is well conserved on a molecular level across all bacteria [1]. Playing an important role in the cell cycle, the proteins involved in forming and positioning the division apparatus have been extensively studied for most model bacteria and are relatively well characterized [7, 23]. The current understanding of cell division and its regulation has predominantly come from studies performed under standard laboratory conditions, which is nutrient rich and relatively stress free. Yet, *in situ*, bacteria occupy a multitude of environmental niches each with a range of variable and fluctuating conditions. This means that bacteria need to have the ability to adapt quickly when their environment changes in order to survive.

One mechanism used by bacteria to adapt to their surroundings is continuing to grow in the absence of division, thereby becoming filamentous. Bacterial filamentation is often associated with an aberrant unregulated response, but this idea underplays the carefully regulated process that underpins filamentation as a survival strategy in response to environmental pressures [3]. Ultimately, filamentation is an important biological mechanism which aids in the survival, pathogenesis and antibiotic resistance of several different bacterial species [3, 4, 82, 94, 98].

How bacterial cell division is regulated to ensure that two viable daughter cells are produced has been extensively studied in the model organism, *Escherichia coli*, [7, 75], under standard laboratory conditions. However, much less is known about how division is regulated under more realistic environmental conditions experienced by bacteria in

their natural habitats. For example, bacteria are able to filament under predation stress in the marine environment [89], during infection of the urinary tract [94, 95] and under antibiotic exposure [4], but the regulation of cell division and filamentation under these conditions is not well understood.

Regulators have been identified, that cause cells to become filamentous such as SulA which is activated as part of the SOS response [119, 121], DamX which is thought to be involved in the UPEC filamentation [126, 129], and several phage-encoded inhibitors [136, 137, 147, 150]. However, these regulators are not essential and filamentation is observed even in their absence [176-178]. In addition to this, given the many conditions in which filamentation is observed, it is likely that multiple, as yet unidentified, regulatory systems exist. This Chapter aims to identify some of these additional genes responsible for cell division inhibition.

To identify potential cell division regulators, a novel, high-throughput screening system was developed in our laboratory [163]. The screen involved the over-expression of an *E. coli* MG1655 shot-gun genomic library and the high-throughput sorting of live, filamentous clones via flow cytometry. The use of over-expression to identify novel genes, does not rely on creating the possibly many conditions that lead to filamentation but instead allows for the selection of genes that when expressed at high levels, will make cells filamentous.

This screen successfully recovered 22 reproducibly filamentous clones, which aligned to 12 distinct loci within the *E. coli* genome (Table 3.1). As expected, some of the genes

from these regions are known cell division genes, including *damX* [126, 127] and *hisH* [179], whilst the function of others including their role in inhibiting cell division are yet to be elucidated.

While the identification of several known regulators supported the veracity of the screening system, ultimately, uncharacterized genes potentially involved in cell division were of the greatest interest. Since these clones contained multiple genes (Table 3.1), the orientation of cloning, literature searches and preliminary bioinformatics was used to select one gene from each clone that did not encode known cell division regulators as likely candidates to cause filamentation. Specifically, these included the genes, *ycjY* (clone D2_3B), *ytfB* (clone D2_5G), *ymfM* (clone D1_8E) and *ykfI* (clone D2_8D) (Table 3.1).

Table 3.1. The genetic loci, clone name and genes present in each clone that caused filamentation from the original screen [163]

Genetic loci	Clone	Genes present
aroB-dam	D2-3D	*aro*B (273- 362/362)
		*dam*X
		dam (1-240/278)
yejH	D1-2H	*yej*H(1-461/573)
ycjY	D2-3B	*ycj*Z (207-1/299)*
		*ycj*Y
ytfA-ytfB	D2-5G	*ytf*B (34-212/212)
rplL-rpoB	D2-10F	*rpl*L
		*rpo*B (1-1227/1342)
Prophage e14	D1-8E	*ymf*L (142-185/185)
		*ymf*M
		oweE (1-92/234)
Prophage CP4-6	D2-8D	*yaf*W (85-105/105)
		*ykf*I
		*thr*W*
hisB-hisA	D2-7F	*his*B (226-355/355)
		*his*H
		*his*A (1-234/245)
Rac prophage	D1-5C	*Kil*
ppiA	D1-5F	*ppi*A
ppiC	D2-11E	*ppi*C
		*ilv*C (198-491/491)*
mutT-coaE	D1-9G	*mut*T (43-129/129)
		*yac*G*
		*yac*F*
		*coa*E*

Each clone contains multiple genes. Some of the open reading frames were partially cloned. These are indicated in brackets as the amino acid position followed by totally number of amino acid in the open reading frame. * indicates genes in the opposite orientation to the expression promoter.

Gene, *ykfI* is part of a toxin/antitoxin system encoded within the CP46-4 prophage region. This toxin shares 60% amino acid sequence homology to another *E. coli* toxin, CtbA (YeeV), which is known to inhibit cell division when over-expressed [138]. YeeV interacts with FtsZ as well as MreB, a cytoskeletal protein required for maintaining rod cell shape, causing a morphological change from rod to lemon-shaped cells [137]. Since YkfI shares sequence homology with YeeV, it is likely that it has a similar function when expressed and subsequently a similar mode of action. However, given that only a filamentous phenotype was observed in the over-expression screen, it is also possible that YkfI only acts to antagonise a component of the cell division machinery (i.e. FtsZ) and not proteins involved in maintaining cell shape (i.e. MreB).

A previous study found that over-expression of *yfkI* led to growth inhibition and reduction in colony forming units (CFU) [180], suggesting that the toxin may be inhibiting an essential component of the cell, thus reducing viability. However its involvement in cell division remains unknown. Interestingly, several toxin/antitoxin systems which inhibit cell division in *E. coli* are also located within prophages [137]. This raises an interesting ecological question about the role of these systems for prophages and how these are in turn benefitting the host cell biology.

The gene, *ycjY* is annotated as a predicted hydrolase of unknown function. This gene is part of an operon that encodes for murein peptide amidases (a type of hydrolase) [181]. Murein hydrolases are enzymes that degrade the peptidoglycan cell wall and are required for re-modelling and splitting of the cell wall during growth and cytokinesis [182]. This operon, is under the regulatory control of *pgrR*, which represses the expression of these

genes during steady-state cell growth [181]. However during a shift in environmental condition, to nutrient starvation [181] or nitrogen depletion [183], the transcription of *ycjY* increases, suggesting that the role of this hydrolase is to degrade the cell wall. This raises questions as to how this gene (if at all) is involved in giving a filamentous phenotype, and more work needs to be done to identify a potential mechanism.

Gene, *ytfB*, encodes a putative cell envelope opacity-associated protein. This is part of a protein family that is also found in *Haemophilus influenzae.* Expression of opacity-associated protein-A (OapA) in *H. influenzae* causes phase variation, resulting in transparent colony phenotype [184, 185]. This colony type contributes to the initial colonisation of the nasopharyngeal mucosal surface in a rat model but not for the subsequent infection [184]. However, this protein family, and in particular, YtfB, has not previously been identified to be involved in cell division, and therefore its potential mechanism in causing a block in division remains unknown.

Finally, the gene, *ymfM* encodes for a putative protein with no known function. It is part of the e14 element, which is a lambdoid-like prophage [155]. Previous studies of this prophage have reported that it contains an SOS-inducible cell division inhibitor called, SfiC, although the actual gene within the phage responsible for this function remains unknown [136, 154]. More recently, bioinformatics analysis of the structure and gene arrangement of the phage narrowed down the source of SfiC to either *ymfM* or *ymfL* [155]. Since the clone from which *ymfM* was identified also contained fragments of *ymfL*, further work needs to be done to determine whether *ymfM* is indeed SfiC, and how it may be acting upon the division machinery to inhibit division.

3.1.2 Chapter Aims and Objectives

It is not yet known if the four genes selected are responsible for the filamentation observed in the screen. This chapter therefore aimed to confirm whether these genes were responsible for the inhibition of division and to characterise their resulting filamentous phenotype. This was achieved by cloning individual open reading frames of the four genes into the expression plasmid, pBAD24. Genes of interest were induced to express and the degree of filamentation was compared to that of the original clones.

3.2 Results

3.2.1 Confirmation of genes from filamentous clones from shot-gun library responsible for cell division inhibition

The genes of interest were tested to confirm whether they were responsible for the filamentation observed in the original clones, by cloning the open reading frame into the expression plasmid pBAD24 in *E. coli* DH5*α*. Cells were induced for gene expression and microscopy was used to determine cell size (For methods refer to Chapter 2 Section 2.8 and 2.10). Cell length distribution of cells expressing the individual open reading frames were compared to the original clones to determination of whether expression of the individual genes of interest caused filamentation to a similar degree and were therefore responsible for the cell division inhibition. For simplicity, pBAD24 expressing the open reading frame of an individual gene will be referred to as gene ORF, and original clone from which the gene was identified will be referred to as gene clone for the remainder of this chapter.

Within this work, the term filamentation is used to define cell growth and DNA replication in the absence of cell division. In cells where the only effect is the complete inhibition of cell division, the cell length is expected to double for each division generation that would have otherwise occurred. This is measured by observing a shift in the mean cell length from one population to another (induced vs. un-induced). As the screen was run over four generations, complete inhibition of division would lead to a 16-fold increase in mean cell length, assuming that the growth rate was not affected. A growth curve of wild-type *E. coli* harbouring pBAD24 grown in LB at 37ºC was used to determine generation time.

A vector only control was included to ensure that the expression of an empty vector alone was not enough to cause filamentation, as well as to give a cell length range for a short cell population. In Figure 3.1, cultures expressing empty plasmid, pBAD24, ranged from approximately 2 μm to 10 μm, with the exception of one cell at 12 μm. Phase-contrast showed that these cells were not filamentous (Figure 3.1). Therefore, a filamentous cell was defined as being greater than 10 μm in cell length.

Over-expression of the predicted hydrolase gene, *ycjY* (*ycjY* ORF) resulted in a mixed population of short (less than 10 μm) and long cells (greater than 10 μm) (Figure 3.1, Row 3). Overall there was an increase in mean cell length to 7.6 ± 4.0μm, which represents a 1.9 fold increase compared to glucose repressed cells (4.0 ± 1.1 μm) (Table 3.2). This was similar to the *ycjY* clone (Figure 3.1, Row 2,) with a mean cell length of 7.4 ± 5.4μm.

The growth rate of the *ycjY* ORF under arabinose induction was effectively identical to that of cells under glucose repression (Figure 3.3C), as well as the pBAD24 control (Figure 3.3A). This was also the case for the *ycjY* clone. This result shows that the expression of *ycjY*, either as the only gene present, or as part of the original clone, does not affect growth rate.

Over-expression of the toxin gene, *ykfI (ykfI* ORF) did not result in an increase in mean cell length, with average cell lengths of 4.1 ± 1.5 μm for the induced sample as compared to 3.8 ± 1.2 μm for un-induced (Table 3.2). However, the *ykfI* clone did increase in cell length (10.8 ± 5.9μm) (Table 3.2).

Upon sequencing of pBAD24 containing the *ykfI* ORF, a mutation was detected, which changed the stop codon (TGA) to a tryptophan (TGG). This change in nucleotide

sequence resulted in the addition of another 78 base pairs to the end of the gene before the next stop codon (TGA) was detected. To ensure that the mutation was not due to an error in cloning, *ykfI* was re-cloned into pBAD24. After colony PCR confirming insertion of the gene, 20 clones containing *ykfI* were screened for filamentation. None resulted in filamentation or lemon-shaped cells, a characteristic observed in the *ykfI* homolog, *cbtA* [137]. These clones were not sequenced to check whether the same mutation was present.

The growth rate of the mutant *ykfI* ORF induced cells was identical to that of cells under glucose repression (Figure 3.3 B). The *ykfI* clone also grew similarly to repressed samples, even though some filamentation (2.7 fold increase) was observed in this population.

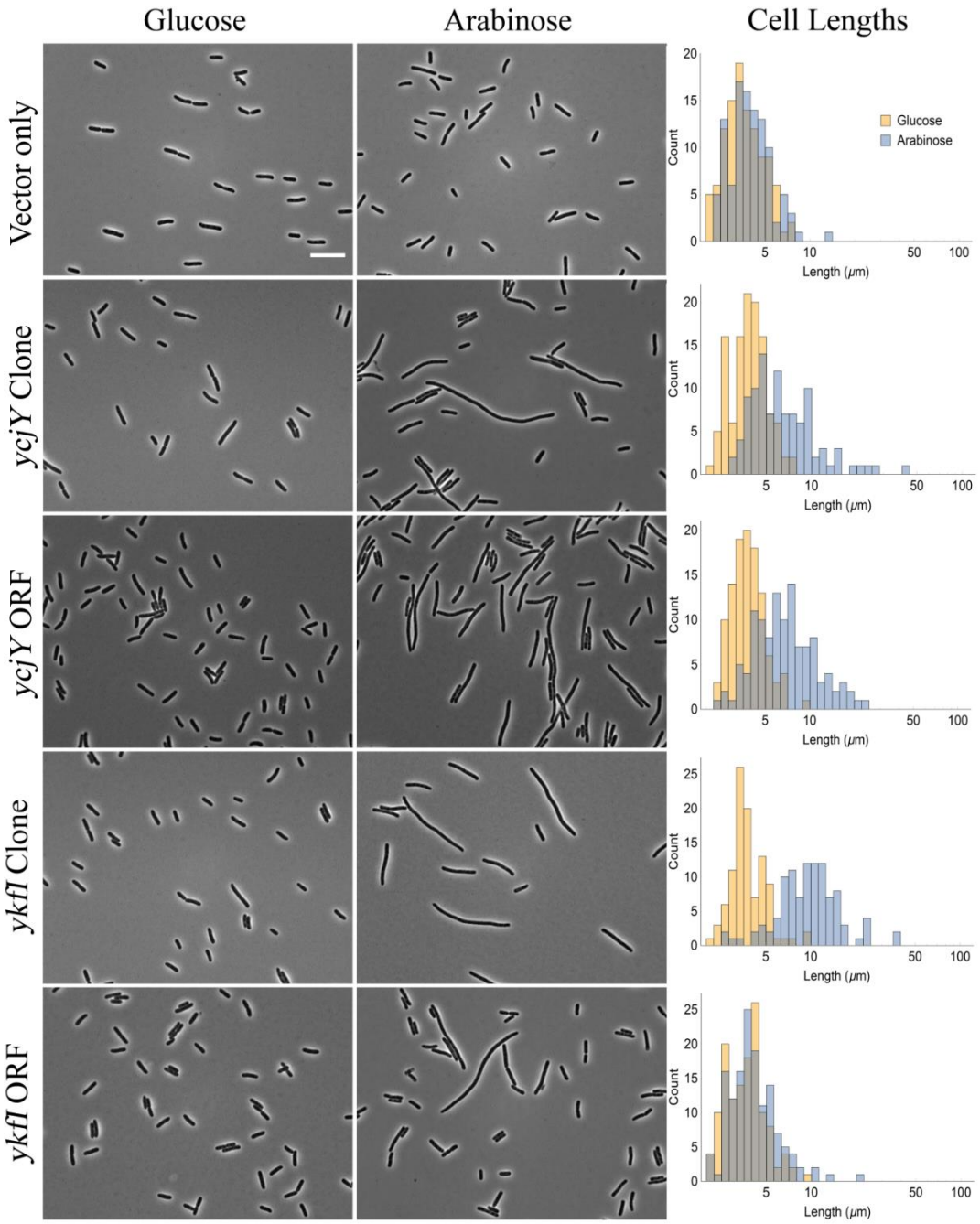

Figure 3.1.Cell length distribution of the over-expression of genes *ycjY* and *ykfI* in DH5a.

Top panel shows the empty vector, pBAD24, grown under 0.2% glucose repression (left) and 0.2% arabinose induction (middle). A comparison of the cell length distribution of the repressed and induced populations is overlayed in a histogram (right). Second panel, shows the original clone from screen containing the gene *ycjY* (*ycjY* clone). Third panel shows the open reading frame of gene the *ycjY* (*ykfI* ORF). Fourth panel, shows the original clone from screen containing the gene *ykfI* (*ykfI* clone). Fifth panel, shows the open reading frame of the gene *ykfI* (*ykfI* ORF). These histograms are representative of one biological replicate. This experiment was done twice, with similar trends observed. At least one hundred cells were counted per sample. Scale bar = 10μm

Over-expression of the phage gene, *ymfM* (*ymfM* ORF) resulted in an almost complete inhibition of division, with a homogenous filamentous population (Figure 3.2, Row 3). This cell length (57.3 ± 19.8µm) was greater than the mean cell length seen in the *ymfM* clone (Figure 3.2, Row 2) of 10.6 ± 6.8µm (Table 3.2). The induced mean length of 57.3 µm was 14.5 times the repressed mean of 4.0 µm (Table 3.2), which is close to the expected 16-fold increase for complete inhibition.

Observation of the growth rate of *ymfM* ORF under arabinose induction showed that while initially cells grew at the same rate as glucose repressed population, growth was inhibited after 100 minutes, with no further growth observed for the remainder of the growth assay (Figure 3.3 D). Interestingly, the *ymfM* clone, continued to grow similarly to the glucose repressed population for a little over 3 hours before growth stopped.

Over-expression of the *ytfB* ORF also gave rise to an increase in cell length (Figure 3.2, Row 5), with majority of induced cells being filamentous (34.6 ± 16.8 µm) (Table 3.2). Expression of the *ytfB* ORF gave a greater increase in cell length (9.1 fold) than the *ytfB* clone (1.8 fold) (Table 3.2).

The growth rate of *ytfB* ORF under arabinose induction revealed that, similar to the *ymfM* ORF, growth was initially comparable to cells grown under glucose repression (Figure 3.3 E). After two hours however, cell growth was inhibited and remained stationary for the rest of the assay, as was the case for *ymfM*. Unlike *ymfM* though, the *ytfB* clone, continued to grow exponentially and at a similar rate as the glucose repressed samples.

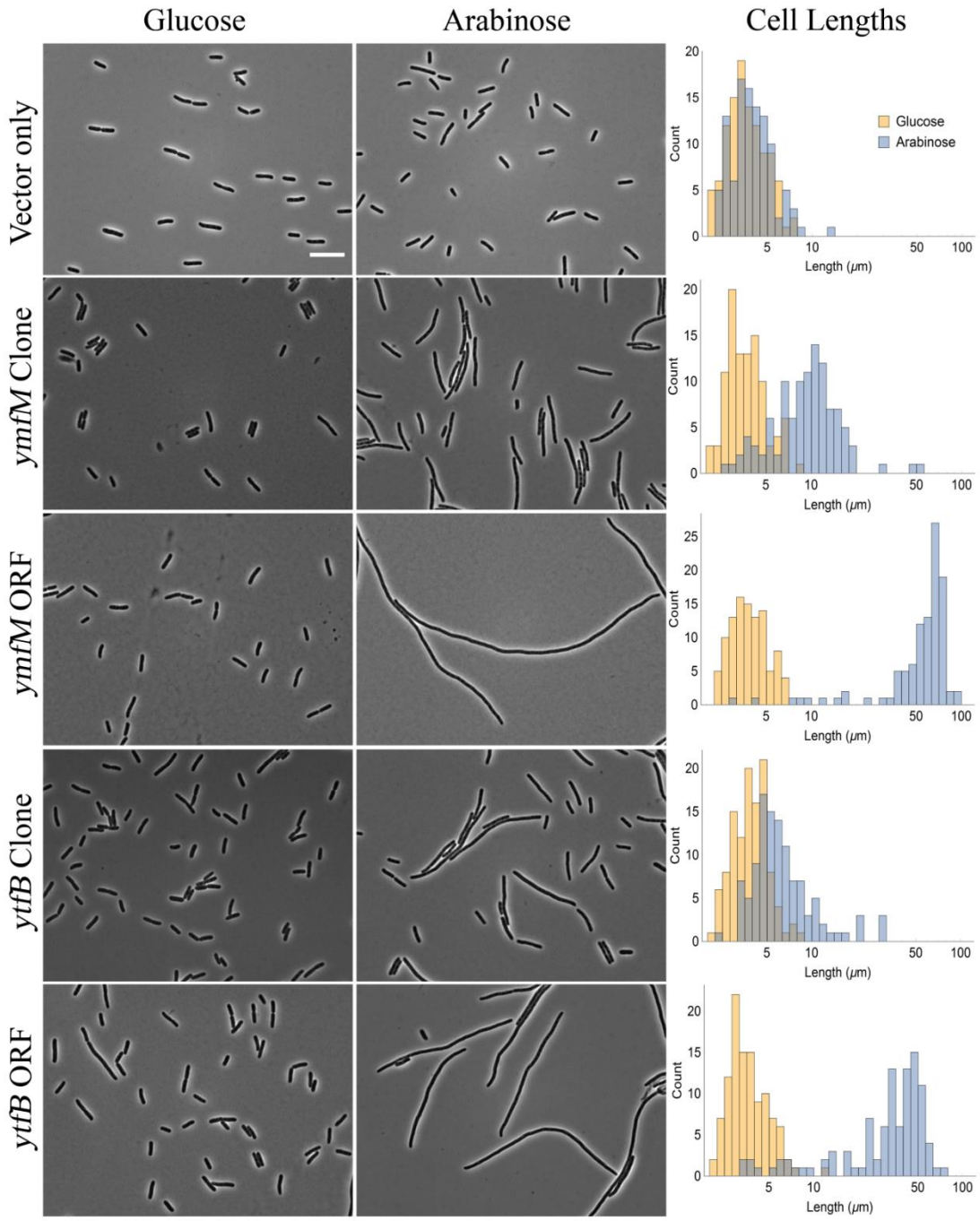

Figure 3.2.Cell length distribution of the over-expression of genes *ymfM* and *ytfB* in DH5a.

Top panel shows the empty vector, pBAD24, grown under 0.2% glucose repression (left) and 0.2% arabinose induction (middle). A comparison of the cell length distribution of the repressed and induced populations is over-layed in a histogram (right). Second panel, shows the original clone from screen containing the gene *ymfM* (*ymfM* clone). Third panel shows the open reading frame of gene the *ymfM* (*ymfM* ORF). Fourth panel, shows the original clone from screen containing the gene *ytfB* (*ytfB* clone). Fifth panel, shows the open reading frame of the gene *ytfB* (*ytfB* ORF). These histograms are representative of one biological replicate. This experiment was done twice, with similar trends observed. At least one hundred cells were counted per sample. Scale bar = 10μm

Table 3.2. Mean cell length and fold increase of length, of genes of interest and their original clones under repression (0.2 % glucose) and induction (0.2% arabinose).

	Mean Cell Length (μm) (±S.D)		Fold Increase
	Glucose	Arabinose	
pBAD24	3.8 (±1.2)	4.2 (±1.5)	1.1
ycjY Clone	4.0 (±1.1)	7.4 (±5.4)	1.9
yjcY ORF	4.0 (±1.1)	7.6 (±4.0)	1.9
ykfI Clone	3.9 (±1.2)	10.8 (±5.9)	2.7
ykfI ORF	3.8 (±1.2)	4.1 (±1.5)	1.1
ymfM Clone	3.8 (±1.3)	10.6 (±6.8)	2.8
ymfM ORF	4.0 (±1.1)	57.3 (±19.8)	14.5
ytfB Clone	4.0 (±1.2)	7.3 (±5.2)	1.8
ytfB ORF	3.8 (±1.4)	34.6 (±16.8)	9.1

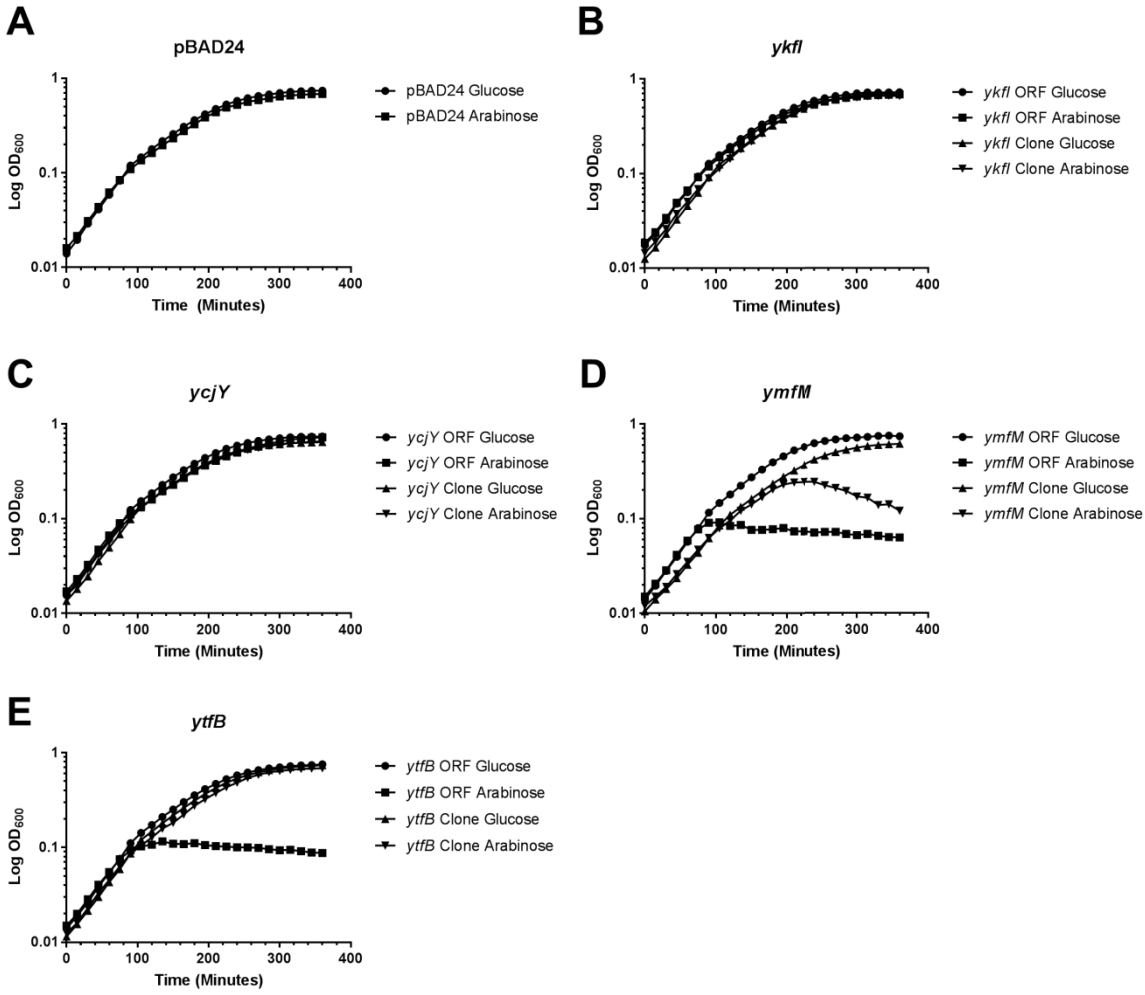

Figure 3.3.Growth curve comparing the growth of individual ORF and their original clones

Open reading frames of genes and the original clones from which they were identified were grown to mid-exponential phase. Samples were diluted and grown for 6 hours under arabinose induction or glucose repression. Optical density (OD) was plotted on a log scale against time in minutes. Empty vector control (A) showed growth was not affected by glucose or arabinose. Panel, (B) shows growth of *ykfI*, (C) of *ycjY*, (D) of *ymfM*, and (E) of *ytfB*

3.3 Discussion

From a recent over-expression screen, several potential candidates for cell division inhibition in *E. coli* were identified. This chapter aimed to confirm the genes from this over-expression screen responsible for the inhibition of division resulting in filamentation when expressed. These included the genes, *ycjY*, *ykfI*, *ymfM* and *ytfB*.

To validate the gene responsible for filamentation, the fold increase of average cell length of cell expressing the ORF was compared to the original clone. As the screen was run over four generations, complete inhibition of division would have theoretically led to a 16-fold increase in the mean cell length. Clones with phenotypes where a large proportion of cells were less than 10μm were considered to be within the normal range of cell size as the cell length distribution of DH5α expressing empty vector pBAD24, ranged from 2 - 10μm (Figure 3.1, Row 1).

Initial over-expression of the clones and individual genes studied here displayed varying degrees of change in cell size, ranging from 1.8 to 14.5 fold increase in average cell length. Of the four genes examined, over-expression of *ymfM* ORF and *ytfB* ORF had the greatest effect of division inhibition (Table 3.2).

The over-expression of the *ycjY* ORF gave a rise to a population of varying cell lengths (Figure 3.1, Row 3). While there was a change in the distribution of cell lengths, the inhibition of division was not prominent. The average cell length of the original clone as compared to the gene only, when expressed was very similar, suggesting that the filamentation observed, albeit slight, was due to the expression of *ycjY*.

The growth rate remained the same as glucose repressed samples (Figure 3.3 C), suggesting that the expression of the gene did not have an adverse effect on growth rate. If the lack of degree of filamentation was due to slow growing cells, this would have been seen in a reduction in growth rate of the arabinose induced sample. However this was not the case and the population was able to grow exponentially due to division events occurring.

Since *ycjY* is a predicted hydrolase, it is most likely not interacting with FtsZ directly, but may be having an indirect effect on division by affecting changes in peptidoglycan synthesis. Peptidoglycan synthesis either during elongation or septation occurs by the coordination of murein synthases and hyrdolases to allow for the insertion of new material. Disruption of this balance can lead to cell lysis [186]. Since no change in the growth was observed, expression of *ycjY* may not be enough to cause cell lysis, but is enough to cause a disruption to the balance of peptidoglycan synthesis and hydrolysis leading to slight increase in cell length.

At this stage, without any more experimental evidence, it is difficult to understand how division, albeit slightly, is being inhibited. Microscopy of the fluorescently tagged protein, may determine whether it localizes to the septal wall or along the length of the cell. Furthermore, inhibition of cell wall synthesis occurs independent to Z ring formation. As a result, if YcjY is causing filamentation via septal wall inhibition, Z rings would be present in the filamentous subpopulation. Since the degree of filamentation was not sufficient be considered filamentous, this gene was not studied further.

The toxin gene, *yfkI*, shares homology to toxin YeeV (CbtA), known to cause cells to become lemon-shaped by interacting with FtsZ and MreB [137]. It was initially

hypothesized that YkfI was acting to only antagonise FtsZ and not MreB as only filaments were observed in the over-expression screen. The expression of the *ykfI* ORF did not cause filamentation. This was an unexpected result as the literature evidence suggested that *ykfI* targets cell division [138], and an increase in cell length from the *ykfI* clone albeit slight (10.8 ± 5.9 μm), was also observed (Figure 3.1). Sequencing of the clone revealed a mutation within the coding region of the gene, which was a possible cause for the lack of phenotypic change. Re-cloning and their subsequent screening did not result in filamentation or lemon-shaped cells.

The lack of phenotype from the over-expression of the *ykfI* ORF is in contrast to recent published work by, Wen et al, 2017 [187], who reported a lemon-shaped morphology after the expression of *ykfI*. Similar to what was seen in this chapter they also observed slight filamentation during co-expression of *ykfI* and *yafW*, although this was not quantified. Furthermore, through a bacterial two-hybrid assay, the study showed an interaction with FtsZ, but not the cytoskeletal protein, MreB.

The difference in the ability to observe a phenotype from the expression of *ykfI* ORF could have been due to the selection of suppressor mutants during the cloning process. YkfI has been previously reported to be lethal with a reduction in colony forming units [180]. It is possible that any leaky expression from pBAD24 was resulting in the generation of suppressor mutants, as a means to overcome the toxic nature of the gene. The original clone, from which *ykfI* was isolated displayed a filamentous sub-population when expressed (Figure 3.1). Co-expression of the antitoxin, *yafW*, is reported to help reduce the lethality of the toxin by acting to prevent the translation of the protein or promoting its degradation [180]. The presence of *yafW* in this clone (although in partial

sequence), was likely reducing lethality and therefore allowing for the partial function of the toxin gene resulting in slight filamentation from the *ykfI* clone.

In contrast to the system used in this study, Wen *et al* [187] used an IPTG inducible plasmid, pCA24N [188], under the tight repression by the laqI^q gene. It is probable that pCA24N was better suited for selecting clones without generating suppressor mutations. As well as this, lemon-shaped cells were observed after 4 hours of pCA24N-*ykfI* expression [187], while *ykfI* ORF expression in our study was done for only 2 hours. There is a chance that expression of some of the re-cloned plasmids may have caused lemon-shaped cells if the experiment was conducted for longer. However, since these re-cloned plasmids were not sequenced, it is difficult to conclude whether the lack of phenotype was due to mutations or insufficient expression time. *YkfI* was not pursued further as other candidates, such as *ymfM* showed stronger filamentous phenotypes.

Expression of *ytfB*, showed a clear inhibition of division, resulting in filamentous cells (Figure 3.2, Row 5), with a 9-fold increase in cell length. This inhibition also led to the eventual cessation of cell growth. The growth rate of *ytfB* under arabinose was identical to that of the glucose repressed cultures until 100 minutes, after which it remained stationary (Figure 3.3 E). The plateau was not due to nutrient exhaustion, as the density of the glucose repressed samples continued to increase. It is possible that over-expression of *ytfB* is affecting the cells by disrupting cell division as well as other cellular processes.

What is interesting is that the original clone continued to grow exponentially, at the same rate as the glucose repressed samples (Figure 3.3). The average cell length of this sample was 7.32 μm, below what was considered to be physiologically relevant inhibition. The only ORF present in this clone was a partial *ytfB* gene. This rescue in growth rate as well

as the reduced cell size of the expressed population indicates that the missing 33 amino acids of the YtfB protein may be important for its ability to inhibit cell division. While YtfB does not share homology to previous known cell division inhibitors, it does share homology to OapA from *H. influenza* [184]. OapA contains a LysM-domain. Prokaryotic proteins containing LysM-domains are able to bind bacterial peptidoglycan [189, 190]. While there is no experimental evidence, it is possible that YtfB is recruited to the septal peptidoglycan via its LysM-domain to exact inhibition of division.

The *ymfM* gene is part of the e14 prophage, which contains an SOS-inducible cell division inhibitor gene called *sfiC*, and the location of *sfiC* has been narrowed down to *ymfM* or *ymfL* through bioinformatics analysis of the phage [136, 155].

Expression of *ymfM* showed the greatest fold increase in mean cell length (14.5 fold-increase) as compared to the other genes tested. This shift was close to the theoretical value for complete repression of cell division (16 fold), suggesting that YmfM is able to efficiently inhibit cell division, whilst not affecting growth rate initially. It is likely that the over-expression of *ymfM* and extensive filamentation is eventually affecting cell growth.

It is interesting that the expression of the original clone took a little longer for the cessation of cell growth. This clone along with the full sequence of *ymfM*; contains partial sequence of *ymfL* and *oweE*, genes adjacent on either side of *ymfM*. While further experimental work would be needed, this slight rescue in growth rate may be due to interactions of one or both of the products of these genes with YmfM.

Expression of *ymfM* and *ytfB* gave the strongest filamentous phenotype from the four genes tested. For *ymfM* the shift in the cell length mean was very close to the theoretical

value of a 16 fold increase (14.5 fold). Over-expression of *ymfM* is able to robustly inhibit cell division, as the occurrence of occasional division would reduce the degree of filamentation. YmfM became the main focus of this PhD research, as not only did it cause a strong filamentation effect, but the literature evidence implied that it was potentially an alternative cell division inhibitor during the SOS response [136]. The inhibition of division by SulA during an SOS response, is well characterised. The fact that other system(s) exist that may contribute to the filamentation seen, was of great interest, and explored further in this work.

Chapter 4. The biological role of YmfM: a potential role in the SOS response

4.1 Introduction

In the previous chapter, Chapter 3, *ymfM* was identified as a potential novel cell division inhibitor, as over-expression from an inducible plasmid caused cells to become filamentous (Chapter 3, Figure 3.2). In this chapter the biological role of *ymfM* is explored. In particular, whether *ymfM* plays an active role in inhibiting cell division during the SOS response is investigated. In a previous study, a novel SOS inducible cell division inhibitor, SfiC, was identified to be encoded somewhere within the e14 prophage [136, 154]. It currently unknown whether *ymfM* encodes for *sfiC* and is responsible for the inhibition of division during the SOS response. The introduction to this chapter will first give an overview of the SOS response in *E. coli* as well as the induction of prophages during the response. This is followed by an overview of the e14 prophage and previous works characterising SfiC.

4.1.1 The SOS Response

The SOS response is a regulatory system which is widespread within bacteria. Its primary function is to detect, and repair DNA damage during cellular stress. The classic example of stress is DNA damage, resulting in single-stranded DNA (ssDNA) breaks. DNA damage can result from exposure to stressors such as oxidative stress, antibiotics or UV exposure [111]. An important feature of the SOS response is the delay of the cell cycle, including the inhibition of division [116]. This inhibition gives the cell sufficient time to repair any DNA damage before committing to producing the two daughter cells, preventing potential deleterious effects.

The regulation of the SOS response is governed by two regulatory proteins which control its suppression and activation [112, 113]. During normal cell growth, the transcriptional regulator, LexA represses over 40 genes in *Escherichia coli*, known as the SOS regulon [114]. This is achieved by LexA dimers binding to consensus DNA targets, with a specific palindromic sequence known as the LexA- or SOS-box [191]. Upon DNA damage, RecA activates the SOS response by binding to ssDNA breaks forming a RecA-DNA filament, also known as activated RecA (RecA*) [192]. RecA* stimulates the auto-proteolytic cleavage of LexA resulting in the de-repression of LexA controlled genes and activation of the SOS regulon [193-195].

Not all LexA controlled genes are switched on at the same time or extent in response to stress. LexA binds to SOS-boxes with different affinities depending on the number and location of the boxes relative to the promoter [114, 196]. As a result some genes are induced early and other are induced only when DNA damage is severe. In addition to this, the SOS response also occurs in a pulse-like pattern and as the response progresses, or more DNA damage occurs, the number of pulses increases [197]. This suggests that SOS genes undergo multiple rounds of induction to deal with DNA damage [198]. Together this helps determine the timing of when the different LexA controlled genes are expressed as appropriate for the level of damage being sensed. That is, some genes will be expressed during early or low levels of SOS induction and others would require a higher level of damage before expression.

Genes under the control of LexA are mainly involved in DNA repair, mutagenesis and arrest in cell division [111]. Of these, the gene encoding SulA is responsible for the cell division inhibition during this time. The presence of SulA leads to filamentous cells, as it directly interacts with the essential cell division protein, FtsZ [117] and prevents the polymerisation of FtsZ into a Z-ring [55, 119]. Once DNA damage is repaired, LexA repression is re-established and FtsZ polymerisation and cell division resumes.

4.1.2 Induction of prophages during SOS

The SOS response can also trigger prophage induction. While integrated into the chromosome, phage DNA is maintained under lysogeny, a repressed state preventing the expression of lytic genes. This state of the phage is known as a prophage. Induction of the prophage results in expression of genes needed for lytic growth and production of viral particles. Repression of prophages of the common lambdoid type occurs via a LexA-like protein called the CI-repressor (CI). CI is responsible for maintaining the lysogenic cycle of phage, preventing it from inducing lysis unnecessarily. Structurally, CI is similar to LexA as it shares homology to the carboxyl-terminal domain of LexA, and is able to interact with RecA*, inducing auto-cleavage [199]. RecA* binds CI at a much slower rate than LexA, and as a result, cleavage of the CI-repressor and prophage induction occurs much later in the SOS response, when the DNA damage is severe [114, 200] .

E. coli K-12 contains nine cryptic prophages. They are called cryptic because they are defective and no longer able to undergo the lytic cycle. It is currently unclear whether genes encoded within these prophages play an active role in *E. coli* during the SOS

response or if their induction is remnants of a once active phage. Two genes in particular, KilR of prophage Rac and DicB of prophage Qin, both cell division inhibitors, have been shown to be induced during antibiotic treatment and their expression aids in resistance [153]. This raises an interesting question of whether these division inhibitors are contributing to the inhibition of division observed during the SOS response.

Precedent exists for prophage genes aiding in the function of host systems. Many prophages can be beneficial to bacteria, encoding virulence factors, toxins, restriction modification systems, antibiotic resistance proteins and contribute to overall bacterial fitness [153, 155, 201]. Cryptic prophages in *E. coli* have been shown to be beneficial in various environments, including osmotic, oxidative and acid stress, biofilm formation and tolerance to antibiotics [153].

4.1.3 The e14 prophage of *E. coli*

One of the nine cryptic prophages contained within *E. coli* K-12 is the e14 prophage. This prophage is integrated within the *icd* gene on the chromosome, and shares lambdoid phage ancestry (Figure 4.1) [155, 161, 202]. The phage has had three major losses of genes in its genome, disabling its lytic cycle [155]. Instead this phage is able to excise as a circular DNA fragment upon induction of an SOS signal [203, 204]. The presence of the e14 prophage has been shown to be beneficial, enhancing biofilm formation and increasing the resistance to acid stress [153].

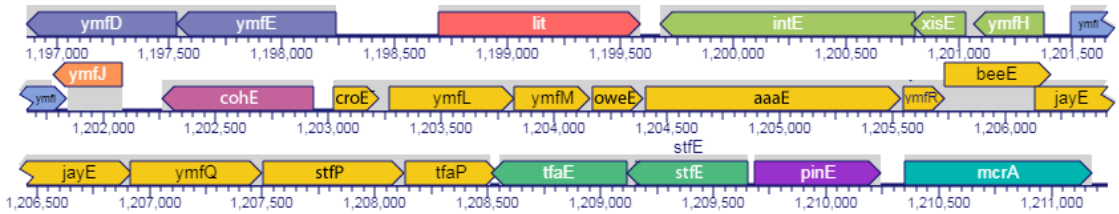

Figure 4.1. A schematic diagram showing the gene arrangement of the e14 prophage

The e14 prophage is inserted on to the chromosome in a site specific manner, within the *icd* gene. Gene *ymfM* is predicted to be encoded in an operon (yellow) with 10 other genes. The lysogenic/lytic switch of the phage is thought to be encoded by genes *cohE* (CI-repressor like) and *croE*.

4.1.4 Identification of another SOS-induced cell division inhibitor, SfiC:

The e14 prophage contains a SOS-inducible cell division inhibitor, SfiC. SfiC was first described in 1983 by D'Ari *et al.,* although they were not able to identify the exact location of this system within the *E. coli* genome [136]. It was later identified to be encoded somewhere within the e14 prophage region [154].

D'Ari *et al*, identified this system by the genetic induction of the SOS response, through the use of a temperature sensitive mutant, *recA441,* also known as *recA-tif*. In this RecA mutant, there are two amino acid substitutions, E38K and I298V [171]. The E38K mutation causes the constitutive expression of RecA441 and therefore the SOS response and, I298V is responsible for its temperature-dependent activation. As such, RecA is activated at the non-permissive temperature of 42^{o}C, thereby inducing the SOS response and filamentation without the need for external means to DNA damage.

D'Ari *et al.* [136] found that even in the absence of the *sulA* gene*,* cells were able to filament when *recA441* was induced, suggesting that this mutant strain of *E. coli* contained another cell division inhibitor which was also activated by the SOS response. As the authors could not locate the exact gene responsible for the filamentation response, they called it the SfiC^{+} phenotype. Filamentation by SfiC was only observed in a *recA441 sulA*-minus background grown at 42^{o}C, when SOS is induced, and no filamentation by SfiC was observed at 42^{o}C in a wild-type *recA*, *sulA*-minus background when SOS is not being induced. From this the authors concluded that the inhibition of division by SfiC was part of the SOS response.

The genetic characterisation of *sfiC* revealed that while it was induced by *recA441*, *sfiC* was not under the repression of LexA. The *lexA(Ts)* mutation causes a temperature dependent inactivation of the LexA repressor and would result in any genes controlled by it to be de-repressed. D'Ari *et al* showed that cells containing *sfiC* did not filament during expression of *lexA(Ts)*, suggesting that it did not require LexA. As mentioned previously, phages contain their own repressor systems, which are LexA-like in nature, and bind to RecA*. The gene *cohE* from e14, is a CI-like repressor, similar in sequence to other bacteriophage CI repressors that are responsive to an SOS signal [155]. As such, it is possible that expression of *sfiC* is regulated by *cohE*.

As well as identifying *sfiC*, D'Ari *et al* [136] were the first to show that FtsZ was most likely the target of both SulA and SfiC. When *sulA* was expressed in an *ftsZ* mutant, *sfiB114*, cells were resistant to effects of SulA. Similarly, mutant *sfiB114* cells did not filament in the presence of SfiC, indicating that like SulA, SfiC inhibited division by targeting FtsZ. However, the filamentation caused by SulA is reversible after recovery from SOS induction, and SfiC-induced filamentation is not[205]. SfiC causes a loss in viability and this might be attributed to the fact that its inhibition of division is irreversible as cells are unable to re-divide and propagate.

In summary, prophages are induced during the SOS response. The e14 prophage has a CI-like repressor suggesting that it is responsive to SOS stimuli. Prophages can encode cell division inhibitors. It has been proposed that e14 has a cell division inhibitor induced by SOS, and it is likely to be under the control of the CI-like repressor. It remains an open question as to which gene from the e14 prophage is responsible for the cell division inhibitory function. Genetic bioinformatics analysis of the arrangement of the phage has

narrowed down this gene to either *ymfL* or *ymfM* [155].Given that this gene is likely up-regulated during an SOS response, it is possible that environmental conditions exist in which it actively contributes to cell division inhibition.

4.1.5 Chapter Aims and Objectives:

The overall aim of this chapter was to understand the biological role of SfiC during the SOS response. This was achieved by first determining whether *ymfM* was the previously identified SfiC. The exact gene responsible for the SfiC phenotype has not been determined but is thought to be encoded by either *ymfL* or *ymfM*. Based on the work presented in Chapter 3, it was hypothesised that YmfM was responsible for the cell division inhibition by SfiC. To confirm this, *ymfL* was cloned and over-expressed to determine if it also resulted in filamentation.

It was next investigated whether *ymfM* could inhibit division during genetic activation of RecA. This was done by expressing mutant *recA, recA441* from an inducible-plasmid, and observing the changes in the degree of filamentation when expressed in strains carrying mutations Δ*ymfM* or Δ*sulA*, and the double-mutant Δ*sulA*Δ*ymfM.* If, in the absence of *ymfM*, cells do not filament as effectively, this would suggest that *ymfM* directly contributes to filamentation during the SOS response.

Finally, the environmental cue inducing the SOS response in which YmfM is needed to inhibit division was explored. This involved inducing SOS using the antibiotic norfloxacin, a fluoroquinolone, known to induce the SOS response [108, 206]. The degree of filamentation response in strains Δ*ymfM*, Δ*sulA* and Δ*sulA*Δ*ymfM* was determined.

4.2 Results

4.2.1 Determining the gene responsible for the *sfiC* phenotype

The e14 prophage contains an SOS-inducible cell division inhibitor, *sfiC*, however the exact gene responsible remains unknown [136, 154]. Analysis of the genome arrangement of the phage and the operon which *ymfM* is a part of, identified that either *ymfL* or *ymfM* were the likely genes responsible for the *sfiC* phenotype [155]. Furthermore, in the over-expression screen that formed the basis of this thesis [163], the DNA fragment containing *ymfM* also contained a partial fragment of the *ymfL* gene. Experimental evidence presented in Chapter 3 showed that when *ymfM* was expressed from an inducible system, filamentation was observed and therefore it is most likely the gene responsible for the *sfiC* phenotype. However, this does not eliminate the possibility that *ymfL* is also acting as a cell division inhibitor and contributing to the phenotype.

To test whether over-expression of *ymfL* was capable of inhibiting division, the gene was cloned into pBAD24 and induced to express. As a positive control for proper induction conditions, *ymfM* was also over-expressed from pBAD24 alongside pBAD-*ymfL*. After two hours of over-expression in 0.2% arabinose, no filamentation was observed (Figure 4.2), showing that of the two genes, *ymfM* is solely responsible for the filamentation phenotype.

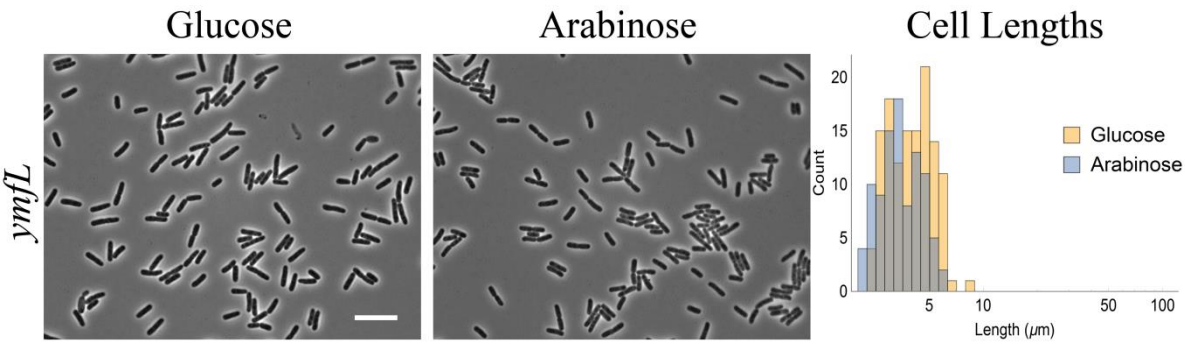

Figure 4.2. Cell length analysis of the over-expression of *ymfL* in *E. coli*

The open reading frame for *ymfL* was cloned into expression plasmid, pBAD24, and was grown under 0.2% glucose repression (left image) and 0.2% arabinose induction (centre image) for two hours. Images on the left and centre were acquired using the Ziess Axioplan microscope at 100x magnification under phase contrast. At least one hundred cells were measured from each population and represented as an overlayed histogram on the right. Count refers to cell count. Scale bar = 10μm

4.2.2 YmfM is involved in the inhibition of division during the SOS response genetically induced by RecA:

From the previous experiment, it is now clear that *ymfM* is likely the previously identified SfiC and should therefore be an SOS-inducible cell division inhibitor independent of SulA. D'Ari *et al.*[136], showed that in the absence of both *sfiC* and *sulA*, cells were unable to filament during *recA441* induction. To show that this could be reproduced with *ymfM*, *recA441* was cloned into pBAD24. This resulted in the plasmid, pBAD-*recA441*. The use of a plasmid based system eliminated the need to generate *recA441* mutations in multiple background strains. Furthermore, the use of mutant *recA* over WT *recA* was

favourable as plasmid expression of wild-type *recA* is unable to elicit an SOS response [207]. Plasmid pBAD-*recA441* was transformed into strains lacking functional copies of either *sulA* or *ymfM* alone, or both.

When induced, *recA441* caused filamentation as expected in a wild-type *E. coli* (BW25113) background after two hours of induced growth (LB supplemented with 0.2% arabinose, 100 µg/mL adenine, at 42ºC). Adenine was added as it has been reported to enhance RecA441 activity [167]. As seen in Figure 4.3, there was an increase in average cell size from 3 μm^3 (un-induced) to 15 μm^3 (induced), as determined by the Coulter counter, compared to the wild-type (short) cell size distribution.

To analyse the cell size distribution a cross correlation was performed to determine how similar the distribution of cell size was between the strains (Table 4.1). A value of 1 indicates that the two distributions being compared are highly correlated and are therefore highly similar. A value of 0 is un-correlated and -1 being perfectly anti-correlated.

The absence of *ymfM* did not affect the degree of filamentation, as the Δ*ymfM*+ pBAD-*recA441* cell distribution (Figure 4.3, green line) was very similar to that of the wild-type + pBAD-*recA441* (Figure 4.3, yellow line) and had a cross correlation of 0.96 (Table 4.1). In the absence of *sulA*, less filamentation was observed as the population shifted toward a shorter cell size distribution (Figure 4.3, red line). This cross correlation comparing wild-type + pBAD-*recA441* and Δ*sulA* + pBAD-recA*441* was 0.62. Finally, cells deleted of both *ymfM* and *sulA* (Figure 4.3, purple line), caused the greatest shift in cell size distribution towards the shorter wild-type population (Figure 4.3, blue line). The short

cell population of wild-type expressing pBAD24 was more correlated with *ΔsulAΔymfM* + pBAD*recA441* than ΔsulA + pBAD-*recA441* (0.62 and 0.22 respectively). While this shift was the greatest, it did not lead to a full recovery to a short cell population. The difference in cell length was not due to a reduction in growth rate, which was similar in all strains tested.

This experiment was repeated again, and the mutant strains showed a similar relationship (Figure S.4). That is the absence of *ymfM* was similar in its cell length distribution to wild-type, while the absence of *sulA* alone was enough to show a lesser degree of filamentation. Again, the absence of both *sulA* and *ymfM* showed the greatest shift towards the shorter cell population as compared to Δ*ymfM* and Δ*sulA* alone.

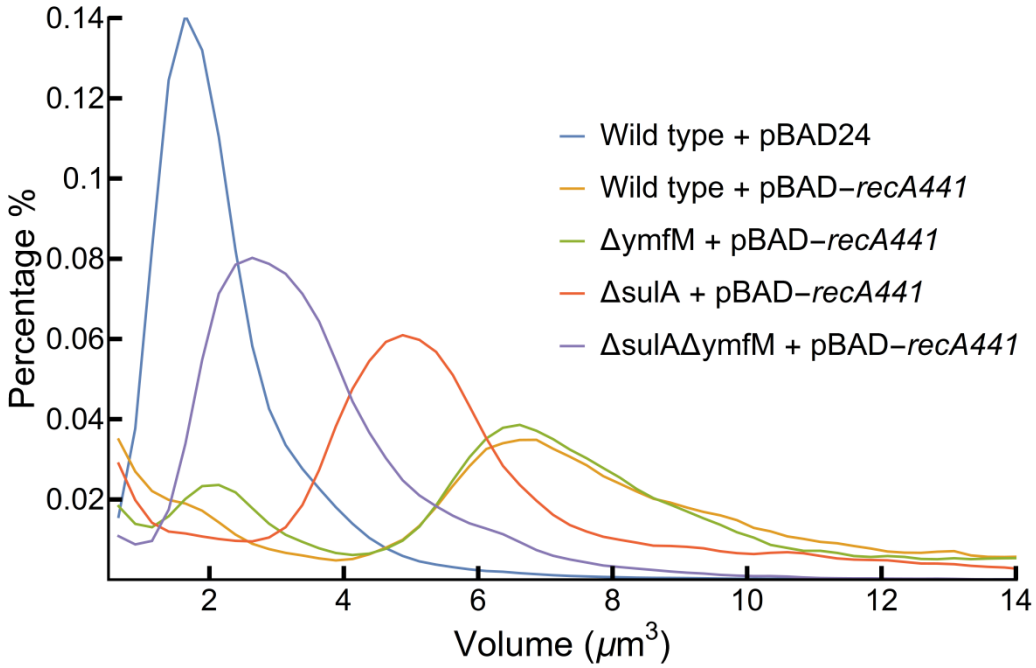

Figure 4.3. Cell volume distribution of WT, Δ*ymfM*, Δ*sulA*, and Δ*sulA*Δ*ymfM* after genetic induction of the SOS response by a temperature-sensitive recA mutant, *recA441*.

Coulter counter analysis of cell size distribution of wild-type (yellow),Δ*ymfM* (green), Δs*ulA*(red), and Δs*ulA*Δ*ymfM* (purple) after two hoursofpBAD-*recA441* induction in LB with 0.2% arabinose and 100 µg/mL adenine, at 42ºC. Samples were compared to wild-type cells expressing empty pBAD24 (blue) not under SOS induction. X-axis represents cell volume (µm^3) and Y-axis represents the percentage of cells at any given volume

Table 4.1 .Average[a] cross correlation[b] analysis of cell volume distribution during pBAD-rec441 expression

	Wild-type + pBAD-*recA441*	*ΔymfM* pBAD-*recA441*	*ΔsulA* pBAD-*recA441*	Δ*sulA*Δ*ymfM* pBAD-*recA441*
Wild-type pBAD24	0.33	0.39	0.22	0.62
Wild-type pBAD-*recA441*		0.96	0.62	0.32
ΔymfM pBAD-*recA441*			0.61	0.45
ΔsulA pBAD-*recA441*				0.52

Average [a] cross correlation[b] of cell volume distribution was determined for wild-type (BW25113), *ΔymfM, ΔymfM,* and *ΔsulAΔymfM* strains expressing pBAD-*recA441* in LB at 42°C for 2 hours with 100 μg/mL adenine.

[a]Average determined from the two biological replicates.

[b]Values vary between -1 and 1, where 1 is perfectly correlated, -1 is anti-correlated, and 0 represents no correlation.

4.2.3 *ymfM* does not contribute to the filamentation seen during norfloxacin-induced SOS

During recA441 induced SOS, the *ymfM* gene contributes to the filamentation observed in the absence of *sulA*, as the double mutant showed the greatest shift towards the shorter cell population as compared to the *sulA* only knockout (Figure 4.3). These experiments were done through genetic activation of the SOS response; however this does not conclusively show whether YmfM is inhibiting division under physiologically relevant SOS inducing conditions.

Antibiotics are known to induce the SOS response by disrupting DNA replication, activating RecA, and causing filamentation [108, 206]. The *ymfM* gene was reported to be significantly up-regulated during norfloxacin treatment [208-210]. Norfloxacin is a fluoroquinolone antibiotic which targets DNA gyrase, an enzyme responsible for the supercoiling of DNA during replication [211, 212]. Inhibiting DNA gyrase leads to double-stranded DNA breaks and the activation of the SOS response, and cell filamentation [108, 211, 212]. It was therefore hypothesised that *ymfM* may play an active role in inhibiting cell division during norfloxacin exposure.

The studies reporting the up-regulation of *ymfM* during norfloxacin exposure did not indicate whether any cellular changes, such as filamentation were observed. Furthermore, each study reported a different concentration of the antibiotic and total time of treatment used [208-210]. To establish which concentration of the antibiotic would result in a filamentous phenotype, the wild-type strain BW25113 was exposed to 25, 50, 100, 150

and 200 ng/mL of norfloxacin for a period of two hours. Consistent filamentation was observed for concentrations greater than 100 ng/mL. Furthermore, extended exposure to 200 ng/mL of Norfloxacin resulted in ballooning at the centre of the filamentous cells (Figure 4.4). Since higher doses resulted in additional phenotypic effects, 100 ng/mL was used to test the involvement of *ymfM* in norfloxacin induced SOS. Wild-type (BW25113), Δ*sulA*, Δ*ymfM* and Δ*sulA*Δ*ymfM*, were exposed to 100 ng/mL norfloxacin over a period of two hours and the cell volume determined using the coulter counter.

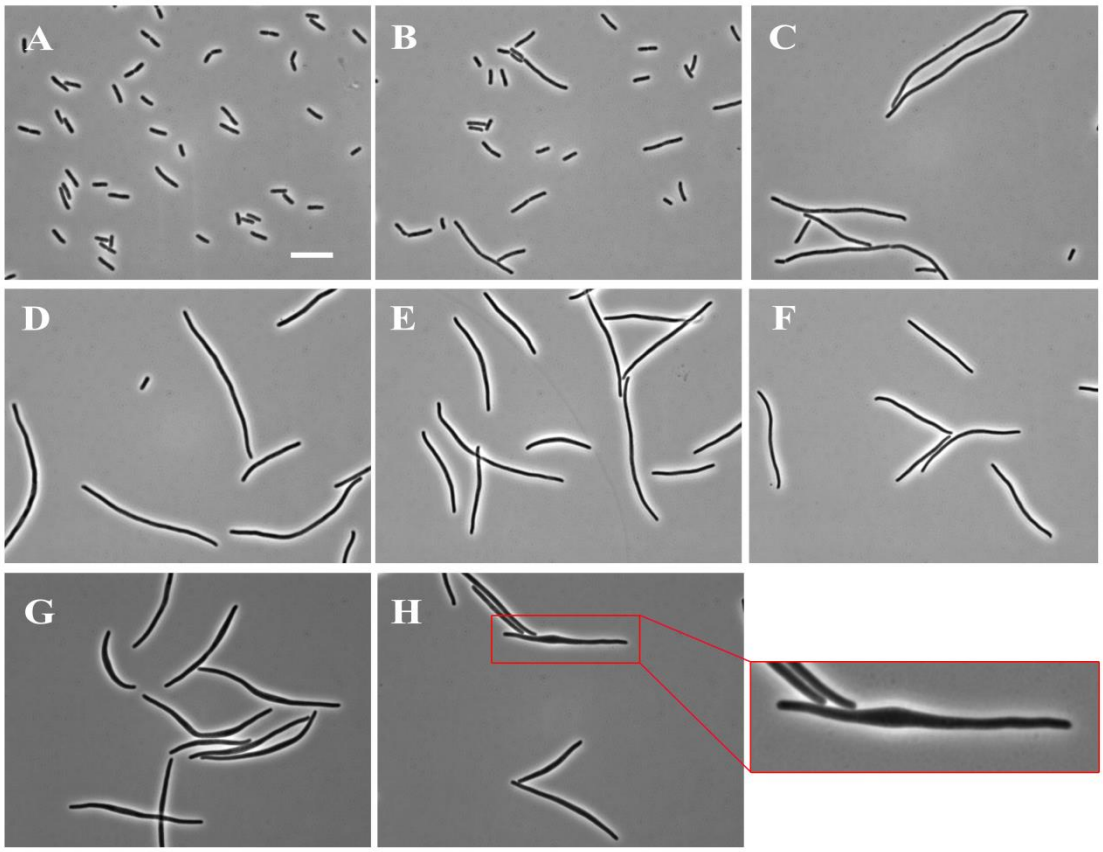

Figure 4.4. Morphological changes of *E. coli* cells exposed to varying concentrations of norfloxacin.

BW25113 cells in mid-exponential growth were exposed to 0 (A), 50 (B), 100 (C), 150 (D), 200 (E) and 250 (F) ng/mL of norfloxacin for two hours. Additional phenotypic changes, including ballooning at the centre of the cell were also observed at 200 ng/mL and above (G and H). Images were acquired using the Ziess Axioplan microscope at 100x magnification under phase contrast. Scale bar = 10µm

BW25113 (wild-type) cells, which contains both *ymfM* and *sulA*, filamented in response to the antibiotic as early as 60 minutes and continued to increase in cell size by 120 minutes (Figure 4.5). This was seen in all three biological replicates, although the cell size distribution varied between the replicates. Nonetheless, this cell size distribution became the basis to compare whether the mutant strains behaved similarly or differently under the same conditions.

In the absence of *sulA*, cells were unable to filament to the same degree as the wild-type. As early as 60 minutes after antibiotic treatment, a shift towards a shorter cell population was seen in all three replicates (Figure 4.5) with an average cross correlation for wild-type and Δ*sulA* being 0.88 (Table 4.2). At 120 minutes of exposure, a bimodal distribution was observed, with a subset population appearing with a similar profile to the short un-exposed cells and the remainder filamenting to varying lengths (Figure 4.5, Row 1). The bimodal distribution is most obvious in replicate one.

In a Δ*ymfM* background, cell size distribution was almost identical to that of the wild-type background at 60 minutes and 120 minutes antibiotic treatment, in replicates one and three (Figure 4.5, rows 1 and 3). However, in replicate two, the Δ*ymfM* background showed a slight shift towards a shorter cell population at 60 minutes, but not at 120 minutes (Figure 4.5, row 2). The average cross correlation (Table 4.2) of wild-type and Δ*ymfM*, 0.98 and 0.97, at 60 and 120 minutes respectively, further highlighting the similarities between the two strains.

In the Δ*sulA*Δ*ymfM* population, cells treated with norfloxacin showed very little difference in its filamentation response compared to the Δ*sulA* population. The average cross correlation for Δ*sulA* and Δ*sulA*Δ*ymfM* was 0.98 and 0.94, at 60 and 120 minutes respectively (Table 4.2). In replicates one and three at 60 minutes (Figure 4.4, rows 1 and 3), the cell size distribution overlayed that of the Δ*sulA* background almost exactly. In replicate two however, the double-knockout showed a slight reduction in cell size, although this relationship was less obvious at 120 minutes. Like Δ*sulA*, a bimodal

distribution also appeared in the double-knockout strain (Figure 4.5). In all three replicates, the short-cell sub-population appears to make up a higher proportion in the double-knockout than the Δ*sulA*. There is very little difference in the cell size distribution of the double-knockout and Δ*sulA* during norfloxacin treatment (Figure 4.5) and this is in contrast to the phenotype observed during *recA441* induced SOS (Figure 4.3), where the double knockout (Δ*sulA*Δ*ymfM*) has a shorter distribution than the Δ*sulA*.

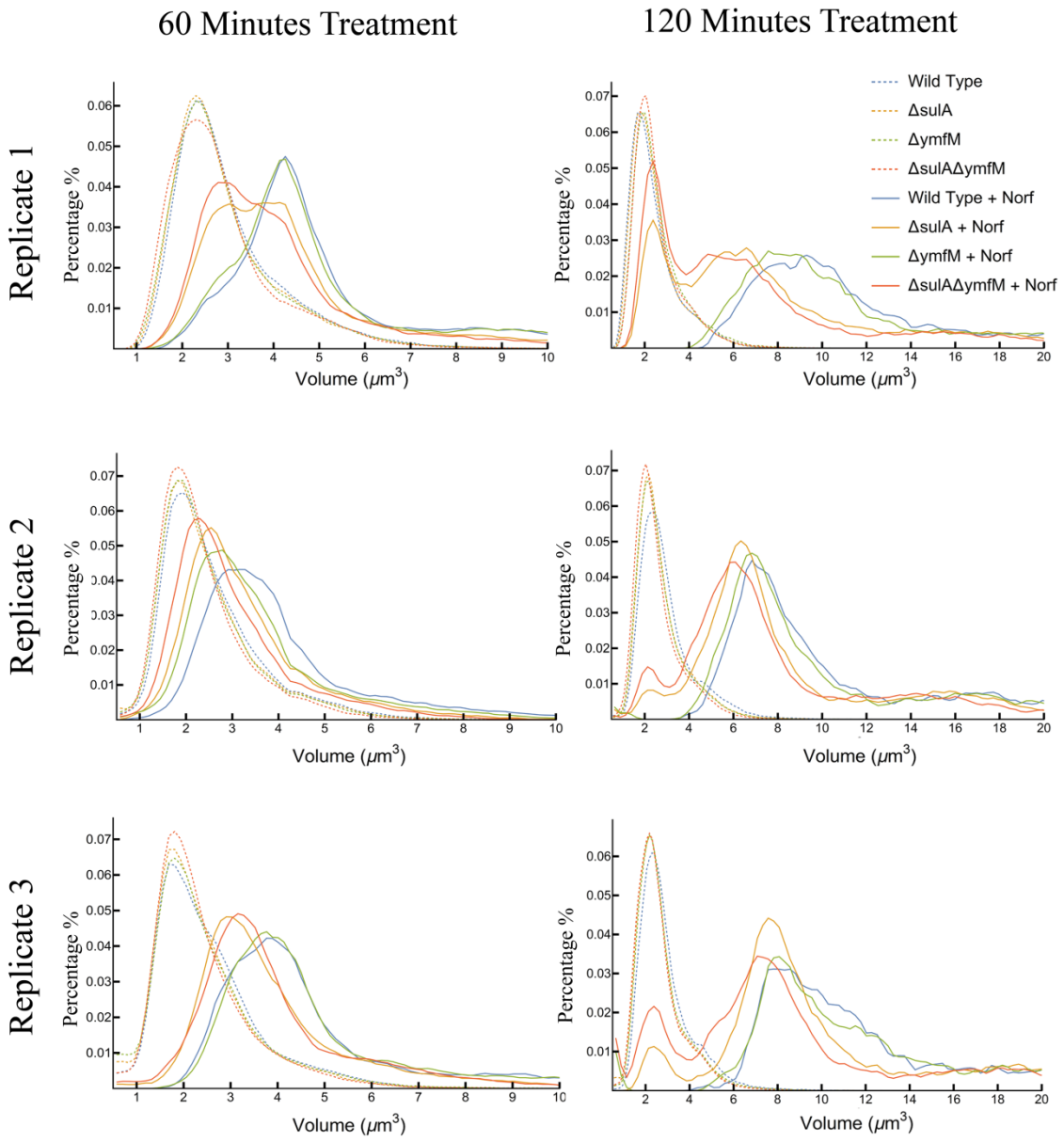

Figure 4.5 Cell volume distribution of WT and mutant *E. coli* treated with Norfloxacin.

Coulter counter analysis of cell size distribution of WT (blue), Δ*ymfM* (green), Δ*sulA* (orange), Δ*sulA*Δ*ymfM* (red) cells without (dashed lines) and with (solid lines) norfloxacin (100ng/mL) treatment over a period of 60 minutes (left column) and 120 minutes (right column). X-axis represents cell volume (μm^3) and Y-axis represents the percentage of cells at any given volume. Experiment was repeated three times, biological replicate one is top row, replicate two is middle row and replicate three is bottom row.

Table 4.2 Average cross correlation analysis of cell volume distribution during Norfloxacin exposure

	60 Minutes			*120 Minutes*		
	ΔymfM	*ΔsulA*	*ΔsulAΔymfM*	*ΔymfM*	*ΔsulA*	*ΔsulAΔymfM*
Wild-type	0.98	0.88	0.82	0.97	0.68	0.52
ΔymfM		0.92	0.88		0.59	0.59
ΔsulA			0.98			0.94

Average [a] cross correlation[b] of cell volume distribution was determined for wild-type (BW25113), *ΔymfM, ΔymfM,* and *ΔsulAΔymfM* strains treated with 100 ng/mL norfloxacin for 60 and 120 minutes.

[a]Average determined from the three biological replicates. For full cross correlation table for each biological replicate, see supplementary data.

[b]Values vary between -1 and 1, where 1 is perfectly correlated, -1 is anti-correlated, and 0 represents no correlation.

4.2.4 Contribution of the entire e14 prophage to norfloxacin-induced filamentation:

The *ymfM* gene is part of an operon with nine other genes, many of which do not have a known function [155]. Transcriptional data showing the up-regulation of *ymfM*, also identified four other genes from the e14 prophage being up-regulated [209]. The norfloxacin filamentation experiments above suggest that *ymfM* is not contributing to filamentation under these conditions which is in contrast to the genetic activation of SOS using *recA441*. To test whether any other e14 genes were contributing to the observed filamentation during norfloxacin exposure, mutant strains lacking the full e14 phage (*Δe14*), and *Δe14ΔsulA* were exposed to norfloxacin and compared to wild-type and *ΔsulAΔymfM*.

Overall the three biological replicates showed variation in the distribution of sizes between each replicate. That is, the trend between wild-type and mutant strains varied in each replicate. In biological replicate one (Figure 4.6, row 1), there was a reduction in the cell size distribution of the *Δe14*strain at both 60 and 120 minutes after norfloxacin treatment, as compared to the wild-type, indicating that the deletion of e14 prophage had an effect on the ability of cells to become filamentous. However the double-knockout of Δs*ulA*Δ*ymfM,* showed a shorter cell size population as compared to Δ*e14*Δ*sulA,* indicating that the e14 prophage was in fact not contributing to the filamentation response. This is best seen at the 120 minute time-point, where there is a higher peak of cells less than 4µm in size in the Δs*ulA*Δ*ymfM* strain as compared to Δ*e14*Δ*sulA*.

In replicate two (Figure 4.6, row 2), at 60 minutes, the cell size of wild-type and Δ*e14* are very similar as their distributions closely overlay each other. This is also observed with

Δ*e14*Δ*sulA* and Δs*ulA*Δ*ymfM*. Similar to what was seen at 60 minutes, there is no difference between Δ*e14*Δ*sulA* and Δs*ulA*Δ*ymfM* at 120 minutes. However, there is a slight shift in cell size, towards the left, of Δ*e14* compared to wild-type. Overall the results of replicate two are consistent with the findings of the previous experiment in which only *ymfM* was deleted (Δ*ymfM,* Figure 4.5).

In replicate three (Figure 4.6, row 3) is similar to replicate two in that the cell size distribution of wild-type is again very similar to that of Δ*e14* at 60 minutes. The double knockout strains have a very similar distribution profile, with a slight shift in the peak of their curves. At 120 minutes, a large shift of events occurring at less than 1μm^3 of the Δ*e14* strain is observed. There is no obvious difference between Δ*sulA*Δ*ymfM* and Δ*e14*Δ*sulA*, at 120 minutes, suggesting that the e14 prophage does not have an additional effect on the ability of cells to filament.

The variations between each replicate made interpretation of the results difficult and to overcome this, more replicates are needed. However, from the average cross correlation (Table 4.3), it appears that the Δe14 strain and wild-type are highly correlated at 60 minutes (0.94). At 120 minutes the cross correlation value is slightly lower (0.78) than the 60 minutes. The Δ*sulA*Δ*ymfM* strain is highly correlated with Δ*e14*Δ*sulA* at both 60 and 120 minutes (0.97 and 0.92 respectively). It is currently concluded that the no additional genes from the e14 prophage are contributing to the filamentation response during norfloxacin exposure. These results are consistent with the results of *ymfM* deletion alone (Figure 4.6), and the e14 prophage does not appear to be contributing to the filamentation response.

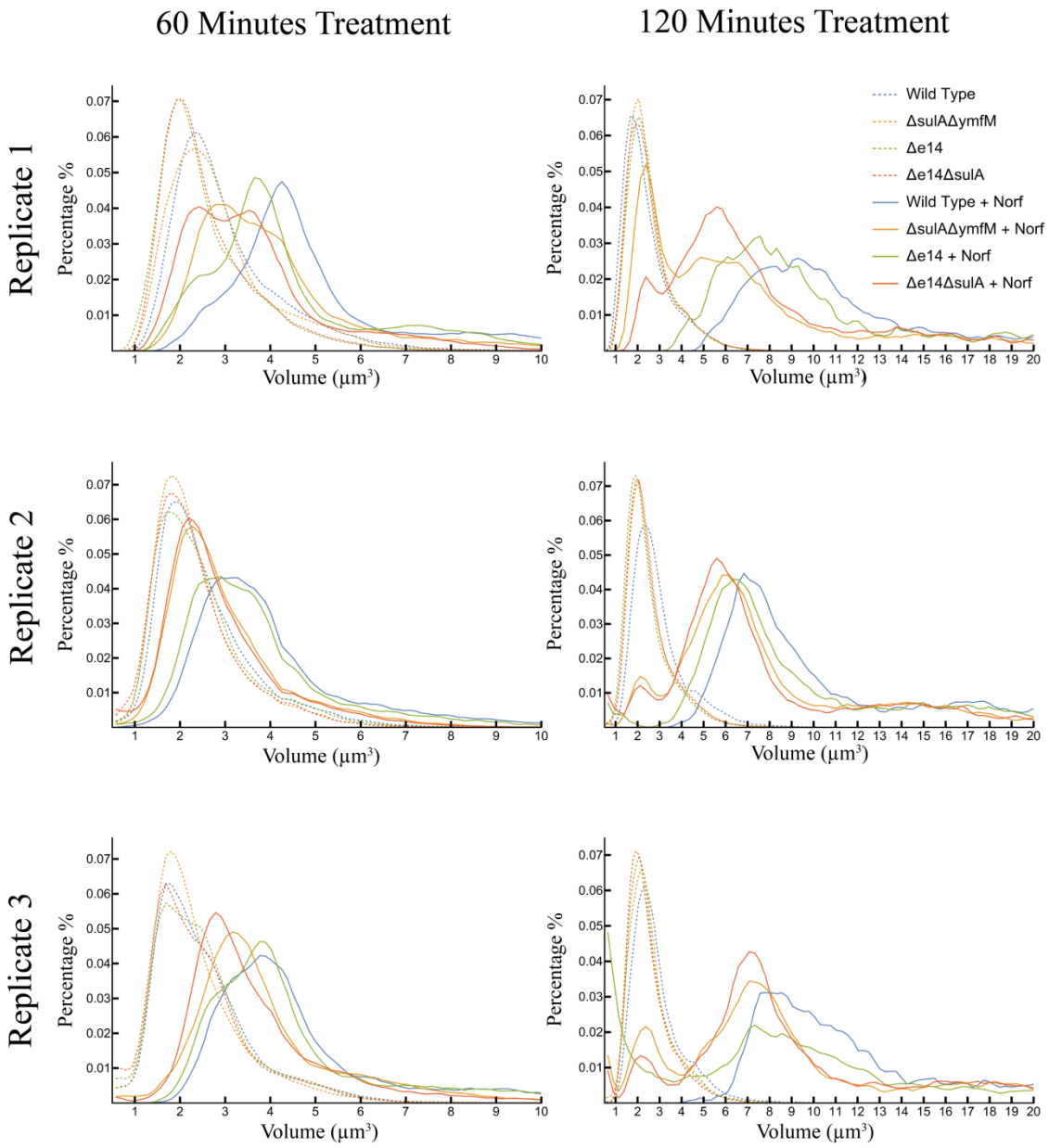

Figure 4.6 Cell volume distribution of e14 mutant treated with Norfloxacin.

Coulter counter analysis of cell size distribution of WT (blue), Δ*sulA*Δ*ymfM* (orange), Δ*e14* (green) and Δ*e14*Δ*sulA* (red) cells, without (dashed lines) no antibiotic added, and with (solid lines) for Norfloxacin (100 ng/mL)treatment over a period of 60 minutes (left column) and 120 minutes (right column). X-axis represents cell volume (µm^3) and Y-axis represents the percentage of cells at any given volume. Experiment was repeated three times, biological replicate one is top row, replicate two is middle row and replicate three is bottom row.

Table 4.3 Average cross correlation analysis of cell volume distribution during Norfloxacin exposure

	60 Minutes			*120 Minutes*		
	ΔsulAΔymfM	*Δe14*	*Δe14ΔsulA*	*ΔsulAΔymfM*	*Δe14*	*Δe14ΔsulA*
Wild-type	0.83	0.94	0.74	0.55	0.78	0.56
ΔsulAΔymfM		0.92	0.97		0.69	0.92
Δe14			0.89			0.75

The average [a] cross correlation[b] of cell volume distribution of wild-type (BW25113), *ΔsulAΔymfM, Δe14,* and *Δe14sulA* strains treated with 100ng/mL norfloxacin for 60 and 120 minutes.

[a] Average determined from the three biological replicates. For full cross correlation table for each biological replicate, see supplementary data.

[b]Values vary between -1 and 1, where 1 is perfectly correlated, -1 is anti-correlated, and 0 represents no correlation.

4.2.5 RecA-independent filamentation mechanism during SOS:

The data from the experiments so far suggest that during norfloxacin exposure, there are other mechanisms independent of SulA which are contributing to filamentation. Unlike the results of the RecA441-mediated SOS, *ymfM* does not appear to contribute to filamentation under norfloxacin treatment. A *recA*-deletion strain was tested to see if cells were able to filament in the absence of *recA*. By using this strain, all genes under the regulatory pathway of RecA will be inactivated and a RecA-mediated SOS response should not occur. We hypothesised that in the absence of RecA, no filamentation should be observed. Interestingly, the results from these experiments showed that, although less than wild-type, filamentation was observed in the absence of RecA at 120 minutes (Figure 4.7). This suggests that during norfloxacin exposure, some of the filamentation observed is not via the RecA (SOS) pathway.

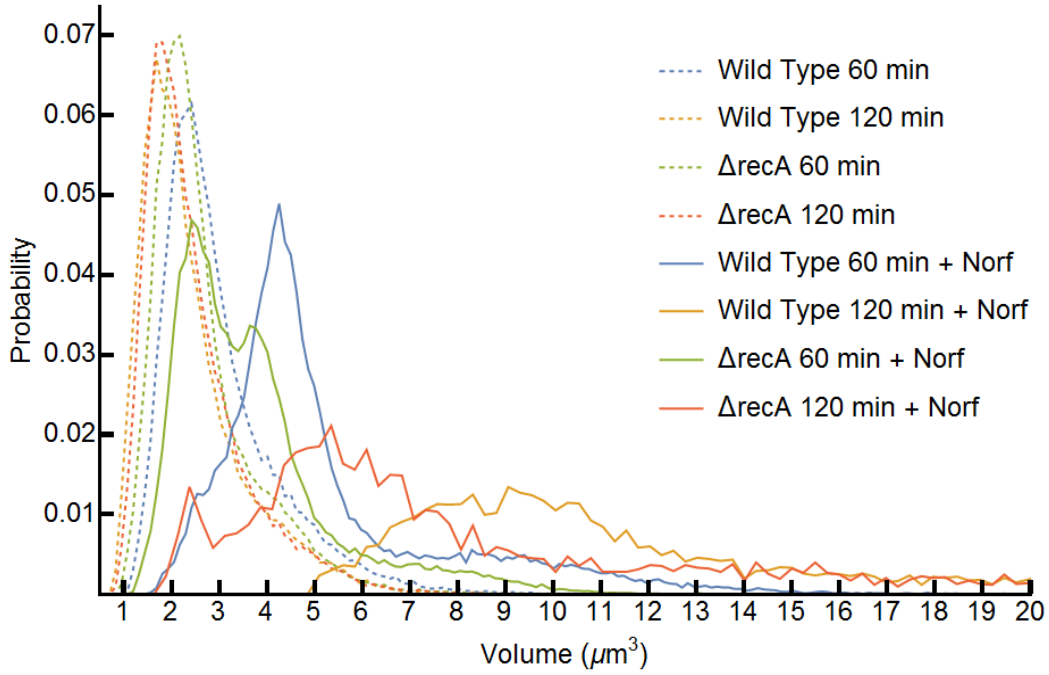

Figure 4.7 Cell volume distribution of wild-type and Δ*recA* *E. coli* K-12 strains treated with norfloxacin

Coulter counter analysis of the cell size of wild-type (BW25113) and *ΔrecA* cells grown with and without 100 ng/mL norfloxacin over a period of 60 minutes and 120 minutes. Cells were grown in LB at 37°C. Dashed lines represent no treatment with norfloxacin and solid lines represent treatment with norfloxacin. X-axis represents cell volume (μm^3) and Y-axis represents the percentage of cells at any given volume.

4.2.6 Changes in expression of *ymfM* during SOS-inducing conditions

Deletion of *ymfM* (in the Δs*ulA*Δ*ymfM* double knock out) shows a change in filamentation lengths during activation of *recA441*, but not during Norfloxacin-induced SOS, even though published transcriptional data shows up-regulation. This discrepancy could be due to two possible reasons. First, cell division inhibition by *ymfM* could be masked by *recA* independent cell division inhibitors (shown to exist in Figure 4.7), similar to how *sulA* was able to hide *ymfM*'s function in the RecA441 experiments (Figure 4.3). A second possibility could be a difference in the up-regulation of *ymfM* by the two different SOS induction conditions used (i.e. RecA441 vs. norfloxacin). To investigate this second possibility, quantitative real-time PCR (qRT-PCR) was used to determine if *ymfM* was indeed up-regulated under the norfloxacin conditions tested, as would expected from previous reports, and if there was a difference in the level of gene expression as a consequence of the different in the two methods employed. As well as *ymfM*, expression of *sulA* (SOS inducible cell division inhibitor), *ymfL* (adjacent to *ymfM*), *croE* (transcriptional regulator, up-stream to *ymfL-ymfM*) and *cohE* (CI-like repressor) were also measured.

Expression of ymfM during Norfloxacin exposure

Cells were exposed to 100 ng/mL of norfloxacin for two hours, with samples taken for RNA extraction and subsequent qRT-PCR at 0 (no treatment), 60 and 120 minutes (details can be found in Section 2.13). Results of the experiment show that expression of *ymfM* was indeed up-regulated during norfloxacin exposure. The expression increased over the

course of the SOS induction, starting at an average of less than one log2-fold change at 60 minutes to five log2-fold change at 120 minutes (Figure 4.8). The expression of *sulA* stays almost consistent over the two time points at around 2 log2-fold change (Figure 4.8). Like *ymfM*, expression of *ymfL* and *croE*, also increased at 120 minutes, with an average of 4 and 3 log2-fold changes, respectively (Figure 4.8). Expression of *cohE*, the Cl-like repressor, did not change over the course of the experiment. While *ymfM* was not up-regulated to a similar degree at 60 minutes as previously published data, the expression results at 120 minutes are comparable to previously published data (Table 4.4) [208-210]. This difference could have been due to variations in experimental design, including concentration, growth conditions and strains used. Nonetheless, the overall trend of *ymfM* being up-regulated during norfloxacin exposure is consistent.

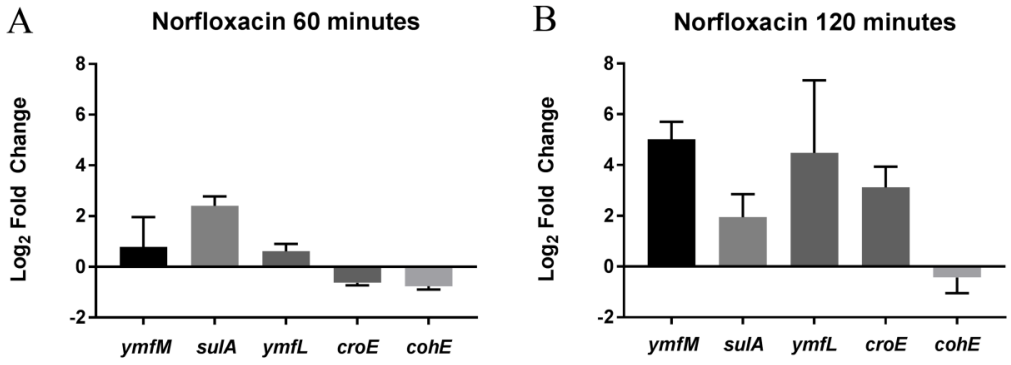

Figure 4.8 Gene expression profile of *E. coli* treated with 100 ng/mL norfloxacin

Average log2 fold change of genes, *sulA, ymfM, ymfL, croE* and *cohE* after 60 minutes (A) and 120 minutes (B) treatment with 100 ng/mL Norfloxacin in the background strain BW25113. Housekeeping genes used for normalization of fold-change were *16S rRNA* and *secA*. The data represent the mean (+SD) from two biological replicates.

Table 4.4. A comparison of log2 fold change of gene expression during norfloxacin exposure

	Norfloxacin concentration	**Time point (mins)**	***sulA***	***ymfL***	***ymfM***	***croE***	***cohE***
This work	100 ng/mL	60	2.4	0.6	0.8	-0.6	-0.8
		120	1.9	4.5	5.0	3.12	-0.4
Faith *et al*. [209]	25 ng/mL	60	3.9	5.4	4.8	1.0	-0.08
Dwyer *et al* [208]	250 ng/mL	60	2.9	5.6	5.9	5.1	1.1
Kohanksi*et al* [210]	250 ng/mL	60	5.5	4.8	4.17	4.28	N.D
		120	4.6	4.7	4.6	4.2	N.D

Transcriptional levels of *sulA, ymfL*, *ymfM, croE* and *cohE*, as determined by qRT-PCR in the current study is compared to previously published expression of these genes. Expression levels are all reported in log2 fold change. N.D Transcriptional data not available

Expression of ymfM during pBAD-recA441 induced SOS

The expression of *ymfM* is up-regulated during norfloxacin exposure suggesting that it is responding to this SOS-inducing condition. However, this change in expression level does not appear to contribute to the filamentation observed under the same conditions (Figure 4.5). To test whether the up-regulation of *ymfM* was greater during *recA441* induction, pBAD-*recA441* was induced to express in a wild-type background (BW25113). When *recA441* was expressed from pBAD24 this time around, it failed to result in filamentation. The results were unexpected as filamentation was previously observed (Figure 4.3), consistent with several previous studies with the *recA441* allele

[136, 167, 213], albeit with a different genetic background to the one used in the present study. Given that more than a year had passed between these experiments, a fresh transformation of pBAD-*recA441* into wild-type *E. coli* was performed in the hopes to overcome this. This still did not result in the expected phenotype and only short cells were observed. This was repeated twice more during which new batches of media, antibiotic, arabinose and adenine were prepared. However, none of these experiments resulted in filamentation.

To further investigate this discrepancy, the original isolate of *E. coli* JM12 [167], in which the *recA441* allele was amplified from its chromosomal location for cloning, was tested for its ability to filament. This was to see whether the issue was limited to the plasmid only. JM12 is known to induce the SOS response when grown under appropriate conditions at the non-permissive temperature of 42ºC, and was the strain used by D'Ari *et al*., [136]. Growth of JM12 at the non-permissive temperature did not result in filamentation (data not shown), showing that both JM12 and pBAD-*recA441* had lost functionality.

D'Ari *et al*., [136] used a minimal growth medium, M63, supplemented with adenine, to activate RecA441 at the non-permissive temperature. It has been reported that minimal media supplemented with adenine aids in RecA441 activity [167]. So far, experiments performed in this current study were done in rich medium, LB. LB was initially preferred, as this allowed a more direct comparison to the norfloxacin-induction experiments that were done in LB. Most importantly, expression of *recA441* from pBAD24 in LB resulted in consistent filamentation earlier (Figure 4.3). Nonetheless, M63 was tested to see if it improved expression of RecA441 and filamentation. *E. coli* JM12 grown in M63 with adenine at 42ºC resulted in an increase in cell size, as determined by Coulter counter, with

a proportion of the population filamentous (Figure 4.9). However, this was not seen with pBAD-*recA441* (data not shown), suggesting that there is another reason for the lack of filamentation with this strain. It is currently hypothesised that leaky expression from pBAD24 may be aiding in the generation of suppressor mutants and the loss of phenotype.

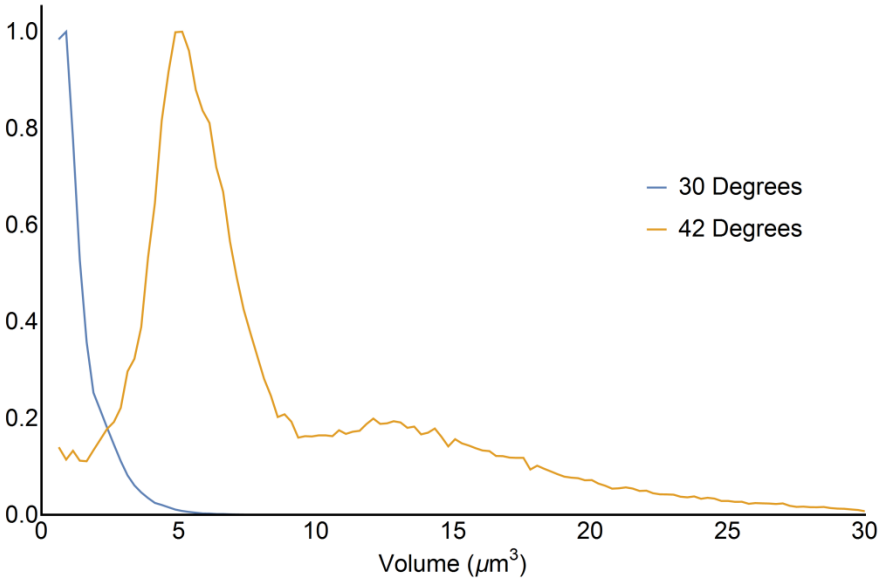

Figure 4.9 The requirement of minimal media for RecA441 activity

Strain JM12 was grown in minimal media, M63, at the permissive temperature (30ºC) to repress *recA441* activity and then at the non-permissive temperature, 42ºC to induce *recA441* with the addition of 100 µg/mL adenine for 2 hours before sampling for Coulter counter. X-axis represents cell volume (µm^3) and the Y-axis has been normalised to a maximum value of 1 for better visualisation. In a non-normalised graph, the maximum bin for the 30ºC sample contains 20% of cells and the 42ºC contains 4.5% of cells.

Expression levels of ymfM from pBAD-ymfM

Given that the transcriptional level of *ymfM* during pBAD-*recA441*-induced SOS was unable to be determined, it is still unclear whether the difference observed in the ability of *ymfM* to contribute to filamentation during *recA441* induction (Figure 4.3) and not during norfloxacin exposure (Figure 4.5) is due to differences in expression levels of *ymfM* under the two different conditions. What is known is that expression of *ymfM* from pBAD24 causes significant inhibition of division (Chapter 3, Figure 3.2). Therefore determining the level of transcriptional change during pBAD-*ymfM* induction may provide insight into the approximate level of *ymfM* expression needed to cause filamentation. Expression of *ymfM* increased by 8.9 log_2-fold after only 60 minutes of pBAD-*ymfM* induction and 11 log2-fold at 120 minutes (Figure 4.10). There was no change in expression of *sulA, ymfL, croE* and *cohE*. The expression level of *ymfM* from the plasmid at 60 minutes is greater than during 120 minutes of norfloxacin (8.9 versus 5.0 Log_2-fold change respectively)

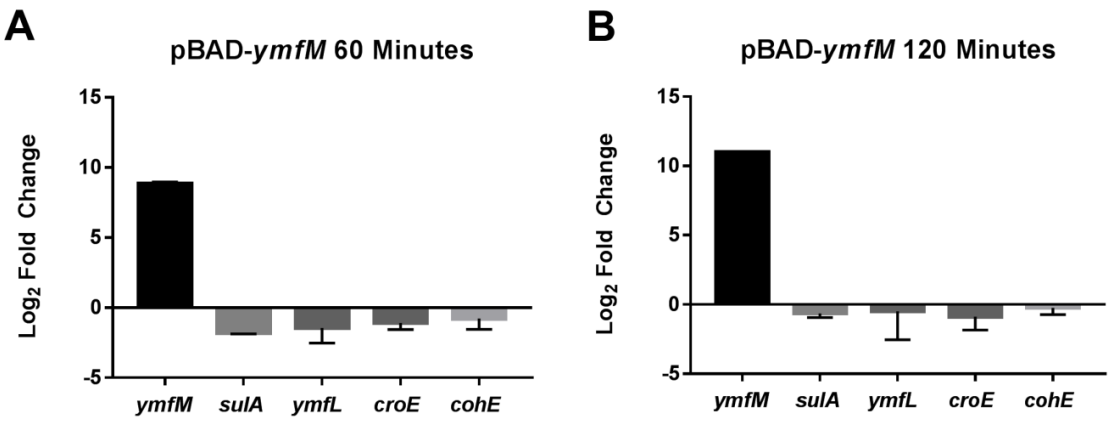

Figure 4.10. Gene expression profile of *E. coli* during pBAD-*ymfM* expression

Average log2 fold change of genes, *sulA, ymfM, ymfL, croE* and *cohE* after (A) 60 minutes and (B) 120 minutes induction of pBAD-*ymfM*, in the background strain BW25113. Cells were grown in LB and 100 µg/mL ampicillin at 37ºC. Expression of pBAD-*ymfM* was induced with 0.2% arabinose and repressed with 0.2% glucose. Transcriptional changes, shown as log2 fold change were determined by comparing CT values from the repressed and induced samples at 60 and 120 minutes. Housekeeping genes used for normalization of fold-change include, *16SrRNA* and *secA*. Mean (+SD) from three biological replicates.

4.3 Discussion

The SOS response is a well characterised pathway most commonly induced by DNA damage [111]. A halt in cell division occurs through the inhibitory actions of SulA during this response and is designed to allow time to repair the damage before the generation of new daughter cells. Once the damage is repaired, division resumes. While the role of SulA is well understood, the role of other cell division inhibitors activated during SOS, such as those encoded within prophages has not been well explored. Given that when over-expressed, *ymfM* leads to filamentation (Chapter 3), and *ymfM* is up-regulated in response to an SOS inducing event such as exposure to antibiotics [208-210], it was hypothesised that *ymfM* may be contributing to the filamentation response during SOS. This chapter subsequently examined the potential role of *ymfM* in inhibiting cell division during chemically- and genetically-induced SOS.

4.3.1 *ymfM* is the previously identified cell division inhibitor, SfiC:

The e14 prophage encodes an SOS-inducible cell division inhibitor, SfiC [136] which based on prophage arrangement was identified to be either *ymfL* or *ymfM* [155]. Since experimental evidence presented in this body of work shows that *ymfM* when over-expressed causes filamentation (Chapter 3, Figure 3.2), it is most likely that *ymfM* is SfiC. However, to eliminate the possibility that *ymfL* was also able to inhibit division *ymfL* was induced to express, resulting in no observable filamentation (Figure 4.2). This shows that *ymfM* is solely responsible for the inhibition of division, and is the previously identified SfiC. This is the first time the gene encoding for SfiC has been identified.

4.3.2 *ymfM* is a cell division inhibitor during RecA-induced SOS:

D'Ari *et al*., characterised SfiC to be a SulA-independent filamentation mechanism induced by the SOS response, which was identified using a temperature sensitive *recA* mutant, *recA441* [136]. The conclusion from data in this chapter is that YmfM is SfiC. To test that YmfM could also act as an alternative cell division inhibitor during SOS as previously reported, RecA441-mediatedSOS was induced in strains devoid of *ymfM* (*ΔymfM*), *sulA* (*ΔsulA*), and both of these genes (*ΔsulAΔymfM*) to see if the absence of any combination of these genes would affect the ability of cells to filament.

In RecA441-mediated SOS, the absence of *sulA* was sufficient to cause a decrease in the extent of filamentation observed compared to wild-type under the same conditions (Figure 2). SulA is a well-defined contributor to the filamentation response during SOS, and so it is not surprising that in the absence of *sulA*, cells filament less effectively. However, the absence of *sulA* alone was not enough to revert to a short wild-type distribution (Figure 4.3), suggesting that other systems are also playing a role in inhibiting division during *recA441* induced SOS. This is a very interesting observation, given that SulA is thought to be responsible for the inhibition of cell division during the SOS response [3, 111].

YmfM may be this additional cell division inhibitor during this SOS response. Interesting though, the absence of *ymfM* alone (Δ*ymfM*), the filamentation profile was identical to that of the wild-type background (Figure 4.3). This result was unexpected, given that the over-expression of *ymfM* from a plasmid causes complete cell division inhibition (Chapter 3, Figure 3.2). If *ymfM* is being induced during RecA441-mediated SOS, then this result suggests that its function is redundant. Given the presence of SulA in the Δ*ymfM* strain and the likely strong induction of SOS from pBAD-*recA441*, there is

probably an excess of SulA such that is able to solely inhibit cell division, masking the inhibitory effects of YmfM.

Interestingly, the deletion of both *sulA* and *ymfM* resulted in a further reduction in cell size as compared to Δ*sulA* alone. This result suggests that during genetic induction of SOS by *recA441*, *ymfM* is contributing to the inhibition of division in the absence of *sulA* during RecA441-mediated SOS. These findings are consistent with the findings of D'Ari *et al*, 1983 [136], who showed that deletion of *sulA* or *sfiC* alone resulted in filamentation and observed only a slight increase in average cell size of *ΔsulAΔsfiC* expressing *recA441*, as compared to the wild-type (short cells) background. Due to the similarities within this body of work and previously published data, we currently conclude that *ymfM* is most likely an alternative cell division inhibitor to SulA during the SOS response.

It should be acknowledged that there was difficulty in reproducing RecA441 experiments, as outlined in the results. Therefore further experimental work is needed to conclusively show that *ymfM* plays an active role in the SOS response. Additionally, as a new plasmid based system was used to activate the expression of RecA441, which has not been reported in the literature before, further characterisation of this allele is needed. This includes determining whether RecA441 acquires proteolytic activity at 30ºC if expression is induced with arabinose as well as its ability to induce SOS when compared to the chromosome *recA441*.

The RecA441 experiments also revealed that there was not a full recovery to a short cell population in the Δ*sulA*Δ*ymfM* background expressing *recA441*. This highlights that other inhibitors are also contributing to filamentation during SOS. Given that over 1000

genes are differentially expressed during the SOS response, it is likely that other yet unidentified SOS-inducible cell division inhibitors exist [214]. A possibility is that prophage encoded cell division inhibitors are contributing the filamentation during the SOS response. For example, *kilR* from prophage Rac and *dicB* from prophage Qin are both cell division inhibitors which have been shown to be up-regulated during treatment with nalidixic acid and azlocillin and are thought to contribute to the resistance of these antibiotics [149, 153, 215]. It is possible that their up-regulation during SOS conditions contributes to the inhibition of cell division.

4.3.3 Finding the biological SOS condition in which YmfM is needed to inhibit division:

YmfM appears to be an active inhibitor of division during SOS under genetic induction (by RecA441). However, the environmental condition(s) under which YmfM inhibits division is unknown. Published transcriptional data was used to identify SOS inducing conditions in which YmfM may be acting to inhibit division. The treatment of *E. coli* with norfloxacin showed up-regulation of *ymfM* expression (Table 3) [208-210]. This SOS inducing antibiotic became a candidate for further investigation.

Exposure of wild-type *E. coli* to norfloxacin resulted in a filamentous phenotype after 60 minutes. Within the three biological replicates, variability in the degree of filamentation response was observed. However, this did not appear to affect the overall trend between the mutant strains within a biological replicate, and are discussed below.

Norfloxacin-induced SOS was very similar to the pBAD-*recA441* induction, in that the absence of *sulA* alone was enough to show a reduction in cell size distribution. Further,

the absence of *ymfM* alone had no effect on the cell size, suggesting that the presence of *sulA* in this strain was enough to inhibit cell division. The obvious difference between Δ*sulA* distribution and wild-type distribution highlights that SulA is the predominant inhibitor of division during SOS induced by norfloxacin.

The lack of complete rescue to the short population in the Δ*sulA* background suggests other inhibitors are also involved. The RecA-mediated experiments (Figure 4.3) showed that *ymfM* was one such inhibitor. This relationship however was not seen under Norfloxacin, as there was a high cross-correlation between Δ*sulA* and Δ*sulAΔymfM*, suggesting that under the conditions tested *ymfM* was not contributing to the observed SulA independent filamentation.

Overall the results of the antibiotic induced SOS showed that SulA alone was a major contributor to the filamentation seen. However the absence of SulA was not enough to get a complete reversal of filamentation, suggesting that other systems are also contributing to cell division inhibition during Norfloxacin treatment.

Experimentally, YmfM did not appear to be such an alternative inhibitor under these conditions as it was during RecA441 mediated SOS. It is possible that these additional cell division inhibitors were masking the effects of YmfM. For example, the nucleoid occlusion protein, SlmA, actively inhibits FtsZ preventing cell division over DNA. It is possible that morphological changes to DNA due to norfloxacin treatment could allow the inhibitory actions of SlmA to mask that of YmfM. As such, DAPI staining should be performed on Norfloxacin induced filaments to determine whether changes in the morphology of the nucleoids is affecting our interpretation of YmfM.

It is also possible that other systems independent of SulA and YmfM are contributing to the filamentation response. As an initial identification step for these inhibitors, a *recA*-deletion strain was used to test whether they are part of the classic SOS response. In a *recA*-deletion background some degree of filamentation was still observed (Figure 4.7), suggesting that RecA independent mechanisms exist which cause filamentation during norfloxacin exposure. This is an interesting observation given that the filamentation response during fluoroquinolone antibiotics treatment is attributed to the activation of the SOS response [206, 211, 216]. However, it is now clear that antibiotics such as norfloxacin are activating cell division inhibition pathways independent of the classic SOS response.

4.3.4 Why does *ymfM* respond differently to genetic and chemical induction of the SOS response?

The results presented so far, have shown *ymfM* to act as an alternative inhibitor under RecA induction but not via norfloxacin exposure. This may be explained by the different level of SOS induction from both methods which will result in a different concentration of YmfM. That is, in genetically induced SOS the concentration of YmfM may be high enough to partially inhibit division whereas via antibiotic exposure it may be low enough that it has no measurable effect.

Quantitative real-time PCR revealed that *ymfM* expression increases in response to Norfloxacin however this response appears to be late, with a 45-fold increase at 120 minutes (Figure 4.8, B). This result is reflective of phage induction during SOS. CI repressors are thought to be cleaved slower than LexA, therefore being induced later

during severe DNA damage [114, 200]. While there is a large relative increase in *ymfM* during norfloxacin induced SOS, these levels do not translate to a physiologically relevant response as no phenotypic change was observed in the absence of *ymfM* at 120 minutes (Figure 4.5).

Expression of *ymfM* from the high-copy plasmid, pBAD24 showed a higher up-regulation at 60 minutes (Figure 4.10), than norfloxacin induction. It is during this higher induction of gene that filamentation is observed. The concentration of YmfM in norfloxacin induced SOS is considerably less than the plasmid concentration. Gene expression of *ymfM* is 4 $\log_2$-fold less during norfloxacin (120 minutes) than during pBAD-*ymfM* (60 minutes). While this result does not indicate the minimal level of *ymfM* needed to inhibit cell division, it does raise the likely possibility that the expression of *ymfM* during norfloxacin treatment is below the minimum concentration of YmfM needed to inhibit division.

Other genes of the e14 phage within the operon containing *ymfM*, including *ymfL* and *croE* were also up-regulated during norfloxacin treatment. *CroE* is annotated as a DNA-binding transcriptional regulator. In lambda phage, after cleavage of the CI-repressor, expression of *cro* is responsible for the switch from lysogenic to lytic growth with the induction of lytic genes downstream of *croE*. qPCR shows that CI-repression and cro-expression system are expressed in response to an SOS signal and cause increased transcription of downstream genes including *ymfL* and *ymfM*.

Ultimately to understand why there was a difference in observed phenotype of the Δ*sulA*Δ*ymfM* strain during RecA441 and norfloxacin mediated SOS, qRT-PCR is required to be performed on cells expressing *recA441*. As explained in the results, this

proved to be technically challenging. While several attempts were made to troubleshoot the lack of filamentation from pBAD-*recA441*, these were unsuccessful. We currently hypothesise that the changes in the functionality of pBAD-*recA441* are possibly due to suppressor mutants appearing in the culture, given that a previously functioning plasmid spontaneously stopped generating the phenotype. To overcome this, the *recA441* allele could be introduced onto the chromosome of the various *sulA* and *ymfM* mutants. The resulting mutant strains could then be grown in minimal media as was done with JM12 (Figure 4.9).

4.3.5 Future directions:

The results presented in this chapter show that YmfM is likely an SOS-inducible cell division inhibitor and is up-regulated during norfloxacin-induced SOS. However the environmental conditions under which YmfM is needed to inhibit division remains unknown. Only one SOS inducing condition, Norfloxacin, was tested in this study. It is a possibility that YmfM is required for a different environmental condition. Therefore testing other methods of SOS induction such as the commonly used antibiotic mitomycin C, UV irradiation, oxidative stress, and acidic pH could provide a better understanding of when YmfM inhibits division [217]. In addition, the e14 prophage has been shown to help *E. coli* cope with acidic environments. It is an attractive thought that perhaps *ymfM* plays an active role during this to inhibit division and should be explored further.

As well as this, knowing the minimum transcriptional level of *ymfM* needed to inhibit division can provide insight into the environmental conditions worth testing. This can be achieved by using a titratable plasmid induction system [218]. Where the minimal induction required for inhibition of division could be first determined by measuring changes in cell lengths before quantification of *ymfM* expression at that level using qRT-PCR. This information could be used to determine how the up-regulation of *ymfM* during norfloxacin treatment compares to *ymfM* levels observed during filamentation. This information could also be used to screen for other environmental stimuli that induce SOS (listed above) and give rise to similar increased expression of *ymfM*

An interesting observation from this chapter was, whether through *recA441* or norfloxacin, there are additional cell division inhibitors activated during an SOS response. It would be interesting to see if the cell division inhibitors during RecA-mediated SOS are also encoded within prophages. This could easily be tested by obtaining various prophage deletions and observing changes in RecA-mediated filamentation.

4.3.6 Conclusions

The main findings of this work showed that *ymfM* is induced by RecA, and contributes to the division inhibition seen during a genetic induction of SOS, but not during norfloxacin treatment. This adds to our current understanding of the cell division regulation during stress, and suggests that several yet unidentified inhibitors may exist which help bacteria filament during the SOS response. While the biological condition in which *ymfM* acts to inhibit division remains unknown, the work presented in this chapter, highlights the wonderful, yet undiscovered intricacies of the SOS response

Chapter 5. A bioinformatics analysis of *ymfM*

5.1 Introduction

In Chapter 3, a novel cell division inhibitor, *ymfM*, was identified by expressing genes contained within DNA fragments known to cause filamentation [163]. In Chapter 4, YmfM was shown to inhibit cell division during RecA441-mediated SOS in the absence of SulA. However, the exact environmental condition in which it functions as well as the complete regulation pathway controlling the function of YmfM remains unclear. In this chapter, a bioinformatics approach was taken to understand the potential regulation pathway of *ymfM*, as well as the context in which YmfM may be functioning.

YmfM is part of the e14 prophage, which is an ancestor of lambda phage [155]. The regulatory switch of the e14 prophage is encoded by genes, *cohE* and *croE* [155]. These genes and their resulting proteins are thought to function together as a system which is similar to the CI repression system from lambda phage [155]. The CI repression system contains two repressors, CI and Cro, which inhibit each other to form a bistable switch that is able to regulate the occurrence of lytic and lysogenic growth [219, 220]. Normally CI is dominant and represses the expression of Cro and downstream genes encoding lytic growth. However, following DNA damage, typically from sources such as antibiotics, oxidative stress and UV irradiation, RecA becomes active which causes the auto-cleavage of CI, allowing expression of *cro* and downstream genes. Once *cro* is expressed, Cro represses the further expression of *cI*. Like CI, CohE from the e14 prophage belongs to the LexA family of transcriptional repressors suggesting that it functions as a phage repressor (pfam: PF00717). In Chapter 4, the expression of *croE* (e14 homolog of *cro*) was up-regulated after norfloxacin induction (Chapter 4, Figure 4.8) strengthening the suggestion that CroE and CohE function as a CI-like repressor system. Furthermore,

ymfM was up-regulated in conjunction with *croE*, implying that CohE and CroE act as a bistable switch, controlling the transcription of downstream genes.

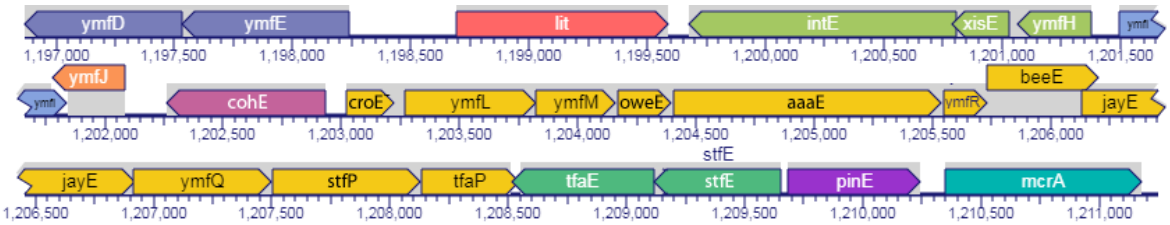

Figure 5.1: The arrangement of the e14 prophage genome within *E. coli*.

The e14 prophage genome is inserted within the *icd* gene of *E. coli*. Genes that are transcribed together are coloured the same. *YmfM* is within the yellow transcript containing ten other genes beginning at *croE*.

YmfM has similarities with the temporal cell division regulator, SulA. SulA inhibits cell division in response to DNA damage as part of the SOS checkpoint control system. Following DNA damage, RecA binds to the damaged single stranded DNA to become active. The expression of *sulA* is repressed by LexA. Activated RecA causes the auto-cleavage LexA and once LexA is cleaved it no longer represses *sulA*, leading to its expression and cell division inhibition. Given that both CohE (putative repressor of *ymfM*) and LexA (*sulA* repressor) are thought to be inactivated by RecA and the expression of both SulA and YmfM cause cell division inhibition, it is possible that there could be some redundancy in their function. This is consistent with the findings of Chapter 4, where the double deletion of *ymfM* and *sulA* was required to reduce cell division inhibition following genetic activation of RecA. However, what isn't clear is how the function of YmfM differs from SulA during the SOS response. For example, is YmfM required at a different stage of the SOS response, such as prolonged SOS induction

following extensive damage? If this is the case, it would require an additional regulation step in combination with the RecA mediated CohE regulation that is thought to exist.

Additional regulation systems may exist which control the expression of *ymfM* in conjunction with the CohE and CroE system. Deep sequencing of the *E. coli* MG1655 transcriptome identified a 116 nucleotide cis-antisense sRNA strand encoded within the 3' end of *ymfL*, and was complementary to the *ymfM* ribosome binding site sequence [221]. Its presence was further confirmed experimentally through northern blotting [221]. The binding of this sRNA strand to the transcribed *ymfM* mRNA ribosome binding site would potentially inhibit translation of the YmfM protein. The sRNA is predicted to be under the control of the σ70 promoter suggesting that it would be constitutively expressed in growing cells [221, 222]. However, it has yet not been demonstrated whether this sRNA regulates the expression of *ymf*M expression. The existence of such an additional regulation systems would further differentiate the activation conditions of YmfM from SulA. SulA only has a single level of up-regulation, through LexA cleavage via RecA. *YmfM* also has a variant of this control, CohE cleavage via RecA, but the presence of an additional control via the sRNA which could further regulate the activation of YmfM for certain conditions (e.g. a later stage of SOS).

Interestingly, the two genes that flank *ymfM*, called *ymfL* and *oweE* (Figure 5.1), are both putative nucleic acid binding proteins. OweE is a homolog of the lambda phage protein O which initiates replication of the lambda phage DNA by binding to the *ori* site within the O gene [223]. It is unknown whether *ymfL, oweE* or any other protein in the e14 prophage plays a role in regulating either the transcription of *ymfM* or sRNA binding to the *ymfM* mRNA ribosome binding site. Therefore, a bioinformatics approach

investigating potential regulation pathways and functional systems controlling *ymfM* will provide a better understanding of how the genes surrounding *ymfM* may control its function.

5.1.1 Chapter Aims and Objectives:

The overall aim of this chapter was to understand the context in which *ymfM* functions. In particular, the first aim was to understand the genetic context in which *ymfM* is found and whether *ymfM* is associated to a particular lifestyle. This was achieved by first determining the prevalence of *ymfM* in the available genomes of living organisms. This would help in distinguishing whether the cell division inhibition function of YmfM is generally applicable to bacterial cell division, or whether it is present only in particular bacterial species. This was then followed by a phylogenetic analysis to measure the distribution of *ymfM* within *E. coli* strains. Examining the presence or absence of *ymfM* to certain branches of the *E. coli* genome phylogenetic tree allowed for the detection of specific environmental conditions in which *ymfM* may be necessary.

The second aim was to understand the relationship of *ymfM* with other genes of the e14 prophage, providing insight into potential genes which function as part of a system with *ymfM*. This was achieved, through using the recently developed technique of community profiling [224], which quantifies the co-maintenance of genes to infer functional proteins systems (i.e. require each other to function). This previously used method was extended to include tests for directionality in gene dependencies. In addition, a cross-correlation of transcriptional regulation using transcriptional databases was performed to identify genes which are co-transcribed. This provided a method,

independent of community profiling, to predict genes that function together. Such large scale transcriptional regulation correlation has previously been used to successfully identify protein systems [209].

5.2 Results

5.2.1 The conservation of *ymfM*

To evaluate the diversity of life containing *ymfM* like genes, the presence of *ymfM* homologs across all organisms represented within the DNA sequence collection was identified using nucleotide sequence similarities. The distribution of *ymfM* in organisms ordered by taxonomy is shown in Table 5.1. *YmfM* is essentially found only within the Enterobacteriaceae, with 81% of homologs being in *E. coli* (Table 5.1). Few homologs were also found in some species of the closely related Gram negative bacteria, *Salmonella* (10%) and *Shigella*(5%) with over 90% sequence homology.

Table 5.1: The distribution of *ymfM* homologs in organisms based on nucleotide sequence

Family	*Genus*	*Species*	Organisms
Enterobacteriaceae			57
	Escherichia		45
		coli	42
		albertii	2
		fergusonii	1
	Salmonella		6
		enterica	6
	Shigella		3
		sonnei	1
		boydii	3
		flexneri	1
	Klebsiella		1
		pneumoniae	1
unclassified Myoviridae			2
	Shigella phage		2
		SfII	1
		SfIV	1

Organisms that have a nucleotide sequence with statistically significant homology to *ymfM* (expected value < 10^{-10}). Table is organised based on taxonomy.

The conservation of the *ymfM* among the homologs identified in Table 1 was analyzed to determine the extent of variation in the nucleotide sequence (339 base pairs). This was done by first generating a consensus sequence, given by the most common nucleotide at each position in the aligned sequences. Each homolog was then compared to this consensus sequence and a fraction conservation plot generated (Figure 5.2). The plot shows that the sequence of *ymfM* is highly conserved, especially at the 5' end of the sequence. Occasional variations are seen toward the 3'-end, although the highest variability in nucleotide is around 50%.

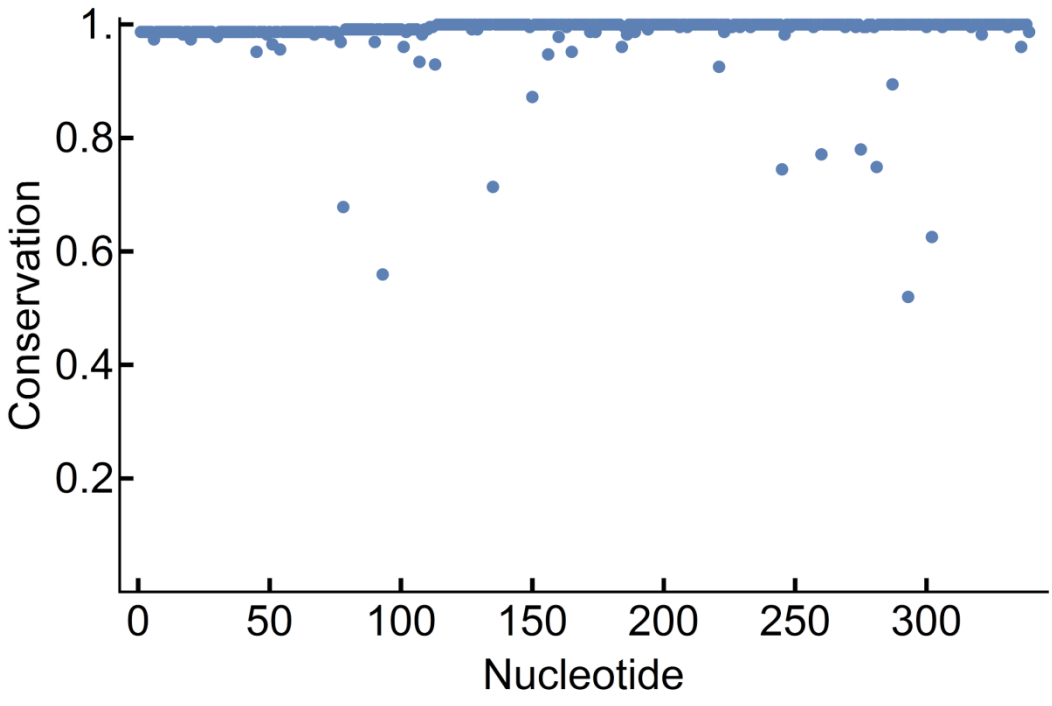

Figure 5.2. Nucleotide sequence conservation of all *ymfM* homologs

The fraction of *ymfM* homologs matching the *ymfM* consensus sequence at each nucleotide. Consensus sequence was determined by the mode of the nucleotide sequence at each position after alignment of all known homologs. A value of 1 on conservation scale is when all homologs have the same nucleotide at that position.

In *E. coli* the strains in which *ymfM* was present, the nucleotide sequence is highly conserved, suggesting it has a conserved function within these strains. Initial blast searches identified *ymfM* in only 45 strains of *E. coli*. This is much less than the number of *E. coli* strains present in the queried collection of genomes (345) suggesting that the role *ymfM* may be more specialized to a specific function required by a subspecies. To understand whether this conservation was clustered to specific strains of *E. coli* the presence and absence of *ymfM* in a range of *E. coli* genomes, including both pathogens and commensals, was determined. The phylogenetic tree of 345 complete *E. coli* genomes was obtained from NCBI (see Chapter 2, Methods and Materials), and each node was colour-coded such that genomes with *ymfM* present were green, genomes with the presence of any other gene within the e14 prophage except *ymfM* were orange, and genomes missing the entire prophage were coloured red (Figure 5.3). The phylogenetic tree shows that *ymfM* as well as the prophage (or its fragments) are not clustered to any specific node of the tree, as green and orange branches are seen throughout. Furthermore, several strains have lost the entire e14 prophage and again this is not specific to any branches.

The orange coded strains on the phylogenetic tree were those that contained at least one gene (except *ymfM*) of the prophage. That is, strains containing only a portion of the e14 prophage. However, the tree does not measure what percentage of the phage was actually present in the orange coded strains. Therefore, each individual gene of the e14 prophage was plotted as a histogram to allow for a better understanding of which portions of the phage were being maintained or lost (Figure 5.4). In this histogram, genes of the prophage appear to be present at discrete frequencies. The first seven genes as well as the last gene of the e14 prophage, *mcrA*, are all present in approximately 10% of strains. Genes from

cohE to *ymfQ* are present in approximately 30% of strains. The genes, *stfP* to *pinE* are the most frequently maintained, with a greater fraction (50% - 70%) of genomes containing these genes. These differences in frequencies suggest that sets of genes in the prophage may function together and subsequently are maintained together.

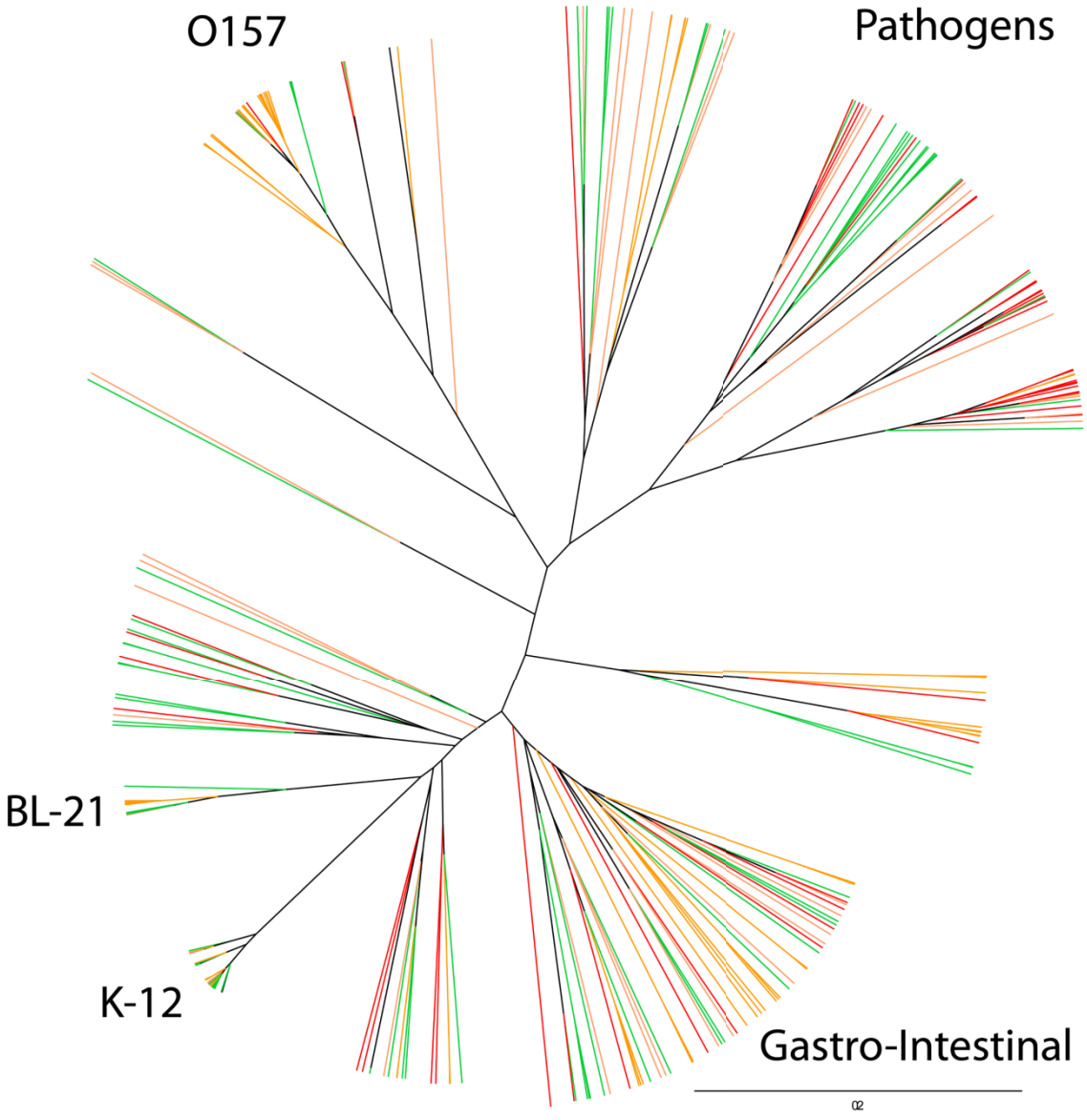

Figure 5.3 A phylogenetic tree of *Escherichia coli* strains showing the presence and absence of various components of the e14 prophage.

The phylogentic tree comprising of 345 strains of *E. coli* is colour-coded to show the presence of *ymfM* (green), at least one gene of the e14 prophage present except *ymfM* (orange), and the absence of the entire e14 prophage (red). General clusters have been manually labeled to show types of strains dominating that cluster based on literature searches. Pathogens include UTI, UPEC and APEC strains. Gastrointestinal includes strains isolated from Humans and Animals. Fifteen outlier strains were omitted to improve visibility. The complete tree is shown in Figure S1.

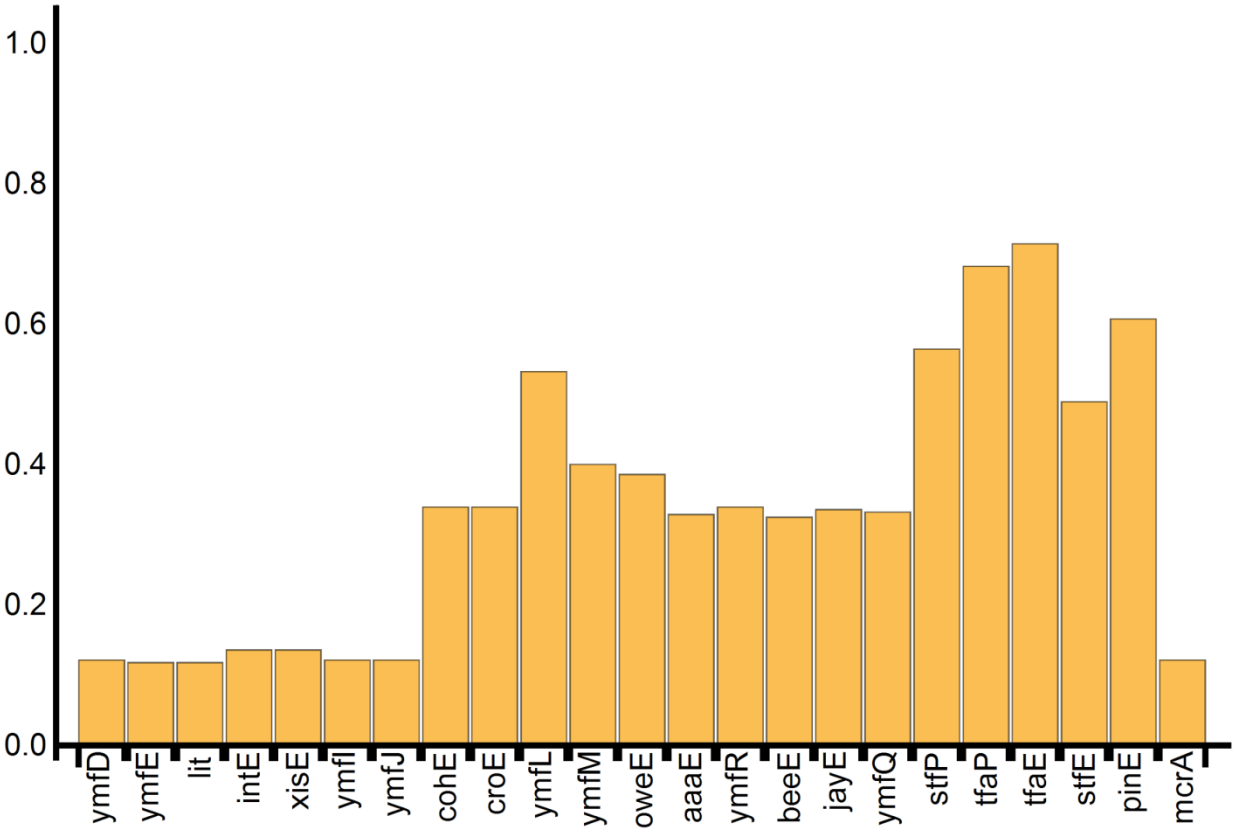

Figure 5.4 The percentage of genomes of *E. coli* containing genes from the e14 prophage

The genes are arranged in the order in which they are located within the e14 prophage on the chromosome, orientated in the forward direction. The y-axis represents the fraction of all complete *E.coli* genomes with the respective gene present.

5.2.2 Community profiling of the genes within e14 prophage

To investigate the potential of genes within the e14 prophage being co-maintained, pair-wise analysis between all gene combinations was performed. The results of this analysis are presented as heat maps (Figures 5.5, 5.6 and 5.7). Figure 5.5 is a heat map of the pair-wise conditional probabilities, which show the probability that a gene (on the x-axis) is present in genomes where a second gene (on the y-axis) is known to be present. This heat map should be read across each row. Each row in the heat map selects the genomes containing the gene specified on the y-axis and then represents the percentage of a specified gene on the x-axis also present in those genomes.

Data from this heat map shows that if any of the early genes (*ymfD* to *ymfJ*) are present, then there is a high probability that the entire prophage is also present (the first 7 rows of the table are all red). The regulatory genes *cohE* and *croE*, are putatively responsible for lysogenic and lytic growth, respectively, are conditional on each other. That is, if one is present in a genome then the other is always (100%) present (*cohE* row, *croE* column and *croE* row, *cohE* column are both red). This is expected as they function together. Additionally, *ymfL* is also always present when either of these two genes exist (*ymfL* column in the *cohE* and *croE* rows). In genomes with *ymfM* present, *ymfL* and *owe* are also essentially always detected (100% and 96% respectively). This relationship is also seen in genomes containing *oweE* where *ymfL* and *ymfM* genes are also always present. However, when *ymf*L is present there is no definitive predictive power of any other gene also being present: *cohE*, *croE, ymfM* and *owe* are often present but only between 64 to 75 % of the time (shown by the yellow colour of the *cohE*, *croE, ymfM* and *owe* columns in the *ymf*L row).

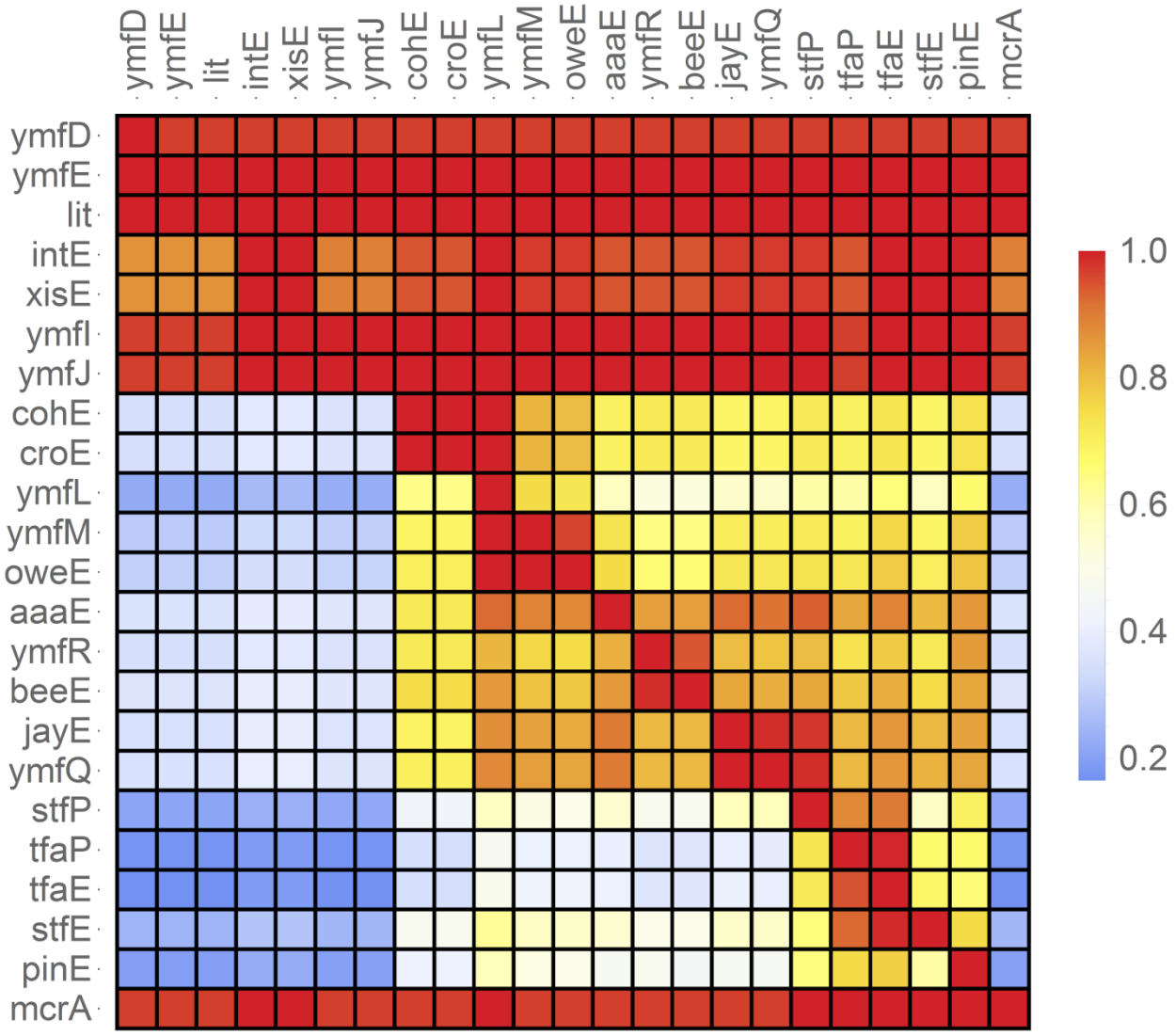

Figure 5.5: Conditional probability for the presence of each gene from the e14 prophage given the presence of any other gene.

The conditional probability is shown as a heat map. That is, the colour of each square shows the probability that the gene at the top of the column (x-axis) is present when the gene at the start of the row (y-axis) is present. Red represents a high probability, blue a low probability

5.2.3 The co-dependency and directional dependency of genes within the e14 prophage

Figure 5.5 shows results of a combination of two different types of dependency, co-dependency and directional dependency. Co-dependency describes two genes that dependent on each other to exist. An example of co-dependency in Figure 5.5 is *cohE* and *croE*. In genomes containing *cohE*, *croE* is present 100% of the time (*cohE* row, *croE* column, red), and similarly in genomes containing *croE*, *cohE* is always present (*croE* row, *cohE* column, red). This co-dependency appears symmetrical on the heat map, as this relationship is the same regardless of which gene is read along the column.

Directional dependency describes the relationship between genes where one gene requires a second gene in order to be present but the second gene does not require the first gene. In this situation the second gene can exist both in the presence and absence of the first gene. An example of this in Figure 5.5 is of *ymfM* and *ymfL,* where in genomes containing *ymfM*, *ymfL* is always present (100%, *ymfM* row, *ymfL* column, red), but conversely in genomes containing *ymfL*, *ymfM* is only sometimes present (75%, *ymfL* row, *ymfM* column, yellow). Directional dependency appears asymmetrically in the heat map (Figure 5).

The relationships observed in this conditional probability were further teased apart to show the co-dependency of two genes (Figure 5.6) and directional dependency (Figure 5.7) of one gene on another. To quantify the degree of co-dependency between genes, the mutual information, a measure of the mutual dependence between the two variables, was calculated between each pair of genes in the e14 prophage. The resulting mutual information values are shown in Figure 5.6. As expected, gene pairs that are symmetric

in the conditional probability have high mutual information value. In particular, *ymfM* and *oweE* have a high mutual information value of 0.9 (where a value of 1 contains maximal mutual information) suggesting that they are co-dependent. Across the rest of the e14 prophage, genes *ymfD* to *ymfJ* are co-dependent on each other with varying degrees, as seen by the red and orange heat boxes. Consistent with the symmetry observed in the conditional probability (Figure 5.5), *cohE* and *croE* have high mutual information suggesting that they exist together in a co-dependent manner. Again, this is not surprising as these two genes function together. Y*mfM* and *ymfL* have low mutual information with a value of 0.54 suggesting that these two genes are not co-dependent but rather directionally dependent.

To help identify directional dependencies, the conditional probability heat map in Figure 5.5 can be filtered for pairs where one gene almost always (>95%) requires the other gene but the reverse is not true; where the other gene is present in genomes containing the first gene less than 80% of the time (Figure 5.7). As expected from the asymmetry in Figure 5.5, *cohE*, *croE, oweE* and *ymfM* are all directionally dependent on *ymfL* (Figure 5.7, *cohE*, *croE, oweE* and *ymfM* rows, *ymfL* column).

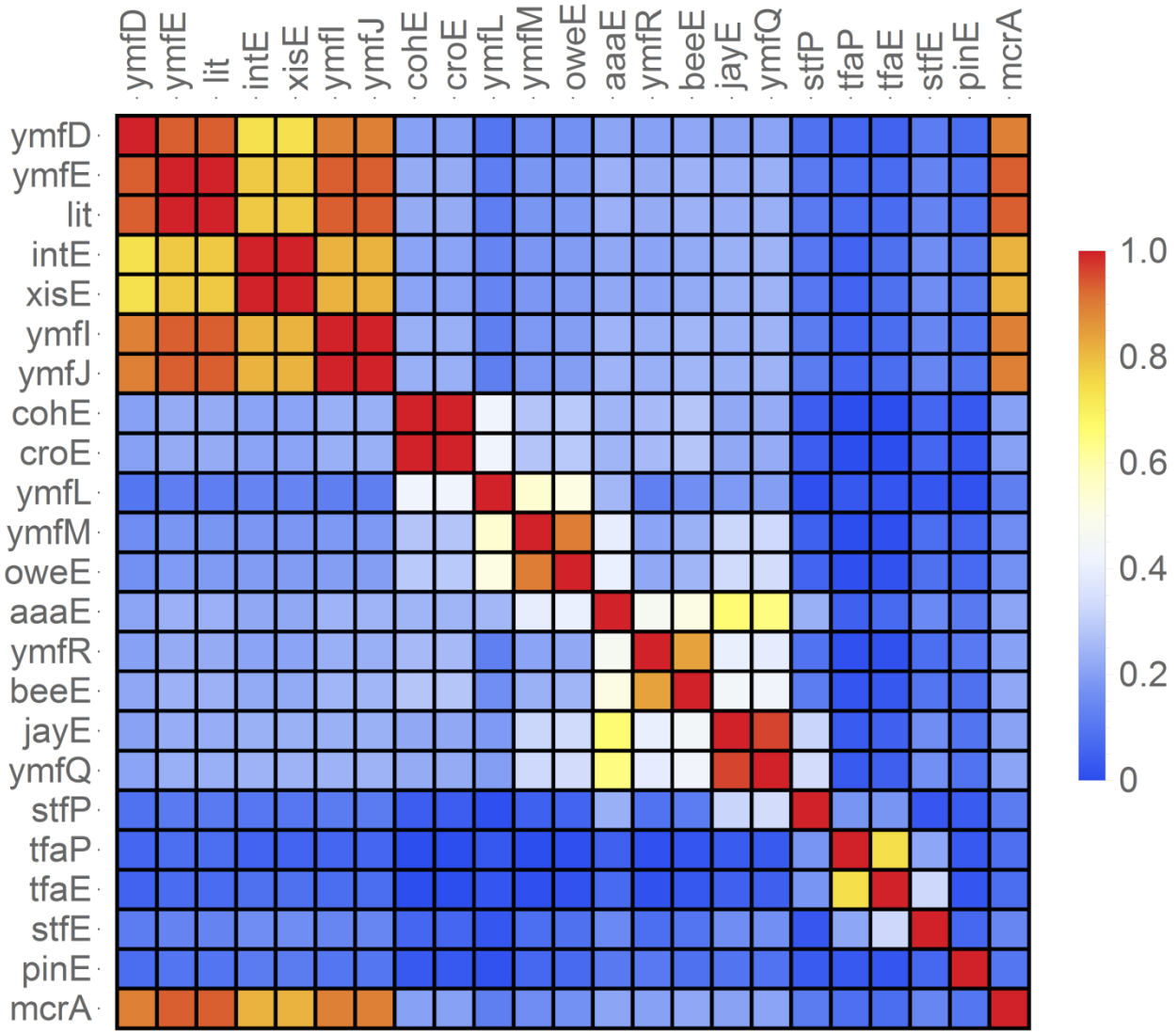

Figure 5.6: Mutual information for all gene combinations of the e14 prophage.

The mutual information is shown as a heat map and measures the probability of two genes co-existing. Red represents strong mutual information (co-existing), blue weak mutual information .

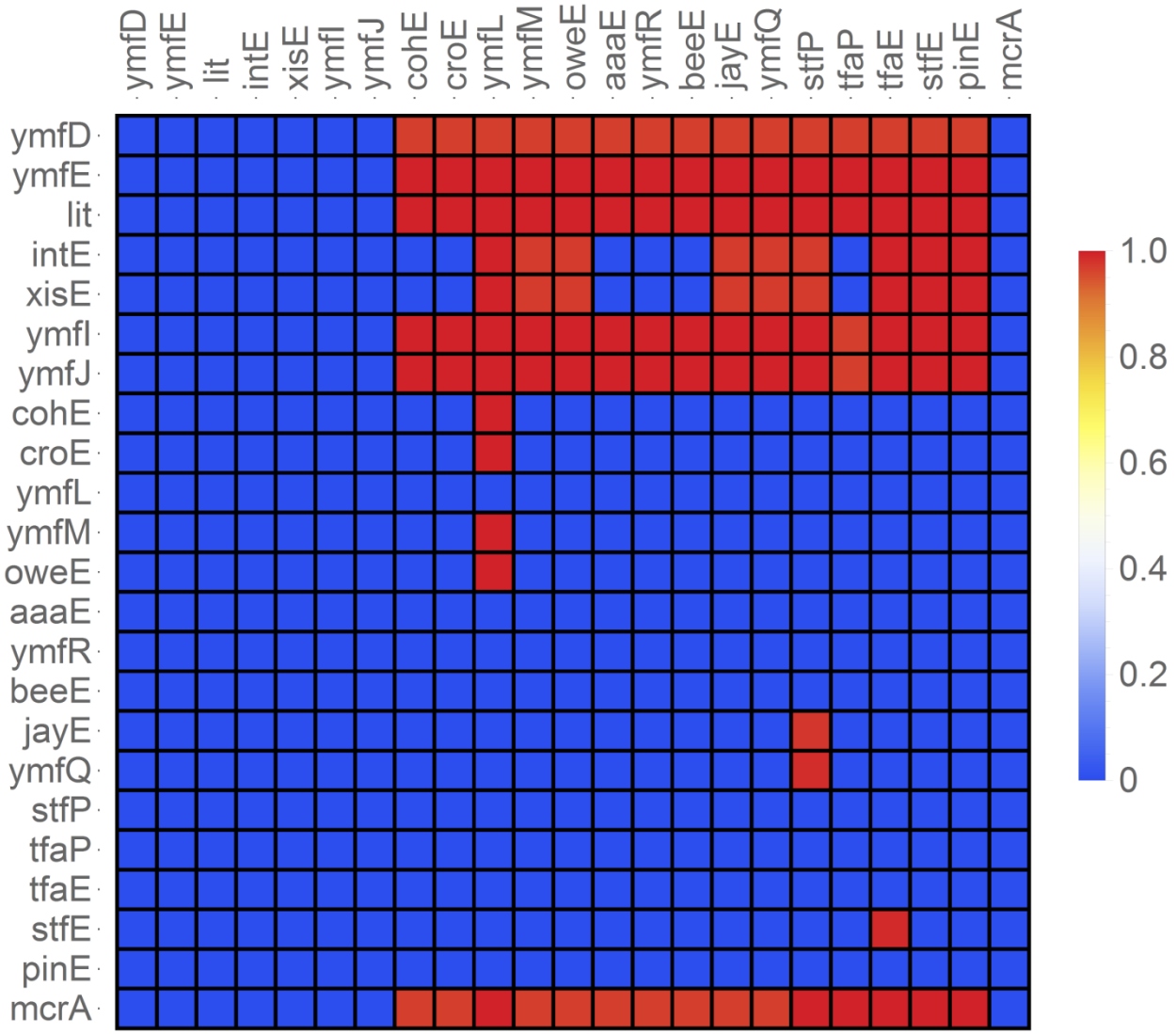

Figure 5.7: Directional probability for all gene combinations of the e14 prophage.

This directional probability is shown as a heat map and measures the directional asymmetry of dependency of genes within the e14 prophage. That is, one gene is dependent on another to be present, while the reverse is not true. Red represents high directional dependency, where the gene at the start of the row (y-axis) requires the gene on the top of the column (x-axis) in order to be present, but the gene at the top of the column can exist without the gene at the start of the row. The red squares have a value > 0.95.

5.2.4 Phylogenetic analysis of *ymfL*

Community profiling showed that a number of genes from the e14 prophage were directionally dependent on *ymfL*. This suggests that *ymfL* has some function that is required by *cohE*, *croE, oweE* and *ymfM* but it also has some function independent of the e14 prophage as it can exist independently. This independent function may be a secondary function that all *ymfL* genes perform or could be the result of *ymfL* being repurposed elsewhere by *E. coli*.

In the case of *ymfL* being repurposed and no longer functioning as a component of the e14 prophage, it is probable that its nucleotide sequence conservation will change to preserve its new function. To test this, a phylogenetic tree containing all *ymfL* homologs found across all complete *E. coli* genomes was made (Figure 5.8). The nodes of the tree were coloured either green when a homolog of *ymfM* was adjacent to the *ymfL* in the respective sequence or red if *ymfM* was not adjacent. This phylogenetic tree clustered into two main groups. The vast majority of nodes in the left hand group had *ymfM* adjacent (green) while the majority of the right hand group were independent of *ymfM* (red).

To examine whether a particular region of *ymfL* varies when it functions with *ymfM*, two consensus sequences were generated, one using the sequences of *ymfL* where *ymfM* was adjacent and one where it was not. The alignment of these two sequences is shown in the supplemental material. Overall, the only area with sustained differences is the last 22 nucleotides where only 2 nucleotides are common between the two sequences.

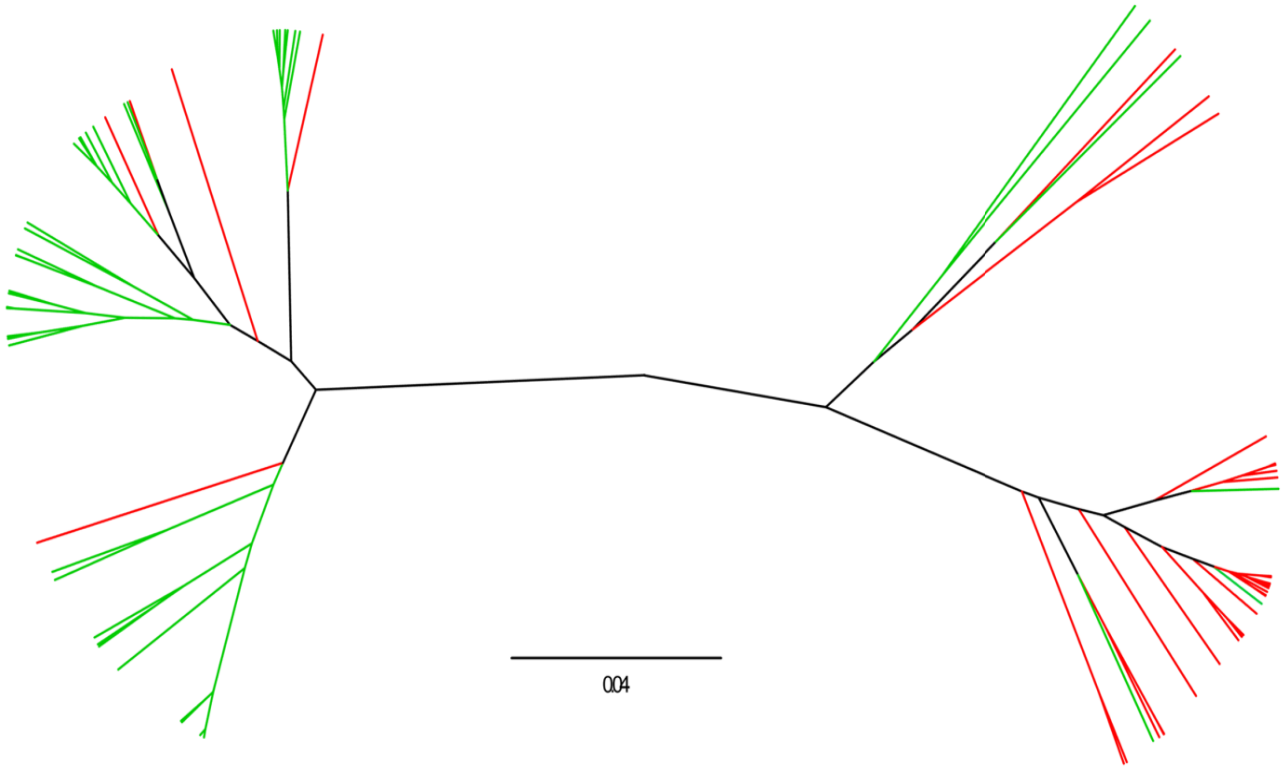

Figure 5.8: Phylogenetic tree of *ymfL* homologs found in *E. coli*.

Nodes of the phylogenetic tree are coloured green if a homolog of *ymfM* is found adjacent to the *ymfL* sequence and red if no *ymfM* homolog is near the *ymfL* gene. Four outlier strains were omitted for visibility. The full tree is shown in Figure S2.

5.2.5 Transcriptional cross-correlation of genes from the e14 prophage from published transcriptional databases

Transcriptional data provides a way to identify genes which are simultaneously transcribed. Community profiling results suggest that *ymfL, ymfM* and *oweE* are co-dependent and likely function together as a system. If these three proteins function together, it is possible that this relationship will be reflected by their simultaneous up-regulation. To test for relationships in transcription between genes in the e14 prophage, pair-wise cross correlations were calculated for each pair of genes using the entire *E .coli* Gene Expression Database. The cross-correlation value ranges from -1 to 1. A value of 1 represents perfect correlation, that is, the transcript levels of the two genes are exactly proportional in all conditions. A value of zero means that the two sets are not linearly correlated. A value of -1 corresponds to two data sets being perfectly anti-correlated, that is, one has low values where the other has high values and vice versa. The results of these calculations are shown in Figure 5.9. Higher values (red panels) show genes whose transcription levels are strongly linearly correlated, values close to zero (blue panels) have no linear predictive power of each other. *CroE* and *cohE* show a low level of cross correlation (0.21), which is consistent with the pair operating as a CI-like repression system [15,16]. Consistent with the genomic analysis, Figure 5.9 shows that the transcription of *ymfL, ymfM,* and *ymfN* (previous annotation of the genes *oweE* and *aaaE*) are strongly linearly correlated.

In order to calculate the cross correlation, each distribution (transcriptional data) had its mean subtracted and was then divided by its standard deviation in order to normalize each distribution. This allowed for the cross correlation to range from -1 (negative correlation) to 1 (positive correlation). While cross correlation values indicate that changes in

transcriptional levels of *ymfL, ymfM,* and *ymfN* occurred synchronous with each other, this does not provide any information as to the magnitude of transcriptional changes within each gene. That is, whether a small increase or decrease in one gene gives rise to a large change in the second gene or vice versa. To examine the sensitivity of transcription levels between *ymfL, ymfM,* and *ymfN*, scatter plots of each pair are shown in Figure 5.10. The red dashed line indicates a symmetric relationship where both transcriptional levels theoretically respond equally; a fold-change in expression of one gene is met with an equal fold change in the other. A symmetric response is expected for proteins in an operon where transcription for all genes occurs at the same time. Examining Figure 5.10, all transcriptional levels respond approximately linearly and are close to symmetric (approximate the red line). Best fit lines shown in green have gradients of 0.84 between *ymfL* and *ymfM*, 0.74 between *ymfL* and *ymfN* and 0.89 between *ymfM* and *ymfN* where perfectly symmetric relationship would have a value of 1.

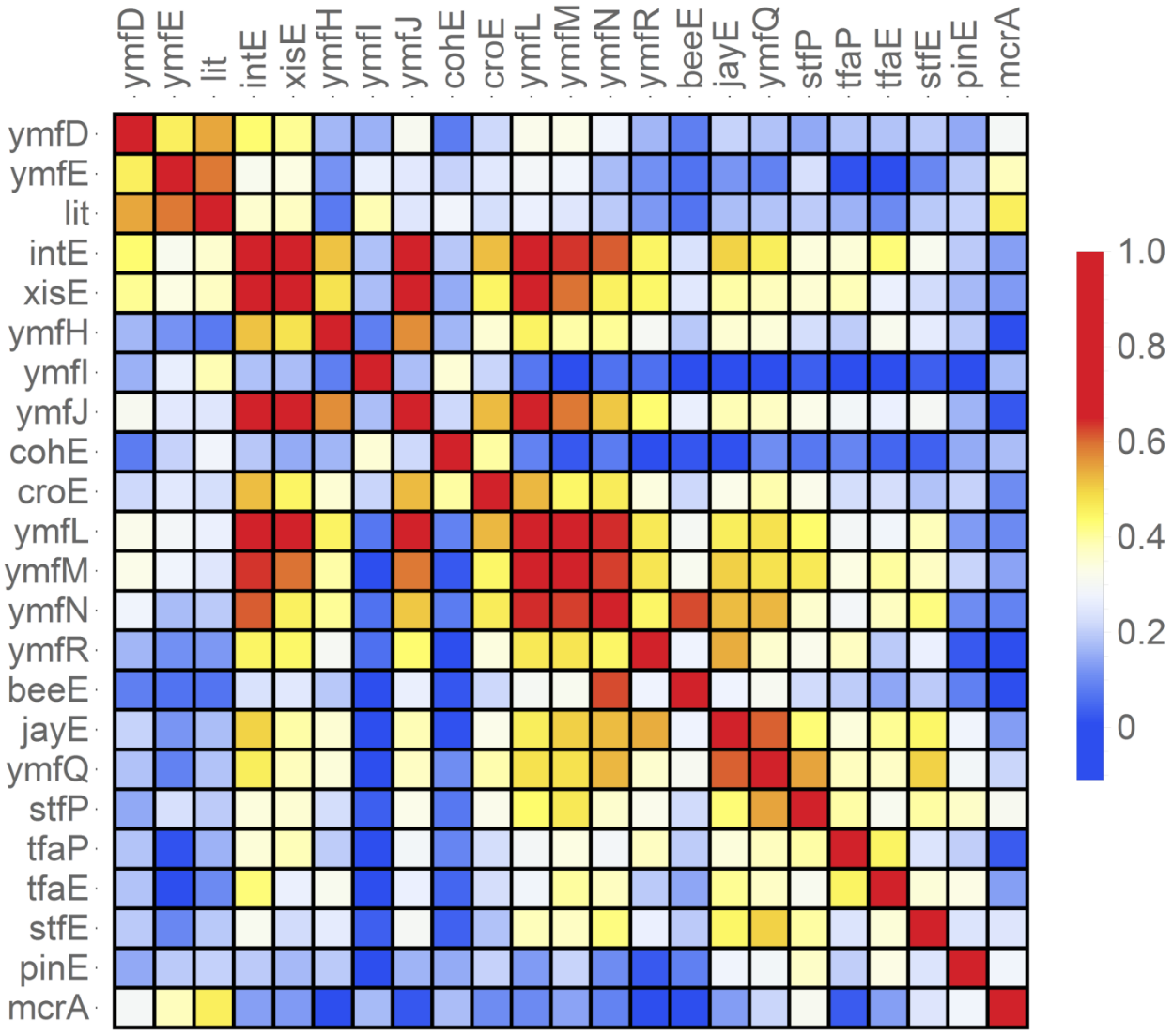

Figure 5.9: Cross correlation of changes within gene transcriptional levels within the e14 prophage. Cross correlation values were calculated using all entries of the *E. coli* Gene Expression Database that included the e14 phage genes. Values closer to 1 (red panels) show genes whose transcription levels are strongly linearly correlated, while values close to zero (blue panels) have little linear predictive power of each other. The colour scale spans the range of measured cross correlation (i.e. there was no strong negative correlations).

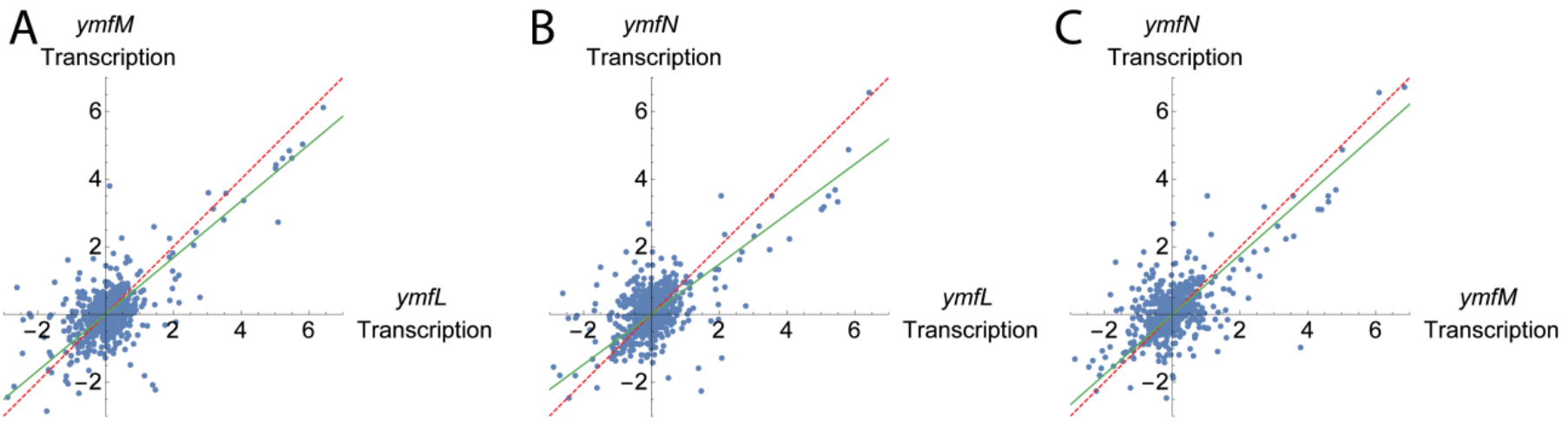

Figure 5.10: Scatterplots of all transcription data for all combinations of *ymfL*, *ymfM* and *ymfN* in the *E. coli* Gene Expression Database.

Values are shown as the $\log_2$ fold change of transcription levels. The red dashed 45 degree line corresponds to a symmetric response where both genes show an equal fold change in transcription levels, indicative of co-expression. Green lines show the line of best fit for each data set with gradients of 0.84, 0.74 and 0.89 for (A), (B) and (C) respectively.

5.3 Discussion

YmfM is a novel cell division inhibitor, which is up-regulated during the SOS response. YmfM seems to have a very similar function to another SOS cell division inhibitor, SulA. Given that both CohE (the putative repressor controlling *ymfM* expression) and LexA (the repressor controlling *sulA* expression) are thought to be inactivated by RecA, and that both SulA and YmfM are cell division inhibitors, it is not clear how their functions differ. Some degree of redundancy in function between SulA and YmfM is consistent with the findings of Chapter 4, where it was shown that the double deletion of *ymfM* and *sulA* was required to minimize cell division inhibition following genetic activation of RecA. The existence of an sRNA which binds to the ribosome binding site of transcribed *ymfM* mRNA suggests that additional regulation of YmfM protein expression may exist on the translational level [221]. The existence such translational control systems in addition to the CroE and CohE transcriptional regulation system would provide a way to differentiate the function of YmfM from SulA.

In this chapter a bioinformatics approach was used to investigate the prevalence of *ymfM* and what dependencies exist between *ymfM* and genes of the e14 prophage. In so doing, the aim of this chapter was to identify potential additional levels of *ymfM* regulation that could conceivably differentiate its expression from SulA.

5.3.1 YmfM is conserved within *E. coli* and is not environment specific

YmfM is confined almost entirely to strains of *E .coli* and, when present, the nucleotide sequence is highly conserved. This level of conservation suggests that *ymfM* has a conserved biological function in *E. coli*. However, since *ymfM* does not cluster to any

specific node or branch of the phylogenetic tree, there is no clear indication that the function of *ymfM* is for a particular environmental niche. Fragments of the e14 prophage can be detected in all nodes suggesting that this phage was acquired before the last common ancestor of these *E. coli* genomes. This is further supported by the presence of homologs in some strains of *Salmonella* and *Shigella* (Table 5.1).

Interestingly every node of the phylogenetic tree also contained the absence of the entire prophage suggesting that e14 is being lost over time and this loss appears to be random and is not node specific. The e14 prophage is able to excise as a circular DNA in response to SOS-inducing conditions [203]. The reintegration of the prophage into the chromosome following excision would almost certainly not be 100% efficient, causing a gradual loss of genes over time. Given the seemingly specialized function of *ymfM*, the occasions where its presence in a cell gives a selective advantage are possibly quite infrequent. If the loss of *ymfM* occurs faster than cells typically experience conditions that apply selection pressures for *ymfM*, most cells will lack *ymfM*. This is quite analogous to the nearly neutral theory of molecular evolution, where genetic variations result from gene mutations occurring faster than selection pressure can suppress, but in this case applying on a whole gene/system level rather than to gene mutation [203, 225]. It is possible that e14 will eventually be lost to all *E. coli* strains because the conditions under which it is lost occur more frequently than the conditions under which it might be beneficial, although it is hard to predict how the rate of loss will change as the e14 prophage becomes more fragmented.

The genes of the e14 prophage are scattered seemingly randomly amongst *E. coli* strains (Figure 5.3), however, three different frequencies of gene presence were observed (Figure

5.4). This suggests that these genes are being lost or maintained cooperatively. If the loss of a single gene incapacitates a system from functioning, there is no longer a use in maintaining the other genes of the system. As a result genes that are being maintained together may indicate that they function together. It is interesting that the gene loss appears to be directional with the first third of the phage present far less than late genes. It is unclear whether this directional loss has an underlying cause, but may indicate that the genes in the latter half of the phage may be selected for. The remainder of the chapter was focused on quantifying and interpreting the degree of co-maintenance.

YmfM functions with YmfL and OweE

Although overall gene presence appeared to cluster into three different frequencies (Figure 5.4), it was not clear whether this was coincidental or if it resulted from these genes co-existing. To test potential gene dependencies, the recently developed technique of community profiling was performed [224]. This technique was further extended to include tests for directionality in gene dependencies by calculating the conditional probabilities of one gene being present given another. From the conditional probability calculations it was identified that *ymfM* and *oweE* likely function together as a system (Figure 5.5) as they are effectively always detected together. This was reiterated through Mutual Information (Figure 5.6) where it was shown that there was a strong co-dependence between *ymfM* and *oweE*, suggesting that they require each other to function.

In the conditional probability (Figure 5.5), *ymfL* was always present when *ymfM* and *oweE* were present suggesting these genes are dependent on *ymfL*. Interesting *ymfL* did not require these genes or any other from the e14 prophage to be present. This asymmetry was detected using the directional probability heat map (Figure 5.7). Phylogenetic

analysis of *ymfL* showed clustering of *ymfL* based on presence of *ymfM* (Figure 5.8) suggesting that two different distinct homologs of *ymfL* exist within *E. coli*, one that functions with *ymfM* and one that may have an alternative function. The last 22 nucleotides of the consensus sequences of the two homologs are heavily divergent, suggesting that the C terminus of *ymfL* may differentiate its function. It is unclear what this alternative function of *ymfL* is, and while interesting, is outside the scope of this study.

Genes, *ymfM* and *oweE* only showed a medium level of mutual information with *ymfL* (Figure 5.6), resulting from the directionality of the conditional probability between these genes (Figure 5.7). If only symmetric metrics were used, such as mutual information, it would have been difficult to correctly identify the relationships between *ymfL* and both *ymfM* and *oweE*. This emphasizes the need to include asymmetric measures including conditional probabilities in conjunction with symmetric metrics previously used (including mutual information [20]) to maximise the information that can be extracted from community profiling.

Considering *ymfM* is dependent on *ymfL* and *oweE*, both of which are putative nucleotide binding proteins, it is probable that *ymfL* and *oweE* regulate *ymfM*'s activity by either affecting the translation of *ymfM* or by directly binding to the resulting YmfM protein. Expression of partial fragment of *ymfL* with full length *ymfM* (Chapter 3, Figure 3.2, *ymfM* Clone) resulted in a reduction in the degree of filamentation as compared to expression of the *ymfM* ORF alone. This indicated that some combination of the partial *ymfL* fragment and the sRNA encoded on the complementary strand of the *ymfL* fragment partially reduced YmfM's ability to inhibit cell division. Further experimental evidence

is required to differentiate whether this was due to the *ymfL* fragment or the sRNA. The role of the *ymfL* fragment and the sRNA can be separated by comparing the degree of filamentation in original clone versus the same fragment with the *ymfL* fragment start codon deleted. This should prevent the translation of the partial *ymfL* sequence but not affect the function of the sRNA. It is also possible that the *ymfL* fragment is only partially functional and that inclusion of the entire *ymfL* gene would more effectively inhibit *ymfM* (i.e. further reduction in the degree of filamentation). This can be tested by co-expressing full-length *ymfL* and *ymfM* from pBAD24 and comparing the degree of filamentation to expressing the *ymfL* fragment and *ymfM*.

Community profiling showed that the putative transcriptional regulators *cohE* and *croE* were co-dependent on each other, as both these genes were found in the presence of each other (Figure 5.5). This is consistent with CroE and CohE acting as a repression switch between maintaining the lysogenic and lytic cycle, respectively [219, 220]. Interestingly these genes were also dependent on *ymfL*, another DNA-binding transcriptional regulator.

5.3.2 Transcriptional regulation of functional systems

Similar to previous large-scale studies [209], transcriptional regulation analysis was performed on e14 genes to provide an independent method to detect what proteins may work together as a system. Consistent with the community profiling results, *ymfM, ymfL* and *oweE* are shown to likely function together as a system.

The relative transcription levels of *ymfM*, *ymfL,* and *oweE* appear to mirror each other; a change in one gene is met with an equal fold change in the others. Such a relationship is

consistent with these three genes being co-transcribed in an operon. This is not surprising given that these genes are annotated as being encoded within the same operon.

YmfL and OweE are both putative nucleic acid binding proteins suggesting that they may operate as negative repressors of *ymfM.* As *ymfM*, *ymfL,* and *oweE* are co-transcribed, all transcriptional level control occurs on all three genes simultaneously. That is, if *ymfL* or *oweE* control the transcription of *ymfM*, they would also control their own transcription. In this scenario, they would act as a self-repressing system generating a negative feedback where, unless inhibited, their expression would repress the further transcription of their own operon. Given the experimental detection of a cis-antisense sRNA strand which is complementary to the *ymfM* ribosome binding site [221], it seems more probable that *ymfL* and *oweE* act to regulate the binding kinetics of the sRNA by binding to RNA rather than DNA, although this idea is admittedly highly speculative.

YmfM is expressed during the SOS response; however, it is also during this time that the e14 prophage excises. It is interesting to consider whether expression of *ymfM* is a benefit to *E. coli*, or whether it benefits the survival of the e14 element, or both. Ultimately, community profiling is unable to answer this question, as it is only sensitive for whether a benefit exists (and hence the genes are maintained). Similar proteins to YmfM, the prophage cell division inhibitors KilR and DicB, respond to certain antibiotics and aid in the development of antibiotic resistance in *E. coli* [16], so it is definitely possible that YmfM has a beneficial role for *E. coli*.

5.3.3 Conclusion

The work presented in this chapter has provided additional evidence of systems within the e14 prophage that work together such as CohE and CroE repression system. As well as this, it has identified a novel relationship between *ymfL*, *ymfM* and *oweE*. This forms the basis for further investigation into the regulatory pathway of *ymfM.* To understand the full role of *ymfM* would require further characterization of this system.

UNIVERSITY OF TECHNOLOGY SYDNEY

Chapter 6. The mechanism of action of YmfM

ithreeinstitute

6.1 Introduction

In Chapter 3, the over-expression of *ymfM* from an inducible plasmid caused a complete inhibition of division leading to filamentous cells. Furthermore, in Chapter 4, YmfM appeared to inhibit division in the absence of SulA during RecA441-mediated SOS. While the results of Chapter 4 gave insight into the possible biological conditions (i.e. SOS response) under which YmfM acts to inhibit division, the exact molecular mechanism of this inhibition is still unclear. In this chapter, the investigation of how YmfM is able to inhibit cell division is initiated. In particular, what stage of division is being inhibited and whether YmfM is acting directly on FtsZ or indirectly through known regulators is explored. For this reason, this introduction gives a relevant overview of cell division, and includes the different known mechanisms of FtsZ inhibition, to remind the reader of the stages of division that can be targeted by an inhibitor.

6.1.1 Overview of cell division

Bacterial cell division involves the localization of the highly conserved protein, FtsZ, at the future division site [14, 226, 227]. FtsZ polymerizes into short protofilaments in a GTP dependent manner [228]. In *E. coli* these protofilaments are bound to the cell membrane via intermediary proteins FtsA and ZipA [25, 26, 29, 31, 229, 230]. These are then able to coalesce into a large filament bundle connected via lateral interactions between protofilaments [231]. The filament bundles assemble into a discontinuous ring-like structure at the division site, called the FtsZ division ring [232]. The early stage of division is defined by the formation of this Z ring, with its associated proteins. Once the Z ring has formed, a number of proteins co-localize with the ring to create a functional

division machine called the divisome, and is referred to as the late stage of division. The divisome drives septal peptidoglycan synthesis and the invagination of the cell envelope [233, 234].

The precise localization and timing of the divisome to mid-cell is coordinated with other cellular functions, in particular DNA replication and chromosome segregation, to give rise to viable daughter cells. Two negative systems known to regulate Z ring positioning to mid-cell include: nucleoid occlusion and the Min protein system [55], although additional systems are likely to exist [9].

6.1.2 FtsZ structure

FtsZ has a general conserved 3D structure (Chapter 1, Figure 1.2), which consists of two independently folding domains, the N-terminal domain comprising the GTP-binding site, and the C-terminal domain, containing the T7 loop [16]. These two domains are linked by the H7 core helix [16]. The assembly of FtsZ into protofilaments occurs in a GTP-dependent manner, with the T7 loop of one FtsZ monomer inserting into the GTP-binding site of the next [17]. This binding activates the GTPase activity of FtsZ, resulting in the hydrolysis of GTP to GDP [22].

6.1.3 Identified modes of FtsZ inhibition

FtsZ inhibition can be achieved either directly or indirectly. Direct inhibitors can act by affecting the GTPase activity of FtsZ [119, 120, 147, 148] or the lateral interactions of protofilaments (high order structures) [53, 58]. While indirect inhibition would come

from utilising the inhibitory actions of another cell division inhibitor [134, 152], by reducing FtsZ cellular levels via transcriptional regulation [135].

Direct inhibitors of FtsZ include, MinC, SlmA, SulA and Kil. The Min system prevents the formation of Z-rings at cell poles by locally inhibiting FtsZ polymerization in these regions [55, 56, 58, 235, 236]. The N-terminal region of MinC interacts with FtsZ for spatial regulation of the Z-ring [72]. MinC prevents polymerisation without affecting the GTPase activity of FtsZ [71], and also prevents lateral interactions of FtsZ protofilaments [58]. SlmA, the nucleoid occlusion protein prevents the Z ring forming over the nucleoid by directly interacting with FtsZ [11, 237, 238]. Like MinC, SlmA prevents polymerisation without affecting the GTPase activity of FtsZ [239].

SulA, is up-regulated as part of the SOS response following DNA damage, giving the cell time to repair the damaged DNA before cell division resumes [198]. SulA directly interacts with FtsZ, as has been shown by the crystal structure in complex with FtsZ in *P. aeruginosa*, where SulA was shown to be bound near the T7 loop of FtsZ [117]. SulA binds to free monomers of FtsZ in a sequestration manner, and inhibits FtsZ polymerisation by reducing the GTPase activity of FtsZ [119, 120]. Kil of bacteriophage λ inhibits cell division leading to filamentation and eventual cell death [133]. Mutations within *ftsZ* that are resistant to the effects of *kil* were found within the T7-loop and GTP-binding domain suggesting that Kil acts to inhibit the GTPase activity of FtsZ [147]. Indeed, i*n vitro,* Kil interacts directly with FtsZ and, like SulA, is able to reduce GTPase activity, as well as disrupt protofilament bundling [147, 148]. While *in vivo kil* requires ZipA to disrupt Z-ring formation, and it has been suggested that ZipA acts to recruit Kil to the FtsZ protofilaments [147].

Indirect inhibitors of FtsZ include two phage-encoded genes, *dicB* and *dicF*. DicB, encoded within the Qin prophage, prevents division indirectly by sequestering MinC. DicB does not share any homology to MinD but is able form a complex with MinC in a similar way to MinD to activate the inhibitory actions of MinC [134]. However, unlike the MinD/MinC complex, the DicB/MinC complex does not localise to the cell membrane, suggesting that DicB activates MinC-mediated cell division inhibition throughout the cell [134]. DicF, also within the *dicB* operon is a small RNA (sRNA), which causes the antisense inhibition of *ftsZ* mRNA, preventing the translation of FtsZ [135].

6.1.4 YmfM, a potential cell division inhibitor

YmfM is a recently identified inhibitor of cell division [163]. When over-expressed, cells become filamentous (Chapter 3) and this inhibition of division contributes to the filamentation during RecA441-mediated SOS response (Chapter 4). A combination of bioinformatics [155], over-expression studies [Chapter 3], and genetic experiments (Chapter 4) has strongly suggested that SfiC, an SOS-inducible cell division inhibitor, is YmfM. As a result, previous studies examining the potential mechanism of SfiC inhibition [136, 154, 205], should also hold true for YmfM. SfiC is suggested to target FtsZ as point mutations of *ftsZ* which conferred resistance to the inhibitory effects of SulA, also conferred resistance to SfiC, implying a common mechanism of action [136, 154].However unlike SulA, the over-production of FtsZ did not overcome the inhibitor effects of SfiC, suggesting that while the mechanism of action may be the same, their binding kinetics or turnover of proteins are different [205].

While the initial characterisation of SfiC has suggested that FtsZ is the ultimate target for the inhibition of division, it is unclear how many degrees of separation there are between YmfM and FtsZ. That is, is YmfM interacting directly with FtsZ, similar to SulA or Kil. Or is YmfM acting indirectly through known cell division inhibitors, similar to the way DicB utilises MinC. Furthermore, from the examples of identified modes of inhibition, it is clear that there are multiple ways in which a cell division inhibitor can act on the division process. Therefore, by initiating investigation into how YmfM inhibits division, this chapter will provide insight into potential mechanisms of a novel phage-encoded gene.

6.1.5 Chapter Aims and Objectives:

The overall aim of this chapter was to investigation how YmfM inhibits cell division leading to filamentation. This was separated into four aims.

The first aim was to identify the stage of division which YmfM acts upon. This involved determining whether YmfM-induced filaments contained Z rings using immunofluoresence microscopy (IFM). The presence of Z rings would indicate that a late stage division component was being targeted, while the function of FtsZ was not being affected. The absence of Z rings would indicate that an early stage of division was being affected.

The second aim was to determine whether YmfM was acting indirectly through known cell division inhibitors. This was achieved by over-expressing *ymfM* in mutant strains lacking SulA, MinC or SlmA, and determining whether filamentation could still occur. The third aim was to understand whether YmfM was localising to the division site to inhibit division through the use of *ymfM-gfp*.

Finally, it was aimed to determine whether YmfM was able to interact with FtsZ *in vitro*, and affect the GTPase activity FtsZ and its ability to polymerise into protofilaments.

6.2 Results

6.2.1 Detecting Z ring formation in cells induced to express *ymfM*

To understand whether *ymfM* expression inhibits cell division at the level of FtsZ assembly or at a later stage of the cell division process, immunofluorescence microscopy (IFM) was used to examine Z ring frequency in cells induced to express *ymfM* from pBAD-*ymfM*. The absence of Z rings in the *ymfM*-induced filamenting cells would imply that *ymfM* expression causes filamentation by inhibiting Z ring formation. If Z rings are present in these cells, this will indicate that FtsZ is able to polymerise and form a ring at the division site, but that effects on other components of the divisome are causing filamentation.

To test whether, *ymfM*-induced filaments contain Z rings, WT (BW25113) cells harbouring pBAD-*ymfM* were grown to mid-exponential phase in glucose (repression of *ymfM*) and arabinose (expression of *ymfM*). Under glucose repression, where the cells are short and dividing with normal frequency, cells contained Z rings, 8.44 μm of cell length per Z ring (Table 6.1), seen as bright green bands at mid-cell (white arrows) (Figure , left column). When *ymfM* expression was induced with arabinose, almost no Z rings were observed along the length of the filamentous cells. Instead FtsZ appeared to be diffused throughout the filament as seen by detection of a signal throughout the filament. Occasional Z rings were seen in this sample, however these were primarily in the few short cells present (Table 6.1). DAPI (DNA) staining showed that induced expression of *ymfM* did not have a drastic effect on nucleoid morphology.

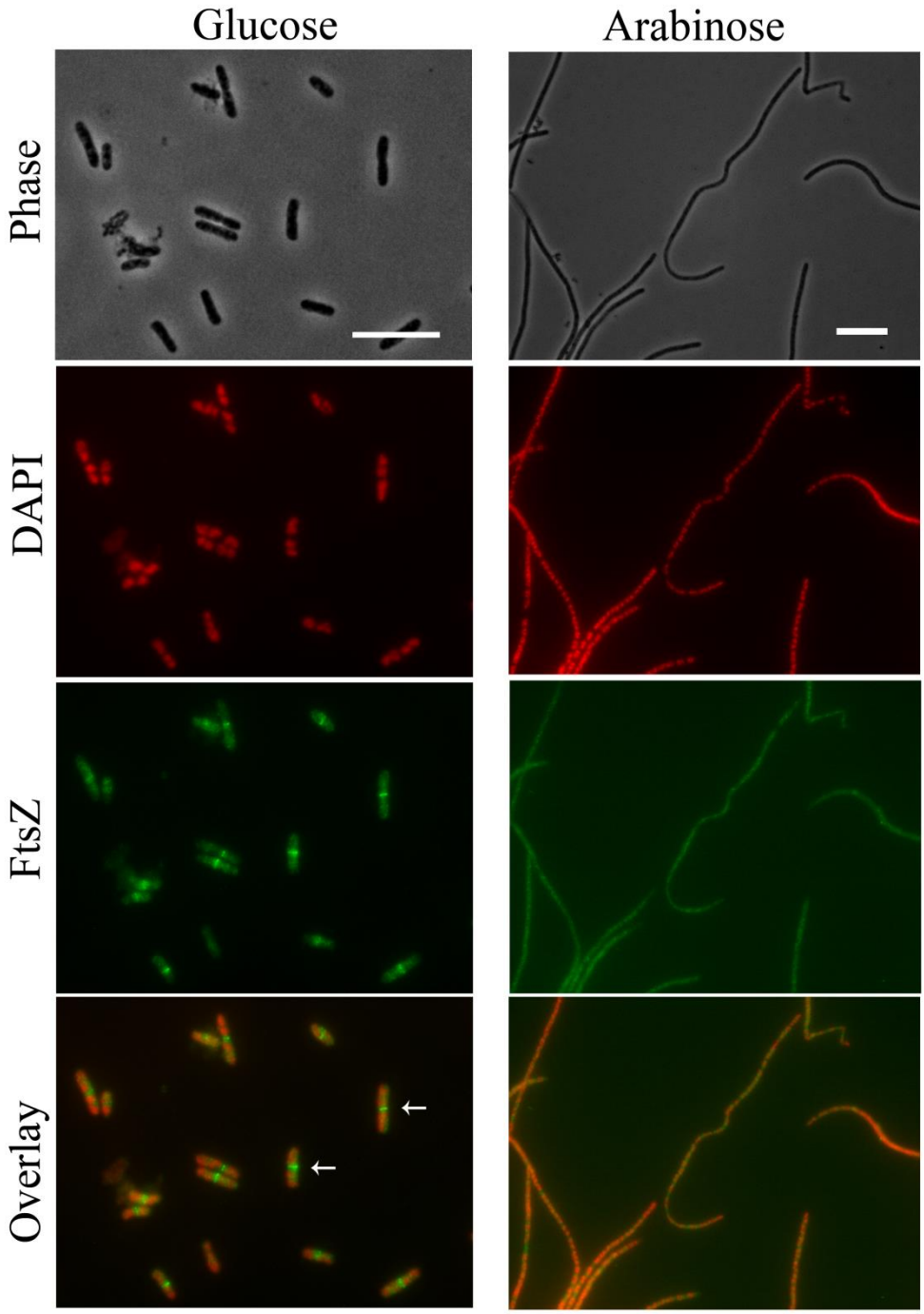

Figure 6.1. BW25113 pBAD-*ymfM* induced filaments have no Z rings.

Immunofluorescence microscopy to visualize Z rings in cells either repressing *ymfM* with 0.2% glucose, (left column) or inducing expression with 0.2% arabinose (right column). Cells were grown in LB for 90 minutes with 100 µg/mL ampicillin at 37ºC. DAPI (nucleoid) staining shows DNA morphology. FtsZ protein labelled with anti-FtsZ antibodies. Bright green band corresponds to Z rings with white arrows highlighting clear examples of rings

Scale bars = 10µm

In additional to cells expressing *ymfM*, IFM was also performed on control samples to ensure that the protocol was optimized for filamentous cells and did not affect the integrity of Z rings. Firstly, an FtsZ-depleted sample was used as a negative control to test the specificity of the *E. coli* FtsZ antibodies. The strain JKD-2 (W3110 *ftsZ::kan*), containing *ftsZ* on a temperature sensitive plasmid [240], was grown at the non-permissive temperature of 42°C to deplete the cell of FtsZ. IFM of these cells showed that FtsZ was not detected, showing that the antibodies were specific to FtsZ (Figure 6.2, right column). Secondly, cephalexin treated cells were used as a positive control for Z rings in filaments (Figure 6.2, left column). Cephalexin is a cephalosporin antibiotic that inhibits peptidoglycan synthesis specifically at the septal site [241]. It prevents cells from dividing as the septal wall is not synthesised and therefore cell filamentation occurs. Since the filamentation by cephalexin occurs via a different pathway to direct FtsZ inhibition, Z rings in cephalexin treated cells are still present. IFM of this sample showed that the protocol was able to detect the presence of Z rings along the length of the filamentous cells (Figure 6.2, left column), with a Z ring detected every 11 μm cell length. Overall the controls show that the IFM procedure was specific for the detection of FtsZ and was not affecting the integrity of Z rings in filaments.

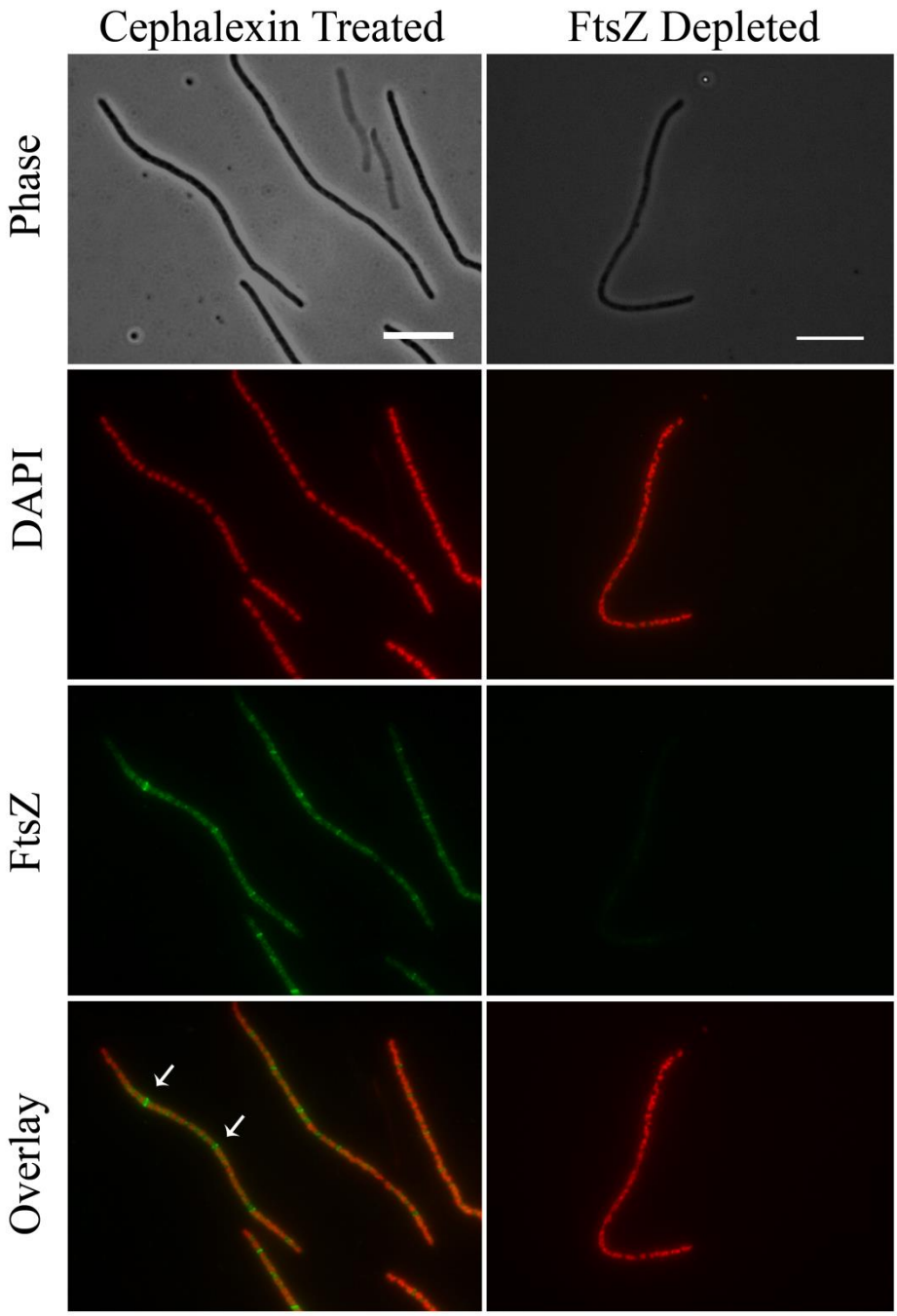

Figure 6.2. Optimisation of immunofluorescence microscopy for detecting the formation of Z rings in filamentous *E. coli*

Cephalexin-treated cells were used as a positive control for Z ring detection in filamentous cells. Cephalexin targets the penicillin binding protein, FtsI, to cause filamentation. As a results Z rings are present in cephalexin treated cells. BW25113 cells were grown to mid-log in the presence of 2 μg/mL cephalexin. The temperature-sensitive *fts*Z mutant strain was used to determine the specificity of the antibodies to FtsZ. At 42°C, cells are depleted of FtsZ and the protein is no longer detected by IFM. DAPI (nucleoid) staining shows DNA morphology. FtsZ protein labelled with anti-ftsZ antibodies. Bright green band corresponds to Z rings with white arrows highlighting clear examples of rings. Scale bar = 10μm

.

Table 6.1. Number of Z rings detected in *ymfM*-induced filament via immunofluorescence microscopy

	pBAD-ymfM [a]		**Cephalexin Control** [b]	
	Glucose Repressed (short)	**Arabinose Induced (long)**	**No cephalexin**	**2 µg/mL cephalexin**
Number of Z rings	60	16 [c]	59	96
µm / Z ring	8.4	224.4	5.79	11.3
Average Cell length (µm)	4.9	35.5	2.93	37.3

[a] Wild-type (BW25113) containing pBAD-*ymfM* were grown in LB supplemented with 0.2% glucose and 0.2% arabinose for two hours. Cells were fixed and processed for immunofluorescence microscopy to visualize Z rings. Approximately 100 cells were counted for each sample.

[b] Wild-type (BW25113) cells were grown to mid-log in the presence and absence of 2 µg/mL of cephalexin in LB at 37°C. 30 cells counted for cephalexin induced filaments

[c] 11 of the Z rings counted were from cells less than 8µm in cell length (short cells)

6.2.2 Measurement of cellular levels of FtsZ in *ymfM*-expressed cells

The results of the IFM showed that in cells over-expressing *ymfM*, Z rings were unable to form. To determine whether this was due to FtsZ mis-localisation or a reduction in cellular levels of FtsZ, western blotting was used to examine the FtsZ levels in these filamentous cells. Cells containing both pBAD24 and pBAD-*ymfM* were grown to mid-log phase with glucose or arabinose, and processed for western blotting using *E. coli* FtsZ antibodies. FtsZ (40 kDa) levels remained constant under arabinose induction of *ymfM* as compared to glucose repression (indicated by black arrow, Figure 6.3). FtsZ was also depleted again using the strain JKD-2 which contains *ftsZ* on a temperature sensitive plasmid. Depletion of FtsZ acted as a control to show that under experimental conditions tested, a reduction in cellular FtsZ levels was able to be detected and the antibodies were specific to FtsZ (Figure 6.4). Western blotting shows that the expression of *ymfM* does not affect FtsZ on a protein level.

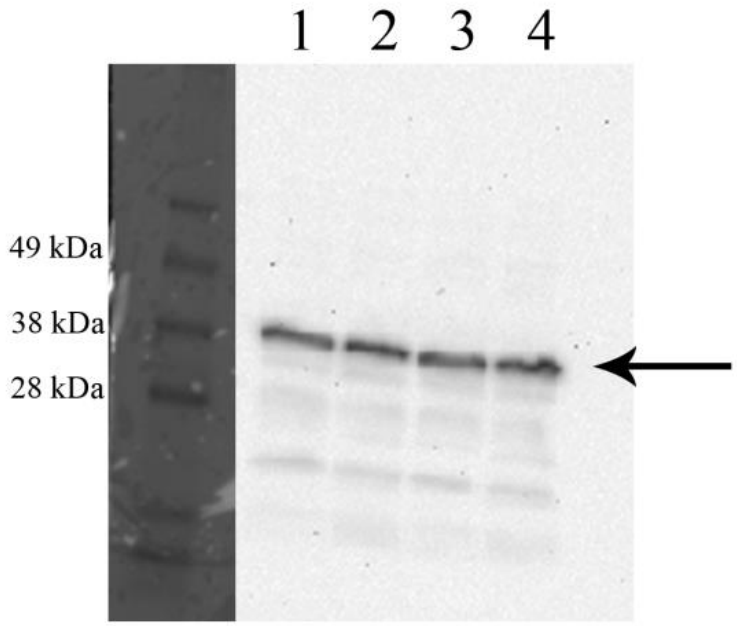

Figure 6.3. Western blot to determine cellular FtsZ levels in *ymfM* expressed cells

BW25113 carrying pBAD24 and pBAD-*ymfM* were grown in LB media at 37^{o}C with glucose (repression) or arabinose (induction) for two hours. Western blot was performed with equal loading of protein for each sample. Lane 1 is of pBAD24, grown in glucose. Lane 2,is of pBAD24 grown in arabinose. Lane 3, is of pBAD-*ymfM* grown in glucose. Lane 4 is of pBAD-*ymfM* grown in arabinose. The black arrow indicates the expected migration point of FtsZ (40 kDa). The ladder is of the same blot and at the same scale, but taken under white trans-illumination light, while the bands of the blot were detected using chemi-illumination. The two channels were then overlayed. Intensities of the each band were quantified giving an arbitrary unit; Lane 1 is 50, Lane 2 is 50.5, Lane 3 is 50.3 and lane 4 is 53.

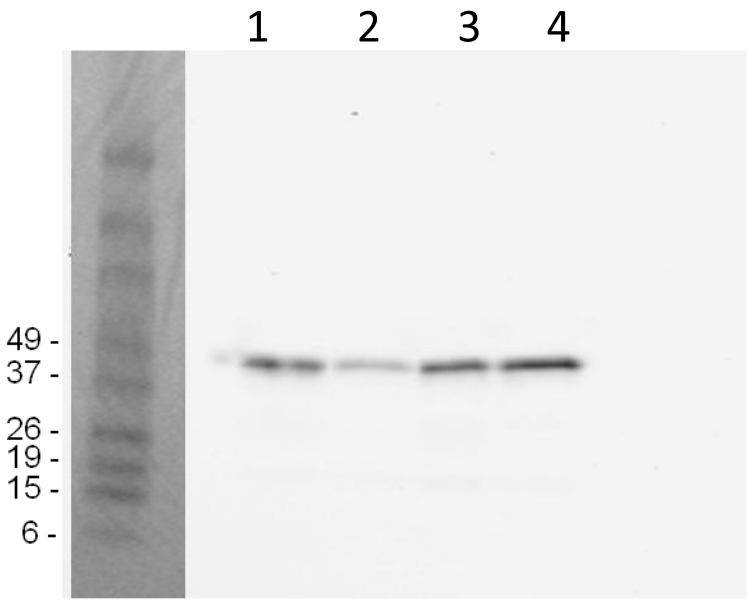

Figure 6.4. Western blot to determine specificity of the antibody to FtsZ

Strain JKD-2 (W3110 *ftsZ::kan*), contains a temperature sensitive plasmid pKD3a encoding for *ftsZ.* This construct allows for the expression of FtsZ and subsequent normal cell division at the permissive temperature of 30^{o}C. At the non-permissive temperature of 42^{o}C, ftsZ is no longer expressed and is depleted from the cells. This strain was grown at both 30^{o}C and 42^{o}C.Western blot was performed with equal loading of protein for each sample. Lane 1, strain JKD-2was grown 30^{o}C. Lane 2, strain JKD-2was grown 42^{o}C to deplete FtsZ. Lane 3, BW25113 (wild-type) grown at 30^{o}C as a control. Lane4, BW25113 (wild-type) grown at 42^{o}C as a control. The ladder is of the same blot and at the same scale, but taken under white trans-illumination light, while the bands of the blot were detected using chemi-illumination. The two channels were then were then overlayed. Intensities of each band were quantified giving an arbitrary unit; Lane 1 is 36, Lane 2 is 16, Lane 3 is 33 and lane 4 is 44.

6.2.3 Inhibition of cell division by YmfM does not rely on known *E. coli* cell division regulators SulA, MinC and SlmA.

The inhibition of division by the expression of *ymfM* appears to target the earliest stage of division as Z rings were not detected via IFM. It is unclear however, whether YmfM is acting directly on FtsZ or indirectly through known inhibitors such as SulA, MinC and SlmA, which act on the early stage of division. In addition to this, there is evidence that other inhibitors, such as prophage encoded DicB, act indirectly on FtsZ by utilising the inhibitory effects of MinC. It was therefore questioned whether YmfM was acting indirectly to prevent Z rings assembly through SulA, MinC or SlmA. If YmfM was acting indirectly through these inhibitors, then their absence would result in no filamentation even when pBAD-*ymfM* is expressed.

Over-expression of *ymfM* in the *sulA* deleted background, JW0941

During times of stress such as DNA damage caused by UV exposure, SulA as part of the SOS response inhibits cell division by directly interacting with FtsZ, resulting in filamentous cells. *E. coli* DH5*α*, the strain used for screening for filamentation-inducing genes [163], has a *recA* mutation (*recA1*). This mutant is deficient in RecA function including the auto-cleavage of the repressor LexA [242]. This means that any genes identified in the original screen would be independent of SulA activity to inhibit division. However as a further confirmatory test, *ymfM* expression from pBAD-*ymfM* was induced in a *sulA*-deletion background, JW0941, for 2 hours after which cells were fixed and analysed using a Coulter counter for cell volume changes. Over-expression of *ymfM* in

the *sulA* mutant resulted in filamentation (20.8±12.7μm^3) to a similar degree as the parent WT strain, BW25113 (18.9 ±14.0μm^3) (Figure 6.5 and Table 6.2).SulA is therefore not responsible for the inhibition of division during the expression of *ymfM*.

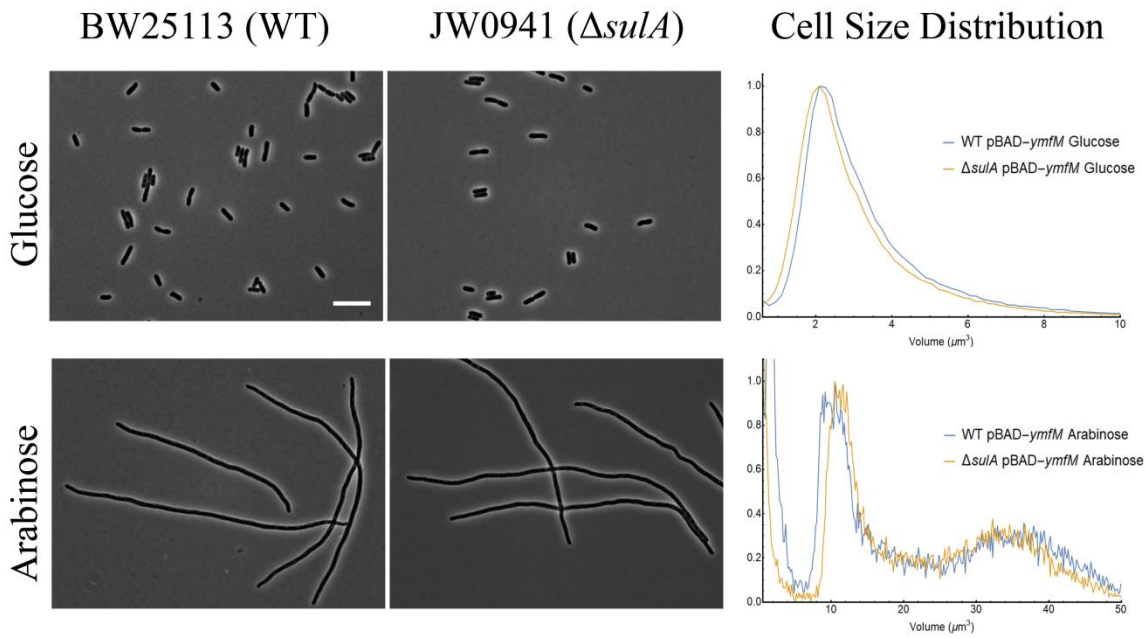

Figure 6.5. Filamentation caused by the over-expression of *ymfM* is independent of the cell division inhibitor, SulA.

Top panel shows ymfM expression repressed in cells of wild-type strain, BW25113 (left) and a *sulA*-deleted strain, JW0941. A comparison cell-length distribution between wild-type and the deletion strain is shown in a distribution plot (right). Bottom panel shows *ymfM* expression induced with arabinose, leading to filamentation in both the wild-type and *sulA*-deletion strains. The cell-size distribution of these two populations is shown in the bottom right panel.

Scale bar = 10μm

Over-expression of *ymfM* in a *minCDE*-deleted background, TB43

The Min system in *E. coli*, comprising of proteins, MinC, MinD and MinE, is a spatial regulator of cell division. These genes were deleted in *E. coli* resulting in the strain TB43 [50]. The absence of these Min proteins results in a mixed population of minicells (small cells lacking DNA) as a result of polar cell division, and mildly filamentous cells [55]. This can be seen in the phase-contrast image on the top row, middle image of Figure 6.6, as well as the cell size distribution (top row, right image), comparing the mutant strain with the WT parent strain, with *ymfM* under glucose repression. Expression of pBAD-*ymfM* caused filamentation in both the parent strain, TB28 (17.9±9.4 μm^3), as well as the mutant strain, TB43 (16.8 ± 10.4 μm^3). The two filamenting populations overlay each other as shown by the cell size distribution plot (Figure 6.6. bottom row, right image). The Min system is therefore not responsible for the inhibition of division during the expression of pBAD-*ymfM.*

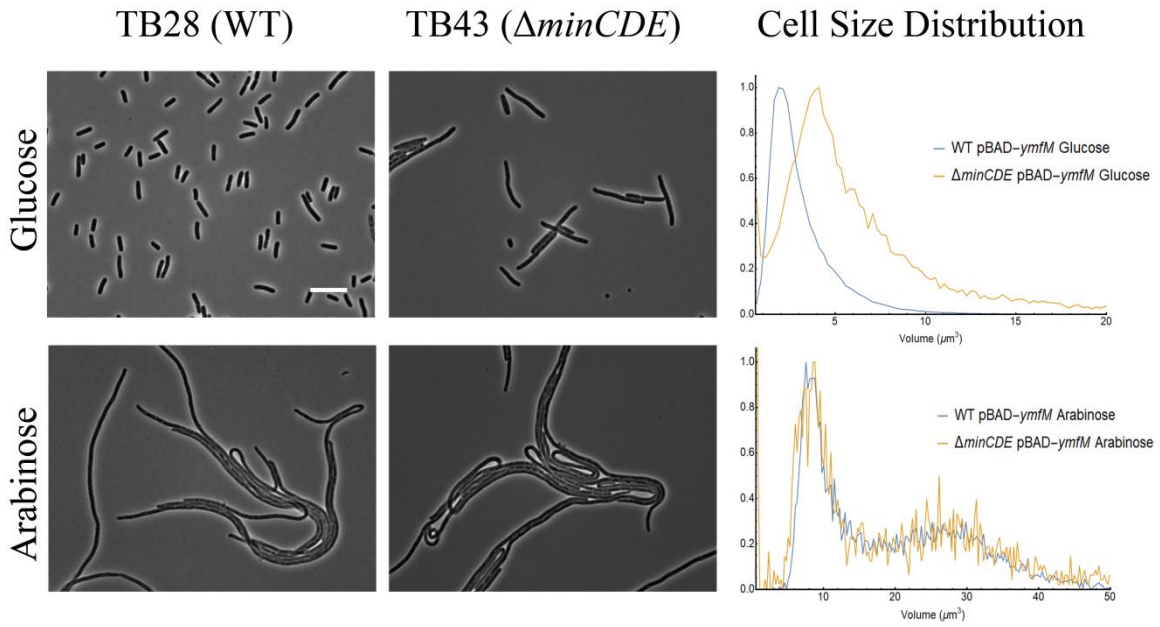

Figure 6.6. Filamentation caused by the over-expression of *ymfM* is independent of the division regulator, the Min system.

Top panel shows *ymfM* repressed in cells of wild-type TB28 (left) and a *minCDE* deletion, TB43 strain (middle). A comparison of cell length distribution between wild-type and deletion strain is shown in a distribution plot (right). Bottom panel shows *ymfM* expression induced from pBAD-*ymfM*, with arabinose leading to filamentation in both the wild-type and deletion strains. The cell size distribution of these two populations is shown in the bottom right panel.

Scale bar = 10μm

Over-expression of *ymfM* in the *slmA*-deleted background, JW5641

SlmA is a nucleoid occlusion protein in *E. coli* that provides spatial and temporal regulation of Z ring assembly during a normal cell cycle. It does this by preventing FtsZ polymerisation and therefore division events occurring over unsegregated DNA[50]. Mutant strain, JW5641, was used to determine whether YmfM requires SlmA to inhibit division. Expression of *ymfM* in the mutant background resulted in filamentation (Figure 6.7), showing that the inhibition of division by YmfM is not mediated through SlmA.

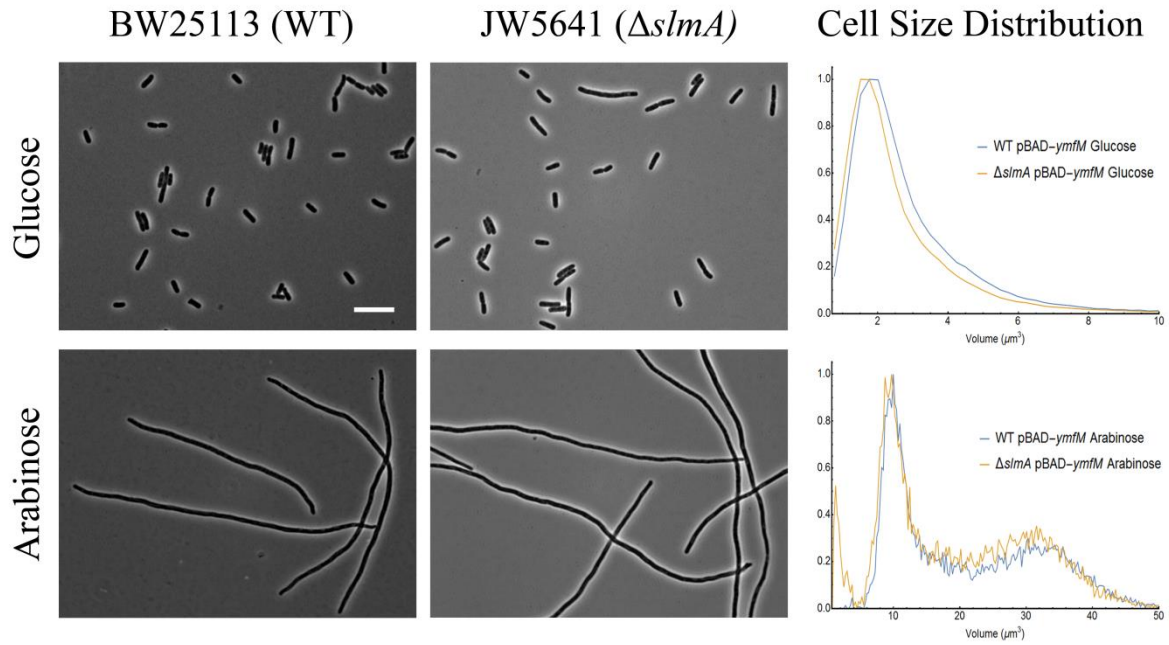

Figure 6.7. Filamentation induced by *ymfM* is independent of the nucleoid occlusion protein, SlmA.

Top panel shows pBAD-*ymfM* expression repressed in cells of wild-type BW25113 (left) and a *slmA* deletion, JW5641 strain (middle). A comparison cell length distribution between wild-type and deletion strain is shown in a distribution plot (right). Bottom panel shows *ymfM* expression induced with arabinose leading to filamentation in both wild-type and deletion strain. The cell size distribution of these two populations is shown in the bottom right panel. Scale bar = 10μm

Table 6.3. Mean cell volume (µm^3) of *ymfM* expressed from pBAD-*ymfM* in mutant backgrounds, as determined by the coulter counter.

Strains[a]	**Mean Cell Volume µm^3 (S.D)**	
	Glucose	Arabinose
BW25113 (WT)	3.5 (2.6)	18.9 (14.0)
JW0941 (Δ*sulA*)	3.1 (2.1)	20.8 (12.7)
JW5461 (Δ*slmA*)	2.78 (2.2)	19.5 (11. 6)
TB28 (Parent to TB43)	3.3 (2.6)	17.9 (9.4)
TB43 (Δ*minCDE*)	6.6 (6.1)	16.8 (10.4)

[a] Refer to Table 2.2 in Chapter 2: Methods and Material for strain information. These strains were harbouring pBAD-*ymfM* and were grown in LB with 100 µg/mL ampicillin at 37^{o}C. The expression of *ymfM* was induced with 0.2% arabinose or induced by 0.2% glucose for 2 hours. Samples were fixed with 3% formaldehyde. Cell length distribution was measured on the coulter counter and reported as a volume (µm^3).

6.2.4 Cellular localisation of YmfM during filamentation, using GFP

To better understand how YmfM was inhibiting division, localisation of YmfM using a GFP tag was planned to be undertaken. This would allow visualisation of whether YmfM is recruited to the division site when it inhibits division, or whether its actions are not site specific resulting in no obvious localisation pattern. Ultimately the objective of this section was to generate a single-copy GFP fusion on the chromosome to visualise localisation of YmfM during conditions in which it is expressed, such as norfloxacin treatment (Chapter 4). An initial proof of concept was testing for functionality of the GFP fusion. To achieve this, *ymfM* was cloned as a *gfp* fusion into pBAD24. Expression from this system would provide an initial way to determine functionality. Unfortunately due to time constraints, only the construction of pBAD-*ymfM-gfp* and expression from the plasmid system was achieved. This section will therefore present the results of *ymfM-gfp* expression from pBAD24.

Testing the functionality of the YmfM-GFP fusion in wild-type *E. coli*

YmfM was tagged at both the C-terminus and N-terminus with super-folding green fluorescent protein (sfGFP) [243], and cloned into pBAD24. Expression from these constructs was compared to the untagged *ymfM* (pBAD-*ymfM*), to determine whether the fluorescent tag would interfere with the function of YmfM. This was achieved by comparing the degree of filamentation observed with GFP tagged variants with untagged YmfM. The untagged and the two tagged GFP constructs were induced with 0.2% arabinose for two hours and cell size was analysed on the Coulter Counter. Expression of the C-terminal GFP tag resulted in a similar filamentation profile (21.8 ± 10.8 μm^3) as

compared to the untagged version (19.2 ± 10.9 μm^3) (Figure 6.8). However, the N-terminal GFP tag, caused a lesser degree of filamentation (13.3 ± 10.9 μm^3) (Figure 6.8), suggesting that the addition of a large protein at the N-terminus was affecting the ability of YmfM to inhibit division.

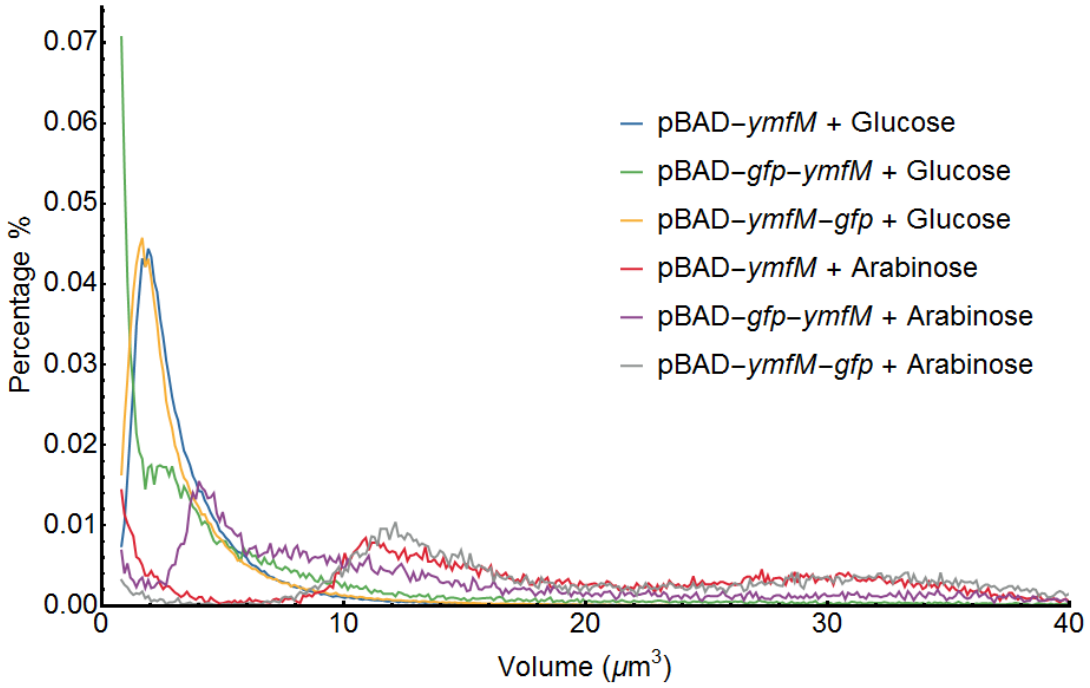

Figure 6.8. Cell size distribution comparison of untagged and GFP tagged YmfM

Cell size distribution of untagged, N-terminally (GFP-YmfM) and, C-terminally (YmfM-GFP) GFP tagged *ymfM* cloned into pBAD24. Cells harbouring these plasmid constructs were grown with either 0.2% glucose for gene repression or 0.2% arabinose for induction in LB for two hours. Samples were analysed on the Coulter Counter and displayed as a histogram showing the distribution of cell volume.

Localisation of YmfM using C-terminally tagged YmfM-GFP

The C-terminal GFP tagged version of YmfM was similar in its ability to cause filamentation compared the untagged version. As a result this construct was used to look for fluorescent signal and potential cellular localization. Cells were grown in either 0.2% glucose to repress or 0.2% arabinose to induce expression of *ymfM-gfp* for one hour. Samples were placed onto agarose pads and imaged live using fluorescence microscopy. Fluorescence was observed only when *ymfM* was induced and the GFP signal was detected uniformly throughout the filament with no specific localisation of YmfM-GFP (Figure 6.9). In addition to this, cells expressing *ymfM-gfp* showed asymmetrical cellular morphological changes including branches and knobs instead of the expected filamentation as seen in the untagged *ymfM* population. Figure 6.10, shows examples of cells displaying these abnormal shapes, suggesting that the addition of the GFP tag at the C-terminus, while still resulting in filamentation of the cells, is having an additional effect on the cell morphology. This additional phenotype was quantified, and 24% of cells/filaments had these abnormal shapes/appendages. As mentioned earlier, due to time constraints, optimising a functional fusion and generating a single-copy variant was not achieved within this body of work and requires further troubleshooting.

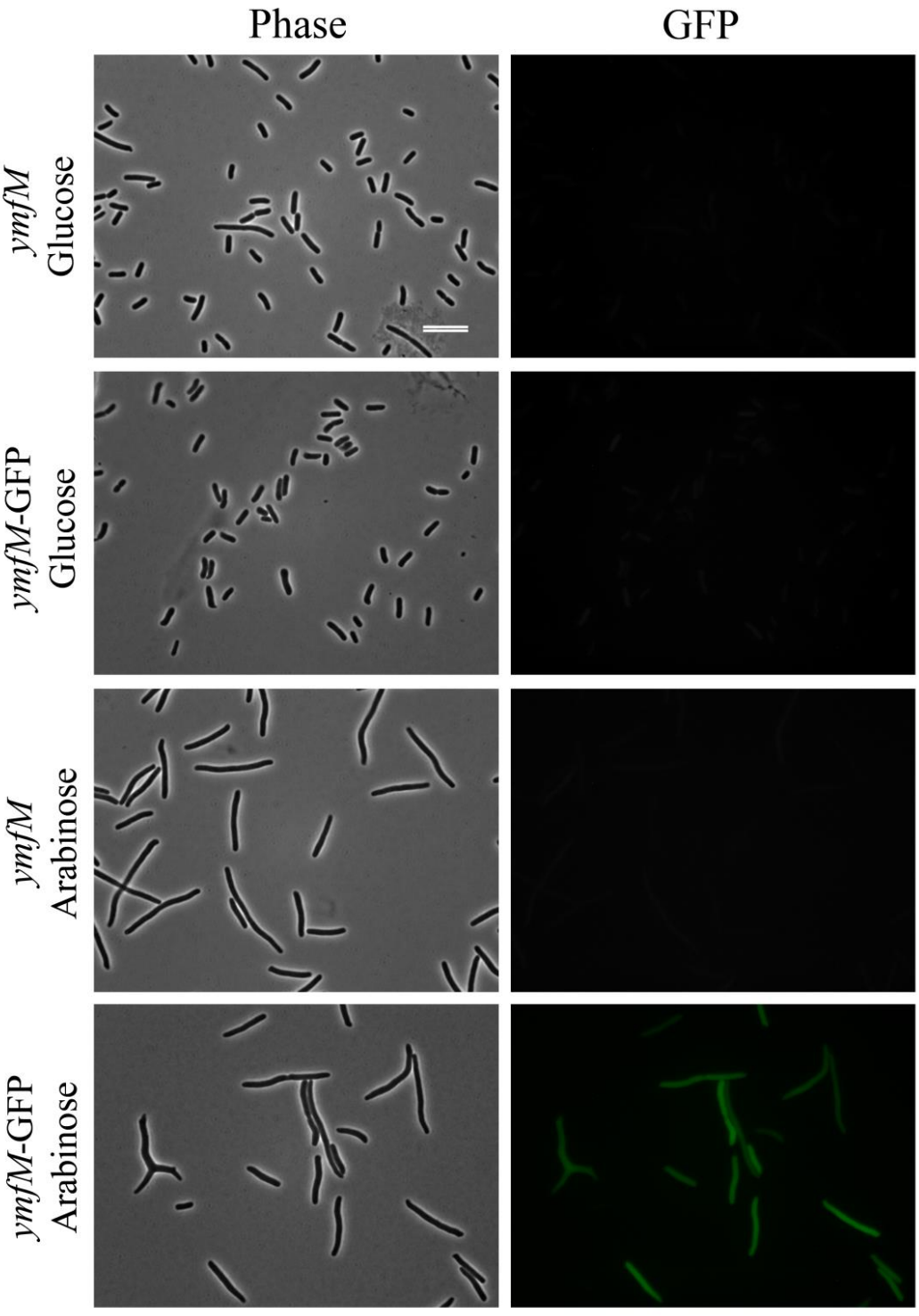

Figure 6.9. Live-cell fluorescent imaging of YmfM-GFP

BW25113 cells carrying pBAD-*ymfM-gfp*, as well as untagged *ymfM,* pBAD-*ymfM* were grown under 0.2% glucose repression (top two panels) and 0.2% arabinose induction (bottom two panels) for 1 hour. Left panel is of phase contrast and right GFP fluorescence. Images were acquired on the Zeiss AxioPlan 2. Scale bar = 10 μm

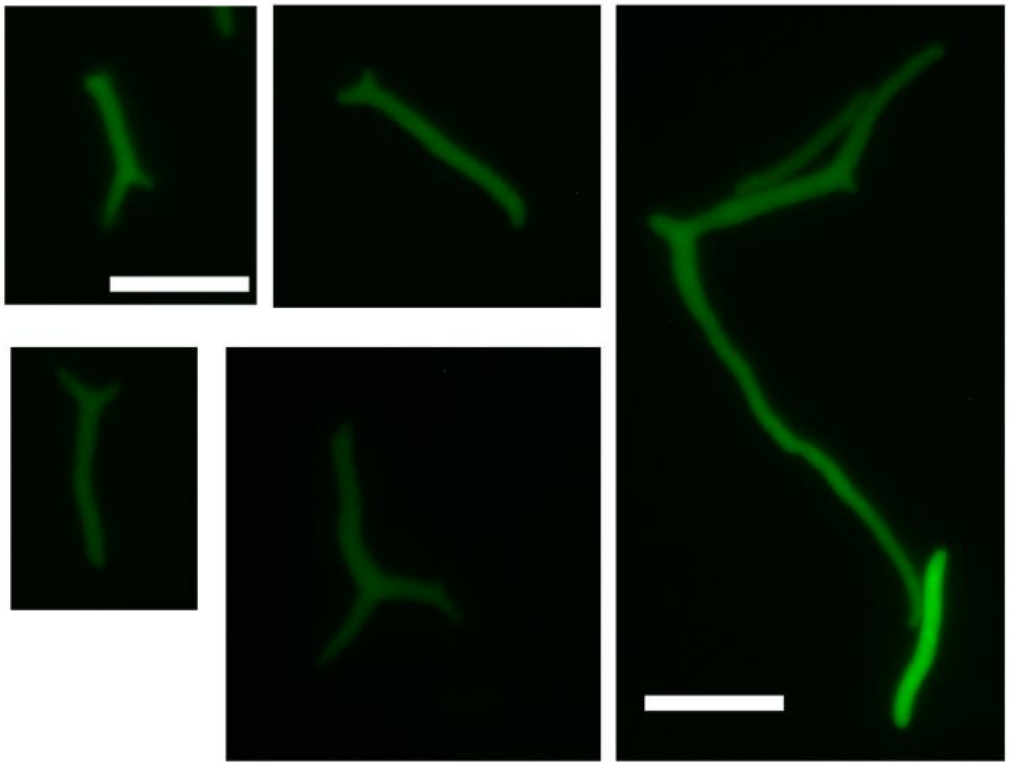

Figure 6.10. Examples of abnormal cell shape observed from YmfM-GFP

Asymmetrical morphology of branching and knobbing in 24% of wild-type *E. coli* cells when C-terminal GFP tagged *ymfM* (pBAD-*ymfM-gfp*) was expressed with 0.2% arabinose for one hour. Scale bar = 10 µm

6.2.5 Optimisation of the over-expression and purification of YmfM for future *in vitro* studies

From the work presented so far, YmfM appears to be acting at the level of Z ring assembly and is independent of the known regulators, SulA, MinC and SlmA. It is unclear whether the inhibitory action of YmfM is through the direct interaction with FtsZ. Early characterisation of SfiC (shown to be *ymfM* in Chapter 5), by D'Ari showed that mutations which made FtsZ resistant to the effects of SulA were also the same for SfiC [136]. This in combination with the findings in this thesis, suggest that YmfM is acting directly with FtsZ. To test this, *in vitro* experimentation, including the ability of FtsZ to polymerise in the presence of YmfM (sedimentation assay) and testing GTPase activity of FtsZ was planned to be undertaken. Such experiments require the purification of both YmfM and FtsZ proteins. YmfM proved to be difficult in the initial stages of protein purification and went as far as troubleshooting this by the time this thesis was completed. This section will therefore outline the steps taken to optimise over-expression and the purification of YmfM.

YmfM was cloned into an-IPTG inducible plasmid, pETMCSIII, which contains an N-terminal His_6 tag immediately upstream to the multiple cloning site and is designed for protein over-production [169]. This resulted in plasmid pET-*his_6-ymfM*. To optimise protein production and solubility, the plasmid construct was transformed into six *E. coli* expression strains including BL21-DE3, BL21-AI, C41-DE3, C43-DE3, B834-DE3, and RIPL. Results from this transformation did not produce any clones except for C43-DE3 which produced several hundred colonies. C43-DE3 is derived from BL21-DE3, and is able to tolerate the production of toxic proteins [244]. The lack of colonies was not due to transformation efficiency as empty plasmid was efficiently transformed into these

electro-competent cells. Since the transformation of the plasmid, pET-*his$_6$-ymfM* was only successful into the strain C43-DE3, protein production and solubility optimisation were carried out in this strain.

To examine whether good overproduction of YmfM could be obtained, strain C43-DE3 containing pET-*his$_6$-ymfM* was induced to express *ymfM* by addition of 1mM IPTG and continued incubation at 37ºC for 3 hours. Cells were lysed using sonication only, as lysozyme (the enzyme commonly used to lyse cells) is a similar size to the YmfM protein (14 kDa and12 kDa, respectively) and with SDS-PAGE migrated the same distance from the well. Soluble and insoluble proteins from the cell lysate were separated using centrifugation and these fractions were run on an SDS-PAGE. When observed using SDS-PAGE, no obvious overproduction band was visible. Instead a thin band was seen at the expected size range, making it difficult to discern whether the band was indeed His_6-tagged YmfM.

To confirm that the band was indeed YmfM, nickel charged affinity resin, Ni NTA, was used to isolate His_6-YmfM from the soluble fraction (Figure 6.11). To do this, a small volume of the resin was added to the soluble fraction and run on an SDS-PAGE alongside the insoluble fraction (Figure 6.11). The whole cell lysate fraction on the SDS PAGE showed slight expression of a product around the predicted size of 12kDa (Figure 6.11, Lane 2). This product was partially soluble, but mostly in the insoluble fraction (Figure 6.11, Lane 3 and 5, respectively).

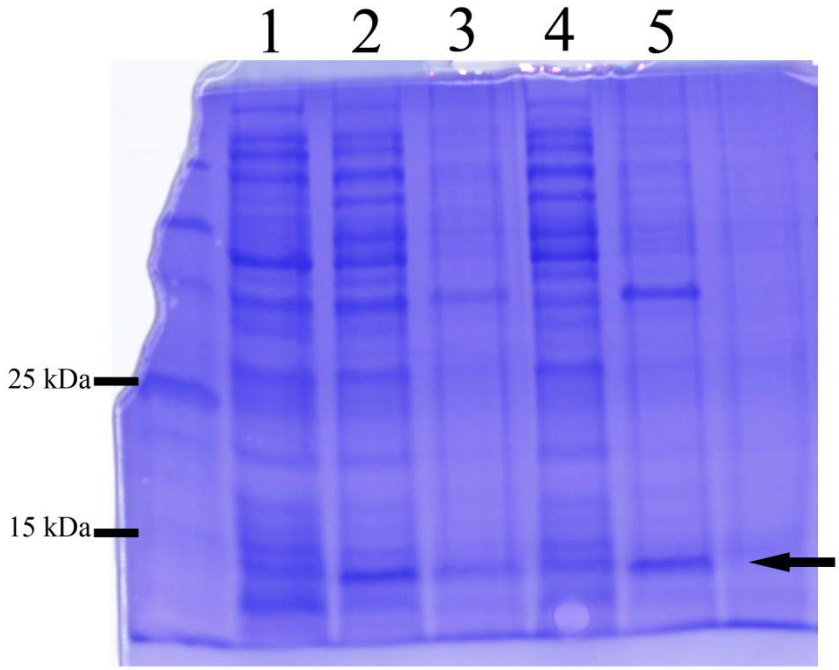

Figure 6.11. 15% SDS-PAGE of the initial overproduction of His_6-YmfM from pETMCSIII in expression strain C41-DE3

Overproduction plasmid containing His tagged YmfM, was induced to express in LB at 37°C for 3 hours using 1mM IPTG. Samples were sonicated to lyse cells and separated into soluble and insoluble fraction using centrifugation. His tagged protein in the soluble fraction was isolated and concentrated using Ni NTA beads. Lane 1 contains whole cell lysate un-induced sample control, Lane 2 contains whole cell lysate of induced sample, Lane 3 contains protein bound to Ni NTA beads from the soluble fraction, Lane 4 contains the wash step following binding to Ni NTA beads, and Lane 5 contains the insoluble fraction. Black arrow shows the expected YmfM (12 kDa) band.

Figure 6.11 indicated that YmfM was being produced, but not a high overproduction, and most of this is within the insoluble fraction. To increase the solubility of YmfM, a range of induction temperatures (30, 25, 18 and 10ºC) was tested. At 30ºC cells were induced for 4 hours, 25ºC for 4 hours, 18ºC for 6 hours, and 10ºC for 24 hours. Cells were lysed by sonication and the soluble and insoluble fraction were separated by centrifugation, and compared to YmfM production in samples induced at 37ºC, using SDS PAGE (Figure 6.12). Only cells induced at 37ºC and 30ºC showed any YmfM production, with both showing only slight expression in the soluble and insoluble fraction (Figure 6.12, top gel). Lowering the induction temperature less than 30ºC did not improve solubility and instead showed no expression of protein as detected by SDS-PAGE (Figure 6.12, bottom gel).

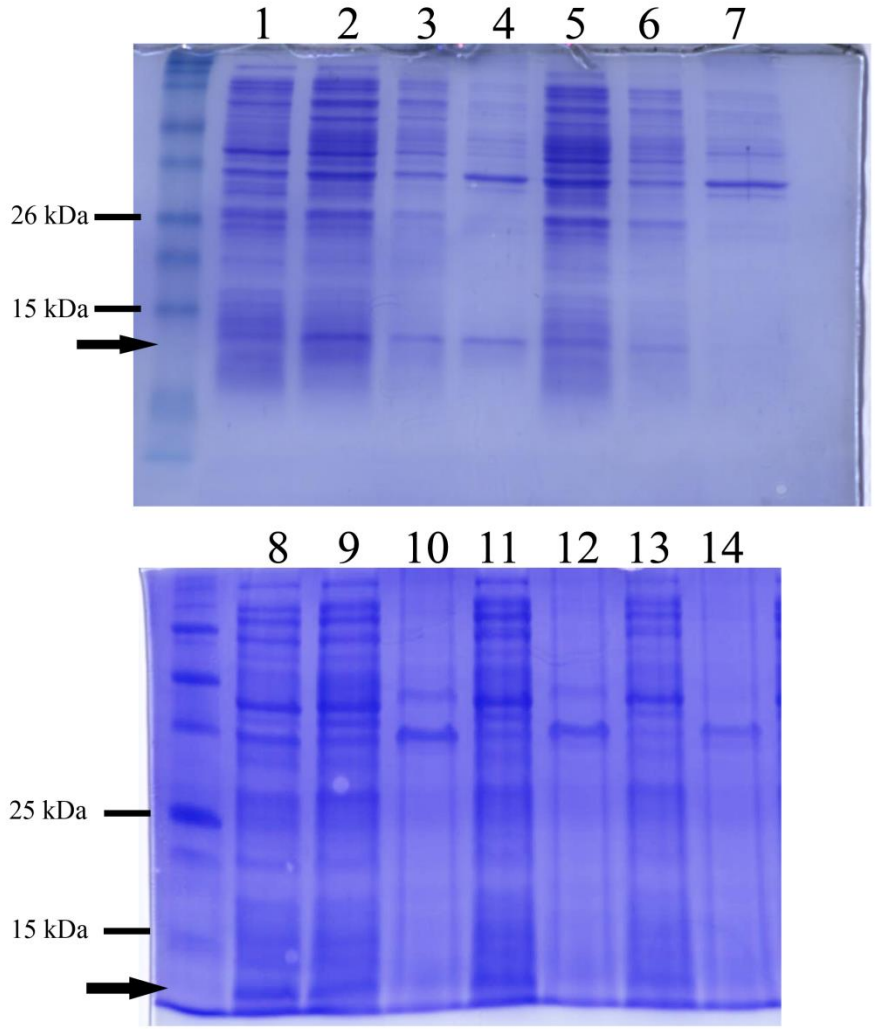

Figure 6.12. SDS PAGE analysis of His_6-YmfM expressed from plasmid pETMCSIII in strain C43-DE3.

Overproduction plasmid containing His-tagged *ymfM*, was induced to express at 37ºC for 3 hours, 30ºC for 4 hours, at 25ºC for 4 hours, 18ºC for 6 hours, and 10ºC for 24 hours using 1mM IPTG. Samples were sonicated to lyse cells and separated into soluble and insoluble fraction using centrifugation. Lane 1 is whole cell lysate of un-induced sample control grown at 37ºC, Lane 2 is whole cell lysate of induced sample at 37ºC, Lane 3 is 37ºC soluble fraction, Lane 4 is 37ºC insoluble fraction, Lane 5 is whole cell lysate of induced sample at 30ºC, Lane 6 is 30ºCsoluble fraction, Lane 7 is 30ºC insoluble fraction, Lane 8 is whole cell lysate of un-induced, Lane 9 is 25ºC soluble fraction, Lane 10 is 25ºC insoluble, Lane 11 is 18ºC soluble fraction, Lane 12 is 18ºC insoluble fraction, Lane 13 is 10ºC soluble fraction, Lane 14 is 10ºC insoluble fraction. Black arrows indicate the expected location of YmfM (12 kDa)

In addition to improving solubility, the possibility that cells were not expressing His6-YmfM efficiently was also explored. A small sample of un-induced cells and induced cells at 37ºC and 18ºC was taken to be visualised under phase-contrast microscopy (Figure 6.13). Microscopy results showed that when grown without IPTG (expression not induced), cells were mainly short, with occasional filaments observed, suggesting potential background leaky gene expression. After 3 hours of IPTG induction at 37ºC, filamentous and short cells were observed (Figure 6.13). Finally at 6 hours of induction at 18ºC, filamentation and cell lysis was seen, indicating that extended induction was lethal to the cells (Figure 6.13).

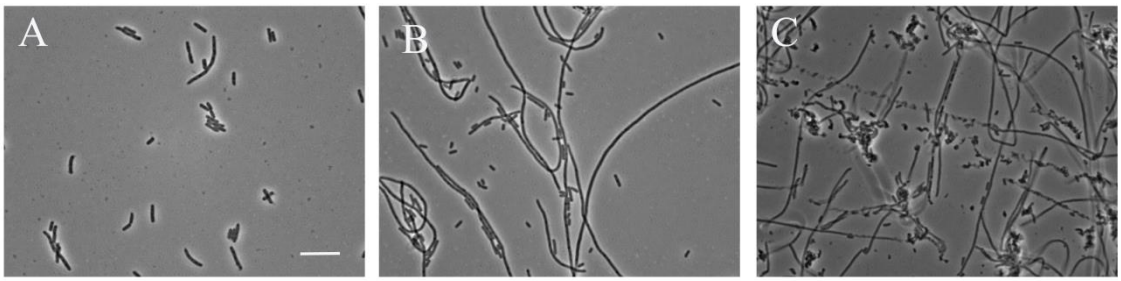

Figure 6.13. Phase-contrast microscopy of C43-DE3 cells expressing pET-his$_6$-*ymfM*.

Strain C43-DE3 containing plasmid, pET-his6-*ymfM*, was grown in LB with 100 µg/mL ampicillin at 37ºC until mid-exponential phase (A). The culture was then induced to express his$_6$-*ymfM* with 1mM IPTG at 37ºC for 3 hours (B) or 18ºC for 6 hours (C). A volume of 1mL of the un-induced and induced samples was taken and in formaldehyde (3%) and viewed with phase-contrast microscopy.

Phase-contrast microscopy of C43-DE3 cells containing pET-his$_6$-*ymfM* showed some filamentation even in the absence of inducer, ITPG, as well as cell lysis after inducing expression for longer periods (Figure). To eliminate the possibility that during cell lysis, YmfM was being secreted into the media, samples of the media were taken during pET-his$_6$-*ymfM* expression at time points ranging from 3 to 24 hours and incubated in a small volume of Ni-NTA resin. This would allow any protein present in the media to be isolated and concentrated for subsequent visualisation on an SDS-PAGE (Figure 6.14). In Figure 6.14, YmfM was not detected in the media, suggesting that YmfM was not being secreted into the media.

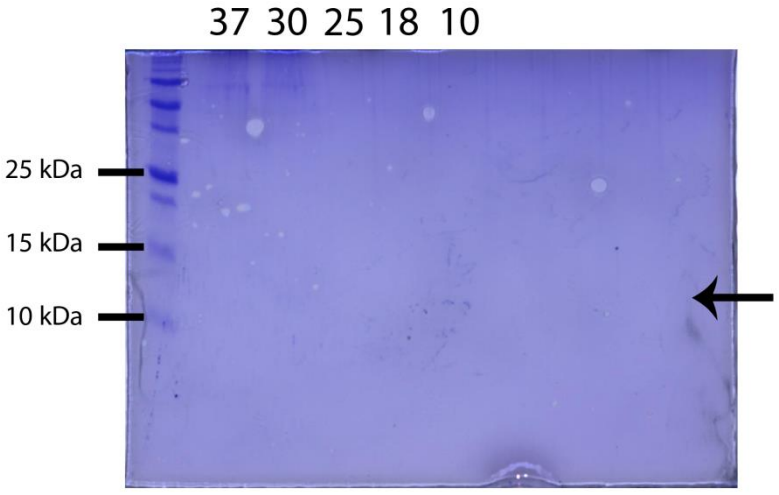

Figure 6.14. SDS-PAGE analysis of possible extracellular YmfM into the media during overproduction

Overproduction plasmid containing His-tagged *ymfM*, was induced to express at 37ºC for 3 hours, 30ºC for 4 hours, at 25ºC for 4 hours, 18ºC for 6 hours, and 10ºC for 24 hours using 1mM IPTG. Cells were pelleted using centrifugation and a small volume of the media was taken to be analysed on a 18% SDS-PAGE. Black arrows indicate the expected location of YmfM (12 kDa)

6.3 Discussion

This research presented in this chapter was performed to initiate the investigation into how YmfM inhibits cell division leading to filamentation. This was done by first by determining the stage of division being inhibited and whether this inhibition occurred indirectly through known temporal and spatial inhibitors, SulA, MinC and SlmA. This was followed by cellular localisation of fluorescently tagged YmfM, and the optimisation of protein purification in preparation for future *in vitro* studies such as the polymerisation and GTPase activity of FtsZ in the presence of YmfM.

6.3.1 YmfM targets early stages of division and is independent of the known cell division inhibitors, SulA, MinC and SlmA

Inhibitors of division can act on different stages of the division cycle, including early stages when FtsZ localizes at mid-cell to form a ring, as well as at a later stage, after the formation of the Z ring. FtsZ-labelled immunofluorescence microscopy showed that YmfM acts during the early stages of division as Z rings were not present in the filamentous cells (Figure 6.1). FtsZ was instead observed throughout the filament suggesting that while FtsZ is present under these conditions, the ability of FtsZ to localize into rings was being inhibited.

Another possibility for the lack of a Z ring in YmfM-induced filaments could have been a result of YmfM affecting cellular concentrations of FtsZ. This has been seen previously with *dicF* from the phage Qin, which encodes for a non-coding RNA that binds *ftsZ* mRNA preventing translation, and therefore reducing the cellular concentration of FtsZ resulting in filamentation[135].To see whether this was the case for *ymfM*, western

immunoblotting was performed. The levels of FtsZ in *ymfM*-expressed filaments were approximately equivalent to that of the repressed and plasmid-only controls, eliminating the possibility that YmfM was preventing Z ring formation by reducing the cellular pool of FtsZ.

Through IFM it is clear that the inhibitory actions of YmfM affect Z ring formation. However, IFM does not indicate whether YmfM is acting by directly interacting with FtsZ or indirectly, through the utilisation of other known cell division inhibitors, such as SulA, MinC and SlmA that target Z ring formation. This is seen with DicB from the prophage Qin which inhibits division indirectly by binding to and activating MinC [134]. No filamentation is seen when DicB is expressed in a strain deleted of the Min system [151]. To investigate if this was the case for YmfM, pBAD-*ymfM* was expressed in *sulA*, *minCDE* and *slmA* deleted backgrounds. In the absence of these genes, mutant strains were still able to filament when *ymfM* was expressed to a similar degree as their wild-type background, showing that YmfM does not require these systems for its inhibitory action. The fact that YmfM cell division inhibition is independent of SulA is not surprising given that YmfM was identified to be an alternative cell division inhibitor to SulA during the SOS response (Chapter 4). Furthermore, this result confirms YmfM as a SulA independent cell division inhibitor. Overall from the IFM and western blotting results it is clear that YmfM is acting at the early stages of division to prevent the assembly of Z rings and is doing this via a pathway that is independent to the well characterised regulators, SulA, MinC and SlmA.

6.3.2 Does YmfM interact directly with FtsZ?

It is currently unclear how YmfM is preventing Z ring formation. Negative regulators of FtsZ such as SulA and Kil act via an FtsZ sequestration method, reducing the GTPase activity of FtsZ, while MinC and SlmA do not affect GTPase activity and are thought to reduce the size of protofilaments. As well as this, mutants in FtsZ which were resistant to the inhibitory effects of SulA were also resistant to the division inhibition of SfiC [136]. As such it is likely that YmfM is acting directly to inhibit FtsZ in a similar manner to SulA.

Troubleshooting overproduction of YmfM

To show that YmfM was directly interacting with FtsZ, protein purification of YmfM was undertaken for *in vitro* studies, including whether YmfM affected GTPase activity and the polymerisation of FtsZ. By the time of this thesis completion, YmfM could not be purified as there was insufficient time. The protein was largely insoluble, indicating a challenging goal of either increasing its solubility or purifying it through denaturation and refolding. In this work, extensive steps were taken to optimise the expression and solubility of the protein.

Plasmid construct of pET-his$_6$-*ymfM* only transformed with high efficiency in the strain C43-DE3. This strain is a mutant variant of the commonly used strain BL21-DE3, and is better at tolerating the toxic effects often associated with protein overproduction[244]. Given that transformation was unsuccessful in BL21-DE3 as well as the several other strains tested, it is likely that the his$_6$-*ymfM* construct was lethal and any leaky expression would be enough for a loss in viability. This idea is supported by the fact that even in the

absence of induction (no IPTG), C43-DE3 containing pET-his$_6$-ymfM occasionally filamented and extended induction with IPTG resulted in cell lysis (Figure 6.13). Lethality of over-expression of phage-encoded inhibitors has been reported in the literature [150]. For the purification of DicB, Yang *et al*, [150] fused a maltose binding protein (MBP) to the N-terminal domain of DicB to reduce toxicity. The addition of tags such as MBP aids in reducing toxicity, increasing protein production and solubility [245-247]. In the future, a similar method, of adding a large globular protein such as MBP or a SUMO tag for the purification of YmfM should be considered [247].

Despite issues with lethality, steps were undertaken to improve expression and solubility of YmfM when produced in C43-DE3. YmfM was best observed from cultures induced at 37^{o}C and 30^{o}C. Initially it appeared that YmfM was not being overproduced as a strong band at the expected size was not observed on an SDS-PAGE (Figure 6.11). In retrospect, given that YmfM is a small protein (12 KDa) even sufficient overproduction will appear as a smaller band due to a less intense signal on the gel.

More importantly, YmfM was only partially soluble (Figure 6.11) when being produced. Lowering the induction temperature with the purpose of increasing solubility, in fact resulted in no expression of the protein as detected by an SDS-PAGE (Figure 6.12). This lack of production at lower temperatures was most likely due to cell lysing during before being able to produce YmfM (Figure 6.13). This is further supported by the fact that no YmfM was detected in the media (Figure 6.14), showing that lack of product seen at lower temperatures was not due to it being leeched into the media, but instead because cells were dying before production of the product.

Overall the time spent troubleshooting the production of YmfM, has highlighted that this protein tends to be insoluble and toxic when overproduced in *E. coli*. Purified YmfM is needed to test for *in vitro* interactions with FtsZ. In the future, for successful purification, several steps will need to be taken to address the solubility and even optimise the expression levels. Firstly, cultures can be grown in glucose repression until a high OD is reached before protein expression is induced. This can help increase the protein yield, even if induction is occurring for a shorter time. As mentioned earlier, using an affinity tag such as MBP will help with protein expression as well as solubility and lethality. However for interaction studies, the addition of relatively large tag may interfere with the ability of YmfM to interact with FtsZ. A cleavage site, such as a TEV protease cleavage site can be included between the MBP tag and YmfM, to generate a tag free protein after purification. Alternatively, expressing YmfM in another organism, such as Bacillus or Saccharomyces may overcome the lethality by producing it in a non-native background.

As an alternative, understanding the binding partners of YmfM *in vivo* may provide insight into conditions needed during protein production. For example the Kil protein is also a lethal cell division inhibitor interacting with FtsZ. In order to purify Kil, Haeusser *et al*. [147], first identified mutations resistant to the inhibitory effects of Kil. Through this, they identified that deletion of ZipA and mutations in FtsZ overcame Kil. They then introduced these *ftsZ* mutations into an expression strain, from which they produced and purified Kil. Using a similar approach, division mutations that are resistant to the inhibitory effects of YmfM can be used to reduce lethality during protein overproduction. These mutants have been previously described [136].

6.3.3 Localisation of YmfM using fluorescence microscopy

As an alternative approach to understanding if YmfM is acting directly on the divisome, localisation of fluorescently tagged YmfM was under taken to give insight into how it may be inhibiting division. Some cell division inhibitors such as MinC and SlmA have obvious localisation patterns, such as near cell poles and over DNA, respectively [11, 248, 249]. To explore this as a possibility for YmfM, GFP-localisation experiments were performed. GFP fusion of *ymfM* was initially cloned into pBAD24 to test for functionality, as this system is the only known way of testing YmfM function. The N-terminal GFP tag resulted in shorter filaments indicating that this region may be required for the inhibitory action of YmfM (Figure 6.8). C-terminally tagged YmfM gave a similar cell size distribution as determined by the coulter counter, as untagged YmfM, and since this fusion appeared to be functional, localisation experiments were performed using this construct. Fluorescence was detected uniformly throughout the cells with no specific localisation pattern. Using a high-copy plasmid with maximum induction may mask the true localisation pattern of YmfM, as YmfM is most likely being produced in excess amounts. To overcome this issue, for future work, using a lower concentration of inducer (arabinose) may help reduce expression levels of *ymfM* from pBAD24. As an alternative, using a low-copy plasmid, with a titratable inducible system, can allow for a more controlled induction of *ymfM*.

Interestingly though, expression of YmfM-GFP resulted in asymmetrical morphological changes including knobbing and branching of filamentous cells (Figure 6.10). This new phenotypic change suggests that the introduction of GFP on the C-terminal end is partially

interfering with YmfM function, as filamentation is still observed with the additional phenotype of branching.

Branching and knobbing phenotypes are most often observed in cells lacking low molecular weight penicillin binding protein, such as PBP 5 [250].As well as seen in when Z rings are incorrectly orientated, so when division occurs, septa doesn't form correctly leading asymmetrical cell poles and branching [251]. While speculative, the observation of this new phenotype suggests that perhaps YmfM does directly contact the divisome to some capacity and the addition of a GFP tag may be sterically interfering with the division process leading to branching. As such, the YmfM-GFP construct is most likely only partially functional as there is an additional phenotype in comparison to untagged YmfM which causes only filamentation. More experimental work is needed to understand this new phenotype and to optimise the functionality of an YmfM-GFP fusion. This could involve fluorescently labelling FtsZ [252, 253] with a tag compatible with GFP and observing Z ring dynamics over-time in cells expressing either untagged YmfM or YmfM-GFP.

Unfortunately using a high copy plasmid which causes such a high over-expression of *ymfM* is not ideal for localisation studies. The pBAD24 expression system was used as a proof of concept for functionality of the fusion. Ultimately, tagging the native copy of *ymfM* and observing localisation during biologically relevant conditions would be ideal and is the next step after the functionality issues have been resolved. Gene expression of *ymfM* is up-regulated during SOS inducing conditions (Chapter 4), and using this will allow for real-time observation of not only how YmfM is activated during the SOS response but also potential localisation patterns. If a functional fusion cannot be achieved,

then the use of YmfM-specific antibodies and subsequent IFM should be explored. This will of course require purification of YmfM in order raise antibodies against it.

6.3.4 Conclusions

The work presented in this Chapter shows that the expression of *ymfM* inhibits the early stages of division when Z rings assemble. This is a novel inhibitor, functioning independently of known regulators, SulA, MinC and SlmA. YmfM does not affect the cellular levels of FtsZ. However it is still unclear whether this inhibition is a result of direct interaction with FtsZ. In previous published work, FtsZ mutants which were resistant to the inhibitory effects of SulA were also resistant to SfiC [136]. As well as this several cell division inhibitors encoded within prophages are known to target FtsZ directly [141, 142, 147, 148, 215]. As such, given that the expression of YmfM results in no Z rings, it is likely that YmfM is directly inhibiting FtsZ. However, further work is required to fully elucidate the molecular mechanism of FtsZ inhibition.

Chapter 7. General Discussion

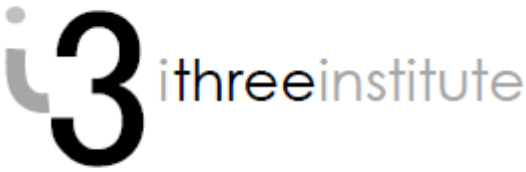

7.1 Introduction

Bacterial cell division is an essential process that is highly regulated to ensure that newborn cells are identical and receive the correct genetic material. While much is known about how cell division occurs, less is known about how this process is regulated under different environmental conditions. Bacteria have the ability to become filamentous in response to predation stress, host immune response, and antibiotics [3, 89]. This transition state is a survival strategy utilised by bacteria. However the underlying molecular mechanisms that enable filamentation are poorly understood. Given the range of conditions under which filamentation is observed, and the fact that only a few inhibitors of cell division have been identified thus far, it is likely that many regulators remain to be discovered.

The overall aim of this thesis was to characterise the molecular and biological function of a novel cell division inhibitor, *ymfM*, encoded within the e14 prophage in *E. coli*. This was achieved by first confirming that *ymfM*, isolated from a recent over-expression library screen [163], was indeed the gene responsible for filamentation (Chapter 3). This was followed by elucidating the involvement of YmfM in inhibiting division during the SOS response through mutational studies (Chapter 4). A bioinformatics approach was then undertaken to determine the conservation and potential regulation pathway of *ymfM* (Chapter 5). Finally, the molecular mechanism underpinning how YmfM acts to inhibit division was explored (Chapter 6).

7.2 Identification of novel cell division inhibitors:

A novel, high-throughput screening system was recently used [163] to identify potential new cell division inhibitors. In this screen, DNA fragments expressed from an inducible plasmid which caused cells to become filamentous were isolated via flow cytometry. Through this screen, several DNA fragments from the *E. coli* genome that cause filamentation when induced from an arabinose inducible plasmid were identified. These fragments often contained multiple genes and so the initial stage of this PhD project was to identify the exact gene responsible for the filamentation observed (Chapter 3). Based on literature evidence and bioinformatics, four genes were chosen to be potentially responsible for filamentation observed in their respective DNA fragments. These included *ymfM, ytfB, ycjY* and *ykfI*.

Initial validation showed that cells over-expressing *ymfM* and *ytfB* had severe inhibition of division, with the greatest fold increase in average cell length (Chapter 3, Figure 3.2 and Table 3.2). Cells over-expressing *ycjY* were a mixed population of filamentous and short cells, while those over-expressing *ykfI* were comparable to the short un-induced population. Since the expression of *ymfM* and *ytfB* were very efficient at inhibiting cell division, these two genes became the focus of research within our lab. YmfM became the primary focus of this PhD, while YtfB was pursued as part of a different project.

Genes *ykfI* and *ycjY* were not pursued further as they did not show a strong filamentation phenotype. Lack of filamentation from cells expressing *ykfI* was unexpected since over-expression of the original clone identifying *ykfI* from the over-expression screen resulted in an increase in average cell length (Chapter 3, Table 3.2). Furthermore, this gene shares

homology to another toxin, *yeeV*, which when expressed causes lemon-shaped cells, through interactions with FtsZ and MreB [138].A study published recently has shown the expression of *ykfI* from an inducible-plasmid causes a lemon-shaped morphology [187]. This is thought to be mediated through an interaction with FtsZ and MreB, although the authors of the study could only show interaction with FtsZ through a bacterial two-hybrid (BATCH), and so it's interaction with MreB remains inconclusive [187].The lack of filamentation and/or lemon-shaped cells observed in this thesis was due the mutations within the stop codon of the ORF of the gene (Chapter 3). It is possible that background leaky expression of this toxin from the pBAD24 [168, 254], would have resulted in suppressor mutants being selected for.

YcjY is predicted to be a hydrolase [181]. Peptidoglycan (PG) hydrolases are important for cell wall elongation and septal wall separation during division [182]. It is unlikely that peptidoglycan cell wall synthesis was being inhibited by *ycjY* over-expression, as cell growth continued to increase consistent with wild-type (Chapter 3 Figure 3.3). However it is possible that *ycjY* is a septal-specific hydrolase and the filamentation observed during *ycjY* over-expression was a result of disruption to the septal PG synthesis.

This original screen was successful in identifying multiple potential cell division inhibitors from a single experiment as it does not rely on creating conditions in which these inhibitors are active. The power of this screen is in its ability to identify genes that may have an overlapping function and as a result would otherwise not be detected by deletion screening systems such as knock-out or transposon insertion libraries. To be effective, these deletion screening systems would require conditions matching the activation conditions of the gene and would require multiple deletions before phenotypic changes are observed (for a redundant system). The main downside of the over-expression

screen used to find the preliminary hits of this work is the lack of certainty whether the filamentation observed is due to identification of a novel cell division inhibitor or due to over-expression of a gene disrupting the function of cellular systems within the cell, causing a cascade of stress responses.

From the experiments performed in Chapter 3, measuring cell length and growth rate changes is not enough to understand how the expression of a gene causes inhibition of division. In retrospect, additional experiments of FtsZ localisation using either fluorescent tags or immunofluorescence microscopy should have been done in conjunction with the over-expression cell length measurements. This would have indicated whether inhibition was occurring during early stages of division (Z ring formation) or later stages (maturation of the divisome).

Overall the results presented in Chapter 3 show that there are still potential unidentified cell division inhibitors. It remains to be seen the physiological conditions in which they are active. It will be particularly interesting to see how they inhibit division and whether this is common to already identified inhibitors or whether they utilise a novel molecular mechanism.

7.3 YmfM is an SOS-inducible cell division inhibitor:

SfiC was identified as a novel SOS-inducible cell division inhibitor encoded within the e14 prophage over 30 years ago [136]. Initial characterisation of this gene by D'Ari *et al*, showed that it was dependent on RecA for induction, but not under the control of the repressor LexA [136]. Since the identification of SfiC, SulA has been studied extensively, with a thorough knowledge of its role during the SOS response as well as its molecular mechanism of inhibiting FtsZ polymerisation [111, 117, 119]. SfiC on the other hand has been left essentially unstudied. Given that SfiC is also another SOS inducible inhibitor; the current model of the SOS pathway is clearly incomplete. Most importantly, why there is a need for multiple cell division inhibitors under SOS induction is currently missing from our understanding of this pathway.

The gene encoding for SfiC was never identified precisely [154], although it was thought to be encoded by *ymfM* or *ymfL* [155]. Over-expression of *ymfL* did not result in filamentation, showing that *ymfM* was solely responsible for the SfiC phenotype. This is the first body of work confirming that the gene encoding SfiC is *ymfM.* Since YmfM is SfiC, any previous results characterising SfiC should also be true for YmfM, including SfiC being an SOS-inducible cell division inhibitor. Through activation of RecA441, it was shown that YmfM was indeed acting to inhibit division during the SOS response (Chapter 4). This filamentation response was only observable in the absence of *sulA*, as the deletion of *sulA* and *ymfM* (Δ*sulA*Δ*ymfM*) filamented to a lesser degree than when only *sulA* was deleted (Δ*sulA*) (Chapter 4, Figure 2).

In the initial experiments, RecA441 activation generated a reproducible distribution of filamentation in each background. That is, the *ΔsulAΔymfM* background consistently filamented to a lesser degree than the *ΔsulA* mutant. This phenotype is consistent with previously published data [136]. As such, it is probable that these findings are accurate. That is, *ymfM* is acting as a novel cell division inhibitor independent of SulA, capable of being induced during the SOS response. However, it is also acknowledged that due to the inability to reproduce this phenotype later in this PhD, more experimental work is needed to conclusively show that YmfM is an alternative cell division inhibitor during SOS.

The absence of *sulA* alone was enough to show a reduction in the degree of filamentation observed during *recA441* expression, indicating that SulA is the primary inhibitor of cell division during the SOS response. However, filamentation is still being observed in the absence of *sulA* and *ymfM* together (Δ*sulA*Δ*ymfM*) suggesting that other cell division inhibitors are also induced by RecA in *E. coli*. This is an interesting observation and to our knowledge has not been reported in the literature before. Potential additional inhibitors could be encoded within prophages. KilR and DicB are known cell division inhibitors which are able to respond to certain antibiotics and are thought to aid in resistance of *E. coli* [153]. It is possible that their up-regulation during the SOS response is contributing to filamentation which becomes apparent in the absence of Δ*sulA*Δ*ymfM*.

While the RecA441-mediated SOS showed the potential involvement of YmfM, during norfloxacin induced SOS, the presence of *ymfM* did not affect filamentation, even in the absence of *sulA*. This is despite qRT-PCR showing *ymfM* expression was up-regulated under this condition (Chapter 4, Figure 4.8). The difference in *ymfM* causing filamentation observed during norfloxacin and RecA441-mediated SOS is most likely due to the levels of *ymfM* expression between these two systems. Induction from pBAD24

can cause up to 1200-fold (10 log2-fold) increase in gene expression [168]. Therefore is it likely that the induction of RecA from pBAD-*recA441* is greater than from an external chemical stimulus. As a result, it is hypothesised that more *ymfM* is being expressed during pBAD-*recA441*induction than during norfloxacin.

A question still outstanding is how much *ymfM* is needed to inhibit division? From qRT-PCR of pBAD-*ymfM* expression, when clear filamentation is observed, *ymfM* was greatly up-regulated, with a 9 log2-fold increase in expression at 60 minutes and 11 log2-fold increase at 120 minutes. This is in contrast to the 5 log2-fold increase at 120 minutes of norfloxacin exposure, where *ymfM* does not cause filamentation. From these, it is unclear how much expression of *ymfM* is needed to see a division inhibitory effect and how this compares to the expression of *ymfM* during induction of RecA441.

Published experimental evidence suggests that translational regulation exists for *ymfM* through an sRNA [221]. The regulatory pathway of this is explored in Chapter 5 and is discussed in detail below. As a result of this potential translational regulation, transcription levels may not actually reflect protein level of YmfM. Therefore, for future studies in addition to qRT-PCR, protein levels should be measured directly using techniques such as western blotting. This would require raising antibodies for YmfM.

Such future studies should involve the use of a titratable plasmid induction system [218], where the minimal induction needed to cause filamentation could be first determined followed by quantification of expression of *ymfM* and protein level at that time point. This level can then be compared to the expression of YmfM during an array of SOS inducing conditions, such as norfloxacin (and other antibiotics), RecA441, acid stress, and UV exposure.

An interesting observation during the norfloxacin induction experiments was that even in the absence of *recA* filamentation was observed. The mechanism of action of this antibiotic is attributed to inhibition of DNA gyrase which leads to double stranded DNA breaks and the activation of the SOS response [108, 206]. However, here it is shown that inhibition of division is occurring independently of the RecA pathway, although not the same extent as when RecA is present. This suggests that norfloxacin is inducing additional unidentified pathways to inhibit division. In the literature, RecA-independent cell division inhibitors have been identified. In *Caulobacter crescentus*, *didA* is a RecA-independent, DNA-damage inducible cell division inhibitor [255]. It has been suggested that *didA* works in partnership with *sidA* (RecA-dependent inhibitor, *sulA* counterpart) to inhibit division following DNA damage. It was proposed by the authors that such a redundancy would provide the cells a fail-safe survival mechanism. This shows that multiple pathways to inhibit cell division following DNA damage exist, that are not solely dependent on RecA. In *E. coli* these RecA-independent pathways should be further investigated as this will provide a more thorough understanding of the global response to DNA damage. To test this global gene expression changes could be analysed using RNA sequencing during SOS induction in a wild-type and Δ*recA* background. The differences in gene expression in the presence and absence of RecA will provide information as to the other potential RecA-independent pathways contributing to the inhibition of division.

It is also interesting to contemplate why *E. coli* would need so many different cell division inhibitors seemly responding to the SOS response? A possibility is that having multiple pathways is important in ensuring the survival of a species. For example, if one inhibitor mutates and is no longer functional, then another may replace its function. The SOS response occurs due to formation of ssDNA breaks caused by a block in DNA replication or as a result of DNA damage. The inhibitory action of SulA is a crucial step, allowing

cells enough time to repair damage before continuing to produce new daughter cells. Having a redundancy in this system, would allow for the inhibition division and the progression of the SOS response to still occur in the event that SulA is no longer functioning.

Overall the work presented in Chapter 4 shows the potential role of *ymfM* during the SOS response. It also highlights that our current understanding of the cell division regulation during the SOS response is incomplete and raises many questions. In particular, what are the benefits of having multiple cell division inhibitors during the SOS response? How do these multiple pathways help *E. coli* cope with stresses and aid in the survival of the population, if at all. Clearly, more work is needed to better understand the different types of cell division inhibitors being induced following the SOS response.

7.4 The regulatory pathway of *ymfM*

A bioinformatics approach was used in Chapter 5 to probe the biological context in which *ymfM* may be acting. In particular, this was used to investigate the regulation pathway of *ymfM* which might give insight into when and where YmfM is acting to inhibit division. Through bioinformatics analysis, it is evident that *ymfM* is highly conserved within *E. coli*. This conservation does not appear to be niche specific as *ymfM* is detected in all nodes of the phylogenetic tree, covering strains of *E. coli* with a range of lifestyles. These results suggest that the inhibitory action of *ymfM* may confer a general benefit to *E. coli*.

The most interesting finding from the bioinformatics analysis was that *ymfM* is consistently associated with *ymfL* and *oweE*. Through conditional and directional probability, it is evident that *ymfM* is dependent on *ymfL*. *YmfL* is always detected when *ymfM* is present, however *ymfL* can be present in the absence of *ymfM*. These results suggest that *ymfL* may be regulating the activity of *ymfM*. In Chapter 4, the DNA fragment from which *ymfM* was identified also contained partial fragments of *ymfL*. When this DNA fragment was over-expressed it filamented to a lesser degree than the over-expression of *ymfM* alone (Chapter 3, Figure 3.2). This supports the idea that *ymfL* may be acting to regulate the inhibitory actions of *ymfM*.

A novel sRNA has been identified to bind the RBS of *ymfM* [221]. It is predicted that the binding of this sRNA to the *ymfM* RBS inhibits translation of this gene. As this sRNA is contained within the 3'-end of *ymfL*, this sRNA was most likely present in DNA fragment from the original screen. This would have partially repressed the function of *ymfM*. The sRNA translational control of YmfM protein synthesis suggests that protein production levels may be less than expected from transcriptional up-regulation. This might explain why even when *ymfM* was up-regulated during norfloxacin, it did not contribute to filamentation.

Multiple levels of control on *ymfM* expression (putative CI-like-repressor and sRNA) may differentiate the function of YmfM from SulA. In Chapter 4, during norfloxacin exposure, the activation of *ymfM* appeared to be delayed as long as possible, suggesting that its function may be more potent and is subsequently reserved for extreme SOS

conditions. The existence of multiple levels of control is similar to other systems in the SOS response which have redundant function. In particular the multiple DNA polymerases are up-regulated during different stages of the SOS response. Low-fidelity polymerases such as PolV, are reserved for extreme late stage SOS, when high-fidelity polymerases have failed to repair lesions. This last-ditch response allows bacteria to repair lesions but in a highly error prone manner [198]. Multiple levels of translational and post-translational regulation exist to avoid this process unless absolutely necessary [256].

While we know that there are multiple levels of transcriptional and translational regulation of *ymfM*, it is still unclear under what conditions these regulators activate the function of YmfM. From the bioinformatics analysis it is clear that looking at transcriptional up-regulation is not sufficient to infer to protein concentration and so it is necessary to look at YmfM protein levels directly to find conditions in which it may be active (as discussed above).

7.5 YmfM inhibits division by targeting Z ring formation

Over-expression of *ymfM* results in a very efficient block in cell division (Chapter 3). This block in division is not due to the induction of the SOS response when YmfM is over-produced in cells. In Chapter 4, qPCR of cells expressing pBAD-*ymfM* (Figure

4.10), showed that SulA was not being up-regulated, suggesting that the inhibitory effects of YmfM is independent of SulA. Therefore, to better understand how YmfM was acting to inhibit division, molecular localisation experiments were carried out in Chapter 5. The expression of *ymfM* inhibits Z ring formation as no Z rings were seen in *ymfM*-induced filaments. This was independent of known cell division inhibitors, SulA, SlmA and MinC which are known to directly inhibit Z ring formation. Furthermore, YmfM is not acting by reducing FtsZ protein levels in the cell, as the cellular concentration of FtsZ was unaffected by *ymfM* expression from pBAD24. D'Ari *et al.,* [136] suggested that FtsZ was the target of the inhibitory action of SfiC. However from this it is unclear whether the inhibition was due to SfiC's direct interaction with FtsZ or was mediated through another cell division inhibitor. We have extended this knowledge by showing that the expression of *ymfM* inhibits the earliest stage of division of when FtsZ assembles into a ring independent of known cell division regulators. While good progress has been made to under YmfM's mechanism of action, it is still unclear whether the lack of Z rings is due to YmfM directly interacting with FtsZ or by interacting with another early division protein such as FtsA and ZipA.

If YmfM is mediating inhibition of FtsZ through FtsA or ZipA, then this can be detected via the use of mutants bypassing the role of FtsA or ZipA [23, 147]. If there is a direct interaction between YmfM and FtsZ, to test for this in an *in vitro* assay would require the purification of YmfM. Such *in vitro* experiments are well described and include testing the ability of FtsZ polymerisation (sedimentation assay) and GTPase activity in the presence of YmfM [257]. While these *in vitro* experiments were the initial goal of this thesis, unfortunately the successful purification of YmfM was not achieved due to toxicity and solubility issues. However, good progress was made towards optimising the

production of YmfM. In retrospect, given that FtsZ mutants which are resistant to the inhibitor effects of SfiC are known [136], this background strain should have been used to minimise lethality of YmfM over-production. In addition to this, future optimisation should include the generation of an expression construct which includes a soluble cleavable tag, such as MPB or SUMO [247]. This tag should be included at the N-terminal region of the protein. Expression of GFP at the N-terminal end of YmfM resulted in less filamentation, suggesting that this region is needed for the inhibitory actions of YmfM. Therefore, addition of large cleavable tag at the N-terminal end might mask the toxic inhibitory actions of YmfM.

7.6 The broader context of YmfM and cell division inhibitors

YmfM is part of the e14 prophage, one of nine cryptic prophages encoded within *E. coli* K-12 [153-155]. These nine cryptic prophages have been shown to be beneficial for *E. coli* and in general, prophages can play a very important role in survivability, adaptation and virulence of their bacterial host [156]. It is interesting that several prophages in *E. coli* encode for cell division inhibitors such as Kil, DicB, DicF, and CbtA [137, 149, 215]. While their original function in an active phage would have been to delay the cell cycle in order to optimise the production of viral particles [162], it appears that they may now act to benefit *E. coli*. For example, both Kil and DicB are both thought to aid *E. coli* in resisting exposure to antibiotics [153]. This suggests that many of these prophage cell division inhibitors may be repurposed by *E. coli* for the benefit of the cell instead of the phage element. As such the beneficial role of YmfM in context to *E. coli* needs to be investigated further.

From this thesis and the literature it is clear that several cell division inhibitors exist [50, 55, 120, 121, 126, 134, 136, 150, 215]. This raises the question, why does *E. coli* need so many different inhibitors to achieve the same ends? The characterisation of spatial inhibitors MinC and SlmA show that they have specialised function to ensure division doesn't occur at cell poles nor over nucleoids respectively. It is probable that temporal inhibitors are equally specialised with respect to their reversibility and the stage of division that they inhibit. By having multiple inhibitors with subtly different properties, cells are likely able to tailor their inhibition in response to different environmental conditions in order to maximise their survivability.

7.7 Concluding remarks

Knowing when and where to divide is crucial for any bacterial population, thus several regulators must be in place to adapt to changing environments, such as those seen during filamentation. The work presented in this thesis, has identified a novel cell division inhibitor encoded within a prophage that is induced by the SOS response. This work highlights that there are still gaps in our current understanding of the SOS response and more work is needed to fully identify the multiple pathways leading to the inhibition of division. Furthermore, characterisation of novel cell division inhibitors not only gives insight into how this highly conserved process is regulated, but also how bacteria are able to adapt to different environments.

Appendix

Supplementary Data

Table S1: Location of genes in *E. coli* strain K-12 substr. MG1655 (NCBI Reference Sequence NC_000913.3) used in this work.

Gene Name	Locus Tag	Start Nucleotide	End Nucleotide	Length (Nucleotides)
ymfD	b1137	1196867	1197532	666
ymfE	b1138	1197533	1198237	705
lit	b1139	1198695	1199588	894
intE	b1140	1199679	1200806	1128
xisE	b1141	1200787	1201032	246
ymfI	b1143	1201497	1201838	342
ymfJ	b1144	1201776	1202084	309
cohE	b1145	1202259	1202933	675
croE	b1146	1203024	1203224	201
ymfL	b1147	1203268	1203825	558
ymfM	b1148	1203822	1204160	339
oweE	b4692	1204170	1204403	234
aaaE	b4693	1204404	1205537	1134
ymfR	b1150	1205549	1205731	183
beeE	b1151	1205731	1206142	412
jayE	b1152	1206143	1206922	780
ymfQ	b1153	1206913	1207497	585
stfP	b1154	1207501	1208130	630
tfaP	b1155	1208132	1208545	414
tfaE	b1156	1208517	1209119	603
stfE	b1157	1209119	1209619	501
pinE	b1158	1209685	1210239	555
mcrA	b1159	1210346	1211179	834

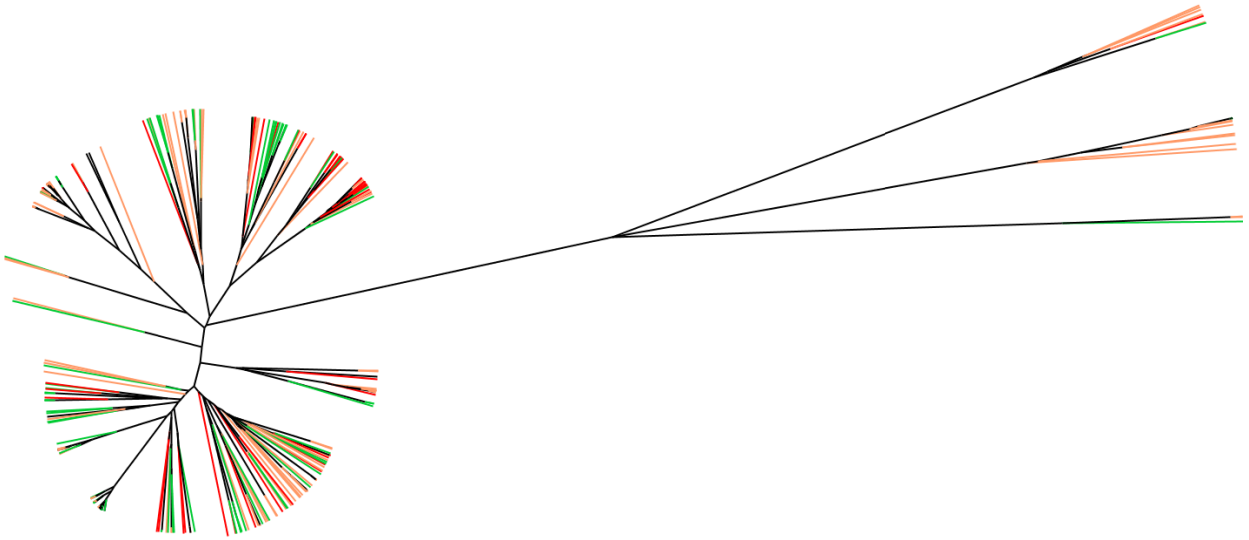

Figure S1: Presence of YmfM and e14 Proteins in *E. coli* including outlier strains

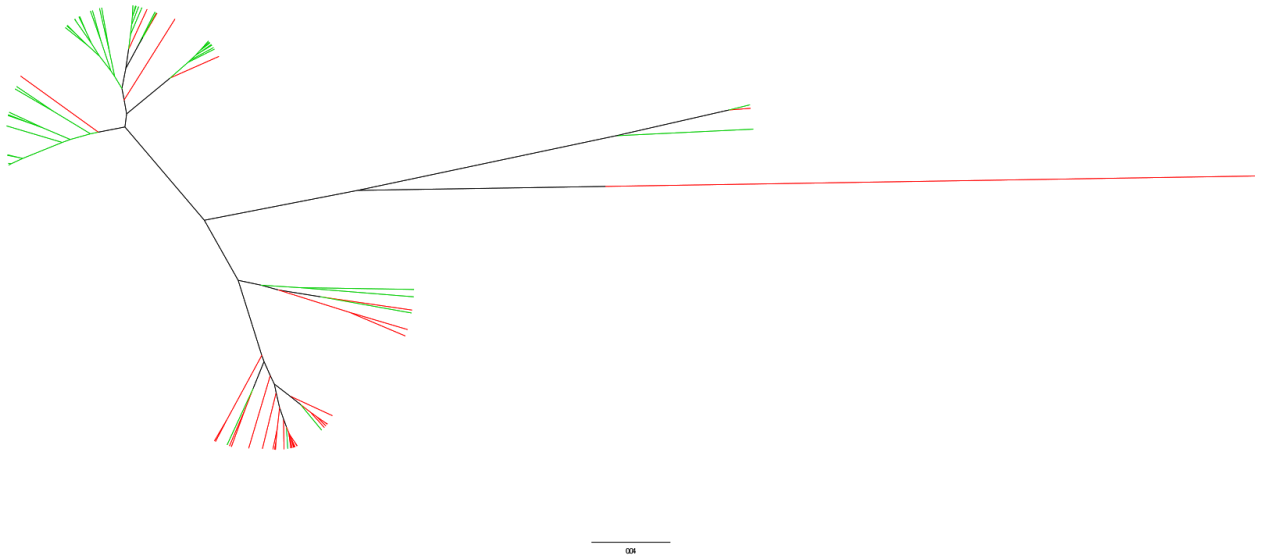

Figure S2: Phylogenetic tree of *ymfL* homologs found in *E. coli* including outlier strains.

```
ymfL Independent        GTGGGTAAGCATCACTGGAAAGTAGAAAAACAGCCTGAGTGGTACGTGAAAGCTGTCAGA          60
ymfL_ymfM_adjacent      GTGGGTAAGCATCACTGGAAAATAGAAAAACAGCCTGAGTGGTACGTGAAAGCTGTCAGA          60
                        ******************** ****************************************

ymfL_Independent        AAAACTATCGCGGCGTTGCCGGGGGGGTTACGCTGAAGCTGCTGAGTGGCTGGATGTAACA         120
ymfL ymfM adjacent      AAAACTATCGCGGCGTTGCCGGGTGGTTACGCTGAAGCGGCTGACTGGCTGGATGTAACA         120
                        ********************** ************** ***** ***************

ymfL Independent        GAGAACGCTTTATTCAACCGCCTTCGTGCAGATGGCGATCAGATTTTCCCGCTGGGATGG         180
ymfL_ymfM_adjacent      GAAAACGCTTTATTCAACCGCCTTCGTGCAGATGGCGATCAGATTTTCCCGCTGGGATGG         180
                        ** ************************************************************

ymfL_Independent        GCAATGATTTTACAGCGCGCGGCTGGCACTCACTACATTGCGGATGCTGTCGCACAGTCT         240
ymfL_ymfM_adjacent      GCAATGGTTTTACAGCGTGCTGGTGGCACTCACTTCATTGCTGATGCTGTGGCGCAGTCT         240
                        ****** ********** ** * *********** ****** ******** ** ******

ymfL_Independent        GCTGGTGGGGTGTTTGTATCGCTTCCTGAAATTGAGGAAGTAGAGAACGCCGATATAAAC         300
ymfL ymfM adjacent      GCAAATGGCGTCTTTGTGTCTCTTCCTGACGTCGAGGATGTGGACAACGCCGATATTAAC         300
                        **   *** ** ***** ** ********  * ***** ** ** ********** ***

ymfL_Independent        CAGCGCCTGCTGGAAGTCATCGAACAGATCGGGAGTTACTCAAAGCAGATTCGTTCGGCA         360
ymfL_ymfM_adjacent      CAGCGCCTGCTGGAAGTCATTGAACAGATCGGCAGTTATTCAAAACAGATTCGTTCAGCA         360
                        ******************** *********** ***** ***** ********** ***

ymfL_Independent        ATCGAAGATGGGGTAGTGGAGCCACACGAGCAGACAGCAATTAATGATGAGTTGTATCTG         420
ymfL_ymfM_adjacent      ATCGAAGACGGTGTAGTGGAACCGCATGAGAAGACAGCAATTAACGACGAGCTGTATCTC         420
                        ******** ** ******** ** ** *** ************* ** *** *******

ymfL Independent        TCAATTTCGAAGCTCCAGGAGCATGCAGCACTGGTCTACAAAATCTTTTGCGCTCCAGAA         480
ymfL_ymfM_adjacent      TCAATTTCGAAGCTGCAGGAGCATGCAGCACTGGTCTACAAAATTTTTTGCATTTCAGAA         480
                        ************** ***************************** ******  * *****

ymfL_Independent        AAGAGTGACGCCCGCGAGTGTGCAGCTCCGGGCGTCGTGGCGTTTTGTGTCTGTGGAGAA         540
ymfL_ymfM_adjacent      AGTAATGACGCCCGCGAGTGTGCAGCTCCGGGCGTCGTGGCGTCTAGTGCCTGTGGAGGT         540
                        *  * ************************************ * *** ********

ymfL_Independent        ACTAACGCATGA------     552
ymfL_ymfM_adjacent      GGAGAAACTAACGCATGA     558
                            *  *
```

Figure S.3 Alignment of consensus sequences of *ymfM* flanked *ymfL* and independent *ymfL*

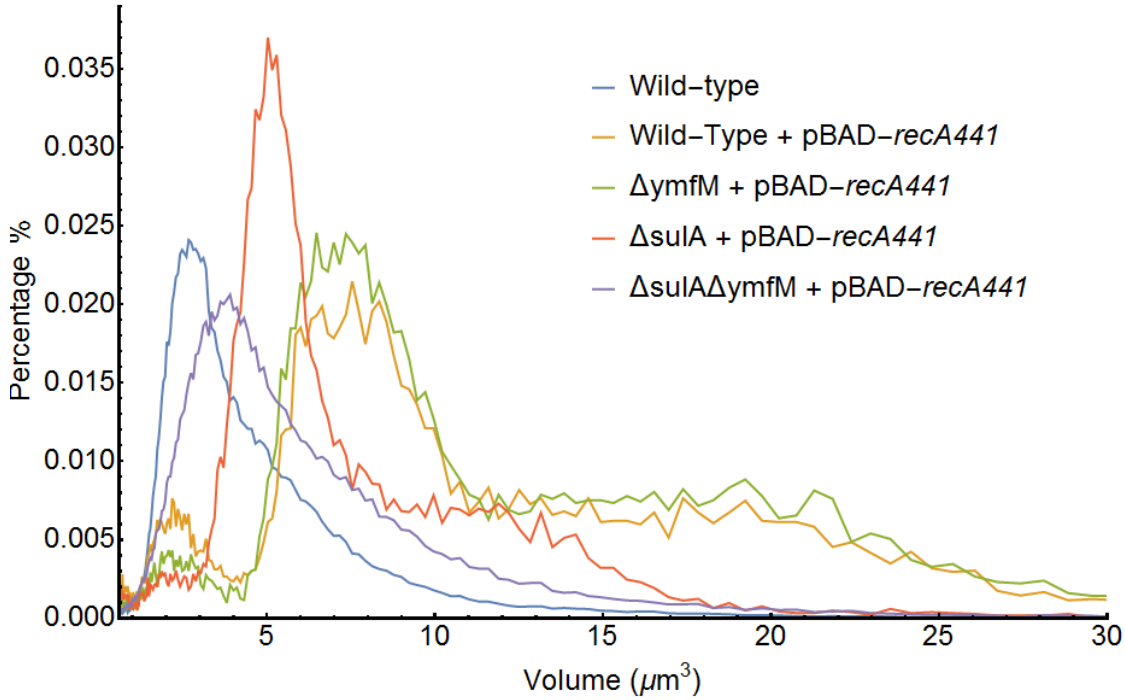

Figure S.4. Cell volume distribution of WT, Δ*ymfM*, Δ*sulA*, and Δ*sulA*Δ*ymfM* after genetic induction of the SOS response by a temperature-sensitive recA mutant, *recA441*.

Coulter counter analysis of cell size distribution of wild-type (yellow),Δ*ymfM* (green), Δs*ulA*(red), and Δs*ulA*Δ*ymfM* (purple) after two hoursofpBAD-*recA441* induction in LB with 0.2% arabinose and 100 µg/mL adenine, at 42ºC. Samples were compared to wild-type cells expressing empty pBAD24 (blue) not under SOS induction. X-axis represents cell volume (µm^3) and Y-axis represents the percentage of cells at any given volume

References

1. Harry, E., L. Monahan, and L. Thompson, *Bacterial cell division: the mechanism and its precison.* Int Rev Cytol, 2006. **253**: p. 27-94.
2. Lock, R.L. and E.J. Harry, *Cell-division inhibitors: new insights for future antibiotics.* Nat Rev Drug Discov, 2008. **7**(4): p. 324-38.
3. Justice, S.S., et al., *Morphological plasticity as a bacterial survival strategy.* Nat Rev Microbiol, 2008. **6**(2): p. 162-8.
4. Bos, J., et al., *Emergence of antibiotic resistance from multinucleated bacterial filaments.* Proc Natl Acad Sci U S A, 2015. **112**(1): p. 178-83.
5. Sass, P. and H. Brotz-Oesterhelt, *Bacterial cell division as a target for new antibiotics.* Curr Opin Microbiol, 2013. **16**(5): p. 522-30.
6. de Boer, P.A., *Advances in understanding E. coli cell fission.* Curr Opin Microbiol, 2010. **13**(6): p. 730-7.
7. den Blaauwen, T., L.W. Hamoen, and P.A. Levin, *The divisome at 25: the road ahead.* Curr Opin Microbiol, 2017. **36**: p. 85-94.
8. Pichoff, S. and J. Lutkenhaus, *Unique and overlapping roles for ZipA and FtsA in septal ring assembly in Escherichia coli.* EMBO J, 2002. **21**(4): p. 685-93.
9. Bailey, M.W., et al., *Evidence for divisome localization mechanisms independent of the Min system and SlmA in Escherichia coli.* PLoS Genet, 2014. **10**(8): p. e1004504.
10. Mannik, J. and M.W. Bailey, *Spatial coordination between chromosomes and cell division proteins in Escherichia coli.* Front Microbiol, 2015. **6**: p. 306.
11. Cho, H., et al., *Nucleoid occlusion factor SlmA is a DNA-activated FtsZ polymerization antagonist.* Proc Natl Acad Sci U S A, 2011. **108**(9): p. 3773-8.
12. Rowlett, V.W. and W. Margolin, *The Min system and other nucleoid-independent regulators of Z ring positioning.* Front Microbiol, 2015. **6**: p. 478.
13. Wang, J.D. and P.A. Levin, *Metabolism, cell growth and the bacterial cell cycle.* Nat Rev Microbiol, 2009. **7**(11): p. 822-7.
14. Bi, E.F. and J. Lutkenhaus, *FtsZ ring structure associated with division in Escherichia coli.* Nature, 1991. **354**(6349): p. 161-4.
15. Schoenemann, K.M. and W. Margolin, *Bacterial Division: FtsZ Treadmills to Build a Beautiful Wall.* Curr Biol, 2017. **27**(8): p. R301-R303.
16. Lowe, J. and L.A. Amos, *Crystal structure of the bacterial cell-division protein FtsZ.* Nature, 1998. **391**(6663): p. 203.
17. Oliva, M.A., S.C. Cordell, and J. Lowe, *Structural insights into FtsZ protofilament formation.* Nat Struct Mol Biol, 2004. **11**(12): p. 1243-50.
18. Matsui, T., et al., *Structural reorganization of the bacterial cell-division protein FtsZ from Staphylococcus aureus.* Acta Crystallogr D Biol Crystallogr, 2012. **68**(Pt 9): p. 1175-88.

19. Oliva, M.A., D. Trambaiolo, and J. Lowe, *Structural insights into the conformational variability of FtsZ.* J Mol Biol, 2007. **373**(5): p. 1229-42.

20. Ma, X. and W. Margolin, *Genetic and functional analyses of the conserved C-terminal core domain of Escherichia coli FtsZ.* J Bacteriol, 1999. **181**(24): p. 7531-44.

21. Mosyak, L., et al., *The bacterial cell-division protein ZipA and its interaction with an FtsZ fragment revealed by X-ray crystallography.* EMBO J, 2000. **19**(13): p. 3179-91.

22. Anderson, D.E., F.J. Gueiros-Filho, and H.P. Erickson, *Assembly dynamics of FtsZ rings in Bacillus subtilis and Escherichia coli and effects of FtsZ-regulating proteins.* J Bacteriol, 2004. **186**(17): p. 5775-81.

23. Haeusser, D.P. and W. Margolin, *Splitsville: structural and functional insights into the dynamic bacterial Z ring.* Nat Rev Microbiol, 2016. **14**(5): p. 305-19.

24. Rico, A.I., M. Krupka, and M. Vicente, *In the beginning, Escherichia coli assembled the proto-ring: an initial phase of division.* J Biol Chem, 2013. **288**(29): p. 20830-6.

25. van den Ent, F. and J. Lowe, *Crystal structure of the cell division protein FtsA from Thermotoga maritima.* EMBO J, 2000. **19**(20): p. 5300-7.

26. Pichoff, S. and J. Lutkenhaus, *Tethering the Z ring to the membrane through a conserved membrane targeting sequence in FtsA.* Mol Microbiol, 2005. **55**(6): p. 1722-34.

27. Szwedziak, P., et al., *FtsA forms actin-like protofilaments.* EMBO J, 2012. **31**(10): p. 2249-60.

28. Loose, M. and T.J. Mitchison, *The bacterial cell division proteins FtsA and FtsZ self-organize into dynamic cytoskeletal patterns.* Nat Cell Biol, 2014. **16**(1): p. 38-46.

29. Hale, C.A. and P.A. de Boer, *Direct binding of FtsZ to ZipA, an essential component of the septal ring structure that mediates cell division in E. coli.* Cell, 1997. **88**(2): p. 175-85.

30. Justice, S.S., J. Garcia-Lara, and L.I. Rothfield, *Cell division inhibitors SulA and MinC/MinD block septum formation at different steps in the assembly of the Escherichia coli division machinery.* Mol Microbiol, 2000. **37**(2): p. 410-23.

31. Hale, C.A. and P.A. de Boer, *Recruitment of ZipA to the septal ring of Escherichia coli is dependent on FtsZ and independent of FtsA.* J Bacteriol, 1999. **181**(1): p. 167-76.

32. Pazos, M., P. Natale, and M. Vicente, *A specific role for the ZipA protein in cell division: stabilization of the FtsZ protein.* J Biol Chem, 2013. **288**(5): p. 3219-26.

33. Dai, K. and J. Lutkenhaus, *The proper ratio of FtsZ to FtsA is required for cell division to occur in Escherichia coli.* J Bacteriol, 1992. **174**(19): p. 6145-51.

34. Dewar, S.J., K.J. Begg, and W.D. Donachie, *Inhibition of cell division initiation by an imbalance in the ratio of FtsA to FtsZ.* J Bacteriol, 1992. **174**(19): p. 6314-6.

35. Rico, A.I., et al., *Role of two essential domains of Escherichia coli FtsA in localization and progression of the division ring.* Mol Microbiol, 2004. **53**(5): p. 1359-71.

36. Geissler, B., D. Shiomi, and W. Margolin, *The ftsA* gain-of-function allele of Escherichia coli and its effects on the stability and dynamics of the Z ring.* Microbiology, 2007. **153**(Pt 3): p. 814-25.

37. Osawa, M. and H.P. Erickson, *Inside-out Z rings--constriction with and without GTP hydrolysis.* Mol Microbiol, 2011. **81**(2): p. 571-9.

38. Osawa, M. and H.P. Erickson, *Liposome division by a simple bacterial division machinery.* Proc Natl Acad Sci U S A, 2013. **110**(27): p. 11000-4.

39. Erickson, H.P., D.E. Anderson, and M. Osawa, *FtsZ in bacterial cytokinesis: cytoskeleton and force generator all in one.* Microbiol Mol Biol Rev, 2010. **74**(4): p. 504-28.

40. Strauss, M.P., et al., *3D-SIM super resolution microscopy reveals a bead-like arrangement for FtsZ and the division machinery: implications for triggering cytokinesis.* PLoS Biol, 2012. **10**(9): p. e1001389.

41. Rowlett, V.W. and W. Margolin, *3D-SIM super-resolution of FtsZ and its membrane tethers in Escherichia coli cells.* Biophys J, 2014. **107**(8): p. L17-20.

42. Daley, D.O., U. Skoglund, and B. Soderstrom, *FtsZ does not initiate membrane constriction at the onset of division.* Sci Rep, 2016. **6**: p. 33138.

43. Bisson-Filho, A.W., et al., *Treadmilling by FtsZ filaments drives peptidoglycan synthesis and bacterial cell division.* Science, 2017. **355**(6326): p. 739-743.

44. Yang, X., et al., *GTPase activity-coupled treadmilling of the bacterial tubulin FtsZ organizes septal cell wall synthesis.* Science, 2017. **355**(6326): p. 744-747.

45. Weiss, D.S., *Bacterial cell division and the septal ring.* Mol Microbiol, 2004. **54**(3): p. 588-97.

46. Buddelmeijer, N. and J. Beckwith, *A complex of the Escherichia coli cell division proteins FtsL, FtsB and FtsQ forms independently of its localization to the septal region.* Mol Microbiol, 2004. **52**(5): p. 1315-27.

47. Gerding, M.A., et al., *Self-enhanced accumulation of FtsN at Division Sites and Roles for Other Proteins with a SPOR domain (DamX, DedD, and RlpA) in Escherichia coli cell constriction.* J Bacteriol, 2009. **191**(24): p. 7383-401.

48. Shen, B. and J. Lutkenhaus, *Differences in MinC/MinD sensitivity between polar and internal Z rings in Escherichia coli.* J Bacteriol, 2011. **193**(2): p. 367-76.

49. Wu, L.J. and J. Errington, *Nucleoid occlusion and bacterial cell division.* Nat Rev Microbiol, 2011. **10**(1): p. 8-12.

50. Bernhardt, T.G. and P.A.J. de Boer, *SlmA, a Nucleoid-Associated, FtsZ Binding Protein Required for Blocking Septal Ring Assembly over Chromosomes in E. coli.* Molecular Cell, 2005. **18**(5): p. 555-564.

51. Cho, H. and T.G. Bernhardt, *Identification of the SlmA active site responsible for blocking bacterial cytokinetic ring assembly over the chromosome.* PLoS Genet, 2013. **9**(2): p. e1003304.

52. Tonthat, N.K., et al., *Molecular mechanism by which the nucleoid occlusion factor, SlmA, keeps cytokinesis in check.* EMBO J, 2011. **30**(1): p. 154-64.

53. Tonthat, N.K., et al., *SlmA forms a higher-order structure on DNA that inhibits cytokinetic Z-ring formation over the nucleoid.* Proc Natl Acad Sci U S A, 2013. **110**(26): p. 10586-91.

54. de Boer, P.A., R.E. Crossley, and L.I. Rothfield, *A division inhibitor and a topological specificity factor coded for by the minicell locus determine proper placement of the division septum in E. coli.* Cell, 1989. **56**(4): p. 641-649.

55. Bi, E. and J. Lutkenhaus, *Cell division inhibitors SulA and MinCD prevent formation of the FtsZ ring.* J Bacteriol, 1993. **175**(4): p. 1118-25.

56. Oliferenko, S., T.G. Chew, and M.K. Balasubramanian, *Positioning cytokinesis.* Genes Dev, 2009. **23**(6): p. 660-674.

57. Lutkenhaus, J., *Assembly dynamics of the bacterial MinCDE system and spatial regulation of the Z ring.* Annu Rev Biochem, 2007. **76**: p. 539-62.

58. Dajkovic, A., et al., *MinC spatially controls bacterial cytokinesis by antagonizing the scaffolding function of FtsZ.* Curr Biol, 2008. **18**(4): p. 235-44.

59. Lutkenhaus, J., *The regulation of bacterial cell division: a time and place for it.* Curr Opin Microbiol, 1998. **1**(2): p. 210-5.

60. Hu, Z. and J. Lutkenhaus, *Topological regulation of cell division in Escherichia coli involves rapid pole to pole oscillation of the division inhibitor MinC under the control of MinD and MinE.* Mol Microbiol, 1999. **34**(1): p. 82-90.

61. Mileykovskaya, E., et al., *Effects of phospholipid composition on MinD-membrane interactions in vitro and in vivo.* J Biol Chem, 2003. **278**(25): p. 22193-8.

62. Taghbalout, A., L. Ma, and L. Rothfield, *Role of MinD-membrane association in Min protein interactions.* J Bacteriol, 2006. **188**(8): p. 2993-3001.

63. Pichoff, S., et al., *Deletion analysis of gene minE which encodes the topological specificity factor of cell division in Escherichia coli.* Mol Microbiol, 1995. **18**(2): p. 321-9.

64. Park, K.T., et al., *The Min oscillator uses MinD-dependent conformational changes in MinE to spatially regulate cytokinesis.* Cell, 2011. **146**(3): p. 396-407.

65. Walsh, J.C., et al., *Non-linear Min protein interactions generate harmonics that signal mid-cell division in Escherichia coli.* PLoS One, 2017. **12**(10): p. e0185947.

66. Walsh, J.C., et al., *Molecular Interactions of the Min Protein System Reproduce Spatiotemporal Patterning in Growing and Dividing Escherichia coli Cells.* PLoS One, 2015. **10**(5): p. e0128148.

67. Zhou, H. and J. Lutkenhaus, *MinC mutants deficient in MinD- and DicB-mediated cell division inhibition due to loss of interaction with MinD, DicB, or a septal component.* J Bacteriol, 2005. **187**(8): p. 2846-57.

68. Zhou, H., et al., *Analysis of MinD mutations reveals residues required for MinE stimulation of the MinD ATPase and residues required for MinC interaction.* J Bacteriol, 2005. **187**(2): p. 629-38.

69. Ghosal, D., et al., *MinCD cell division proteins form alternating copolymeric cytomotive filaments.* Nat Commun, 2014. **5**: p. 5341.

70. Conti, J., M.G. Viola, and J.L. Camberg, *The bacterial cell division regulators MinD and MinC form polymers in the presence of nucleotide.* FEBS Lett, 2015. **589**(2): p. 201-6.

71. Hu, Z., et al., *The MinC component of the division site selection system in Escherichia coli interacts with FtsZ to prevent polymerization.* Proc Natl Acad Sci U S A, 1999. **96**(26): p. 14819-24.

72. Hu, Z. and J. Lutkenhaus, *Analysis of MinC reveals two independent domains involved in interaction with MinD and FtsZ.* J Bacteriol, 2000. **182**(14): p. 3965-71.

73. Margolin, W., *Spatial regulation of cytokinesis in bacteria.* Curr Opin Microbiol, 2001. **4**(6): p. 647-52.

74. Yu, X.C. and W. Margolin, *FtsZ ring clusters in min and partition mutants: role of both the Min system and the nucleoid in regulating FtsZ ring localization.* Mol Microbiol, 1999. **32**(2): p. 315-26.

75. Lutkenhaus, J., S. Pichoff, and S. Du, *Bacterial cytokinesis: From Z ring to divisome.* Cytoskeleton (Hoboken), 2012. **69**(10): p. 778-90.

76. Rodrigues, C.D. and E.J. Harry, *The Min System and Nucleoid Occlusion Are Not Required for Identifying the Division Site in Bacillus subtilis but Ensure Its Efficient Utilization.* PLoS Genet, 2012. **8**(3): p. e1002561.

77. Chien, A.C., N.S. Hill, and P.A. Levin, *Cell size control in bacteria.* Curr Biol, 2012. **22**(9): p. R340-9.

78. Young, K.D., *The selective value of bacterial shape.* Microbiol Mol Biol Rev, 2006. **70**(3): p. 660-703.

79. Pernthaler, J., *Predation on prokaryotes in the water column and its ecological implications.* Nat Rev Microbiol, 2005. **3**(7): p. 537-46.

80. Queck, S.Y., et al., *The role of quorum sensing mediated developmental traits in the resistance of Serratia marcescens biofilms against protozoan grazing.* Environ Microbiol, 2006. **8**(6): p. 1017-25.

81. Matz, C. and K. Jurgens, *High motility reduces grazing mortality of planktonic bacteria.* Appl Environ Microbiol, 2005. **71**(2): p. 921-9.

82. Yang, D.C., K.M. Blair, and N.R. Salama, *Staying in Shape: the Impact of Cell Shape on Bacterial Survival in Diverse Environments.* Microbiol Mol Biol Rev, 2016. **80**(1): p. 187-203.

83. Mulvey, M.A., J.D. Schilling, and S.J. Hultgren, *Establishment of a persistent Escherichia coli reservoir during the acute phase of a bladder infection.* Infect Immun, 2001. **69**(7): p. 4572-9.

84. Ferrero, R.L. and A. Lee, *Motility of Campylobacter jejuni in a viscous environment: comparison with conventional rod-shaped bacteria.* J Gen Microbiol, 1988. **134**(1): p. 53-9.

85. Szymanski, C.M., et al., *Campylobacter jejuni motility and invasion of Caco-2 cells.* Infect Immun, 1995. **63**(11): p. 4295-300.

86. Vinette, K.M., et al., *Growth of Helicobacter pylori in a long spiral form does not alter expression of immunodominant proteins.* BMC Microbiol, 2002. **2**: p. 24.

87. Justice, S.S., et al., *Bacterial differentiation, development, and disease: mechanisms for survival.* FEMS Microbiol Lett, 2014. **360**(1): p. 1-8.

88. Jurgens, K. and C. Matz, *Predation as a shaping force for the phenotypic and genotypic composition of planktonic bacteria.* Antonie Van Leeuwenhoek, 2002. **81**(1-4): p. 413-34.

89. Hahn, M.W., E.R. Moore, and M.G. Hofle, *Bacterial filament formation, a defense mechanism against flagellate grazing, is growth rate controlled in bacteria of different phyla.* Appl Environ Microbiol, 1999. **65**(1): p. 25-35.

90. Corno, G. and K. Jurgens, *Direct and indirect effects of protist predation on population size structure of a bacterial strain with high phenotypic plasticity.* Appl Environ Microbiol, 2006. **72**(1): p. 78-86.

91. Leroy, M., et al., *Multiple consecutive lavage samplings reveal greater burden of disease and provide direct access to the nontypeable Haemophilus influenzae biofilm in experimental otitis media.* Infect Immun, 2007. **75**(8): p. 4158-72.

92. Champion, J.A. and S. Mitragotri, *Role of target geometry in phagocytosis.* Proc Natl Acad Sci U S A, 2006. **103**(13): p. 4930-4.

93. Doshi, N. and S. Mitragotri, *Macrophages recognize size and shape of their targets.* PLoS One, 2010. **5**(4): p. e10051.

94. Horvath, D.J., Jr., et al., *Morphological plasticity promotes resistance to phagocyte killing of uropathogenic Escherichia coli.* Microbes Infect, 2011. **13**(5): p. 426-37.

95. Hunstad, D.A. and S.S. Justice, *Intracellular lifestyles and immune evasion strategies of uropathogenic Escherichia coli.* Annu Rev Microbiol, 2010. **64**: p. 203-21.

96. Justice, S.S., et al., *Filamentation by Escherichia coli subverts innate defenses during urinary tract infection.* Proc Natl Acad Sci U S A, 2006. **103**(52): p. 19884-9.

97. Foxman, B., *Epidemiology of urinary tract infections: Incidence, morbidity, and economic costs.* Disease-a-Month, 2003. **49**(2): p. 53-70.

98. Justice, S.S., et al., *Differentiation and developmental pathways of uropathogenic Escherichia coli in urinary tract pathogenesis.* Proc Natl Acad Sci U S A, 2004. **101**(5): p. 1333-8.

99. Chen, S.L., et al., *Identification of genes subject to positive selection in uropathogenic strains of Escherichia coli: a comparative genomics approach.* Proc Natl Acad Sci U S A, 2006. **103**(15): p. 5977-82.

100. Anderson, G.G., et al., *Intracellular bacterial biofilm-like pods in urinary tract infections.* Science, 2003. **301**(5629): p. 105-7.

101. Anderson, G.G., S.M. Martin, and S.J. Hultgren, *Host subversion by formation of intracellular bacterial communities in the urinary tract.* Microbes Infect, 2004. **6**(12): p. 1094-101.

102. Haraoka, M., et al., *Neutrophil recruitment and resistance to urinary tract infection.* J Infect Dis, 1999. **180**(4): p. 1220-9.

103. Chauhan, A., et al., *Mycobacterium tuberculosis cells growing in macrophages are filamentous and deficient in FtsZ rings.* J Bacteriol, 2006. **188**(5): p. 1856-65.

104. Rosenberger, C.M. and B.B. Finlay, *Macrophages inhibit Salmonella typhimurium replication through MEK/ERK kinase and phagocyte NADPH oxidase activities.* J Biol Chem, 2002. **277**(21): p. 18753-62.

105. Wainwright, M., et al., *Morphological changes (including filamentation) in Escherichia coli grown under starvation conditions on silicon wafers and other surfaces.* Lett Appl Microbiol, 1999. **29**(4): p. 224-7.

106. Maki, N., et al., *Motility and chemotaxis of filamentous cells of Escherichia coli.* J Bacteriol, 2000. **182**(15): p. 4337-42.

107. Comber, K.R., R.J. Boon, and R. Sutherland, *Comparative effects of amoxycillin and ampicillin on the morphology of Escherichia coli in vivo and correlation with activity.* Antimicrob Agents Chemother, 1977. **12**(6): p. 736-44.

108. Elliott, T.S., A. Shelton, and D. Greenwood, *The response of Escherichia coli to ciprofloxacin and norfloxacin.* J Med Microbiol, 1987. **23**(1): p. 83-8.

109. Suzuki, H., J. Pangborn, and W.W. Kilgore, *Filamentous cells of Escherichia coli formed in the presence of mitomycin.* J Bacteriol, 1967. **93**(2): p. 683-8.

110. Chen, K., et al., *Modified virulence of antibiotic-induced Burkholderia pseudomallei filaments.* Antimicrob Agents Chemother, 2005. **49**(3): p. 1002-9.

111. Simmons, L.A., et al., *The SOS Regulatory Network.* EcoSal Plus, 2008. **3**(1).

112. Little, J.W., *Mechanism of specific LexA cleavage: autodigestion and the role of RecA coprotease.* Biochimie, 1991. **73**(4): p. 411-21.

113. Little, J.W., *The SOS regulatory system: control of its state by the level of RecA protease.* J Mol Biol, 1983. **167**(4): p. 791-808.

114. Butala, M., D. Zgur-Bertok, and S.J. Busby, *The bacterial LexA transcriptional repressor.* Cell Mol Life Sci, 2009. **66**(1): p. 82-93.

115. Janion, C., *Inducible SOS response system of DNA repair and mutagenesis in Escherichia coli.* Int J Biol Sci, 2008. **4**(6): p. 338-44.

116. Huisman, O., R. D'Ari, and S. Gottesman, *Cell-division control in Escherichia coli: specific induction of the SOS function SfiA protein is sufficient to block septation.* Proc Natl Acad Sci U S A, 1984. **81**(14): p. 4490-4.

117. Cordell, S.C., E.J. Robinson, and J. Lowe, *Crystal structure of the SOS cell division inhibitor SulA and in complex with FtsZ.* Proc Natl Acad Sci U S A, 2003. **100**(13): p. 7889-94.

118. Dajkovic, A., A. Mukherjee, and J. Lutkenhaus, *Investigation of regulation of FtsZ assembly by SulA and development of a model for FtsZ polymerization.* J Bacteriol, 2008. **190**(7): p. 2513-26.

119. Chen, Y., S.L. Milam, and H.P. Erickson, *SulA Inhibits Assembly of FtsZ by a Simple Sequestration Mechanism.* Biochemistry, 2012. **51**(14): p. 3100-9.

120. Mukherjee, A., C. Cao, and J. Lutkenhaus, *Inhibition of FtsZ polymerization by SulA, an inhibitor of septation in Escherichia coli.* Proc Natl Acad Sci U S A, 1998. **95**(6): p. 2885-90.

121. Trusca, D., et al., *Bacterial SOS checkpoint protein SulA inhibits polymerization of purified FtsZ cell division protein.* J Bacteriol, 1998. **180**(15): p. 3946-53.

122. Dai, K., et al., *Mutations in ftsZ that confer resistance to SulA affect the interaction of FtsZ with GTP.* J Bacteriol, 1994. **176**(1): p. 130-6.

123. Mizusawa, S. and S. Gottesman, *Protein degradation in Escherichia coli: the lon gene controls the stability of sulA protein.* Proc Natl Acad Sci U S A, 1983. **80**(2): p. 358-62.

124. Li, B., et al., *SOS regulatory elements are essential for UPEC pathogenesis.* Microbes Infect, 2010. **12**(8-9): p. 662-8.

125. Andersen, T.E., et al., *Escherichia coli Uropathogenesis in vitro: Invasion, Cellular Escape and Secondary Infection Analyzed in a Human Bladder Cell Infection Model.* Infect Immun, 2012.

126. Khandige, S., et al., *DamX Controls Reversible Cell Morphology Switching in Uropathogenic Escherichia coli.* MBio, 2016. **7**(4).

127. Lyngstadaas, A., A. Lobner-Olesen, and E. Boye, *Characterization of three genes in the dam-containing operon of Escherichia coli.* Mol Gen Genet, 1995. **247**(5): p. 546-54.

128. Yahashiri, A., M.A. Jorgenson, and D.S. Weiss, *The SPOR Domain, a Widely Conserved Peptidoglycan Binding Domain That Targets Proteins to the Site of Cell Division.* J Bacteriol, 2017. **199**(14).

129. Arends, S.J., et al., *Discovery and characterization of three new Escherichia coli septal ring proteins that contain a SPOR domain: DamX, DedD, and RlpA.* J Bacteriol, 2010. **192**(1): p. 242-55.

130. Lopez-Garrido, J. and J. Casadesus, *The DamX protein of Escherichia coli and Salmonella enterica.* Gut Microbes, 2010. **1**(4): p. 285-288.

131. Lopez-Garrido, J., et al., *Identification of the Salmonella enterica damX gene product, an inner membrane protein involved in bile resistance.* J Bacteriol, 2010. **192**(3): p. 893-5.

132. Penades, J.R., et al., *Bacteriophage-mediated spread of bacterial virulence genes.* Curr Opin Microbiol, 2015. **23**: p. 171-8.

133. Greer, H., *The kil gene of bacteriophage lambda.* Virology, 1975. **66**(2): p. 589-604.

134. Johnson, J.E., L.L. Lackner, and P.A. de Boer, *Targeting of (D)MinC/MinD and (D)MinC/DicB complexes to septal rings in Escherichia coli suggests a multistep mechanism for MinC-mediated destruction of nascent FtsZ rings.* J Bacteriol, 2002. **184**(11): p. 2951-62.

135. Balasubramanian, D., et al., *A Prophage-Encoded Small RNA Controls Metabolism and Cell Division in Escherichia coli.* mSystems, 2016. **1**(1).

136. D'Ari, R. and O. Huisman, *Novel mechanism of cell division inhibition associated with the SOS response in Escherichia coli.* J Bacteriol, 1983. **156**(1): p. 243-50.

137. Tan, Q., N. Awano, and M. Inouye, *YeeV is an Escherichia coli toxin that inhibits cell division by targeting the cytoskeleton proteins, FtsZ and MreB.* Mol Microbiol, 2011. **79**(1): p. 109-18.

138. Yamaguchi, Y., J.H. Park, and M. Inouye, *Toxin-antitoxin systems in bacteria and archaea.* Annu Rev Genet, 2011. **45**: p. 61-79.

139. Wang, X. and T.K. Wood, *Toxin-antitoxin systems influence biofilm and persister cell formation and the general stress response.* Appl Environ Microbiol, 2011. **77**(16): p. 5577-83.

140. Norton, J.P. and M.A. Mulvey, *Toxin-antitoxin systems are important for niche-specific colonization and stress resistance of uropathogenic Escherichia coli.* PLoS Pathog, 2012. **8**(10): p. e1002954.

141. Masuda, H., et al., *YeeU enhances the bundling of cytoskeletal polymers of MreB and FtsZ, antagonizing the CbtA (YeeV) toxicity in Escherichia coli.* Mol Microbiol, 2012. **84**(5): p. 979-89.

142. Heller, D.M., M. Tavag, and A. Hochschild, *CbtA toxin of Escherichia coli inhibits cell division and cell elongation via direct and independent interactions with FtsZ and MreB.* PLoS Genet, 2017. **13**(9): p. e1007007.

143. Fenton, A.K. and K. Gerdes, *Direct interaction of FtsZ and MreB is required for septum synthesis and cell division in Escherichia coli.* EMBO J, 2013. **32**(13): p. 1953-65.

144. Schumacher, M.A. and W. Zeng, *Structures of the nucleoid occlusion protein SlmA bound to DNA and the C-terminal domain of the cytoskeletal protein FtsZ.* Proc Natl Acad Sci U S A, 2016. **113**(18): p. 4988-93.

145. Du, S. and J. Lutkenhaus, *SlmA antagonism of FtsZ assembly employs a two-pronged mechanism like MinCD.* PLoS Genet, 2014. **10**(7): p. e1004460.

146. Shen, B. and J. Lutkenhaus, *Examination of the interaction between FtsZ and MinCN in E. coli suggests how MinC disrupts Z rings.* Mol Microbiol, 2010. **75**(5): p. 1285-98.

147. Haeusser, D.P., et al., *The Kil peptide of bacteriophage lambda blocks Escherichia coli cytokinesis via ZipA-dependent inhibition of FtsZ assembly.* PLoS Genet, 2014. **10**(3): p. e1004217.

148. Hernandez-Rocamora, V.M., et al., *Evidence That Bacteriophage lambda Kil Peptide Inhibits Bacterial Cell Division by Disrupting FtsZ Protofilaments and Sequestering Protein Subunits.* J Biol Chem, 2015. **290**(33): p. 20325-35.

149. Cam, K., et al., *Identification and sequence of gene dicB: translation of the division inhibitor from an in-phase internal start.* Nucleic Acids Res, 1988. **16**(14A): p. 6327-38.

150. Yang, S., et al., *Characterization of DicB by partially masking its potent inhibitory activity of cell division.* Open Biol, 2016. **6**(7).

151. de Boer, P.A., R.E. Crossley, and L.I. Rothfield, *Central role for the Escherichia coli minC gene product in two different cell division-inhibition systems.* Proc Natl Acad Sci U S A, 1990. **87**(3): p. 1129-33.

152. Johnson, J.E., et al., *ZipA is required for targeting of DMinC/DicB, but not DMinC/MinD, complexes to septal ring assemblies in Escherichia coli.* J Bacteriol, 2004. **186**(8): p. 2418-29.

153. Wang, X., et al., *Cryptic prophages help bacteria cope with adverse environments.* Nat Commun, 2010. **1**: p. 147.

154. Maguin, E., et al., *SOS-associated division inhibition gene sfiC is part of excisable element e14 in Escherichia coli.* J Bacteriol, 1986. **168**(1): p. 464-6.

155. Mehta, P., S. Casjens, and S. Krishnaswamy, *Analysis of the lambdoid prophage element e14 in the E. coli K-12 genome.* BMC Microbiol, 2004. **4**: p. 4.

156. Argov, T., et al., *Temperate bacteriophages as regulators of host behavior.* Curr Opin Microbiol, 2017. **38**: p. 81-87.

157. Brussow, H., C. Canchaya, and W.D. Hardt, *Phages and the evolution of bacterial pathogens: from genomic rearrangements to lysogenic conversion.* Microbiol Mol Biol Rev, 2004. **68**(3): p. 560-602, table of contents.

158. Brown-Jaque, M., W. Calero-Caceres, and M. Muniesa, *Transfer of antibiotic-resistance genes via phage-related mobile elements.* Plasmid, 2015. **79**: p. 1-7.

159. Colomer-Lluch, M., J. Jofre, and M. Muniesa, *Antibiotic resistance genes in the bacteriophage DNA fraction of environmental samples.* PLoS One, 2011. **6**(3): p. e17549.

160. Shousha, A., et al., *Bacteriophages Isolated from Chicken Meat and the Horizontal Transfer of Antimicrobial Resistance Genes.* Appl Environ Microbiol, 2015. **81**(14): p. 4600-6.

161. Casjens, S., *Prophages and bacterial genomics: what have we learned so far?* Mol Microbiol, 2003. **49**(2): p. 277-300.

162. Comeau, A.M., et al., *Modular architecture of the T4 phage superfamily: a conserved core genome and a plastic periphery.* Virology, 2007. **362**(2): p. 384-96.

163. Burke, C., et al., *Harnessing single cell sorting to identify cell division genes and regulators in bacteria.* PLoS One, 2013. **8**(4): p. e60964.

164. Datsenko, K.A. and B.L. Wanner, *One-step inactivation of chromosomal genes in Escherichia coli K-12 using PCR products.* Proc Natl Acad Sci U S A, 2000. **97**(12): p. 6640-5.

165. Baba, T., et al., *Construction of Escherichia coli K-12 in-frame, single-gene knockout mutants: the Keio collection.* Mol Syst Biol, 2006. **2**: p. 2006 0008.

166. Bernhardt, T.G. and P.A. de Boer, *The Escherichia coli amidase AmiC is a periplasmic septal ring component exported via the twin-arginine transport pathway.* Mol Microbiol, 2003. **48**(5): p. 1171-82.

167. Castellazzi, M., J. George, and G. Buttin, *Prophage induction and cell division in E. coli. I. Further characterization of the thermosensitive mutation tif-1 whose expression mimics the effect of UV irradiation.* Mol Gen Genet, 1972. **119**(2): p. 139-52.

168. Guzman, L.M., et al., *Tight regulation, modulation, and high-level expression by vectors containing the arabinose PBAD promoter.* J Bacteriol, 1995. **177**(14): p. 4121-30.

169. Neylon, C., et al., *Interaction of the Escherichia coli replication terminator protein (Tus) with DNA: a model derived from DNA-binding studies of mutant proteins by surface plasmon resonance.* Biochemistry, 2000. **39**(39): p. 11989-99.

170. Cherepanov, P.P. and W. Wackernagel, *Gene disruption in Escherichia coli: TcR and KmR cassettes with the option of Flp-catalyzed excision of the antibiotic-resistance determinant.* Gene, 1995. **158**(1): p. 9-14.

171. Knight, K.L., et al., *Identification of the amino acid substitutions in two mutant forms of the recA protein from Escherichia coli: recA441 and recA629.* J Biol Chem, 1984. **259**(18): p. 11279-83.

172. Addinall, S.G., E. Bi, and J. Lutkenhaus, *FtsZ ring formation in fts mutants.* J Bacteriol, 1996. **178**(13): p. 3877-84.

173. Morgulis, A., et al., *Database indexing for production MegaBLAST searches.* Bioinformatics, 2008. **24**(16): p. 1757-64.

174. Cover, T.M., J.A. Thomas, and NetLibrary Inc., *Elements of information theory*. 2006, Wiley-Interscience,: Hoboken, N.J. p. xxiii, 748 p. ill.

175. Katoh, K., J. Rozewicki, and K.D. Yamada, *MAFFT online service: multiple sequence alignment, interactive sequence choice and visualization.* Brief Bioinform, 2017.

176. Kawarai, T., et al., *SulA-independent filamentation of Escherichia coli during growth after release from high hydrostatic pressure treatment.* Appl Microbiol Biotechnol, 2004. **64**(2): p. 255-62.

177. Gibert, I. and J. Casadesus, *sulA-independent division inhibition in his-constitutive strains of Salmonella typhimurium.* FEMS Microbiol Lett, 1990. **57**(3): p. 205-10.

178. Henry, T., F. Garcia-Del Portillo, and J.P. Gorvel, *Identification of Salmonella functions critical for bacterial cell division within eukaryotic cells.* Mol Microbiol, 2005. **56**(1): p. 252-67.

179. Frandsen, N. and R. D'Ari, *Excess histidine enzymes cause AICAR-independent filamentation in Escherichia coli.* Mol Gen Genet, 1993. **240**(3): p. 348-54.

180. Brown, J.M. and K.J. Shaw, *A novel family of Escherichia coli toxin-antitoxin gene pairs.* J Bacteriol, 2003. **185**(22): p. 6600-8.

181. Shimada, T., K. Yamazaki, and A. Ishihama, *Novel regulator PgrR for switch control of peptidoglycan recycling in Escherichia coli.* Genes Cells, 2013. **18**(2): p. 123-34.

182. Uehara, T. and T.G. Bernhardt, *More than just lysins: peptidoglycan hydrolases tailor the cell wall.* Curr Opin Microbiol, 2011. **14**(6): p. 698-703.

183. Choi, U., et al., *Increased expression of genes involved in uptake and degradation of murein tripeptide under nitrogen starvation in Escherichia coli.* FEMS Microbiol Lett, 2016. **363**(14).

184. Weiser, J.N., et al., *Identification and characterization of a cell envelope protein of Haemophilus influenzae contributing to phase variation in colony opacity and nasopharyngeal colonization.* Mol Microbiol, 1995. **17**(3): p. 555-64.

185. Prasadarao, N.V., et al., *Opacity-associated protein A contributes to the binding of Haemophilus influenzae to chang epithelial cells.* Infect Immun, 1999. **67**(8): p. 4153-60.

186. Meisel, U., J.V. Holtje, and W. Vollmer, *Overproduction of inactive variants of the murein synthase PBP1B causes lysis in Escherichia coli.* J Bacteriol, 2003. **185**(18): p. 5342-8.

187. Wen, Z., et al., *Interaction of Type IV Toxin/Antitoxin Systems in Cryptic Prophages of Escherichia coli K-12.* Toxins (Basel), 2017. **9**(3).

188. Kitagawa, M., et al., *Complete set of ORF clones of Escherichia coli ASKA library (a complete set of E. coli K-12 ORF archive): unique resources for biological research.* DNA Res, 2005. **12**(5): p. 291-9.

189. Buist, G., et al., *LysM, a widely distributed protein motif for binding to (peptido)glycans.* Mol Microbiol, 2008. **68**(4): p. 838-47.

190. Mesnage, S., et al., *Molecular basis for bacterial peptidoglycan recognition by LysM domains.* Nat Commun, 2014. **5**: p. 4269.

191. Fernandez De Henestrosa, A.R., et al., *Identification of additional genes belonging to the LexA regulon in Escherichia coli.* Mol Microbiol, 2000. **35**(6): p. 1560-72.

192. Chen, Z., H. Yang, and N.P. Pavletich, *Mechanism of homologous recombination from the RecA-ssDNA/dsDNA structures.* Nature, 2008. **453**(7194): p. 489-4.

193. Giese, K.C., C.B. Michalowski, and J.W. Little, *RecA-dependent cleavage of LexA dimers.* J Mol Biol, 2008. **377**(1): p. 148-61.

194. Kovacic, L., et al., *Structural insight into LexA-RecA* interaction.* Nucleic Acids Res, 2013. **41**(21): p. 9901-10.

195. Gruenig, M.C., et al., *RecA-mediated SOS induction requires an extended filament conformation but no ATP hydrolysis.* Mol Microbiol, 2008. **69**(5): p. 1165-79.

196. Courcelle, J., et al., *Comparative gene expression profiles following UV exposure in wild-type and SOS-deficient Escherichia coli.* Genetics, 2001. **158**(1): p. 41-64.

197. Friedman, N., et al., *Precise temporal modulation in the response of the SOS DNA repair network in individual bacteria.* PLoS Biol, 2005. **3**(7): p. e238.

198. Michel, B., *After 30 years of study, the bacterial SOS response still surprises us.* PLoS Biol, 2005. **3**(7): p. e255.

199. Sauer, R.T., M.J. Ross, and M. Ptashne, *Cleavage of the lambda and P22 repressors by recA protein.* J Biol Chem, 1982. **257**(8): p. 4458-62.

200. Slilaty, S.N., J.A. Rupley, and J.W. Little, *Intramolecular cleavage of LexA and phage lambda repressors: dependence of kinetics on repressor concentration, pH, temperature, and solvent.* Biochemistry, 1986. **25**(22): p. 6866-75.

201. Fornelos, N., D.F. Browning, and M. Butala, *The Use and Abuse of LexA by Mobile Genetic Elements.* Trends Microbiol, 2016. **24**(5): p. 391-401.

202. Hill, C.W., J.A. Gray, and H. Brody, *Use of the isocitrate dehydrogenase structural gene for attachment of e14 in Escherichia coli K-12.* J Bacteriol, 1989. **171**(7): p. 4083-4.

203. Greener, A. and C.W. Hill, *Identification of a novel genetic element in Escherichia coli K-12.* J Bacteriol, 1980. **144**(1): p. 312-21.

204. Brody, H., A. Greener, and C.W. Hill, *Excision and reintegration of the Escherichia coli K-12 chromosomal element e14.* J Bacteriol, 1985. **161**(3): p. 1112-7.

205. Maguin, E., J. Lutkenhaus, and R. D'Ari, *Reversibility of SOS-associated division inhibition in Escherichia coli.* J Bacteriol, 1986. **166**(3): p. 733-8.

206. Pohlhaus, J.R. and K.N. Kreuzer, *Norfloxacin-induced DNA gyrase cleavage complexes block Escherichia coli replication forks, causing double-stranded breaks in vivo.* Mol Microbiol, 2005. **56**(6): p. 1416-29.

207. Uhlin, B.E. and A.J. Clark, *Overproduction of the Escherichia coli recA protein without stimulation of its proteolytic activity.* J Bacteriol, 1981. **148**(1): p. 386-90.

208. Dwyer, D.J., et al., *Antibiotics induce redox-related physiological alterations as part of their lethality.* Proc Natl Acad Sci U S A, 2014. **111**(20): p. E2100-9.

209. Faith, J.J., et al., *Large-scale mapping and validation of Escherichia coli transcriptional regulation from a compendium of expression profiles.* PLoS Biol, 2007. **5**(1): p. e8.

210. Kohanski, M.A., et al., *A common mechanism of cellular death induced by bactericidal antibiotics.* Cell, 2007. **130**(5): p. 797-810.

211. Kohanski, M.A., D.J. Dwyer, and J.J. Collins, *How antibiotics kill bacteria: from targets to networks.* Nat Rev Microbiol, 2010. **8**(6): p. 423-35.

212. Drlica, K. and X. Zhao, *DNA gyrase, topoisomerase IV, and the 4-quinolones.* Microbiol Mol Biol Rev, 1997. **61**(3): p. 377-92.

213. Huisman, O., R. D'Ari, and J. George, *Dissociation of tsl-tif-induced filamentation and recA protein synthesis in Escherichia coli K-12.* J Bacteriol, 1980. **142**(3): p. 819-28.

214. Khil, P.P. and R.D. Camerini-Otero, *Over 1000 genes are involved in the DNA damage response of Escherichia coli.* Mol Microbiol, 2002. **44**(1): p. 89-105.

215. Conter, A., J.P. Bouche, and M. Dassain, *Identification of a new inhibitor of essential division gene ftsZ as the kil gene of defective prophage Rac.* J Bacteriol, 1996. **178**(17): p. 5100-4.

216. Phillips, I., et al., *Induction of the SOS response by new 4-quinolones.* J Antimicrob Chemother, 1987. **20**(5): p. 631-8.

217. Erill, I., S. Campoy, and J. Barbe, *Aeons of distress: an evolutionary perspective on the bacterial SOS response.* FEMS Microbiol Rev, 2007. **31**(6): p. 637-56.

218. Marschall, L., P. Sagmeister, and C. Herwig, *Tunable recombinant protein expression in E. coli: promoter systems and genetic constraints.* Appl Microbiol Biotechnol, 2017. **101**(2): p. 501-512.

219. Folkmanis, A., et al., *The essential role of the cro gene in lytic development by bacteriophage lambda.* Virology, 1977. **81**(2): p. 352-62.

220. Schubert, R.A., et al., *Cro's role in the CI Cro bistable switch is critical for {lambda}'s transition from lysogeny to lytic development.* Genes Dev, 2007. **21**(19): p. 2461-72.

221. Shinhara, A., et al., *Deep sequencing reveals as-yet-undiscovered small RNAs in Escherichia coli.* BMC Genomics, 2011. **12**: p. 428.

222. Paget, M.S. and J.D. Helmann, *The sigma70 family of sigma factors.* Genome Biol, 2003. **4**(1): p. 203.

223. Casjens, S.R. and R.W. Hendrix, *Bacteriophage lambda: Early pioneer and still relevant.* Virology, 2015. **479-480**: p. 310-30.

224. Jiao, D., W. Han, and Y. Ye, *Functional association prediction by community profiling.* Methods, 2017. **129**: p. 8-17.

225. Ohta, T., *Slightly deleterious mutant substitutions in evolution.* Nature, 1973. **246**(5428): p. 96-8.

226. Lowe, J. and L.A. Amos, *Crystal structure of the bacterial cell-division protein FtsZ.* Nature, 1998. **391**(6663): p. 203-6.

227. van den Ent, F., L. Amos, and J. Lowe, *Bacterial ancestry of actin and tubulin.* Curr Opin Microbiol, 2001. **4**(6): p. 634-8.

228. de Boer, P., R. Crossley, and L. Rothfield, *The essential bacterial cell-division protein FtsZ is a GTPase.* Nature, 1992. **359**(6392): p. 254-6.

229. Errington, J., R.A. Daniel, and D.J. Scheffers, *Cytokinesis in bacteria.* Microbiol Mol Biol Rev, 2003. **67**(1): p. 52-65, table of contents.

230. Pichoff, S., et al., *FtsA mutants impaired for self-interaction bypass ZipA suggesting a model in which FtsA's self-interaction competes with its ability to recruit downstream division proteins.* Mol Microbiol, 2012. **83**(1): p. 151-67.

231. Erickson, H.P., et al., *Bacterial cell division protein FtsZ assembles into protofilament sheets and minirings, structural homologs of tubulin polymers.* Proc Natl Acad Sci U S A, 1996. **93**(1): p. 519-23.

232. Lutkenhaus, J., *FtsZ ring in bacterial cytokinesis.* Mol Microbiol, 1993. **9**(3): p. 403-9.

233. Aakre, C.D. and M.T. Laub, *Asymmetric cell division: a persistent issue?* Dev Cell, 2012. **22**(2): p. 235-6.

234. Du, S. and J. Lutkenhaus, *Assembly and activation of the Escherichia coli divisome.* Mol Microbiol, 2017. **105**(2): p. 177-187.

235. Hernandez-Rocamora, V.M., et al., *MinC protein shortens FtsZ protofilaments by preferentially interacting with GDP-bound subunits.* J Biol Chem, 2013. **288**(34): p. 24625-35.

236. Arumugam, S., Z. Petrasek, and P. Schwille, *MinCDE exploits the dynamic nature of FtsZ filaments for its spatial regulation.* Proc Natl Acad Sci U S A, 2014. **111**(13): p. E1192-200.

237. Adams, D.W., L.J. Wu, and J. Errington, *Cell cycle regulation by the bacterial nucleoid.* Curr Opin Microbiol, 2014. **22**: p. 94-101.

238. Bernhardt, T.G. and P.A. de Boer, *SlmA, a nucleoid-associated, FtsZ binding protein required for blocking septal ring assembly over Chromosomes in E. coli.* Mol Cell, 2005. **18**(5): p. 555-64.

239. Cabre, E.J., et al., *The Nucleoid Occlusion SlmA Protein Accelerates the Disassembly of the FtsZ Protein Polymers without Affecting Their GTPase Activity.* PLoS One, 2015. **10**(5): p. e0126434.

240. Dai, K. and J. Lutkenhaus, *ftsZ is an essential cell division gene in Escherichia coli.* J Bacteriol, 1991. **173**(11): p. 3500-6.

241. Pogliano, J., et al., *Inactivation of FtsI inhibits constriction of the FtsZ cytokinetic ring and delays the assembly of FtsZ rings at potential division sites.* Proc Natl Acad Sci U S A, 1997. **94**(2): p. 559-64.

242. Lauder, S.D. and S.C. Kowalczykowski, *Negative co-dominant inhibition of recA protein function. Biochemical properties of the recA1, recA13 and recA56 proteins and the effect of recA56 protein on the activities of the wild-type recA protein function in vitro.* J Mol Biol, 1993. **234**(1): p. 72-86.

243. Pedelacq, J.D., et al., *Engineering and characterization of a superfolder green fluorescent protein.* Nat Biotechnol, 2006. **24**(1): p. 79-88.

244. Miroux, B. and J.E. Walker, *Over-production of proteins in Escherichia coli: mutant hosts that allow synthesis of some membrane proteins and globular proteins at high levels.* J Mol Biol, 1996. **260**(3): p. 289-98.

245. Moon, A.F., et al., *A synergistic approach to protein crystallization: combination of a fixed-arm carrier with surface entropy reduction.* Protein Sci, 2010. **19**(5): p. 901-13.

246. Kapust, R.B. and D.S. Waugh, *Escherichia coli maltose-binding protein is uncommonly effective at promoting the solubility of polypeptides to which it is fused.* Protein Sci, 1999. **8**(8): p. 1668-74.

247. Young, C.L., Z.T. Britton, and A.S. Robinson, *Recombinant protein expression and purification: a comprehensive review of affinity tags and microbial applications.* Biotechnol J, 2012. **7**(5): p. 620-34.

248. Mannik, J., et al., *Robustness and accuracy of cell division in Escherichia coli in diverse cell shapes.* Proc Natl Acad Sci U S A, 2012. **109**(18): p. 6957-62.

249. Bisicchia, P., et al., *MinC, MinD, and MinE drive counter-oscillation of early-cell-division proteins prior to Escherichia coli septum formation.* MBio, 2013. **4**(6): p. e00856-13.

250. Potluri, L.P., M.A. de Pedro, and K.D. Young, *Escherichia coli low-molecular-weight penicillin-binding proteins help orient septal FtsZ, and their absence leads to asymmetric cell division and branching.* Mol Microbiol, 2012. **84**(2): p. 203-24.

251. Wells, V.L. and W. Margolin, *A new slant to the Z ring and bacterial cell branch formation.* Mol Microbiol, 2012. **84**(2): p. 199-202.

252. Moore, D.A., et al., *Probing for Binding Regions of the FtsZ Protein Surface through Site-Directed Insertions: Discovery of Fully Functional FtsZ-Fluorescent Proteins.* J Bacteriol, 2017. **199**(1).

253. Buss, J., et al., *In vivo organization of the FtsZ-ring by ZapA and ZapB revealed by quantitative super-resolution microscopy.* Mol Microbiol, 2013. **89**(6): p. 1099-120.

254. Lee, N., C. Francklyn, and E.P. Hamilton, *Arabinose-induced binding of AraC protein to araI2 activates the araBAD operon promoter.* Proc Natl Acad Sci U S A, 1987. **84**(24): p. 8814-8.

255. Modell, J.W., et al., *A DNA damage-induced, SOS-independent checkpoint regulates cell division in Caulobacter crescentus.* PLoS Biol, 2014. **12**(10): p. e1001977.

256. Robinson, A., et al., *Regulation of Mutagenic DNA Polymerase V Activation in Space and Time.* PLoS Genet, 2015. **11**(8): p. e1005482.

257. Krol, E. and D.J. Scheffers, *FtsZ polymerization assays: simple protocols and considerations.* J Vis Exp, 2013(81): p. e50844.